Fundamentals and Applications of Mo and Nb Alloying in High Performance Steels

Volume 1

CBMM | IMOA | TMS

Fundamentals and Applications of Mo and Nb Alloying in High Performance Steels

Volume 1

Fundamentals and Applications of Mo and Nb Alloying in High Performance Steels

Volume 1

Proceedings of the First International Symposium on Fundamentals and Applications of Mo and Nb Alloying in High Performance Steels. Held in Taipei, Taiwan, 7–8 November 2011.

Published by CBMM and IMOA

Production work by The Minerals, Metals & Materials Society (TMS)

Editorial support provided by Beta Technology Ltd, UK

ISBN 978-0-615-67631-9

Printed in the United States of America.

TABLE OF CONTENTS
Fundamentals and Applications of Mo and Nb Alloying in High Performance Steels

Preface vii
About IMOA ix
About CBMM xi

Physical Metallurgy of Mo and Nb Alloyed Steels

On Austenite Conditioning and Recrystallization Control of Higher Grade Linepipe Steels (X100) with Niobium and Molybdenum Additions 3
S.V. Subramanian and Y. Yang

Effect of Niobium and Molybdenum on Phase Transformations in Advanced Low-Carbon Steels 23
M. Militzer, F. Fazeli, and T. Jia

Austenite Processing and Phase Transformation of Niobium and Molybdenum Alloyed High Performance Structural Steel 37
C.J. Shang, C.L. Miao, and S.V. Subramanian

The Effect of Niobium Additions on the Microstructural Morphology in the Heat-Affected Zone of Low-Carbon Steels 63
J.R. Yang and C.Y. Huang

Synergies of Niobium and Boron Microalloying in Molybdenum Based Bainitic and Martensitic Steels 83
H. Mohrbacher

Effects of Ti-Mo and Ti-Nb Complex Additions on Interphase Precipitation in Low-Carbon Steels 109
H.W. Yen, C.Y. Huang, and J.R. Yang

Applications of Mo and Nb Alloyed Steels

Application of Niobium-Molybdenum Strengthening Mechanisms in High Strength Linepipe Steels 121
J.M. Gray

Effects of Microalloying and Hot Rolling Parameters on Toughness and Yield Strength of API X80 Grade Steel Strips 135
K. Kim

Seismic and Fire Resistant Niobium-Molybdenum-Bearing Long and Plate Products 155
S.G. Jansto

Metallurgy of Two Types of Precipitation Hardened High Strength Flat-Rolled Products for Automobile Applications 173
Y. Hosoya, T. Urabe, Y. Funakawa, and Y. Ono

The Use of Molybdenum and Niobium in Ultra-High Strength Multiphase Steels 185
H. Mohrbacher

Influence of Titanium and Niobium on the Strength-Ductility-Hole Expansion Ratio Balance of Hot-Rolled Low-Carbon High-Strength Steel Sheets 209
K. Kamibayashi, Y. Tanabe, Y. Takemoto, I. Shimizu, and T. Senuma

Progress in Press Hardening Technology and Innovative Alloying Designs 227
J. Bian

Common Acronyms and Abbreviations 239

Author Index 245

Subject Index 247

Preface

Niobium and molybdenum are neighboring elements in the periodic table having atomic numbers 41 and 42 respectively. Both are important alloying elements in steel, improving essential properties such as strength, toughness, as well as corrosion and heat resistance. Although there have been great advances in steel technology over the last four decades, the industry currently faces the most serious sustainability challenges ever, with regard to energy conservation, reduction of CO_2 emissions and generally the more efficient use of resources. Continuous innovative development of steels with properties specifically tailored to fulfill these demands is absolutely vital. Consistent with this strategy and the goal of achieving "more with less" this *First Symposium on Fundamentals and Applications of Mo and Nb Alloying in High Performance Steels* was precisely striving to encourage progress in this field.

The metallurgical effects of both elements have been the subject of countless publications. Most typically, niobium has the strongest grain refining effect of all alloying elements whereas molybdenum is famous for its excellent hardenability effect. Beyond their established effects, both elements have more unique metallurgical influences when applied in combination and often show interesting synergies. It is exactly these synergies that can raise the performance of steels to the next higher level fulfilling the ever-more stringent industrial and socio-economic needs.

The symposium was a collaborative initiative providing a platform for leading experts from steel mills, research organizations and professionals from academic institutions, to closely focus on such interesting combinations of two potent alloying elements. Furthermore the meeting constituted a perfect occasion for discussing future collaborations, exchanging ideas and viewpoints, and fostering genuine critical thinking among the attendees.

The International Molybdenum Association (IMOA) representing the global molybdenum industry and the leading Brazilian niobium producer Companhia Brasileira de Metalurgia e Mineração (CBMM) joined forces in organizing and sponsoring this unique symposium. Both organizations have a long history of actively promoting metallurgical research and development.

The National Taiwan University (NTU) and China Steel Corporation (CSC) kindly hosted the symposium in the Taiwanese capital Taipei. Even though Taiwan is a small island, its steel production ranks in the top 20 and its steel consumption per capita ranks in the top three in the world. More importantly, Taiwanese steel technology and metallurgical research are top class, thus providing the right environment with respect to the ambitions set for this symposium.

The one and a half day symposium presented carefully selected, invited talks focusing on aspects of niobium and molybdenum alloying along the processing chain and with respect to particular applications. The symposium also served as a forum for the exchange of experience and expertise in this field. Attention to detail and exhaustive discussions allowed the audience to get an in-depth picture on the various effects and synergies of molybdenum and niobium in steel. These proceedings seek to capture and preserve the tremendous amount of information presented and exchanged during the symposium and to make it available to a broader audience.

Hardy Mohrbacher
NiobelCon
Editor-in-Chief

The International Molybdenum Association (IMOA)

IMOA represents 85% of mine production plus all conversion capacity in established markets and a growing proportion of production in developing markets, including the largest mines in China. It also represents traders, downstream processors, consumers and other industry participants.

The Association is dedicated to serving the best interests of its members and works continually to enhance the reputation of the industry. The key areas of activity are:

- Proactive development of existing and potential new markets around the world through a network of technical, industry and application experts.
- Representing members in the increasingly global regulatory arena, engaging in science-based dialogue in support of the adoption of appropriate levels of regulation.
- Collecting, disseminating and maintaining statistics on the molybdenum market, excluding price and related information.
- Acting as a central repository of information about molybdenum, its properties, uses and products.

In addition IMOA's Annual General Meeting provides a secure forum for networking, exchanging views and ideas to the benefit of a wide cross section of the industry – producers, converters, traders, intermediate producers and users – within the bounds of international competition law.

Tim Outerridge
IMOA Secretary-General

Companhia Brasileira de Metalurgia e Mineração - CBMM

Brazilian company CBMM is the world's leading niobium supplier, with 40 years of investment and research in niobium technology and the application of the element across a wide spectrum of important end uses. The company's operations are fully integrated, from mine to final products, and its goals are not only to satisfy the worldwide niobium demand in the form of ferroalloys, oxides or pure metal, but also to provide a framework of technological development with the objective of identifying how the element can be employed to maximum effect to enable industry to overcome many of today's major worldwide technical challenges. Through this strategy, CBMM seeks to develop its business in a commercially sensitive manner growing wisely and in a sustainable way, thereby always being conscious of energy savings, cost reductions and environmental protection.

CBMM's niobium research and development program is conducted in a manner consistent with the objectives set out above. The company's mineral resources are unrivalled in quantity and quality but CBMM are constantly striving to improve the flexibility and efficiency of both their own operations and to enhance the value which more effective and efficient use of the element can deliver to its valued customers.

CBMM boasts a strong technical group for developing niobium applications, acting together with industries, universities, research institutes and end users. The company is currently involved in more than 60 research projects around the world and is continually identifying new research partners with whom collaboration can be mutually beneficial.

Traditionally, niobium is applied as a microalloying element to obtain higher strength in steels that are mainly used in the automotive industry, high-pressure gas transmission pipelines and a wide variety of important structural applications. Niobium is also used in stainless steel mostly for automotive exhaust lines, in nickel-based super-alloys for land–based and aircraft turbines as well as in heat resistant steels for power generation. Other special applications include superconducting alloys for nuclear magnetic resonance imaging, electronic ceramics and camera lenses.

CBMM's participation in this important high profile symposium, addressing the mutual benefits of niobium and molybdenum in high performance steel alloys is testimony to its declared strategy of aiming for constantly improving products through technical innovation.

Marcos Stuart
Technical Director
CBMM

Physical Metallurgy of Mo and Nb Alloyed Steels

Fundamentals and Applications of Mo and Nb Alloying in High Performance Steels – Volume 1
Edited by Hardy Mohrbacher
CBMM, IMOA and TMS, 2014

ON AUSTENITE CONDITIONING AND RECRYSTALLIZATION CONTROL OF HIGHER GRADE LINEPIPE STEELS (X100) WITH NIOBIUM AND MOLYBDENUM ADDITIONS

S.V. Subramanian[1] and Y. Yang[1, 2]

[1]McMaster University Department of Materials Science and Engineering,
Hamilton, Canada
[2]University of Science and Technology Beijing
Beijing, China

Keywords: Linepipe, X100, X120, Microstructure, Precipitation, EBSD, High Angle Boundaries, TEM, Segregation, Charpy Toughness, Niobium, Molybdenum, Grain Refinement, Phase Transformation, Atom Probe, HAZ, Recrystallization

Abstract

In higher strength linepipe steels (API Grade X100), research on structure-property correlation studies has underscored the importance of control of the density and dispersion of crystallographic high angle boundaries, which are effective as micro-crack arresters to suppress brittle fracture, in addition to morphological microstructure design to impart high strength and fracture toughness associated with resistance to ductile fracture. The control of density and dispersion of high angle boundaries, in turn, requires: (i) austenite grain refinement prior to pancaking, (ii) large strain accumulation by suppressing static recrystallization through strain-induced precipitation of NbC with adequate Zener drag force (NbC precipitate) and solute drag (Nb dissolved in matrix) in order to prevent boundary break away, and (iii) adequate hardenability to promote transformation at low temperature under accelerated cooling conditions to produce a lath structure with high angle boundaries by a displacive rather than a diffusive mechanism. The role of niobium microalloying on austenite conditioning and recrystallization control will be discussed in the light of quantitative modeling of strain induced precipitation of NbC and its interaction with recovery, and the effect of Zener and solute drag on boundary mobility and recrystallization. In order to promote transformation of pancaked austenite within a low temperature window, alloying with molybdenum is found to be effective, as molybdenum operates synergistically with solute niobium to promote transformation at a low temperature to give a fine lath structure having a high density of high angle boundaries. A combination of techniques involving EBSD, HRTEM and atom probe was used to characterize morphological structure, selection of crystallographic variants, nano-scale precipitates and solute dispersion in API Grade X100 containing niobium and molybdenum addition. The concept of hierarchical control on the evolution of microstructure with high density and dispersion of high angle boundaries will be discussed to achieve the target domain size in higher strength linepipe steels, with emphasis on Nb-Mo design in the base chemistry.

Background

Control of density and dispersion of high angle boundaries, which are super-imposed on the microstructural morphology, is the quintessential requirement for improving the fracture behavior of higher grade linepipe steels. Since high angle boundaries act as barriers to microcrack propagation, it should be possible in principle to control brittle fracture initiation if microcracks could be arrested by high angle boundaries before they could grow to attain the critical Griffith crack length to spread across the grains, in accordance with the Cottrell-Petch model for brittle fracture [1]. If the occurrence of cleavage planes with low fracture stress is coincident with the fracture path, it is to be expected that brittle fracture will be aided by such incidence of crystallographic orientation. Thus, it is essential to understand texture evolution when processing linepipe steels and its consequence on brittle fracture behavior of linepipes.

In an early work on the ductile to brittle transition temperature in a bainitic steel with high yield strength (700 MPa), Gladman and Pickering [2] showed that the Ductile Brittle Transition Temperature (DBTT) is raised by a coarse austenite grain size, but the mechanism was not clarified, see Figure 1. John Knott [3] suggested that grain boundaries of coarse austenite grains are invariably associated with coarse carbide particles, which could crack to nucleate brittle fracture that could grow to the Griffith crack length to spread across the grains. However, in low interstitial high strength linepipe steels, such coarse carbides are seldom observed. On the other hand, brittle fracture is promoted by a low density of high angle boundaries occurring in coarse austenite grains in the heat affected zone when using high heat input welding. These large austenite grains are associated with a large interspacing of high angle boundaries, which are too large to arrest growth of micro-cracks from a dislocation pile-up which consequently reaches the critical Griffith crack length to trigger brittle fracture in accordance with the Cottrell-Petch model for brittle fracture. This hypothesis underscores the importance of control of density and dispersion of high angle boundaries to suppress brittle fracture in the design and development of higher grade linepipe steels. Linepipe produced from thermo-mechanically processed microalloyed steels is prone to exhibiting unpredictable failure, characterized by transition from ductile to brittle fracture behavior in full scale burst testing of pipes. This is attributed to a high intensity of {100} <110> texture component according to a recent study on burst testing of linepipe [4]. The objective of the present work is to characterize the morphological and crystallographic features of higher grade linepipe steels in order to correlate morphological structure, crystallographic features (texture and boundary misorientations) with strength and fracture behavior of linepipe steel plate and the HAZ region. The control of density and dispersion of high angle boundaries in X100 based on high molybdenum-low niobium design will be examined in comparison with a recent cost-effective development of X100 based on low molybdenum-higher niobium multi-phase design.

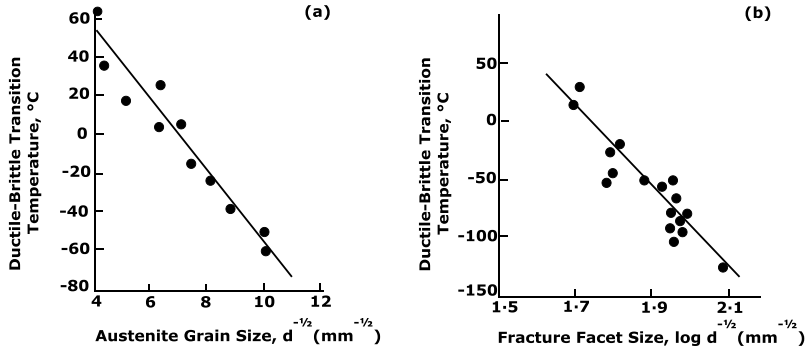

Figure 1. Effect of grain size on the ductile-brittle transition temperature in bainite-martensite structures; (a) effect of austenite grain size on a 700 MPa proof stress bainitic steel, (b) effect of fracture facet size in bainite-martensite structures, T. Gladman and F.B. Pickering [2].

Experimental

The experimental work consisted of EBSD characterization of linepipe steels to generate a comprehensive data-base on the density and dispersion of high angle boundaries of steel samples thermo-mechanically processed under laboratory and industrial rolling conditions. The data-base comprises base chemistry, thermo-mechanical rolling parameters, pancaked austenite grain size as revealed by special metallographic etchants, EBSD characterization of density and dispersion of high angle boundaries in hot rolled plates and Gleeble samples subjected to thermal simulation of temperature cycles characteristic of HAZ region of welded plates, intensity of {100} <110> texture from EBSD, and physical properties relating to strength and fracture behavior.

Results

EBSD Investigations on Bench-marked Higher Grade Linepipe Steels

Figure 2 shows a typical optical microstructure of pancaked austenite as revealed by metallographic etching of laboratory rolled and quenched HTP (High Temperature Processing) steel sample-B2. Figure 3 shows a band contrast map from EBSD of the corresponding region of the pancaked austenite grain. The variation in the density of high angle boundaries is mapped as a function of distance using line scans at any specific location in the pancaked austenite grain. The line scan closer to the pancaked austenite grain boundary is compared with two other locations in the interior of the austenite grain in Figure 3. It should be noted that only high angle boundaries above 35º are found to be effective in arresting cracks. The density (number count) of high angle boundaries with misorientations greater than 45º is high at the austenite grain boundary. The density of high angle boundaries decreases in the interior of the austenite grain. Thus in the middle of a large pancaked austenite grain, the interspacing of high angle boundaries is too large to arrest the growth of a micro-crack before it could reach the critical Griffith crack length for initiating brittle fracture. The crystallographic high angle boundaries associated with

microstructural constituents determine the domain size, which acts as the effective grain size of this complex optical microstructure in the Hall-Petch equation used to predict impact transition temperature. Table I summarizes sample identification, controlled rolling and accelerated cooling parameters, fracture behavior in DWTT (Drop-Weight Tear Test), impact toughness at -20 ºC, intensity of {100} <110> texture component, and interspacing of high angle boundaries. Figure 4 is a plot of variation in the dispersion of average interspacing of high angle boundaries in the vicinity of austenite grain boundaries compared to the middle region of the austenite grain in different steel samples examined in this investigation.

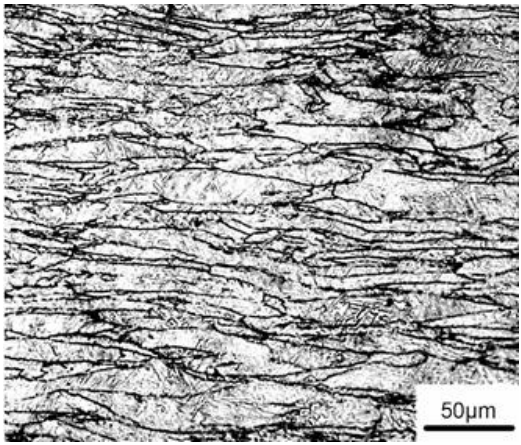

Figure 2. Optical microstructure of pancaked austenite grains in HTP steel sample-B2.

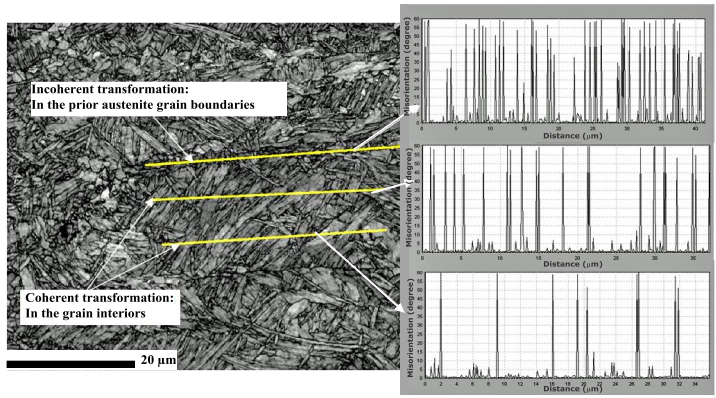

Figure 3. Band contrast map of sample-B2 plotting degree of misorientation along each line scan within a grain.

Table I. Compilation of Processing Parameters, Physical Properties, Texture, Prior Austenite Grain Size and Interspacing of High Angle Boundaries for Higher Niobium HTP (0.04%C, 0.095%Nb) Steels in Comparison with High Molybdenum-Nb-V Steels

Sample ID		Process			DWTT (SA%)	Average impact toughness at -20 ºC (J)	{100}<011> Texture component (deviation = 20°)	Prior austenite grain size (microns)	Interspacing of high angle boundaries (>15 degree) (microns)
		Deformation below Tnr	Temp. of last pass (ºC)	Cooling rate (ºC/s)					
HTP	B1	61.7%	940	≥30		-	2.59%	<25	1.91
	B2	61.7%	850	≥30		-	4.22%	<25	1.31
	B3	61.7%	800	≥30		-	1.85%	<20	1.65
	X90	62~67%	880~ 860	15~18	97% (-15 ºC)	370	2.7%	<25	3
	W20	0		32		278	4.17%	<30	4.1
	W50	0		5.1		64	5.84%	>45	11.2
C (X100)		69%	790	35	95% (-15 ºC)	174	2.44%	<25	2.10
Large strain C1		80%	790	35		250	0.892%	<25	1.55
B (X120) with boron		69%	790	34	100% (-15 ºC)	178	0.205%	<25	1.30

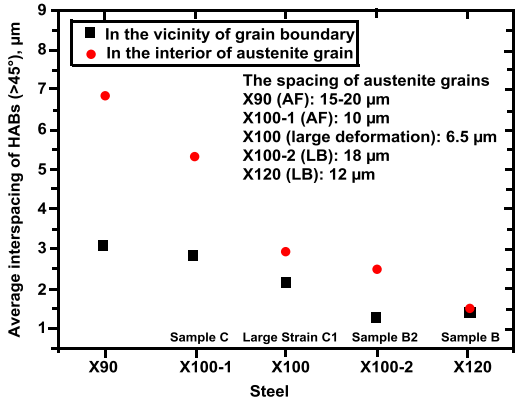

Figure 4. Average interspacing of high angle boundaries near the grain boundary and in the middle of pancaked austenite grains observed in different grades of linepipe steels.

Salient points from EBSD studies on base plates are summarized below:

(i) The density and dispersion of high angle boundaries obtained in HTP sample B3, subjected to high cooling rate under laboratory conditions, are comparable to those obtained in high molybdenum, high vanadium low niobium sample C (X100). Recent industrial trials on HTP have confirmed the feasibility of producing X100 based on HTP chemistry by using large strain accumulation and a high cooling rate in excess of 25 ºC/s.

(ii) The effect of large strain accumulation combined with accelerated cooling is clearly to promote a high density of high angle boundaries as shown by mill rolled X90 based on HTP chemistry.

(iii) The effect of increasing strain accumulation by increasing the total reduction below the no-recrystallization temperature, Tnr, from 69 to 80% in high Mo-Nb-V microalloyed steel of X100 grade is to increase the density of high angle boundaries and decrease the interspacing of high angle boundaries from 2.10 to 1.55 µm.

(iv) The effect of boron addition to X100 is to promote X120 grade with a further increase in the density and uniformity of dispersion of higher angle boundaries. The structure exhibits a very low intensity of {100} <110> texture and a domain size of less than 2 µm. More importantly, the structure exhibits a remarkable uniformity of dispersion of high angle boundaries and is associated with minimal variation in the interspacing of high angle boundaries from the grain boundary to the interior of austenite grain as shown in the plot in Figure 4.

(v) In the absence of strain accumulation by prior deformation, the effect of a moderately low cooling rate (5 ºC/s), characteristic of high heat input welding at 50 kJ/cm, “W-50”, is to promote a microstructure of granular bainite, which exhibits predominantly low angle misorientations (<10º). At a relatively high cooling rate (25 ºC/s) corresponding to cooling schedules for low heat input welding of 20 kJ/cm, W-20, the microstructure is

lower bainite with a well delineated lath structure, which exhibits high angle misorientations (> 45º). The loss of toughness in higher heat input welding correlates with the loss of high angle boundaries in the HAZ region of HTP in W-50.

(vi) A low intensity of (100) <110> texture component is found to correlate well with a high density and uniform dispersion of high angle boundaries. The upstream refinement of austenite grains in X120 is remarkably good in producing pancaked austenite grains of less than 10 μm thickness. High density and uniformity of dispersion of high angle boundaries causes the domain size to be less than 2 μm in X120. The structure is coupled with low intensity {100} <110> texture. Thus, the structure of X120 is identified as a target structure to aim for in order to control brittle fracture in higher grade linepipe steels.

Control of Density and Dispersion of High Angle Boundaries

The functional role of niobium microalloying in API Grade X80 linepipe may be summarized as follows:

(i) Strain induced precipitates of niobium carbo-nitride are used to pin austenite grain boundaries during thermo-mechanical rolling, which prevents recrystallization of austenite (by Zener drag).
(ii) Niobium solute retards boundary mobility through solute drag and hence retards recrystallization. (Retardation of recrystallization of austenite by solute drag).
(iii) Niobium retained in solid solution at the completion of finish rolling will aid in the formation of acicular ferrite upon accelerated cooling (Transformation hardening due to solute niobium in austenite).
(iv) Upon transformation and holding at coiling temperature, the ferrite matrix is supersaturated with niobium and carbon that will result in fine precipitation of NbC in ferrite, which will contribute some additional strength by the precipitate hardening mechanism.

In higher grade linepipe steels such as X100 and X120, it has become essential to suppress competition from brittle fracture in niobium microalloyed steels. This warrants control of a high density and good dispersion of high angle boundaries, which, in turn, requires (i) austenite grain refinement prior to pancaking, (ii) large strain accumulation, by suppressing static recrystallization through strain-induced precipitation of NbC with adequate Zener drag force and solute drag due to niobium dissolved in the matrix in order to prevent boundary break away, and (iii) adequate hardenability, to promote transformation at low temperature under accelerated cooling conditions to produce lath structures with high angle boundaries by a displacive rather than a diffusion mechanism. These are examined in further detail below in three separate modules.

Module-1 Austenite Grain Refinement Prior to Pancaking. Grain refinement of austenite in upstream processing of HTP: Since a large interspacing of high angle boundaries associated with coarse austenite grains raises the DBTT, grain refinement of austenite before pancaking is an essential step to lower the DBTT well below the operating temperature of linepipes. Three potential strategies for grain refinement of austenite upstream are: (i) grain refinement by static or dynamic recrystallization, (ii) prevention of grain coarsening of austenite grains by upstream

precipitation of duplex precipitates of TiN and NbCN, and (iii) control of recrystallization nucleation kinetics by prior deformation.

Significant grain coarsening of austenite will occur in the high temperature window up-stream because of the thermodynamic driving force for reduction of surface energy by coarsening of austenite grains due to a capillarity effect, and high diffusion kinetics at elevated temperature. Grain coarsening of austenite can be counteracted by Zener pinning of boundaries by second phase particles. Recent work on X100 and X120 has confirmed that if a good dispersion of TiN particles is engineered in austenite, epitaxial growth of NbC will occur on pre-existing TiN particles, obviating the large undercooling associated with strain induced precipitation in upstream processing. These particles are found to be very effective in retarding the grain coarsening of austenite.

Analysis of an extensive data-base of DWTT results has underscored the importance of austenite grain refinement prior to pancaking. The laboratory research has led to the development of optimized high temperature processing (OHTP) of higher niobium steel for refining austenite grain size before pancaking. By imparting a deformation of 25% pass reduction at 1000 ºC to a sample of HTP base chemistry with an initial average austenite grain size of 80 µm (from a prior deformation at 1070 ºC), it is shown that recrystallized austenite grains are formed within seconds but these refined austenite grains do not coarsen significantly for up to 240 seconds of holding time [5]. It is further shown that niobium carbide precipitates are effective in stopping recrystallization fully for pancaking of austenite only below about 900 ºC, and therefore there is significant potential for partial recrystallization in between these temperatures, particularly 960-920 ºC. This can be safely avoided without grain coarsening of austenite by carrying out the last pass of roughing at 1000 ºC and rapidly cooling within a short time to the start of finish rolling close to 900 ºC. This is the metallurgical basis for austenite conditioning of higher niobium low molybdenum steel, particularly in modern mills with large capacity (10,000 tons) and the high productivity environment of thermo-mechanical rolling of heavy gauge (27 mm thick) and very wide (5000 mm) X80 plates using the higher niobium, low interstitial, HTP steel design.

Module-2 Strain Accumulation in Pancaked Austenite Grains During Controlled Rolling. Physically based models are developed to analyze quantitatively time-evolution of strain induced precipitation of NbC during thermo-mechanical rolling for single pass deformation following the approach of Dutta and Sellars [6] and its interaction with recovery and recrystallization explicitly following the approach of Zurob et al. [7]. NbC precipitates nucleating on dislocations pin the dislocations impeding the recovery process. The effect of molybdenum is to delay the onset of strain induced precipitation, which allows recovery to precede strain induced precipitation, thereby lowering the driving force for recrystallization. Zurob's work has clarified that while strain induced precipitation occurs within a second or with a slight delay of 4-6 seconds with high Mn or Mo addition, the pinning of austenite boundaries takes a much longer time, involving tens of seconds for precipitates to grow adequately to exert the required Zener pinning force on boundaries to stop recrystallization. The model considers the time evolution of driving force for recrystallization, as influenced by Zener drag due to strain induced precipitates of NbC, and solute drag due to niobium dissolved in the matrix. The model for single pass deformation is the building block for multi-pass rolling. However, the phenomenology is rendered complex by

continuous fresh nucleation of precipitates on new dislocations during multi-pass rolling. More basic science work is in progress to capture recrystallization nucleation kinetics and growth in multi-pass rolling.

Stress relaxation has turned out to be a powerful technique for investigation of time evolution of strain induced precipitation and its interaction with recovery and recrystallization [8]. Previous work on stress relaxation studies in high niobium-high manganese steel by Banks et al. has shown that pinning of dislocations by nucleation of strain induced precipitates on dislocations impedes recovery at short times [9]. This has to be distinguished from Zener pinning of grain boundaries which occurs at much longer times, retarding recrystallization. Since the stored energy from dislocation density is the driving force for both recovery and recrystallization, physically based modeling is a valuable tool to interpret the results from coupling of recovery and recrystallization. The optimum design of base chemistry and rolling schedule is to control the strain induced precipitation kinetics to maximize the pinning force, while ensuring adequate solute niobium to prevent the boundary from breaking away from its solute atmosphere during finish rolling of niobium microalloyed steels [10].

Module-3 Transformation Control. Austenite with (i) large strain accumulation and (ii) adequate solute niobium, should be transformed under (iii) accelerated cooling conditions, to produce bainitic ferrite microstructures at low transformation temperatures in order to obtain a target domain size of about 2 μm to meet X100 requirements. The scale of the bainitic microstructure decreases as the driving force for transformation and the strength of austenite are increased. One way of simultaneously increasing the driving force and the austenite strength is to reduce the transformation temperature as demonstrated by Bhadeshia and Singh [11]. In order to promote coherent transformation of pancaked austenite in a low temperature window, alloying with molybdenum and niobium is found to be effective. Molybdenum operates synergistically with solute niobium to promote transformation at low temperature to give a fine lath structure with a high density of high angle boundaries. The effect of molybdenum addition to niobium bearing higher strength linepipe grade steels on structure and properties is investigated by comparing high molybdenum-low niobium with higher niobium-low molybdenum alloy design.

Investigations of Structure and Properties of Nb-Mo Bearing Higher Grade Linepipe Steels

Table II shows the composition of high molybdenum, low niobium high V steel with and without boron addition. The base chemistry of the higher niobium low molybdenum multi-phase X100 steel is also included in Table II. The physical properties of the three steels are summarized in Table III.

Table II. Base Chemistry of Low Niobium (0.04%) - High Molybdenum (0.4%) Steels with and without Boron and Higher Niobium (0.08%) - Low Molybdenum (0.26%) Steel

Steel	C (wt%)	Mn (wt%)	B (ppm)	Nb (wt%)	V (wt%)	Mo (wt%)	N (ppm)	Remarks
Steel B Mo-Nb-V-B	0.041	1.6~1.7	8	0.038	0.069	0.4	47	X120
Steel C Mo-Nb-V	0.065	1.67	1	0.047	0.07	0.4	59	X100
Multi-phase 0.08 Nb-0.25 Mo	0.07	1.75	-	0.081	-	0.26	≤ 40	X100 Multi-phase

Table III. Physical Properties of Low Niobium-High Molybdenum with and without Boron Compared to Higher Niobium-Low Molybdenum Multiphase Steel

Grade	R_m (MPa)	$R_{t0.5}$ (MPa)	Elongation A%	Avg. Charpy energy (J) at test temperature		Shear avg (%)
Steel B (X120) Mo-Nb-V-B [Nb 0.038, Mo 0.4, B 0.008]	907	810.6	16.75	-5 °C	241	100
				-15 °C	178	100
Steel C (X100) Mo-Nb-V [Nb 0.047, Mo 0.4]	792.9	690.6	19.5	-5 °C	249	100
				-15 °C	174	95
Multi phase (X100) Nb 0.081, Mo 0.26	909	708	(UEL 8) A-30	-20 °C	233	100

Previous work by Serin et al. [12] on nucleation kinetics of ferrite has shown that niobium is effective in inhibiting ferrite nucleation on austenite boundaries. The incubation time for ferrite nucleation is increased by a factor of 10 by niobium addition in C-Mn steel, which is comparable to that of boron. Niobium is also reported to decrease growth kinetics of ferrite by a factor of four compared to a reference C-Mn steel, which is attributed to interphase precipitation. Zhao et al. [13] have investigated the transformation characteristics of Mo-Nb-Cu-B low carbon steel under isothermal and continuous cooling conditions; molybdenum and niobium are shown to retard ferrite nucleation. The concept of hierarchical evolution of microstructure is used to promote multi-phase microstructures, comprising acicular ferrite at austenite grain boundaries by interrupted holding, and bainitic ferrite sheaves in the residual austenite matrix by quenching, in order to achieve adequate strength and toughness.

In the present investigation, in the absence of boron, a large reduction below Tnr (>70%) is required to ensure adequate strain accumulation to achieve X100 grade. Excellent strength with high density and dispersion of high angle boundaries are achieved with boron addition. The microstructure exhibits well pancaked austenite grains of uniform thickness of about 10 μm. High angle boundaries occur between bainitic ferrite laths, which nucleate from austenite grain boundaries and extend to the middle of the austenite grains. Pole figure analysis has confirmed that high angle boundaries are formed between crystallographic units belonging to different Bain groups within each packet. The target structure for high toughness is characterized by well distributed packets within an austenite grain, and more importantly a large number of crystallographic units belonging to different Bain groups occurring within each packet, configured such that adjacent crystallographic units belong to different Bain groups. There is an optimum temperature window of transformation corresponding to an optimum cooling rate in which a large number of crystallographic units belonging to different Bain groups is obtained to give a high density of high angle boundaries. Hara et al. have shown the pronounced effect of niobium and molybdenum addition on lowering transformation temperature of low carbon bainitic steel containing boron [14]. At a cooling rate of 30 ºC/s, the transformation temperature of boron containing steels is lowered by 50 ºC with 0.04% niobium, and by 60 ºC with 0.4% molybdenum addition respectively. Mohrbacher has provided a comprehensive review of the hardenability effect of molybdenum and niobium alloying in plate steels [15]. The refinement of austenite grain size prior to pancaking, a large reduction (>70%) below Tnr to promote a large Sv factor (grain boundary area per unit volume) in pancaked austenite with large strain accumulation and high cooling rates are demonstrated to be important processing parameters in low niobium-high molybdenum-high vanadium steels to achieve X100 properties.

High Resolution TEM Characterization of Micro–chemistry of Nano-scale Ti-Nb Precipitates in High Molybdenum – Low Niobium – High Vanadium Microalloyed X100 Steels

Ti-Nb microalloyed linepipe steels are designed for titanium rich nitride precipitation at elevated temperature. These precipitates are thermodynamically stable to pin austenite boundaries during high temperature excursions associated with high heat input welding in order to prevent austenite grain coarsening. Strain induced niobium rich carbide precipitates occur at relatively large undercooling (>100 °C) during thermo-mechanical rolling, inhibiting recovery and recrystallization, thereby aiding strain accumulation [16]. If NbC grows epitaxially on pre-existing TiN particles, it will obviate the need for strain induced precipitation at large undercoolings. NbC will start growing at elevated temperature once the thermodynamic potential for precipitation occurs at the phase boundary. High resolution TEM has confirmed that in both X100 without boron addition and X120 with boron addition, a good dispersion of precipitates occurs. NbC grows on two opposite faces of cubic TiN precipitates exhibiting a dumb-bell appearance, as shown in Figure 5. The number density of the dumb-bell precipitates increases with boron addition. This finding is new and significant, as this can be used to advantage in austenite grain refinement prior to pancaking. These TiNb(CN) precipitates will retard the kinetics of grain coarsening of austenite in the HAZ region during high heat input welding.

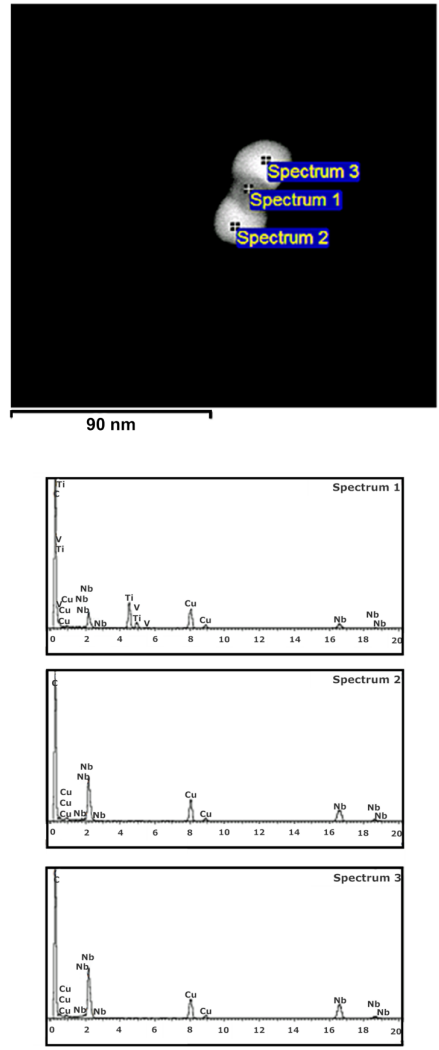

Figure 5. Ti-Nb nano-scale precipitate from X100 linepipe steel extracted by carbon replica. The middle spectrum shows a titanium rich phase. The top and bottom spectra show niobium rich phases attached to the two opposite faces of the cubic TiN.

Atom Probe Results in High Molybdenum - Low Niobium - High Vanadium Microalloyed X100 Steel

In higher grade linepipe steel, strain accumulated pancaked austenite is rapidly cooled at 35 ºC/s and the transformation occurs at a low temperature giving the lath structure. Under these conditions, it is believed that para-equilibrium holds with only carbon partitioning; by contrast, substitutional solutes like niobium do not partition as their diffusion coefficient is orders of magnitude lower than that of an interstitial solute like carbon. The residual austenite will be enriched in carbon, which could transform to hard and embrittling martensite, and the resulting hard MA product could initiate a microcrack. This phenomenon occurs in the heat affected zone, which promotes brittle fracture in the absence of crack arresters in the form of high angle boundaries. Atom probe examination has confirmed the occurrence of segregation of carbon at grain boundaries, but there is no segregation of substitutional solute, including niobium, at the grain boundaries. Atom probe analysis has also confirmed that niobium is evenly distributed in the matrix and there is no clustering of niobium. Figure 6 shows a map of carbon atoms as well as concentration profiles of solutes; both show significant segregation of carbon at the grain boundary. Figure 7 shows that the niobium distribution in the matrix is even. There is no evidence of niobium clusters in the matrix of the X100 linepipe that was examined [17].

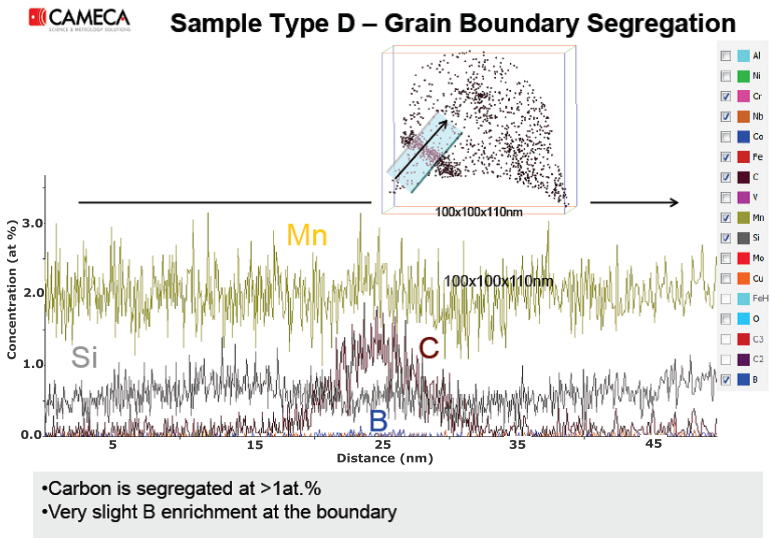

Figure 6. Atom map of carbon atoms (top) and concentration profiles of C, B, Si and Mn (bottom). Significant segregation of carbon was noted at the grain boundary.

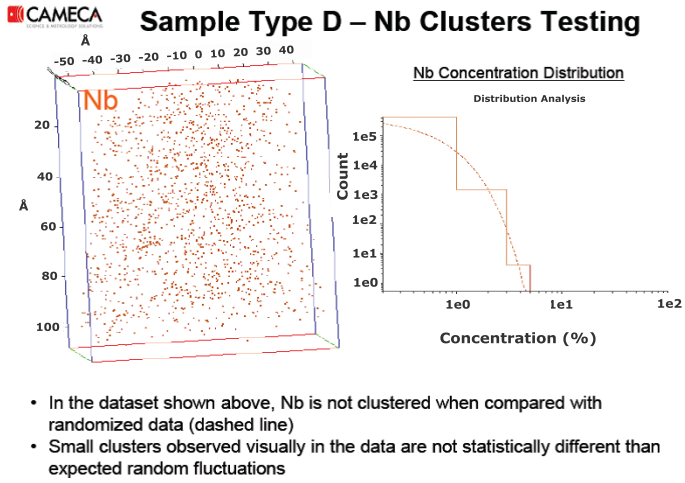

Figure 7. Niobium atom distribution with no clustering of niobium in the matrix.

Development of X100 Based on Higher Niobium - Low Molybdenum Multi-phase Processing

The recent development of multi-phase X100 is a cost effective alloy design based on higher niobium - low molybdenum, which holds considerable promise. The approach is based on the concept of hierarchical evolution of microstructure by coherent transformation. The strategy is to adopt a two step processing: the first one is to interrupt and hold at the required temperature to promote an adequate amount of "ferrite" at austenite grain boundaries and the second process step is to quench and promote coherent transformation of austenite enriched in carbon to obtain bainitic ferrite. Figure 8 shows a typical microstructure of X100 from multi-phase processing of the higher niobium-low molybdenum chemistry.

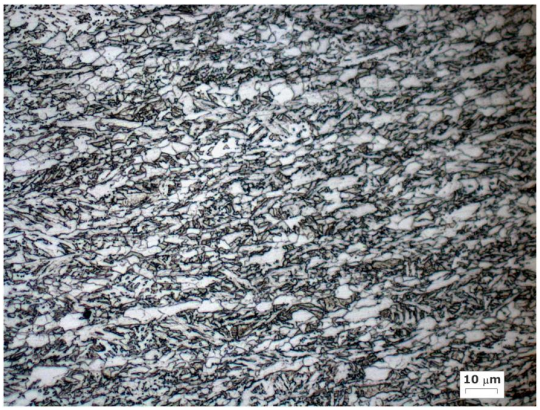

Figure 8. Optical microstructure of multi-phase X100 based on low molybdenum (0.275%) higher niobium (0.08%).

Control of Density and Dispersion of High Angle Boundaries to Suppress Brittle Fracture in Single Pass HAZ of Multi-phase X100

The effect of heat input in single pass welding HAZ simulation on the toughness of the HAZ in higher niobium-low molybdenum multi-phase X100 was investigated. This provides a window of opportunity to study the hierarchical evolution of high angle boundaries as a function of cooling rate on a fixed, higher niobium-low molybdenum chemistry in coherent transformation of austenite without interference from dislocations due to deformation. Figure 9 shows Charpy impact toughness plotted as a function of heat input, SEM pictures of corresponding fracture surfaces, and a schematic diagram of different Bain groups from pole figure analysis, which are color coded. High angle boundaries occur between crystallographic units belonging to different Bain groups, which can be distinguished by interfaces of adjoining regions of two different colors. The one sample that exhibited ductile fracture showed a high density and dispersion of high angle boundaries, which occur within each packet, in addition to high angle boundaries occurring between the two adjoining packets within an austenite grain.

High angle boundaries within the packet are shown to occur between crystallographic units belonging to different Bain groups, whereas low angle boundaries occur between crystallographic units belonging to the same Bain group. Therefore, the target structure for a high density of high angle boundaries is identified as one where a high number density of crystallographic units belonging to different Bain groups occur within each packet and, more importantly, where the crystallographic units are arranged to maximize the interface between different Bain groups. Since bainitic ferrite laths belonging to different Bain groups nucleate on austenite grain boundaries, it is surmised that austenite grain size control is the key to promote a high density of high angle boundaries to suppress brittle fracture. This concept is also validated in X120 with a domain size of less than 2 μm. In this case, the pancaked austenite size is of

5-10 μm thickness, and high angle boundaries occur between bainitic ferrite nucleating from austenite grain boundaries and propagating to the middle of the pancaked austenite grains.

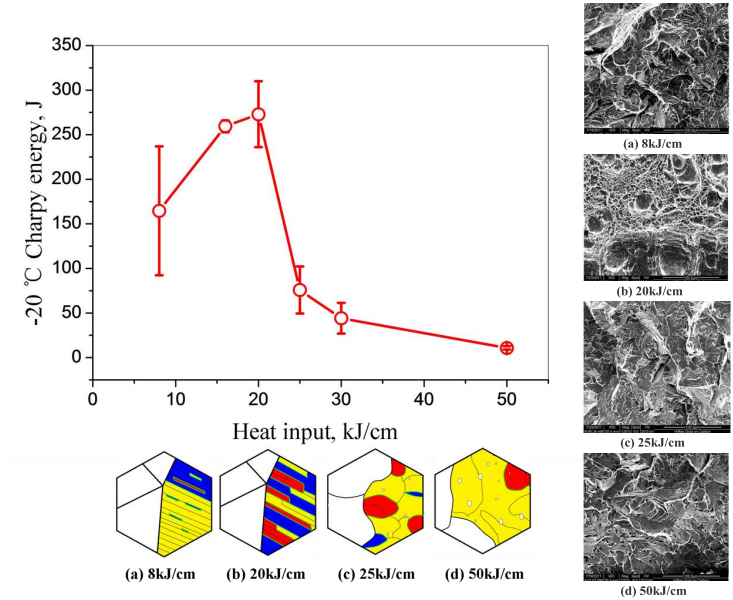

Figure 9. Charpy toughness at -20 °C plotted against heat input; SEM fracture surface, and schematic of Bain groups occurring within a packet of austenite grain obtained for each of the four heat inputs examined. High angle boundaries occur between two distinctly different Bain groups as revealed by different color [18].

Conclusions

1. High density and good dispersion of high angle boundaries are essential to suppress brittle fracture.

2. High angle boundaries are shown to form in the target structure between crystallographic units belonging to different Bain Groups occurring within each packet in an austenite grain, in addition to those formed between packets.

3. The control of density and dispersion of high angle boundaries in plate rolling requires: (i) austenite grain refinement prior to pancaking, (ii) large strain accumulation by large reduction below the temperature of no recrystallization Tnr, and (iii) adequate hardenability to promote transformation at low temperature under accelerated cooling conditions to produce a lath structure with high angle boundaries by the displacive rather than diffusive mechanism.

4. X100 based on high molybdenum-low niobium design: A high density of high angle boundaries can be obtained by increasing the hardenability of the base chemistry in X100. This can be achieved with a high molybdenum addition (0.4 wt%) to traditionally alloyed medium niobium (0.045 wt%) and 0.08%V steel. The steel is designed for thermo-mechanical rolling and accelerated cooling in a conventional mill.

5. However, newer X100 alloy and processing designs have emerged based on a higher niobium-low molybdenum multi-phase concept: X100 with a minimum of 6% uniform elongation to meet strain-based design is based on higher niobium (0.08%) and low molybdenum contents. Two step processing is used involving interrupted holding to promote ferrite at prior austenite grain boundaries and quenching the residual austenite to produce bainitic ferrite so as to produce a dual phase structure. This steel composition is the lowest cost design which exploits the advanced processing capabilities of a modern mill.

Acknowledgements

The authors wish to thank Dr. Gianluigi Botton, Dr. Glynis de Silveira and Dr. Carmen Andrei for help with high resolution TEM, and Mr. Chris Butcher, BIMR for help with ESBD. The funding support by CBMM, Brazil is gratefully acknowledged.

The authors wish to thank (i) Chinese Government for the award of scholarships to You Yang to do research at McMaster University, (ii) Dr. Laurie Collins of Evraz Inc NA, Regina, Canada for research support, (iii) Sha Steel for supply of steels and technical support and (iv) Dr. Chengjia Shang, USTB, China for collaborative research.

References

1. Alan Cottrell, "Brittle Fracture From Pile-ups in Polycrystalline Iron," *Yield, Flow and Fracture of Polycrystals*, ed. T.N. Baker (Applied Science Publishers, 1983), 123-129.

2. T. Gladman and F.B. Pickering, "Effect of Grain Size on the Mechanical Properties of Ferrous Materials," *Yield, Flow and Fracture of Polycrystals*, ed. T.N. Baker, (Applied Science Publishers, 1983), 141-198.

3. J.F. Knott, "Cleavage Fracture and the Toughness of Structural Steels," *Yield, Flow and Fracture of Polycrystals*, ed. T.N. Baker, (Applied Science Publishers), 81-99.

4. I. Psyhmintsey et al., "Effect of Microstructure and Texture on Shear Fracture in X80 Line Pipe Designed for 11.8 MPa Gas Pressure" (Paper presented at the Ostend Conference, November, 2009).

5. C.L. Miao et al., "Recrystallization and Strain Accumulation Behavior of High Niobium-bearing Linepipe Steel in Plate and Strip Rolling," *Materials Science and Engineering A*, 527 (2010), 4985-4992.

6. B. Dutta, E.J. Palmiere, and C.M. Sellars, "Modelling the Kinetics of Strain Induced Precipitation in Nb Microalloyed Steels," *Acta Materialia*, 49 (2001), 785.

7. H.S. Zurob et al., "Modeling Recrystallization of Microalloyed Austenite: Effect of Coupling Recovery, Precipitation and Recrystallization," *Acta Materialia*, 50 (2002), 3075.

8. C.L. Miao et al., "Refinement of Prior Austenite Grain in Advanced Pipeline Steel," *Frontiers Materials Science China*, 4 (2010), 197-201.

9. K.M. Banks et al., "High Temperature Processing and Accelerated Cooling of X65 Line Pipe Steel on a 4000T Plate Mill" (Paper presented in the Proceedings of the International Conference on Microalloying, Pittsburgh, June 2007).

10. H. Zurob et al., "Analysis of the Effect of Mn on the Recrystallization Kinetics of High Nb Steel: An Example of Physically Based Model," *The Iron and Steel Institute of Japan International*, 45 (5) (2005), 713-722.

11. S.B. Singh and H.K.D.H. Bhadeshia, "Estimation of Bainite Plate-thickness in Low-alloy Steels," *Materials Science and Engineering* A, 245 (1) (1998), 72-79.

12. B. Sarin et al., *Memoires Scientifiques de la Revue de Metallurgie*, June, 5, (1978), 355-369.

13. Y.T. Zhao et al., "The Metastable Austenite Transformation in Mo-Nb-Cu-B Low Carbon Steel," *Materials Science and Engineering A*, 433 (2006), 169-174.

14. T. Hara et al., “Role of Combined Addition of Niobium and Boron and of Molybdenum and Boron on Hardenability in Low Carbon Steels,” *Iron and Steel Institute of Japan International*, 44 (8) (2004), 1431-1440.

15. H. Mohrbacher, “Mo and Nb Alloying in Plate Steels for High Performance Applications” (Paper presented at the Proceedings of the International Symposium on the Recent Developments in Plate Mill, AIST, Winter Park, Colorado 19-22 June 2011).

16. E.J. Palmiere, C.M. Sellars, and S.V. Subramanian, “Modeling of Thermomechanical Rolling” (Paper presented at the International Symposium Niobium 2001, AIME-TMS, Orlando, U.S.A, December 2001), 501- 526.

17. S.V. Subramanian et al., “Characterization of Nano-scale Precipitates in Microalloyed Steel” (Paper presented at the Proceedings of the International Conference: Advances on Analytical Techniques and Characterization of Materials (ATCOM), Ranchi, India, 5-7 July, 2011).

18. S.V. Subramanian et al., “EBSD Characterization of HAZ from Single and Multi-pass Welding of Niobium Microalloyed Line Pipe Steels” (Paper presented at the Proceedings of the TMS-CBMM Seminar on Welding of Pipeline Steels, Araxa, 28-29 November, 2011).

Fundamentals and Applications of Mo and Nb Alloying in High Performance Steels – Volume 1
Edited by Hardy Mohrbacher
CBMM, IMOA and TMS, 2014

EFFECT OF NIOBIUM AND MOLYBDENUM ON PHASE TRANSFORMATIONS IN ADVANCED LOW-CARBON STEELS

M. Militzer, F. Fazeli and T. Jia

The Centre for Metallurgical Process Engineering,
The University of British Columbia,
Vancouver, BC, Canada V6T 1Z4

Keywords: X65, X80, Phase Transformation, Linepipe, Solute Drag, Niobium, Molybdenum, CCT, Thermal Simulation, Modelling, Kinetics

Abstract

Advanced high strength steels are frequently microalloyed with Nb and/or Mo. Both elements are known to have a tremendous effect on the austenite-ferrite transformation, which constitutes the key metallurgical tool to tailor the properties. The effects of Nb on the continuous cooling transformation behavior are quantified for two linepipe steels by separately controlling the austenite grain size and the content of Nb in solution. One of the investigated steels is an X80 grade that also contains Mo and the transformation studies are used to quantify the synergistic role of Nb and Mo. Bringing Nb into solution decreases the transformation temperature by up to 100 °C for accelerated cooling conditions. The experimental results are described in the framework of phenomenological models for the austenite-to-ferrite transformation. In particular the effect of Nb and Mo on the apparent austenite-ferrite interface mobility is analyzed.

Introduction

The use of Nb and Mo is a critical aspect for developing advanced low carbon high strength steels, e.g. for automotive and pipeline applications. Over the past 60 years Nb has increasingly been employed as a microalloying element to engineer state-of-the-art flat and bar products [1,2,3]. Adding Nb is particularly effective in refining ferrite microstructures but Nb may also act as a precipitation strengthener when fine Nb(CN) precipitates form. One of the striking features of Nb addition is the increase of the austenite recrystallization temperature and this is utilized in thermo-mechanical controlled processing [4,5,6]. Furthermore, Nb in solution promotes formation of acicular ferrite constituents and shifts austenite decomposition to lower temperatures [6,7,8]. The effect on phase transformation is very profound, such that only a few ppm of dissolved Nb changes the decomposition kinetics dramatically. The amount of dissolved Nb at the onset of the austenite decomposition may potentially differ from the nominal Nb content of the steel depending on the processing conditions. For example, in plate rolling some of the Nb may precipitate in austenite whereas this is less likely in strip rolling due to shorter processing times. Despite these important industrial implications and a significant body of research work including numerous experimental observations, the influence of Nb in solution on austenite decomposition has yet to be quantified unambiguously, [9,10,11]. In particular, the role of systematically varied Nb levels in solution needs to be quantified for a given steel chemistry to exclude potential additional effects on phase transformation when taking the more traditional approach of studying a number of steels with different Nb contents.

Mo is another element with a major effect on the austenite decomposition kinetics. There is a large body of work on the effect of Mo on the transformation kinetics showing that Mo delays the ferrite formation, can lead to incomplete transformation and, as a result, the separation of the ferrite and bainite portions in the overall transformation through the emergence of the bainite bay in the time-temperature-transformation diagrams with increasing Mo content [12,13]. Thus, adding Mo is a very efficient strategy to tailor the phase transformation such that under the constraints of an industrial processing line the desired multi-phase microstructure can be formed that is required to attain the property targets of the steel product [14]. Similar to Nb, Mo also delays the recrystallization in ferrite and austenite. Even though many steels contain both Nb and Mo, there is surprisingly little quantitative information on their combined effects on the austenite decomposition kinetics [15,16].

The present paper describes systematic studies to quantify the effect of Nb in solution on ferrite formation in two Nb microalloyed linepipe grades, one of which is also alloyed with Mo. A novel experimental methodology permits to vary the content of dissolved Nb in austenite while maintaining an invariant austenite grain size. Recording the subsequent decomposition kinetics of austenite enables quantification of the role of various Nb contents in solution. Based on the experimental observations, a solute drag parameter for Nb is incorporated into a model for the ferrite transformation-start temperature during continuous cooling. Further, the effect of Nb on the migration rate of the ferrite-austenite interface is analyzed in terms of an apparent interface mobility.

Materials and Experimental Methodology

The current study includes two commercial linepipe steel grades, i.e. an X65 and an X80 steel both microalloyed with Nb. The steel chemistries are shown in Table I. The X80 steel contains also Mo as an alloying addition. The *Ae3* temperatures of these two steels are 839 °C and 823 °C, respectively, as determined by Thermo-Calc using the Fe2000 data-base. From these materials two types of samples were machined for continuous cooling transformation (CCT) studies, i.e. tubular specimens with a wall thickness of 1 mm when no deformation step is included in the test procedures and, for tests with deformation, solid samples having a cylindrical working zone with a 6 mm diameter.

Table I. Chemical Composition of Investigated Steels (Key Elements in wt%)

Steel	C	Mn	Nb	Ti	Mo	N
X65	0.06	1.49	0.047	-	-	0.0094
X80	0.06	1.65	0.034	0.012	0.24	0.005

The CCT tests were conducted in a Gleeble 3500 thermo-mechanical simulator equipped with a dilatometer. To study the effect of Nb in solution on the phase transformation kinetics, austenitizing treatment schedules were developed that enabled independent variation of the austenite grain size and the amount of Nb in solution. For the X65 steel a thermo-mechanical treatment was employed that replicates key features of a hot rolling process, as shown in Figure 1. First, the samples were reheated at 1200 °C for 2 mins to bring all Nb into solution. This was followed by a deformation step in compression (true strain of 0.3) at 1050 °C to refine the austenite grain size through recrystallization. An average austenite grain size of 40 μm

resulted from this thermo-mechanical treatment. The deformation conditions at 1050 °C were selected to avoid re-precipitation of Nb. Then, the samples were cooled at 100 °C/s to 900 °C where they were held for selected times to obtain different levels of re-precipitation of Nb and, thus, different amounts of Nb in solution. Austenite grain growth during the holding at 900 °C is negligible. The amount of Nb in solution was estimated from a precipitation study by Park et al. [17], on a steel with a similar chemistry (0.08 wt%C, 1.21 wt%Mn, 0.038 wt%Nb, 0.0017 wt%N), i.e. 281 ppm at 0 min (all Nb in solution), 230 ppm at 2 mins and 44 ppm at 20 mins, respectively.

For the X80 steel, a similar re-precipitation step was conducted at 900 °C after having brought all Nb in solution but without a deformation step, i.e. employing thermal cycles that are similar to those in the weld heat affected zone (HAZ). For CCT studies with larger austenite grain sizes (here 26 μm) the samples were directly cooled from a suitable reheat condition (here 5 s at 1250 °C) to 900 °C, see Figure 2(a), whereas for smaller austenite grain sizes a two-step reheating procedure can be employed, see Figure 2(b). Here the sample is quenched from the solution temperature to room temperature and then quickly reheated to a selected temperature in austenite (e.g. 950 °C for a grain size of 5 μm) before conducting the precipitation heat treatment at 900 °C. Even though the Nb content in the X80 steel is similar to that in the steel studied by Park et al. [17], the precipitation kinetics are expected to be different due to the presence of Ti and Mo. In particular, the addition of Mo reduces the rate of Nb(CN) precipitation in austenite [18]. Thus, systematic age hardening studies were performed at 610 °C for samples that had been exposed to different holding times at 900 °C. The peak strength increment observed in these aging experiments was taken as a measure of the apparent volume fraction of Nb precipitated during aging. From this volume fraction one can estimate the amount of Nb that was in solution before aging, i.e. that had not been precipitated at 900 °C. From these studies it was concluded that the degree of re-precipitation of Nb was approximately 64% after 20 mins holding at 900 °C which is significantly less than in the X65 steel (93%). Then, the following Nb levels in solution were adopted for the X80 steel: 204 ppm for 0 mins and 73 ppm for 20 mins holding at 900 °C.

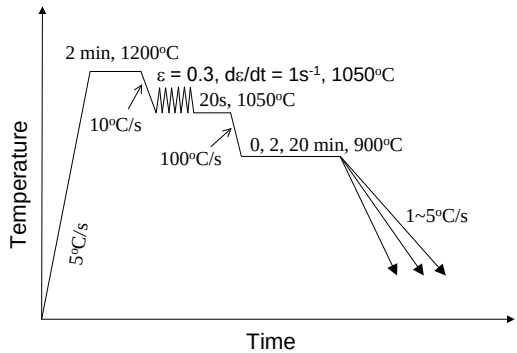

Figure 1. Thermo-mechanical processing path of CCT tests for X65 steel.

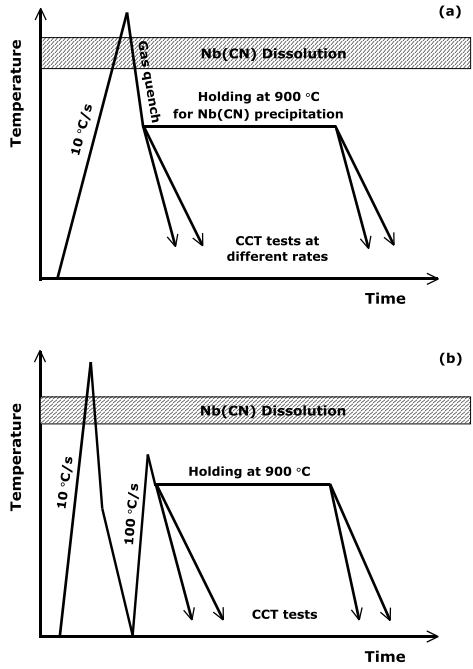

Figure 2. Processing paths for CCT tests in X80 steel; (a) large austenite grain size, (b) small austenite grain size.

Experimental Results

Effect of Nb on the Austenite-to-Ferrite Transformation

Figure 3 shows the austenite decomposition kinetics in the X65 steel as a function of temperature during cooling at 5 °C/s. Having more Nb in solution systematically lowers the transformation temperatures. Considering the cases of 20 min holding at 900 °C vs no holding, i.e. almost full re-precipitation of Nb vs all Nb in solution, shows a decrease of transformation temperatures of about 50 °C in the initial transformation stages of up to 50% transformed when bringing all Nb in solution. The microstructures obtained in these two CCT tests are shown in Figure 4. For the higher transformation temperature (i.e. Nb re-precipitated) a fine grained ferrite structure is observed with a mixture of polygonal and irregular grains; these ferrite structures are often termed as "acicular ferrite" even though the ferrite may not form on inclusions or large precipitates for which a truly acicular growth had first been observed. In the case of Nb in solution where the transformation is shifted to lower temperatures, the resulting microstructure is a clear mixture of polygonal ferrite that has formed at prior austenite grain boundaries and

bainitic ferrite inside the prior austenite grains. The ferrite fractions for the three cases shown in Figure 3 increase from 0.25 to 0.31 and 0.47 when reducing the Nb level in solution by increasing the holding time at 900 °C. These experimental observations provide further evidence that Nb in solution delays the ferrite formation thereby promoting a more bainitic microstructure for a given cooling condition in the investigated steel.

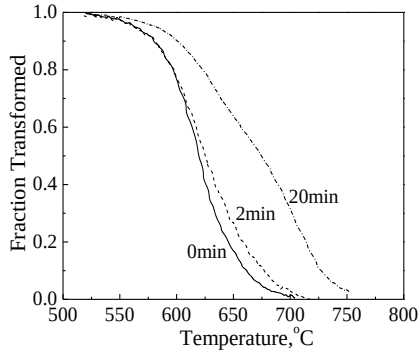

Figure 3. Effect of Nb in solution on the austenite decomposition kinetics in the X65 steel cooled at 5 °C/s.

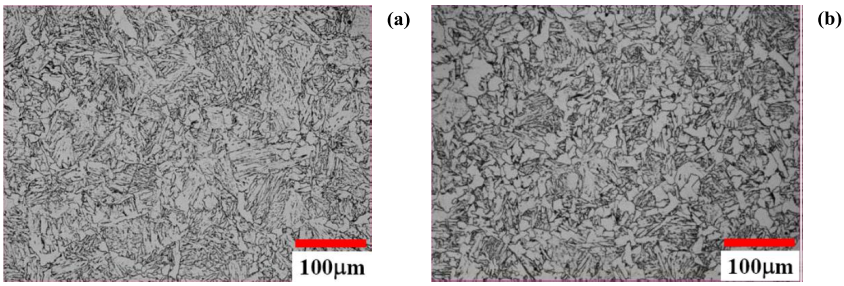

Figure 4. Microstructures in the X65 steel when cooled at 5 °C/s for (a) Nb in solution (no holding at 900 °C) and (b) Nb re-precipitated (20 min holding at 900 °C).

Effect of Nb and Mo on the Austenite-to-Ferrite Transformation

In the X80 steel a similar trend as in the X65 steel was observed for the effect of Nb in solution on the austenite decomposition kinetics. Increasing the amount of Nb in solution delays the transformation and lowers the transformation temperature. As illustrated in Figure 5, the transformation temperature can be lowered by approximately 100 °C for accelerated cooling conditions with a cooling rate of 30 °C/s and a prior austenite grain size of 5 μm. The resulting microstructures are shown in Figure 6. Lowering the transformation temperature leads to a transition from a fine-grained polygonal ferrite microstructure to a fine-grained but more irregular ferrite microstructure with an increased fraction of bainitic ferrite. In both cases randomly distributed fine martensite/austenite (M/A) islands are observed with an average size of approximately 1 μm.

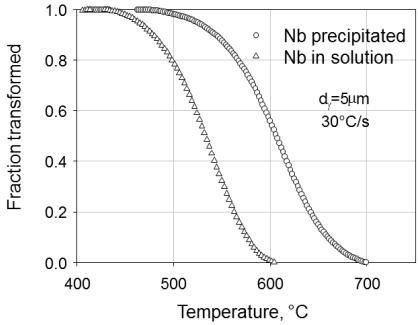

Figure 5. Effect of Nb in solution on the austenite decomposition kinetics in the X80 steel with a prior austenite grain size of 5 μm cooled at 30 °C/s.

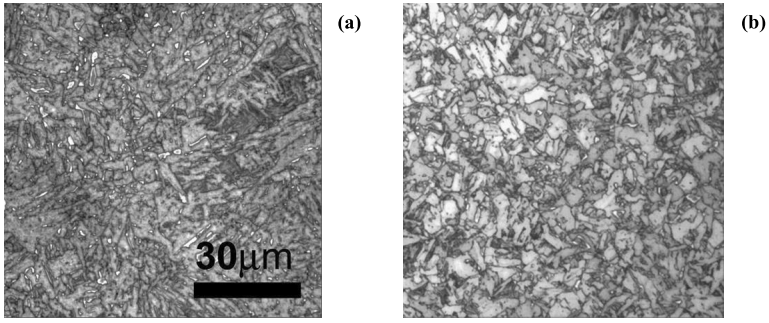

Figure 6. Microstructures in the X80 steel with a prior austenite grain size of 5 μm cooled at 30 °C/s for (a) Nb in solution (no holding at 900 °C) and (b) Nb re-precipitated (20 min holding at 900 °C).

The role of Nb may in detail be somewhat different than in the X65 steel since in the X80 steel Mo is also present in solution. Mo is known to similarly delay the ferrite formation. To evaluate potential synergistic effects of Nb and Mo on the kinetics of the austenite-to-ferrite transformation, additional systematic CCT tests were performed at a cooling rate of 1 °C/s using samples with a prior austenite grain size of 26 μm and different holding times at 900 °C. The measured kinetics of austenite decomposition, in terms of total fraction transformed versus temperature, is shown in Figure 7. It can be readily observed that the transformation shifts systematically to lower temperatures as the Nb content of austenite increases by decreasing the holding times at 900 °C from 20 to 6, 1 and 0 mins. Metallographic studies confirmed that polygonal ferrite constitutes more than 60% of the microstructure for all the examined cases.

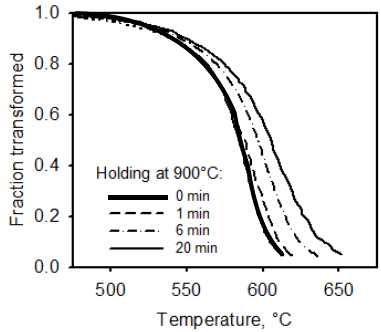

Figure 7. Effect of Nb in solution on the austenite decomposition kinetics in the X80 steel with a prior austenite grain size of 26 μm cooled at 1 °C/s.

Discussion

Transformation Start Model

The variation of Nb content in austenite due to Nb(CN) precipitation at 900 °C is too small to explain the observed effect on austenite decomposition in terms of the underlying thermodynamics, i.e. the driving pressure for transformation. Thus, Nb in solution is expected to affect kinetic factors, in particular the apparent mobility of the austenite-ferrite interface. For the delay in transformation-start also the effect of Nb on nucleation may be important, but a measurable transformation-start involves the early growth of ferrite grains. A ferrite-start model previously proposed for plain low carbon steels is being adopted here to analyze the role of Nb in the initial transformation stages [19]. The model considers early carbon diffusion controlled growth of ferrite grains nucleated at austenite grain corners at a temperature, T_N. The original model has been extended to include solute drag of Nb that slows down the growth rate of ferrite. The modified growth rate equation can be formulated as [20]:

$$\frac{dR_f}{dt} = D_C \frac{C^\gamma - C_o}{C^\gamma - C^\alpha} \frac{1}{R_f} \left(1 + \frac{D_C \alpha C_{Nb}}{R_f} \right)^{-1} \quad (1)$$

where R_f is the radius of the growing ferrite grain, D_C is the carbon diffusivity in austenite [21], C_o is the average carbon concentration, C^α and C^γ are the carbon equilibrium concentrations in ferrite and austenite, respectively, C_{Nb} denotes the concentration of Nb in solution and α is a constant related to the intensity of the solute-interface interaction. The carbon equilibrium concentrations are calculated with Thermo-Calc using the Fe2000 database and assuming ortho-equilibrium (i.e. full equilibrium for all alloying elements). Measurable transformation-start (i.e. 5% transformed) is assumed to be associated with nucleation site saturation at prior austenite grain boundary sites. Ferrite nucleation is presumed to cease once the carbon enrichment of the entire grain boundary area attains a critical level, C^*, i.e.:

$$R_f > \frac{1}{\sqrt{2}} \frac{C^* - C_o}{C^\gamma - C_o} d_\gamma \quad (2)$$

is the condition to calculate the transformation-start temperature, T_S. The three adjustable parameters, i.e. T_N, C^* and α, have been determined from the experimental ferrite transformation start temperatures as summarized in Table II. In this analysis, the parameter α that describes the role of Nb is similar in both steels that have comparable Nb levels. Also, the values for C^*/C_o fall in the same range for both steels but the apparent undercooling ($Ae3 - T_N$) for nucleation is much larger in the X80 steel, i.e. 123 °C vs 59 °C in the X65 steel. A possible reason for this difference may be that in the X65 steel Nb is the only microalloying element whereas the X80 steel also contains Mo and Ti. In particular, Mo delays the onset of ferrite transformation significantly.

Table II. Ferrite Transformation-start Parameters

Steel	T_N **(°C)**	C^*/C_o	α **(s/μm)/(at.ppm)**
X65	780	2.43	0.013
X80	700	$1.74 + 6.8\mu m/d_\gamma$	0.043

Apparent Austenite-Ferrite Interface Mobility

The overall kinetics of the formation of ferrite can be more rigorously analyzed to quantify the effect of Nb on the apparent austenite-ferrite interface mobility, M, for the investigated transformation scenarios. For this analysis, the formation of polygonal ferrite is considered. To this end, two main tasks have to be dealt with. Firstly, a suitable assumption for the growth geometry has to be established such that the interface velocity can be extracted from the measured transformation kinetics. Secondly, an appropriate kinetic model has to be adopted to interpret the interface velocity in terms of the interface mobility. As clearly seen in the micrograph shown in Figure 4(b), ferrite forms essentially as films along prior austenite grain boundaries and grows inwards to consume the austenite grain. A suitable geometry to describe this situation is a spherical austenite grain with an outer ferrite shell growing towards the grain interior [22]. This is relevant for cooling scenarios where nucleation site saturation occurs at

austenite grain boundaries and the overall kinetics is mainly controlled by subsequent thickening of the ferrite shell. The growth rate of ferrite in low carbon steels can be explained by a mixed-mode approach [22], in which the interface velocity, v_α, is related to the mobility term and the chemical driving pressure acting on the ferrite-austenite interface, $\Delta G_{\text{int}}^{\gamma\to\alpha}$, i.e.

$$v_\alpha = M\Delta G_{\text{int}}^{\gamma\to\alpha} \tag{3}$$

The driving pressure can be quantified based on the difference between the interfacial carbon concentration, C_{int}^{γ}, and the equilibrium carbon content of austenite, C_{eq}^{γ}, with respect to para-equilibrium. The assumed geometry and the carbon concentration profile during the transformation are illustrated schematically in Figure 8. The interfacial carbon concentration at the austenite side is *a priori* unknown in the mixed-mode growth scenario. It evolves with time and has to be determined by solving carbon flux equations across the interface and within the austenite. Numerical procedures have been proposed to self-consistently extract M and C_{int}^{γ} from this analysis [23,24].

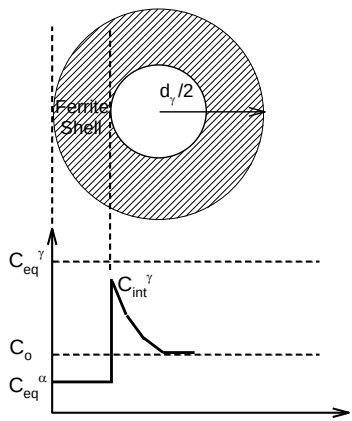

Figure 8. Schematic illustration of carbon profile within the domain consisting of a spherical austenite grain with an outer ferrite shell.

Figure 9 shows the apparent mobility in the X65 steel as a function of temperature for the ferrite portion of the CCT data shown in Figure 3. For a given temperature the apparent mobility decreases with increasing amount of Nb in solution. Interestingly, however, the apparent mobility decreases with increasing temperature. In the case with very little Nb remaining in solution it appears that a maximum of the apparent mobility is obtained at approximately 650 °C. The effect of cooling rate on apparent mobility is shown in Figure 10 for the situation that all Nb is in solution. Here, the occurrence of a maximum in the apparent mobility at an intermediate transformation temperature is clearly observed for lower cooling rates. Another striking feature of Figure 10 is that the apparent mobility is not only a function of temperature but also depends

on cooling rate. The observations for the apparent mobility are similar in the X80 steel, as illustrated in Figure 11. Clearly, the apparent mobility decreases with increasing Nb content in solution as well as with increasing temperature.

One may rationalize these findings considering a solute drag effect of Nb on the migrating austenite-ferrite interface. Classical solute drag models [25] predict that the solute drag effect increases with solute concentration. This is consistent with the observation that the apparent mobility decreases with increasing solute Nb content. Further, the solute drag pressure depends on the interface velocity and shows a maximum at intermediate velocity values. This may explain the surprising temperature trend and the effect of cooling rate on the apparent interface mobility. It will be important to conduct a rigorous solute drag analysis on the extracted mobility data following approaches previously applied to other low carbon steels (without Nb microalloying) and Fe-Mn alloys [26,27]. This will permit evaluation of whether or not classical solute drag theories lead to a consistent description of the effect of Nb in solution on the austenite-to-ferrite transformation. For the X80 steel, it will also be important to analyze more rigorously the synergistic role of Nb and Mo.

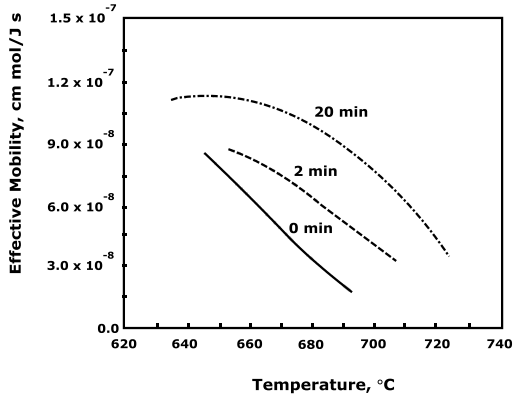

Figure 9. Effect of Nb in solution on effective mobility of austenite-ferrite interface in X65 steel cooled at 5 °C/s.

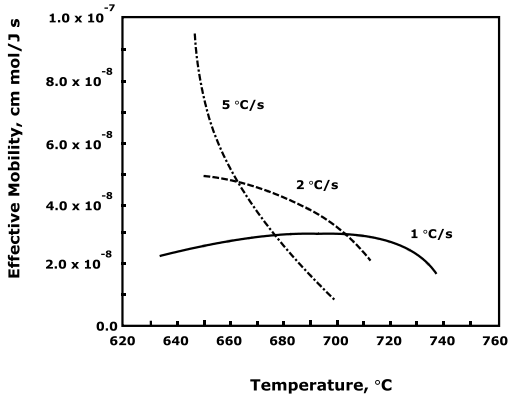

Figure 10. Effect of cooling rate on effective mobility of austenite-ferrite interface in X65 steel with all Nb in solution.

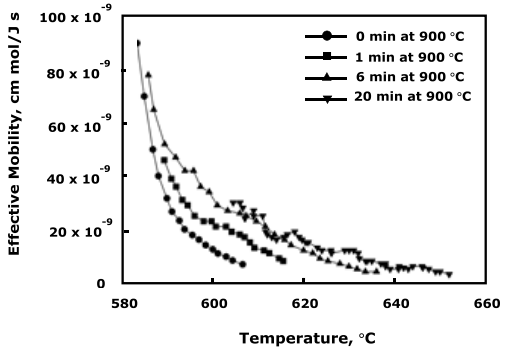

Figure 11. Effect of Nb in solution on effective mobility of austenite-ferrite interface in X80 steel with an austenite grain size of 26 μm cooled at 1 °C/s.

Conclusions

This paper provides a renewed in-depth investigation of the solute drag effect of Nb and Mo on the austenite decomposition in linepipe steels. A particularly significant role of Nb is confirmed that is of paramount importance when thermo-mechanically processing or welding these steels as the amount of Nb in solution may vary as a function of the employed process path or welding conditions. Further, the synergistic effects of Nb with Mo require further detailed studies. It is proposed to employ a rigorous solute drag analysis to quantify the effects of Nb and/or Mo on the austenite-to-ferrite transformation. This analysis will have to be extended to the bainite transformation. Bainitic transformation products are increasingly sought in higher strength linepipe steels and other state-of-the-art high-strength steels. Preliminary studies for the X80 steel indicate that bringing Nb into solution has also a marked effect on the bainite transformation [28].

Acknowledgements

We acknowledge the financial support received from the Natural Sciences and Engineering Research Council of Canada, Evraz Inc. NA and TransCanada Pipelines Ltd. with gratitude. Further, we would like to thank Sepehr Gerami, Thomas Garcin and Jennifer Reichert for their assistance in experimental and analyzing work.

References

1. W.B. Morrison, "Microalloy Steels – The Beginning," *Materials Science and Technology*, 25 (9) (2009), 1066-1073.

2. A.J. DeArdo et al., "On Strength of Microalloyed Steels: An Interpretive Review," *Materials Science and Technology*, 25 (9) (2009), 1074-1082.

3. Y. Terada et al., "Development of API X100 UOE Line Pipe," *Nippon Steel Technical Report (Japan)*, 72 (1997), 47-52.

4. J.D. Jones and A.B. Rothwell, "Controlled Rolling of Low-carbon Niobium-treated Mild Steels," *Special Report*, 108, ISI, London (1968), 78.

5. I. Weiss and J.J. Jonas, "Interaction Between Recrystallization and Precipitation During the High Temperature Deformation of HSLA Steels," *Metallurgical Transactions A*, 10 (7) (1979), 831-840.

6. A. Yoshie et al., "Modelling of Microstructural Evolution and Mechanical Properties of Steel Plates Produced by Thermo-mechanical Control Process," *Iron and Steel Institute of Japan International*, 32 (1992), 395-404.

7. W.B. Morrison, "The Influence of Small Niobium Additions on the Properties of Carbon-manganese Steels," *Journal of the Iron and Steel Institute*, 201 (4) (1963), 317-325.

8. S. Okaguchi, T. Hashimoto, and H. Ohtani, "Effect of Niobium, Vanadium and Titanium on Transformation Behavior of HSLA Steel in Accelerated Cooling" (Paper presented at the International Conference on Physical Metallurgy of Thermomechanical Processing of Steels and Other Metals, THERMEC-88, Keidanren Kaikan, Tokyo 6-10 June 1988), (1) 330-336.

9. Y.J.M. Brechet et al., "Effect of Nb on Ferrite Recrystallization and Austenite Decomposition in Microallyed Steels," *Steel Research International*, 78 (3) (2007), 210-215.

10. C. Fossaert et al., "The Effect of Niobium on the Hardenability of Microalloyed Austenite," *Metallurgical and Materials Transactions A*, 26 (1) (1995), 21-30.

11. Y. Takahama and J. Sietsma, "Mobility Analysis of the Austenite to Ferrite Transformation in Nb Microalloyed Steel by Phase Field Modelling," *Iron and Steel Institute of Japan International*, 48 (4) (2008), 512-517.

12. W.T. Reynolds Jr. et al., "The Incomplete Transformation Phenomenon in Fe-C-Mo Alloys," *Metallurgical Transactions A*, 21 (6) (1990), 1433-1463.

13. H.I. Aaronson, W.T. Reynolds Jr., and G.R. Purdy, "The Incomplete Transformation Phenomenon in Steel," *Metallurgical and Materials Transactions A*, 37 (6) (2006), 1731-1745.

14. H. Mohrbacher, "Mo and Nb Alloying in Plate Steels for High-performance Applications" (Paper presented at the The International Symposium on the Recent Developments in Plate Steels, AIST, Warrendale, PA, 19-22 June, 2011), 169-179.

15. P.A. Manohar et al., "Grain Growth Predictions in Microalloyed Steels," *Iron and Steel Institute of Japan International*, 36 (2) (1996), 194-200.

16. N. Isasti et al., "Effect of Composition and Deformation on Coarse-grained Austenite Transformation in Nb-Mo Microalloyed Steels," *Metallurgical and Materials Transactions A*, 42 (12) (2011), 3729-3742.

17. J.S. Park et al., "Dissolution and Precipitation Kinetics of Nb (C,N) in Austenite of a Low Carbon Nb-Microalloyed Steel," *Metallurgical and Materials Transactions A*, 40 (3), 2009, 560-568.

18. J.M. Gray, "Evolution of Microalloyed Linepipe Steels with Particular Emphasis on the 'Near Stoichiometry' Low Carbon, 0.10 Percent Niobium 'HTP' Concept," *Journal of Iron and Steel Research International*, 18 (1-2) (2011), 652-657.

19. M. Militzer, R. Pandi, and E.B. Hawbolt, "Ferrite Nucleation and Growth During Continuous Cooling," *Metallurgical and Materials Transactions A*, 27 (6) (1996), 1547-1556.

20. M. Militzer, F. Fazeli, and H. Azizi-Alizamini, "Modelling of Microstructure Evolution in Advanced High Strength Steels," *La Metallurgica Italiana*, (4) (2011), 35-41.

21. J. Ågren, “A Revised Expression for the Diffusivity of Carbon in Binary Fe C Austenite,” *Scripta Metallurgica*, 20 (11) (1986), 1507-1510.

22. R.G. Kamat et al., “The Principle of Additivity and the Proeutectoid Ferrite Transformation,” *Metallurgical Transactions A*, 23 (9) (1992), 2469-2480.

23. J. Sietsma and S. van der Zwaag, “A Concise Model for Mixed-mode Phase Transformations in the Solid State,” *Acta Materialia*, 52 (14) (2004), 4143-4152.

24. F. Fazeli, “Modelling the Austenite Decomposition into Ferrite and Bainite” (Ph.D. thesis, The University of British Columbia, Vancouver, 2005).

25. J.W. Cahn, “The Impurity-drag Effect in Grain Boundary Motion,” *Acta Metallurgica*, 10 (9) (1962), 789-798.

26. F. Fazeli and M. Militzer, “Application of Solute Drag Theory to Model Ferrite Formation in Multiphase Steels,” *Metallurgical and Materials Transactions A*, 36 (6) (2005), 1395-1405.

27. T. Jia and M. Militzer, “Modelling Phase Transformation Kinetics in Fe–Mn Alloys,” *Iron and Steel Institute of Japan International*, 52 (4) (2012), 644-649.

28. F. Fazeli et al., “Modelling the Effect of Nb on Austenite Decomposition in Advanced Steels” (Paper presented at The International Symposium on the Recent Developments in Plate Steels, AIST, Warrendale, PA, 19-22 June 2011), 343-350.

Fundamentals and Applications of Mo and Nb Alloying in High Performance Steels – Volume 1
Edited by Hardy Mohrbacher
CBMM, IMOA and TMS, 2014

AUSTENITE PROCESSING AND PHASE TRANSFORMATION OF NIOBIUM AND MOLYBDENUM ALLOYED HIGH PERFORMANCE STRUCTURAL STEEL

C.J. Shang[1], C.L. Miao[2] and S.V. Subramanian[3]

[1]University of Science and Technology Beijing, School of Materials Science and Engineering
Beijing, 100083, China
[2]Shougang Steel Group, Research Institute of Technology
Beijing, 100041, China
[3]McMaster University, Hamilton, Department of Materials Science and Engineering
Ontario L814L7, Canada

Keywords: High Performance Steel, Niobium, Molybdenum, Austenite Processing, Phase Transformation, Stress Relaxation, Thermal Simulation, CCT, Microstructure, Recrystallization, Austenite Grain Size, X80, X70, Dislocation Density, Microstructure

Abstract

Grain refinement and phase transformation control are significant issues for high performance structural steels. The use of a higher Nb content in low carbon Mn steel has an important effect on refining the prior austenite grains at intercritical temperatures by static recrystallization. The mechanism by which higher Nb levels produce ultra refinement of austenite is that recrystallization kinetics need longer incubation times and longer finish times, and higher solute Nb can slow down the mobility of recrystallized grain boundaries, and suppress grain coarsening effectively. Meanwhile, higher Nb can also suppress the softening between passes, and may increase the possibility of partial DRX (Dynamic Recrystallization) caused by high strain accumulation during hot strip finish rolling. Therefore, the start temperature of finish rolling should be lower to prevent DRX. Additionally, Nb and Mo are key elements for affecting phase transformation. Comparing results from an experimental Mn-Cr-Nb steel with Mn-Cr and Mn-Mo steels with higher Nb levels shows that a higher Nb content is beneficial in stabilizing austenite and widening the window for acicular ferrite and bainite formation during continuous accelerated cooling; whereas, Mo additions in low carbon higher Nb bearing steels widen the window for acicular ferrite and bainite transformation further. However, in order to obtain an optimum microstructure in low carbon-Mn-Nb-Mo steels, the ultra refined austenite should be cooled at a rate of more than 10 ºC/s, and the finish cooling temperature should be below 450 ºC.

Introduction

In order to meet the requirement of high performance, various metallurgical phenomena of Nb bearing low carbon low alloyed steels need to be controlled during the hot rolling and accelerated cooling process. No matter which rolling process is employed, grain refinement and strain accumulation of prior austenite grains are the key issues for obtaining excellent mechanical properties. In general, microstructure and properties are influenced by recovery of dislocations, static and dynamic recrystallization of austenite and precipitation. Literature [1] proves that increasing the Nb content in steel is the most effective method to retard SRX (Static

Recrystallization) compared with using other microalloying elements. Based on this characteristic, the higher Nb approach has been applied to rolled steel in a relatively higher non-recrystallization temperature range, the so-called high temperature process (HTP) [2]. Recent researchers [3,4] have shown that, in X80 pipeline steel, using a higher Nb content approach, the prior austenite grains can be refined from typically 80 microns to 10-20 microns and the elongated prior austenite grains can be flattened to several microns. Such a refinement effect is achieved by so-called "intercritical austenite processing" (IAP). According to the physical metallurgy principle of higher Nb bearing low carbon low alloyed steel, the rough rolling process should be optimized at an intercritical temperature to obtain an ultra fine and homogeneous prior austenite grain size by static recrystallization (SRX) with the solute dragging effect of dissolved Nb, while during the finish rolling process, the austenite should be flattened and strain accumulated in the non-recrystallization temperature range by not only precipitation but also the dragging effect of solute Nb.

Phase transformation after controlled rolling is another key factor affecting mechanical properties of steel, especially toughness. Generally, for low carbon low alloyed steel, Mo and Nb play important roles in phase transformation. Additionally, the accelerated cooling rate also significantly affects phase transformation. For the purpose of achieving high strength, high toughness and low cost, optimization of alloy design should be based on implementing an optimum TMCP process.

In this paper, the role of higher Nb contents on refining prior-austenite and accumulating strain in austenite will be introduced. Furthermore, the effect of Nb and Mo on phase transformation will be revealed. A skeleton map of an optimum TMCP process can be outlined for developing high strength, high toughness Nb bearing low carbon low alloyed structural steel.

Austenite Processing of Higher Nb Bearing Steel

Ultra Refining Prior Austenite Grains by Intercritical Static Recrystallization

Four low carbon steels were used for stress relaxation tests, as shown in Table I, therein, s1, s2 and s3 are laboratory steels with different Nb contents ranging from 0.012 wt% to 0.10 wt%, which were used to investigate the effect of niobium on recrystallization and precipitation behavior, and the possibility of grain refinement. Figure 1 presents the process cycle for the stress relaxation tests, after 25% reduction at a 1 s^{-1} strain rate at different temperatures, the specimens were held for 400 s at constant strain, and the stress-time curves were recorded. Actually, the stress relaxation method [5,6] can supply enough data to analyze the whole softening behavior as discrete events and can be used to characterize recovery or recrystallization behaviors, solute dragging and precipitation pinning. It is considered that more precise results can be obtained for isothermal recrystallization kinetics by the stress relaxation method [7].

Table I. Chemical Compositions of Experimental Steels Wt%

	C	Mn	Nb	Si	N(ppm)	Ni+Ti+Cu+Cr
s1	0.04	1.71	0.012	-	≤40	-
s2	0.04	1.76	0.063	-	≤40	-
s3	0.04	1.72	0.10	-	≤40	-
Industrial High Mn	0.04	1.75	0.095	0.22	≤40	<1.0 wt%

Figure 2 shows the stress relaxation curves of steels having different Nb contents, at 1050 °C and 1000 °C. According to Figure 2(a), no precipitation hardening was found at 1050 °C, and recrystallization softening occurs in all three steels after deformation, but the onset times of recrystallization are different; 0.10%Nb steel has the longest incubation period, less than 2 s, but the time for the 0.012%Nb steel is shorter than 0.5 s. Moreover, the 0.10%Nb steel needs a longer time to complete the recrystallization process compared with the other two steels. From the morphology of the austenite grains in Figure 3, partial recrystallization occurs in the 0.10%Nb steel at 2 s. Additionally, it is evident that most grains in the 0.10%Nb steel have finished complete recrystallization at 30 s, which is in agreement with the results of the stress relaxation test at 1050 °C.

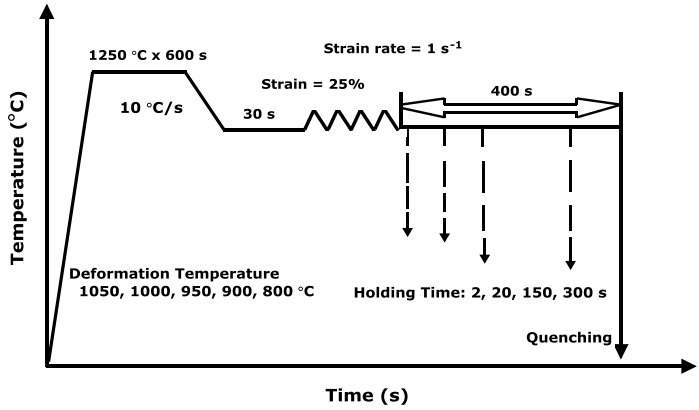

Figure 1. Schematic diagram of stress relaxation tests.

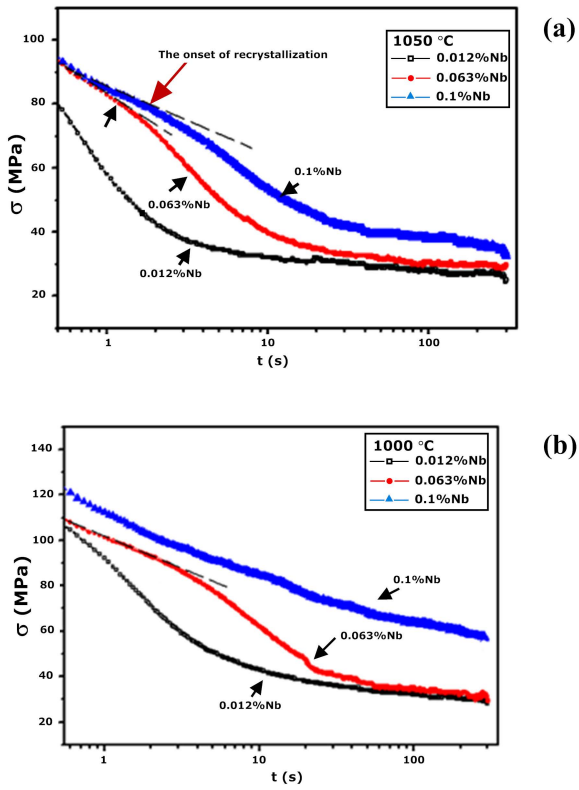

Figure 2. Stress relaxation curves; (a) 1050 °C, (b) 1000 °C.

Likewise, Figure 2(b) presents obvious recrystallization softening for the 0.063%Nb steel and 0.012%Nb steels at 1000 ºC. Incubation time of recrystallization increased as the temperature decreased. It is interesting to see from the curve of the 0.10%Nb steel at 1000 ºC that no obvious accelerated softening by recrystallization as well as no suppressed softening by precipitation occurs. Actually, TEM observations on the specimen from the 0.10%Nb steel after 300 s holding did not reveal strain-induced precipitated particles [4]. Combined with the etching results of austenite grains shown in Figure 4, there is a very slow recrystallization process, which is also time dependent, just as in the case at 1050 ºC.

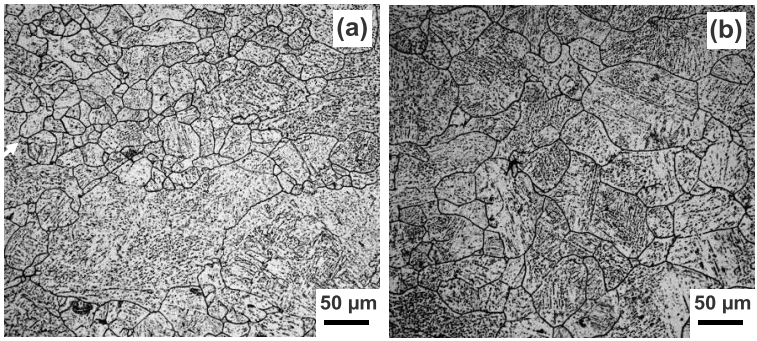

Figure 3. Morphology of austenite grains at 1050 °C; (a) 0.1%Nb - 2 s, (b) 0.1%Nb - 30 s.

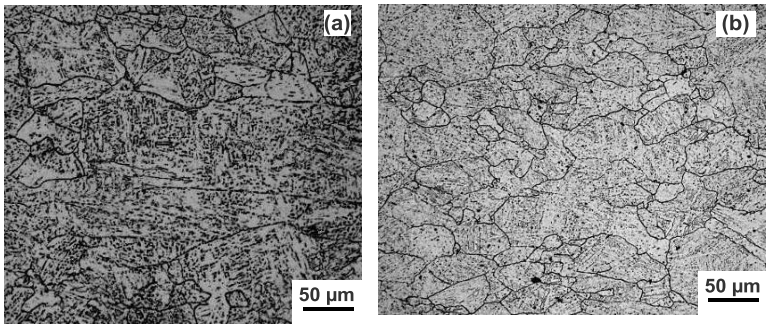

Figure 4. Morphology of austenite grains at 1000 °C; (a) 0.1%Nb - 30 s, (b) 0.1%Nb - 300 s.

Stress relaxation curves can effectively reflect recrystallization softening and precipitation hardening behavior [8]. From Figure 5, the curves from the 0.10%Nb steel at 950 ºC and 900 ºC both show the softening rates being reduced by strain-induced precipitation at 5 s and 3 s, respectively. It is also shown by TEM observation that precipitates are not found in the specimens of the 0.10%Nb steel at 2 s from 950 °C to 850 °C, however, after holding for 20 s, particles with a size ≤50 nm were observed, as shown in Figure 6.

The recrystallization behavior of a commercial higher Nb X80 pipeline steel was also examined. Its chemical composition is shown in Table I. The stress relaxation method was also employed for further research on recovery, recrystallization and precipitation, and a schematic of the process is shown in Figure 7.

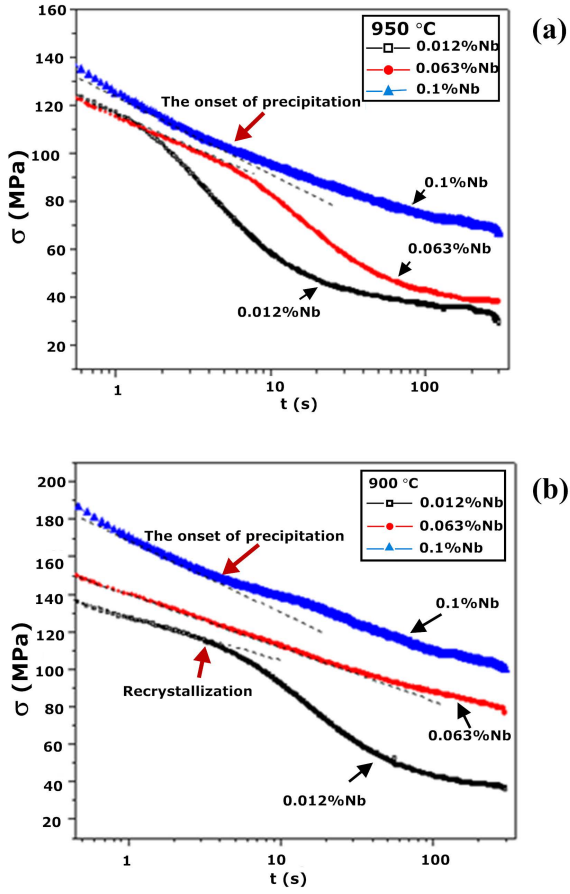

Figure 5. Stress relaxation curves at different temperatures; (a) 950 °C, (b) 900 °C.

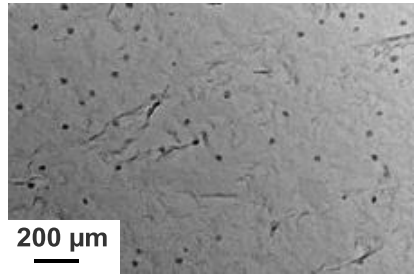

Figure 6. Morphology of strain induced precipitates at 950 °C in 0.1%Nb steel after delay of 20 s.

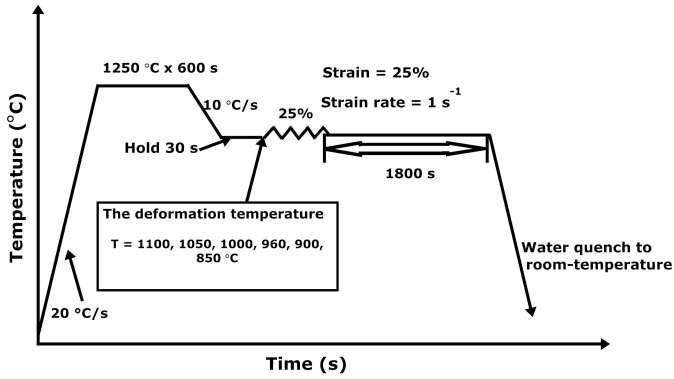

Figure 7. Thermomechanical process of stress relaxation tests for industrial steel.

Stress-relaxation curves for the industrial steel were measured at different temperatures. As shown in Figures 8(a) and (b), the stress level in the initial period falls quickly at 1100 ºC and 1050 ºC, due to the occurrence of recovery and recrystallization. When static recrystallization occurs, the relaxation time hardly reached 1 s, and the recrystallization stop time also is similar to the results from double compression tests. Once the relaxation temperature was decreased to 1000 ºC, as shown in Figure 8(c), visible softening behavior caused by recrystallization does not appear within 100 s. Neither is a hardening platform, resulting from strain-induced precipitation, clearly observed in this curve, that is to say, there are no precipitated particles available that can have their effect on dislocation mobility. Figure 8(d) indicates that strain-induced precipitation occurs after 25% prior deformation at 900 °C, and hardening behavior occurred after relaxing for 4 s.

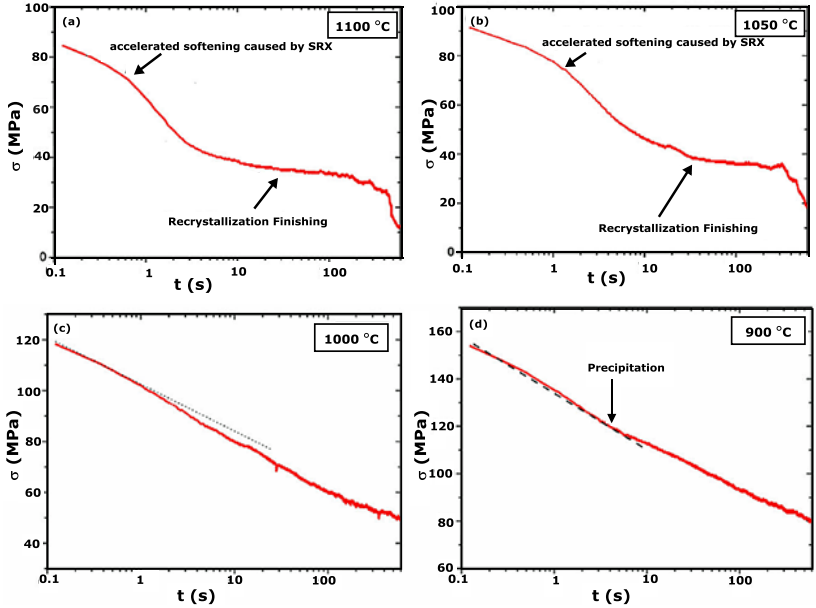

Figure 8. Stress-relaxation curves of Nb-bearing industrial steel at different temperatures; (a) 1100 °C, (b) 1050 °C, (c) 1000 °C, (d) 900 °C.

Likewise, similar thermo-simulation tests were also carried out on the industrial steel, as shown in Figure 9, and a statistical analysis of grain size distribution from the samples was analyzed by the software *image Pro* based on grain data in five different regions of each tested sample.

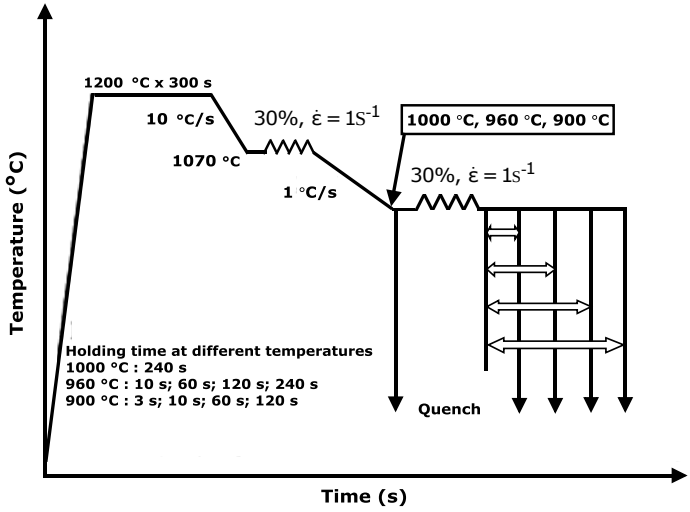

Figure 9. Thermomechanical schedule for observing morphology of prior austenite grains.

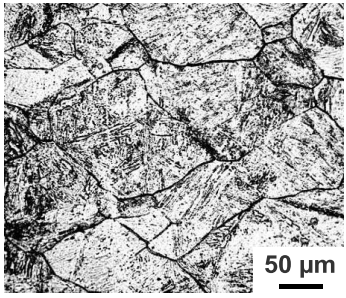

Figure 10. Morphology of the prior austenite grains.
(30% deformation at 1070 °C).

Figure 10 shows the morphology of statically recrystallized grains after 30% deformation at 1070 °C, it can be seen that the average size of completely recrystallized austenite grains is more than 80 µm. The accelerated recrystallization after the execution of one pass at 1070 °C is still time-dependent, as is the recrystallization of this steel after single deformation at 1050 °C. The recrystallization finishes in a very short time (less than 20 s). The morphology of the prior austenite grains after deformation and holding for 10 s, 60 s and 240 s is illustrated in Figure 11. Austenite grains after holding the sample for 10 s, Figure 11 (a), are homogenous and very fine, the average grain size is only about 19 µm, i.e. most austenite grains have finished SRX. Even

when holding for 240 s at 1000 °C, the average grain size is still less than 28 microns. The growth rate of recrystallized grains is relatively much slower compared with that at 1070 °C and this can be explained by the slow coarsening rate of recrystallized grains which results from the intense dragging effect of solute Nb.

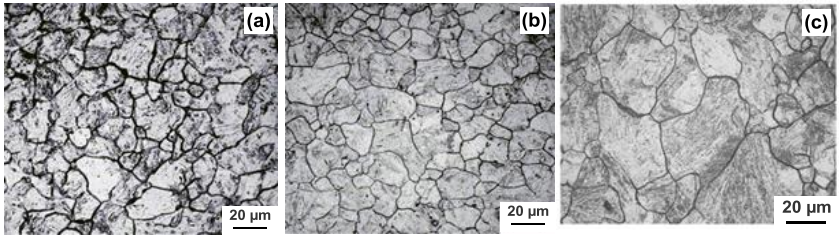

Figure 11. Stress relaxation curves of industrial steel under different conditions, and morphology of austenite grains at different times; (a) 10 s, (b) 60 s, (c) 240 s.

Preventing Dynamic Recrystallization by Optimizing Finish Rolling Process

In the present study, steels of two types (S and I) were analyzed, as shown in Table II. Steels of the first type (S2 and S3) were cast in the laboratory to solely investigate the effect of Nb on flow stress and DRX. The influence of other micro-alloyed elements can be eliminated. The steels of the second type (I2 and I4) were industrial X80 pipeline steels, with the aim to understand strain accumulation behavior during multi-pass rolling at relatively high temperatures. Cylindrical specimens of $\Phi 8 \times 10$ mm were prepared for the research on DRX before testing in a Gleeble-3800 thermo-mechanical simulator. The simulation schedule is shown in Figure 12. Specimens were reheated to 1100 °C for 120 s and then cooled to the test temperature (900-1100 °C) at 10 °C/s. After holding for 30 s at this temperature, the samples were compressed with 60% deformation at constant strain rates of 0.05-2 s^{-1}, and then quenched immediately.

Table II. Chemical Compositions of Investigated Steels

ID	C	Mn	Nb	Si	Mo	Cu+Ti+Ni+Cr
s2	0.037	1.76	0.063	-	-	
s3	0.031	1.72	0.10	-	-	
I2	0.044	1.83	0.092	0.18	0.249	0.54
I4	0.048	1.81	0.067	0.20	0.284	0.49

Figure 12 illustrates the simulated process of multi-pass rolling. Therein, the reductions and pass intervals are based on actual hot strip rolling of X80 pipeline steel. Strain-stress data were recorded for all simulated tests, and mean flow stress (MFS) values were calculated [9] in the analysis of this process.

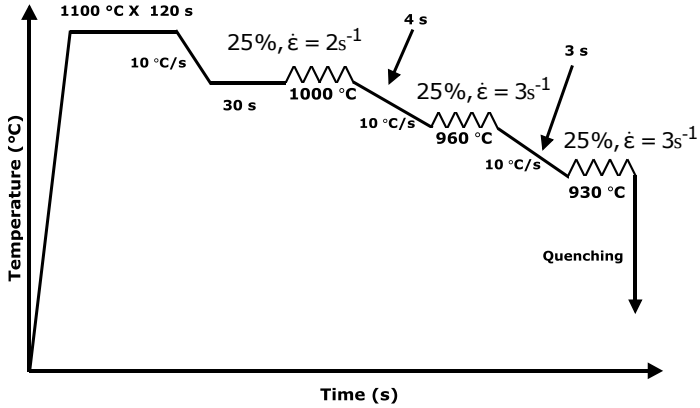

Figure 12. Schematic of simulated process for multi-pass deformation.

Figure 13 illustrates the stress-true strain curves and the evolution of mean flow stress in multi-pass rolling. There is a stress peak in the second pass for the industrial higher Nb steel and, also, its MFS value is decreased in the second pass. The decrease of the MFS value implies occurrence of DRX/MDRX during rolling, however the MFS value of the medium Nb steel increases steadily during rolling. The softening caused by DRX is only found in the higher Nb steel and hence the final stress values of these two steels are similar. Actually, the higher Nb steel has a larger critical strain value, so the occurrence of DRX can be explained by higher strain accumulation associated with the high Nb content. Moreover, the occurrence of DRX will generate serious mixed grain microstructures which have a negative impact on the toughness of the steel [10].

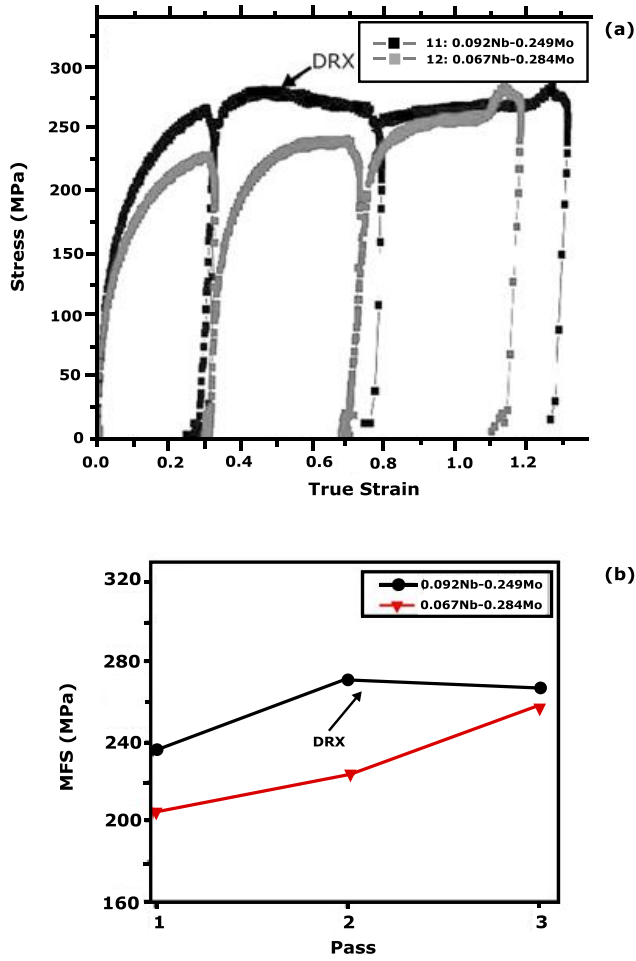

Figure 13. (a) True stress-strain curves and (b) mean flow stress (MFS) of multi-pass rolling.

A plane strain thermomechanical-simulation machine was used to investigate strain accumulation in the industrial steel, Table I; the schedule based on industrial rolling of X80 strip is shown in Figure 14 and was designed to focus on the effect of rolling temperature. Two finish rolling start temperatures were chosen, 940 °C and 910 °C, respectively, and true stress-strain curves were obtained.

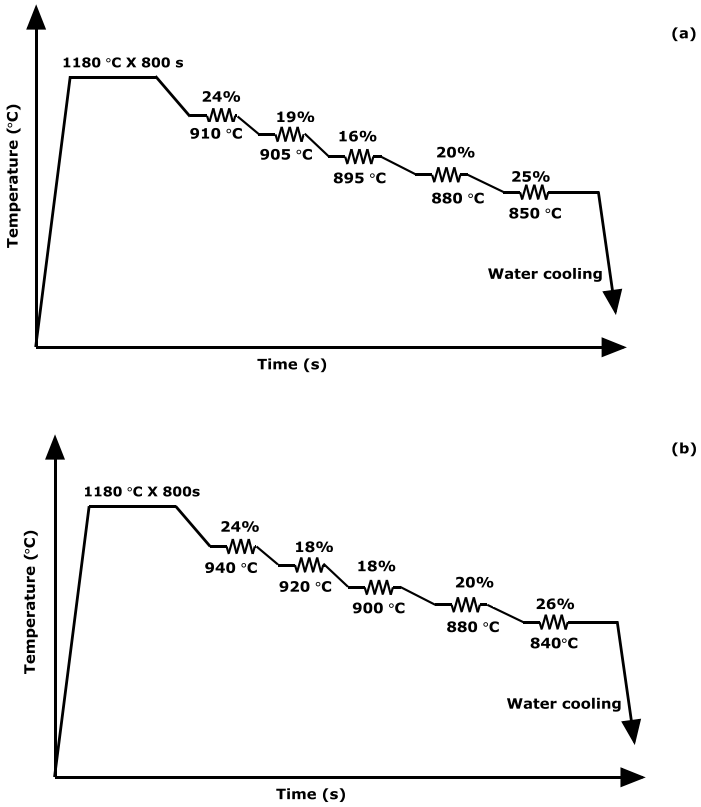

Figure 14. Schedule of plane strain tests.

In the high Mn higher Nb steel, the kinetics of strain-induced precipitation Nb(C,N) is offset by the higher Mn content [11]. The speed of finish rolling is very fast in industrial tandem rolling (the interstand time is very short), so there is hardly any available Nb(C,N) precipitated between passes. However, the dragging effect is still very strong. In this case, the strain accumulation by

rolling passes will easily reach a high level. Once the accumulated-strain exceeds a critical strain, dynamic recrystallization will take place [12].

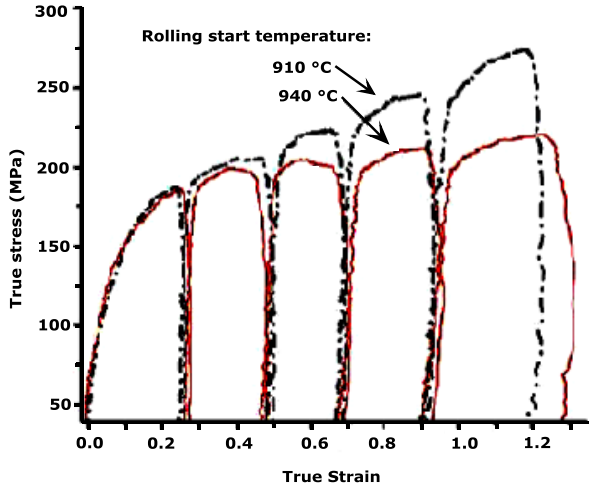

Figure 15. True stress-strain curves at different steps of plane strain simulation.

Figure 15 shows stress-strain curves measured in the plane strain test. In the first case where finish rolling starts at 910 °C, the stress value increases steadily. Yet, when the start/finish rolling temperature is raised to 940 °C, the characteristics of the stress-strain curve in the third pass indicate the occurrence of dynamic recrystallization. The same conclusion can be obtained when analyzing the mean flow stress (MFS). A drop of the MFS indicates the occurrence of DRX [13], as shown in Figure 16. In dynamic recrystallization, the relationship between the critical strain value and deformation temperature is inverse [14] which means that the critical strain value decreases with increasing temperature. If the rolling process (rolling reduction, strain rate, etc.) is not well defined, dynamic recrystallization is more likely to take place in a high temperature deformation process.

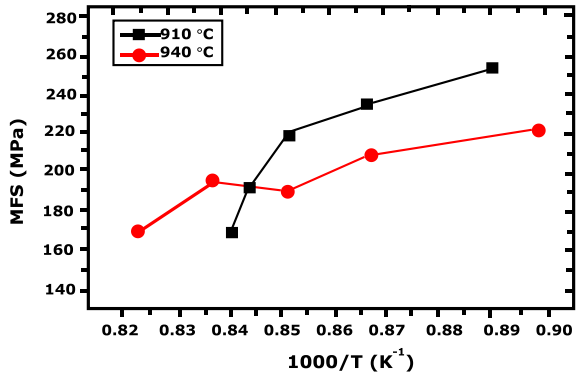

Figure 16. Mean flow stress (MFS) at different steps of plane strain simulation.

Prior austenite grains as shown in Figure 17(a) are homogeneous, for a rolling start temperature of 910 °C. However, austenite grains are non-uniform in Figure 17(b) for a start/finish rolling temperature of 940 °C and there is a grain layer, which is composed of small size grains among some coarse grains. Their morphology is like a necklace, which is probably caused by the occurrence of partial dynamic recrystallization. Generally, complete dynamic recrystallization evidently refines grain size, but partial dynamic recrystallization leads to serious mixed grain microstructures and a loss of dislocation density which would not be of benefit to strain accumulation in the austenite, resulting in a drop of yield strength.

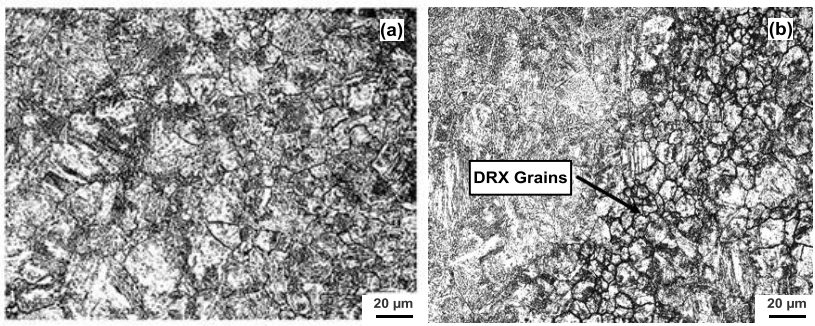

Figure 17. Morphology of prior austenite grains (vertical direction of rolling) for a start rolling temperature of (a) 910 °C, (b) 940 °C.

Combining these above characteristics of high Mn high Nb steel, a skeleton map can be outlined for optimization of the rolling schedule. Deforming above 1050 °C allows break up of coarse austenite grains, but due to the absence of precipitates and solute dragging effect in this temperature regime, grain growth and coarsening behavior is fast. Controlling rough rolling to further refine austenite grains, complete recrystallization will happen after deforming in the temperature range close to 1000 °C. The dragging effect from solute Nb can effectively retard the growth and coarsening of grains so that a homogeneous and fine grain structure can be obtained before finish rolling. Partial recrystallization must be avoided during finish rolling. By decreasing the rolling temperature and controlling reduction in each pass, pancaked austenite grains with a small width, will be obtained. Whether in plate or in strip rolling, high S_v (grain boundary area per unit volume) is always a key aim to acquire good properties for the steel. The flow stress level reflects the dislocation density. Actually, the flow stress behavior, both during and after deformation, is a key factor in determining the final dislocation density. The influence of the Nb content on flow stress behavior during deformation varies depending on temperatures and strain rates. In actual production, plate rolling has the metallurgical characteristics of a low strain rate and large deformation. Thus, higher Nb steels can provide a large advantage in effectively suppressing DRX behavior at high temperatures. A higher stress level or S_v is therefore easier to obtain at low temperature. However, in hot strip rolling a larger strain rate will be applied. Thus the influence of the Nb content on flow stress behavior will diminish during the finish rolling process. The main influencing factors for the final stress level are the softening and hardening behavior after deformation, which have a close correlation with the solute Nb content and precipitation. A high amount of solute Nb can prevent significant recovery between passes. Thus a higher Nb content can suppress softening between pass intervals, and may result in higher strain accumulation [15]. Although DRX of higher Nb steel requires a higher critical stress value, strain accumulation can still exceed it. Therefore the onset of DRX for higher Nb steel is more easily achieved during hot strip rolling (finish rolling process) with relatively high start rolling temperatures. However, by decreasing the finish rolling temperature, the DRX of high Mn higher Nb steel can be restrained, and a higher and steady MFS can be achieved. As a consequence, a homogeneous grain structure and a high S_v will be obtained.

Phase Transformation Characterization and Optimum Control of Process

Low carbon, high Mn, high Nb, Cr (Mo) alloy design has been accepted for the development of high strength pipeline and other infrastructural steels. Generally, Cr and Mo are added for solid solution strengthening. Solutes Cr, Mo and Nb also have an effect of increasing the hardenability. Actually, 0.04-0.08%C, 1.8-2.0%Mn and 0.08-0.1%Nb steel can transform to acicular ferrite and/or bainite by TMCP [16]. Cr, Mo, Ni and Cu can be added for further strengthening and/or increased hardenability. As the costs of Mo and Ni are relatively high, the added amount of alloying element should be justified by the strength grade required and also by the actual TMCP facility available. Nevertheless, the phase transformation characteristics of each alloying element should be understood, and the key processing parameters to produce the optimum microstructure in each kind of alloyed steel should be revealed.

The compositions of three experimental steels used in the research are shown in Table III. The Mn-Mo-Nb steel is the composition of conventional X70, and the Mn-Cr-Nb^+ and Mn-Mo-Nb^+ steel are higher Nb bearing grades used for X80 pipeline steel.

Table III. Chemical Composition of Three Experimental Steels in wt%

Experimental Steel	C	Si	Mn	Nb	Mo	Cr	Other microalloy elements
Mn-Mo-Nb	0.050	0.23	1.52	0.052	0.18	-	Ni+Al+Cu+Ti+V =0.09
Mn-Cr-Nb$^+$	0.043	0.16	1.90	0.091	-	0.29	Ni+Ti+Cu=0.42
Mn-Mo-Nb$^+$	0.026	0.14	1.92	0.090	0.15	-	Ni+Ti+Cu=0.42

Effect of Higher Nb and Mo on Continuous Cooling Phase Transformation

Static CCT diagrams for the steels were obtained by the thermal simulator FORMASTER. The specimens (3 mm diameter ×10 mm) were heated to 1000 ºC at 20 ºC/s, soaked for 500 s, and cooled to 900 ºC. After holding for 10 s at 900 ºC, the specimens were cooled to room temperature at rates of 0.5, 1, 3, 5, 10, 15, 20 ºC/s, respectively.

The CCT diagrams of the Mn-Mo-Nb and Mn-Cr-Nb$^+$ steels are shown in Figure 18(a). It can be seen that at lower cooling rates, the Mn-Mo-Nb steel is more likely to transform into ferrite-pearlite. When the cooling rate is higher than 5 ºC/s, the CCT curves of the two steels tend to be similar. When the cooling rate is larger than 10 ºC/s, both steels transform in the acicular ferrite and bainite zone. It is noticeable that the final phase transformation temperature of the Mn-Cr-Nb$^+$ steel is lower than that of the Mn-Mo-Nb steel. It can be concluded from a comparison of the results that the austenite of the higher Nb bearing steel is more stable, even without a Mo addition. Therefore, Mn-Mo-Nb steel can be replaced by Mn-Cr-Nb$^+$ steel, because identical phase transformation can be obtained when using a cooling rate of more than 10-15 ºC/s under accelerated cooling conditions. The key point of replacing Mn-Mo-Nb steel by Mn-Cr-Nb$^+$ steel is that the type and proportion of Mn-Cr-Nb$^+$ intermediate temperature transformation product can be controlled by cooling rate and final cooling temperature control within a certain range, however, cooling rate and cooling stop temperature are usually constrained by the mill facility. Furthermore, there is some difference between the physical metallurgy of a continuous hot rolling mill and a steckel-mill. All the factors stated above can influence the strength and toughness of pipeline steels. Considering the limitations of the facility, addition of Mo is taken account of in the higher Nb bearing alloy design.

Static CCT curves of the Mn-Mo-Nb$^+$ and Mn-Cr-Nb$^+$ steels are compared in Figure 18(b). The starting transformation temperature of the Mn-Cr-Nb$^+$ steel is higher than that of Mn-Mo-Nb$^+$ steel, and the ferrite and bainite zones of the Mn-Cr-Nb$^+$ steel are larger than those of the Mn-Mo-Nb$^+$ steel. That is because the addition of Mo retards the transformation to ferrite and pearlite, shifting the whole ferrite zone to longer times. It can also be concluded from Figure 18(b) that at higher cooling rates, the bainite transformation zone of the Mn-Cr-Nb$^+$ steel is wider. That is to say, with a higher starting transformation temperature it is feasible to obtain acicular ferrite and bainite. However, at lower cooling rates, bainite formation is more likely in Mn-Mo-Nb$^+$ steel.

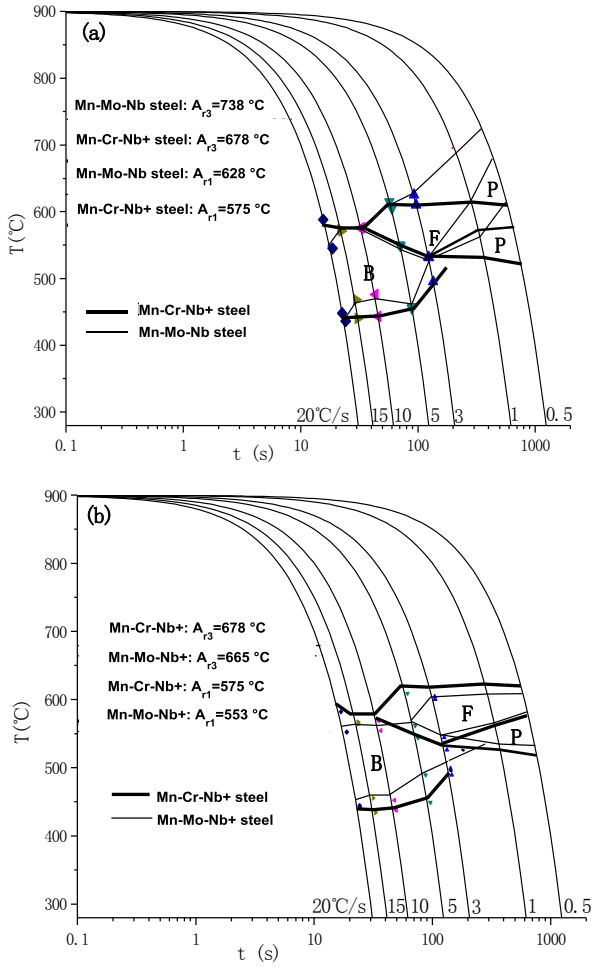

Figure 18. CCT diagram of experimental steels; (a) Mn-Mo-Nb and Mn-Cr-Nb+ steels, (b) Mn-Mo-Nb+ and Mn-Cr-Nb+ steels.
(Ar temperatures determined by continuous cooling from 900 ºC at 0.05 ºC/s).

Continuously cooled microstructures of the Mn-Cr-Nb^{+} steel at different cooling rates are shown in Figure 19. It can be seen that in Figure 19(a) and (b), at a cooling rate of 1 ºC/s, the microstructure is mostly composed of polygonal ferrite and quasi-polygonal ferrite, a small quantity of degenerate pearlite can also be observed. At a cooling rate of 5 ºC/s, the microstructure, Figure 19(c), is mostly composed of fine acicular ferrite, and a little polygonal ferrite. The microstructure at 10 ºC/s, Figure 19(d), is mostly evenly distributed acicular ferrite and when the cooling rate reaches 15 ºC/s, the microstructure, Figure 19(e) and (f), evolves to acicular ferrite and bainite, which are much finer than obtained at lower cooling rates.

Figure 20 shows that at a cooling rate of 3 ºC/s, more and finer bainite microstructures are formed. Mo can prohibit the phase transformation of austenite to ferrite, and increase the nucleation sites and thus a finer microstructure can be obtained in the presence of Mo. Moreover, the addition of Mo can promote the generation of bainite at relatively low cooling rates. Therefore, in industrial rolling, adding some Mo is a good choice to meet the requirement of strength.

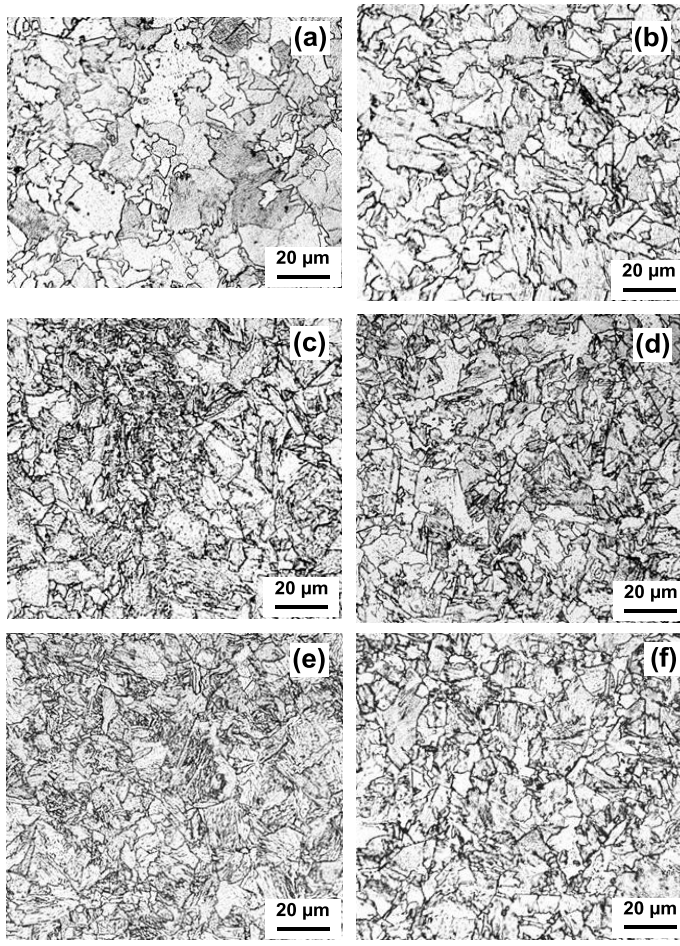

Figure 19. Continuous cooling microstructure of Mn-Cr-Nb+ steel; (a) 0.5 °C/s, (b) 1 °C/s, (c) 5 °C/s, (d) 10 °C/s, (e) 15 °C/s, (f) 20 °C/s.

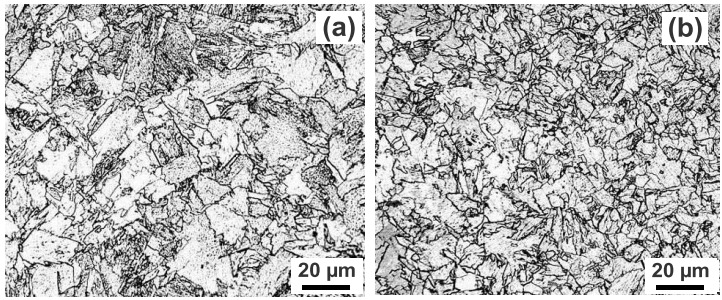

Figure 20. Microstructure of steels continuously cooled at 3 °C/s;
(a) Mn-Cr-Nb+, (b) Mn-Mo-Nb+.

Intermediate Phase Transformation Characteristics, Control of Cooling Start and Stop Temperature

Isothermal phase transformation research was also performed with the FORMASTER. The samples were heated to 1100 ºC at 20 ºC/s, held for 300 s, and then cooled to 650, 600, 550, 500 ºC at 60 ºC/s, respectively. After holding for 900 s at the above temperatures, the specimens were quenched to room temperature.

The microstructure of the Mn-Cr-Nb+ steel after isothermal treatment is shown in Figure 21. For the specimen held at 650 ºC for 900 s, only a small amount of ferrite is formed, while at 600 ºC and 550 ºC the main product of isothermal transformation is polygonal ferrite and/or quasi-polygonal ferrite. The quantity of these phases obviously decreases with decreasing temperature. Therefore, the nose temperature of reconstructive transformation should be at around 600 ºC. However, while isothermally treated at 500 ºC, most of the austenite transforms into an intermediate transformation microstructure of acicular ferrite and/or bainite.

It can be concluded from all the experimental results presented above that there are two transformation temperature windows for the Mn-Cr-Nb^{+} steel. One is at around 600 ºC, in which polygonal ferrite and quasi-polygonal ferrite are formed. At 550 ºC however, austenite is in a metastable state, the transformation is restrained, so only a small amount of grain boundary allotriomorphic ferrite is formed. Then at around 500 ºC, an intermediate transformation microstructure, such as bainite, can be obtained. Therefore, in order to control the acicular ferrite and bainite microstructure, the steel should be cooled down below 500 ºC.

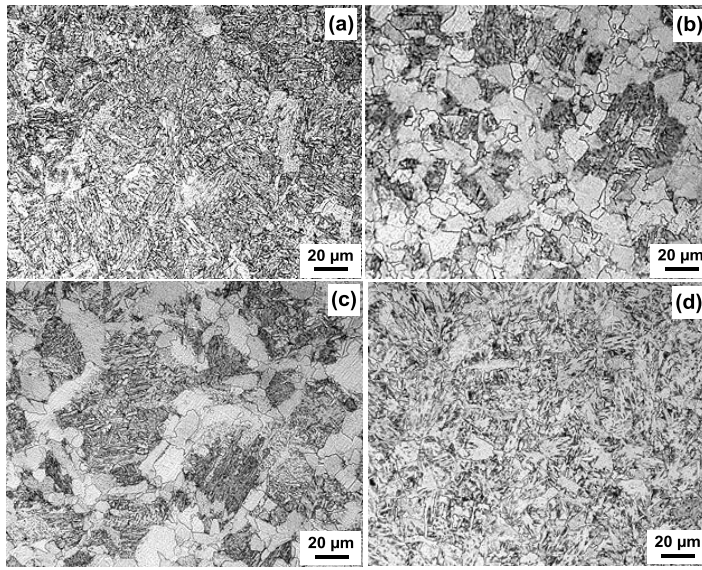

Figure 21. Microstructure of Mn-Cr-Nb^{+} steel after isothermal treatment at different temperatures for 900 s; (a) 650 ºC, (b) 600 ºC, (c) 550 ºC, (d) 500 ºC.

Thermal simulation samples of Φ8 mm × 15 mm were obtained to study the optimum accelerated cooling stop temperature of the Mn-Cr-Nb^{+} steel. The specimens were heated to 1200 ºC at 20 ºC/s, soaked for 300 s, compressed at 850 ºC for 30%, accelerated cooled to 600, 550, 500, 450 ºC, respectively at a rate of 10 ºC/s, and then quenched to room temperature. The influence of different accelerated cooling stop temperatures on phase transformation is shown in Figure 22. It can be seen from Figure 22(a) that the microstructure of the specimen cooled to 600 ºC and then quenched is mainly composed of lath bainite and/or martensite formed during quenching, while after continuous accelerated cooling to 550 ºC, Figure 22(b), only a small amount of acicular ferrite is formed on transformation. After cooling to 500 ºC, Figure 22(c), the microstructure is mostly composed of acicular ferrite. The black spots dispersed in the matrix are the product of quenched residual austenite (MA phase). It can be clearly seen from Figure 22(d) that after cooling to 450 ºC at a rate of 10 ºC/s the transformation to intermediate phase is almost totally completed, and both the amount and size of the MA constituents decrease.

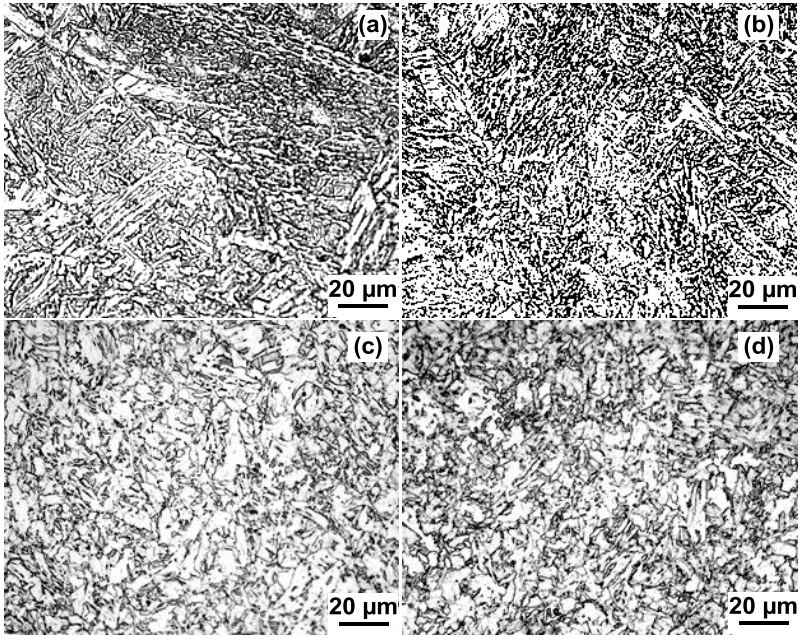

Figure 22. Microstructure after quenching at different temperatures after accelerated cooling at 10 °C /sec; (a) 600 °C, (b) 550 °C, (c) 500 °C, (d) 450 °C.

Conclusions

1. Analysis of stress relaxation data has shown that in the absence of precipitates, the recrystallization behavior of higher Nb steels is time dependent. At decreasing temperatures the recrystallization kinetics require a longer incubation time and longer finish time. This characteristic of higher Nb steel creates a new temperature window around 1000 ºC, without showing obvious accelerated softening by recrystallization as well as no suppressed softening by precipitation. Homogeneous and fine grains are generated prior to the finish rolling in which austenite grains will be fully flattened. This improvement of prior austenite grain condition has a large positive effect on the final properties of the steel.

2. The results of multi-pass rolling simulation indicate that higher Nb can suppress the softening between passes. It may also increase the possibility of partial DRX caused by excessive strain accumulation during hot strip finish rolling. Therefore the start temperature of finish rolling should be lower than 940 °C to fully flatten austenite grains and to accumulate strain or S_v.

3. Analysis of isothermal heat treatment and continuous cooling transformation data and microstructures of Nb and Mo alloyed low carbon steel, makes it clear that in order to obtain an ideal microstructure, the cooling rate after rolling should be controlled to more than 10 ºC/s and the final end cooling temperature should be controlled to below 450 ºC. Addition of Mo can retard the transformation to ferrite and pearlite and produce more acicular ferrite in higher Nb bearing steels at lower cooling rates.

Acknowledgement

This work was supported by the National Basic Research Program of China ("973" Program). The authors are grateful for the support from CITIC and CBMM.

References

1. L.J. Cuddy, *Thermomechanical Processing of Microalloyed Austenite,* ed A.J. DeArdo, G.H. Ratz, and P.J. Wray (Warrendale, PA: The Metallurgical Society of AIME, 1982), 129.

2. K. Hulka, J.M. Gray, and F. Heisterkamp, "Metallurgical Concept and Full-scale Testing of a High Toughness, H2S Resistant 0.03% C-0.10% Nb Steel" (Niobium Technical Report NbTR16/90[R], Companhia Brasileira de Metalurgia & Mineração, Sao Paulo, Brazil, 1990).

3. C.L. Miao et al., "Recrystallization and Strain Accumulation Behaviors of High Nb-bearing Line Pipe Steel in Plate and Strip Rolling," *Materials Science and Engineering A*, 527 (2010), 4985-4992.

4. C.L. Miao et al., "Recrystallization, Precipitation Behaviors and Refinement of Austenite Grains in High Mn High Nb Steel," *Metallurgical and Materials Transactions A*, 43 (2012), 665-676.

5. L.P. Karjalainen, "Stress Relaxation Method for Investigation of Softening Kinetics in Hot Deformation," *Materials Science and Technology*, 11 (6) (1995), 557-565.

6. C.L. Miao et al., "Studies on Softening Kinetics of Niobium Microalloyed Steel Using Stress Relaxation Technique," *Frontiers of Materials Science in China*, 4 (2) (2010), 197-201.

7. J. Kliber and I. Schindler, "Recrystallization/Precipitation Behavior in Microalloyed Steels," *Journal of Materials Processing Technology*, 60 (1996), 597-602.

8. W.J. Liu and J.J. Jonas, "A Stress Relaxation Method for Following Carbonitride Precipitation in Austenite at Hot Working Temperatures," *Metallurgical Transactions A*, 19A (1988), 1430-1413.

9. T.M. Maccagno et al., "Determination of Recrystallization Stop Temperature from Rolling Mill Logs and Comparison with Laboratory Simulation Results," *Iron and Steel Institute of Japan International*, 34 (11) (1994), 917-922.

10. T.X. Cui et al., “Effect of the Composition and Process on Microstructure and Properties of X80 Pipeline Hot Strip Steel,” *Iron and Steel Institute of Japan International*, 44 (2009), 55-59.

11. H.S. Zurob et al., “Analysis of the Effect of Mn on the Recrystallization Kinetics of High Nb Steel: An Example of Physically-based Alloy Design,” *Iron and Steel Institute of Japan International*, 45 (2005), 713-722.

12. A.I. Fernández, P. Uranga, and B. López, “Dynamic Recrystallization Behavior Covering a Wide Austenite Grain Size Range in Nb and Nb–Ti Microalloyed Steels,” *Materials Science and Engineering A*, 361 (2003), 367-376.

13. J.X. Dong, F. Siciliano, and J.J. Jonas, “Effect of Silicon on the Kinetics of Nb(C,N) Precipitation During the Hot Working of Nb-bearing Steels,” *Iron and Steel Institute of Japan International*, 40 (6) (2000) 613-618.

14. K. Minami et al., “Mathematical Modeling of Mean Flow Stress During the Hot Strip Rolling of Nb Steels,” *Iron and Steel Institute of Japan International*, 36 (12) (1996), 1507-1515.

15. C.L. Miao, G.D. Zhang, and C.J. Shang, “Effect of Nb Content on Hot Flow Stress, Dynamic Recrystallization and Strain Accumulation Behaviors in Low Carbon Bainitic Steel,” *Materials Science Forum*, 62 (2010), 654-656.

16. C.L. Miao et al., “Grain Refinement and Microstructure Control of HTP X80 Pipeline Steel,” *Iron and Steel Institute of Japan International*, 3 (015) (2009).

Fundamentals and Applications of Mo and Nb Alloying in High Performance Steels – Volume 1
Edited by Hardy Mohrbacher
CBMM, IMOA and TMS, 2014

THE EFFECT OF NIOBIUM ADDITIONS ON THE MICROSTRUCTURAL MORPHOLOGY IN THE HEAT-AFFECTED ZONE OF LOW-CARBON STEELS

J.R. Yang[1] and C.Y. Huang[2]

[1]Department of Materials Science and Engineering, National Taiwan University,
1 Roosevelt Rd., Sec. 4, Taipei, Taiwan, R.O.C.
[2]Iron and Steel R&D Department, China Steel Corporation,
Kaohsiung, Taiwan, R.O.C.

Keywords: Niobium, Coarse Grained Heat Affected Zone, Thermal Simulation, Widmanstätten Ferrite, Bainite, Interlocking Ferrite Structure, TEM, Heat Input, Charpy Toughness, Microstructure, Phase Transformation

Abstract

With the purpose of evaluating the effect of niobium additions on the microstructures of the HAZ (heat-affected zone) in mild steels, a plain C-Mn steel (without niobium) and three niobium containing steels with 0.01, 0.02 and 0.04 wt%Nb respectively, were investigated through simulated HAZ experiments at heat inputs of 20, 50 and 80 kJ/cm. The microstructures of simulated coarse-grained HAZ's have been examined by optical metallography and transmission electron microscopy. It was found that the addition of niobium had a significant effect on the transformation in the HAZ. For high energy heat inputs (80 and 50 kJ/cm), the addition of niobium retarded the pearlite formation, even in the case of the 0.01 wt%Nb containing steel. The microstructures of the coarse-grained HAZ of niobium-containing steels consisted mainly of secondary Widmanstätten ferrite, but that of the niobium-free steel contained a large amount of pearlite as well as secondary Widmanstätten ferrite. At the low energy heat input level (20 kJ/cm), the microstructures of the coarse-grained HAZ of the niobium-containing steels were all similar and consisted mainly of interlocking ferrite plates with small amounts of bainite and Widmanstätten ferrite; while that of the niobium-free steel comprised Widmanstätten ferrite and martensite with a small quantity of pearlite. The results from Charpy impact tests indicated that the niobium-containing steels with a simulated HAZ heat input of 20 kJ/cm possessed higher toughness than those treated at heat inputs of 50 and 80 kJ/cm. It is proposed that the interlocking ferrite structure, which forms in the HAZ of the niobium-containing steels after simulation of a 20 kJ/cm heat input level, improves the toughness property.

Introduction

Nb-microalloyed steels have been studied extensively over the past four decades. Plenty of investigators have studied austenite recrystallisation behaviour in these kinds of steels, and have shown that the addition of Nb can substantially retard the recrystalisation of austenite during hot rolling [1-3]. It is well known that the principal strengthening of these steels is derived from precipitation of finely dispersed niobium carbonitrides Nb(CN) in a ferrite matrix. Nb(CN) can also be utilised in the refinement of austenite grains if austenite conditioning has been controlled. The use of these products, which have been applied in such areas as ships, buildings, automotive

and earthmoving equipment and pipelines etc., usually involves fabrication by welding. It is known that high-energy welding processes such as submerged-arc or electro-slag welding usually cause a brittle microstructure in the heat-affected zone (HAZ) of niobium-containing steels [4,5]. At the highest range of temperatures in the weld thermal cycle, niobium carbonitrides, which are effective in pinning the austenite grain-boundaries, tend to dissolve. This results in rapid coarsening of austenite grains in the HAZ adjacent to the fusion line. Niobium taken into solid-solution in coarse-grained austenite will have a strong effect on the subsequent transformation [6-9]. Some researchers have studied the HAZ of niobium-containing steels [10-13], however, considerable confusion exists in the literature, particularly with regard to the effect of niobium on the microstructural morphology in the HAZ. The classification of microstructures, on the basis of morphology, is of considerable use in the study of structure-property relationships. Therefore further studies are needed to clearly characterise the various ferrite morphologies in the HAZ.

The aim of the present work is to determine the effect of niobium additions on the coarse-grained HAZ microstructures after thermal simulations performed on a Gleeble 1500 machine (manufactured by Duffers Scientific, Inc.). The toughness of each microstructure has also been evaluated in order to define the relationship between microstructure and toughness.

Experimental Procedure

The investigation involved four different steels. A plain C-Mn steel was selected as the reference material. To find out the effect of Nb addition, three other steels with the same C-Mn base composition but alloyed with 0.01, 0.02 and 0.039 wt%Nb respectively, were also investigated. The chemical compositions of the steels are given in Table I; the reference steel (without Nb) is designated as steel O, and the 0.01, 0.02 and 0.039 wt%Nb containing steels identified as L, M and H, respectively. All steels were prepared by vacuum melting, then cast into 100 kg ingots with a thickness of 210 mm. The ingots were homogenised at 1200 °C for 2 h and then hot rolled in several passes, by 20% reduction per pass, to plates of 20 mm thickness with a finishing temperature of 850 °C. The plates were air cooled to room temperature after hot rolling.

Table I. Chemical Compositions (wt%) of the Steels Studied

Steel	C	Si	Mn	P	S	Nb	Al	N*
O	0.127	0.29	1.36	0.017	0.008	-	0.029	54
L	0.128	0.29	1.47	0.018	0.008	0.010	0.032	83
M	0.124	0.30	1.37	0.017	0.008	0.020	0.037	54
H	0.125	0.29	1.36	0.017	0.008	0.039	0.031	56

*N in ppm

The simulated HAZ experiments were carried out on a Gleeble 1500 machine. Before thermal simulation, the representative weld thermal cycles from actual welding had been obtained as described below. Test beads were deposited on 20 mm thick steel plates, using the bead on plate technique, by submerged-arc welding at three different heat inputs: 20, 50 and 80 kJ/cm. The thermal cycles were measured at the location of the coarse-grained region in the HAZ close to the fusion boundary. The thermal cycles are shown in Figure 1; the peak temperatures were approaching 1400 °C for the three cycles and cooling times between 800 and 500 °C ($\Delta t_{8/5}$) for

the heat inputs of 80, 50 and 20 kJ/cm were 220, 102 and 16 s, respectively. The specimens to be used for simulation were sectioned from the as-rolled plates along the rolling direction as bars of dimensions 11 x 11 x 56 mm. A Gleeble 1500 machine was employed to reproduce repesentative coarse grained HAZ microstructures in the samples. After the Gleeble thermal simulation cycles, the Charpy specimens were prepared in the standard form of 10 x 10 x 55 mm. Notches were located in the uniform microstructural region at the centre of the specimens and Charpy impact tests were carried out at 0, -20, -40 and -60 °C.

The optical metallography specimens were prepared from the coarse-grained HAZ region of Charpy specimens. The specimens were mechanically polished and then etched in 2% Nital solution. Hardness measurements were made on optical specimens using a Vickers hardness tester. A load of 300 g was used in order to make the indentation on the individual phases. Transmission electron microscopy samples were prepared from 0.25 mm thick discs slit from the coarse grained HAZ region of the Charpy specimens. The discs were mechanically ground down to a thickness of 0.05 mm on 1200 grit SiC paper; the specimens were then single-jet electropolished using a 5% perchloric acid, 25% glycerol and 70% ethanol mixture at ambient temperature and 60 V polishing potential. The electron microscopy was carried out using a JEM 2000 EX transmission electron microscope operated at 200 kV.

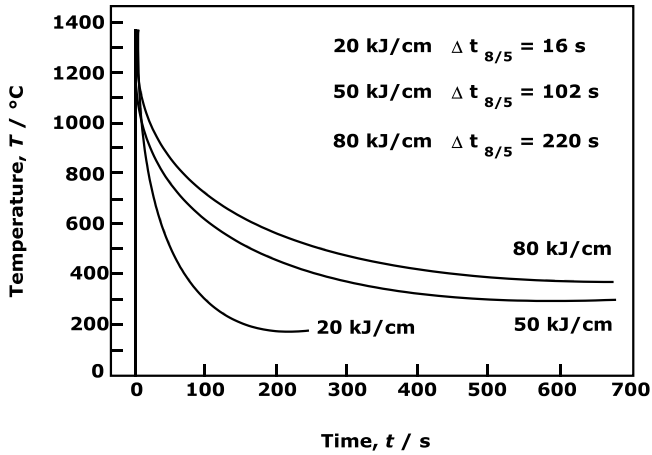

Figure 1. Thermal cycles of HAZ simulations corresponding to the real thermal cycles for three heat inputs: 80, 50 and 20 kJ/cm.

Results and Discussion

Optical Metallography

The optical microstructures of the as-rolled steels were all similar, and consisted of banded structures of equiaxed ferrite and pearlite as shown in Figures 2(a) and (b). Steel H possessed the smallest ferrite grain size (about 20 μm) of the three niobium containing steels studied. The electron micrographs, Figures 2(c) and (d), revealed large quantities of fine niobium carbonitride particles scattered in the ferrite matrix. The high ingot reheating temperature (1200 °C) allowed most of the niobium carbonitrides to dissolve in the austenite as the maximum solubility of niobium in steel H is about 0.037 wt% in austenite, based on the solubility product equation for NbC proposed by Irvine et al. [8] as follows:

$$\log[Nb][C] = -6770/T+2.26, \quad (1)$$

where the solubilities are expressed in wt% as a function of absolute temperature.

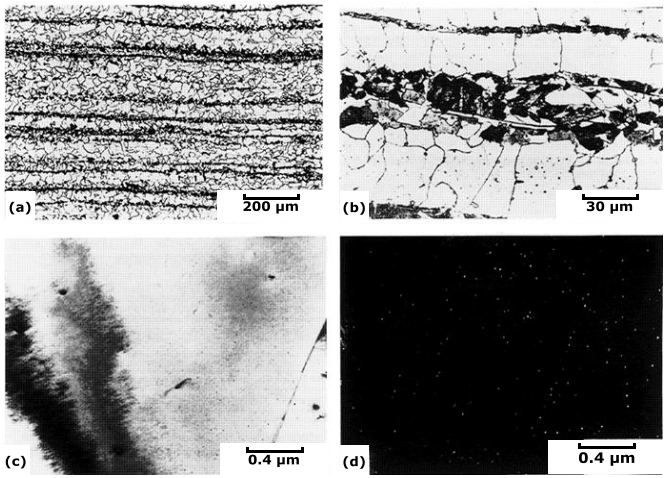

Figure 2. Microstructure of the as-rolled steel H; (a) and (b): Optical micrographs, (c) and (d): Bright and dark field images from electron micrographs.

In microalloyed steels, where strong carbide-forming elements are present in concentrations less than 0.1 wt%, it is often possible to obtain the ferrite in a supersaturated condition with little or no carbide precipitation taking place during the $\gamma \rightarrow \alpha$ reaction [14]. However, in the thermo-mechanical process for producing the as-rolled steel H, the finish-rolling at a low temperature (850 °C) would accumulate strain in the deformed austenite and promote the very finely dispersed niobium carbonitride precipitates as observed in this steel (0.039 wt%Nb). Indeed,

while the steel was cooled through the transformation temperature of ferrite, carbide particles formed in the ferrite matrix due to interface precipitation.

The typical structure in a low-alloy steel HAZ is characterised by a very coarse prior austenite grain size with allotriomorphic ferrite layers formed during cooling after welding. The allotriomorphic ferrite which nucleates at the prior austenite grain boundaries tends to grow along the austenite boundaries at a rate faster than in the direction normal to the boundary plane. When the cooling time from 800 to 500 °C is short, the layers of allotriomorphic ferrite become thin or even disappear. It is believed [15,16] that during continuous cooling, the transformation temperature of Widmanstätten ferrite is just below that of allotriomorphic ferrite. In the coarse-grained region of the HAZ, there are usually two kinds of Widmanstätten ferrite to be found, primary and secondary Widmanstätten ferrite [15,17]. Secondary Widmanstätten ferrite nucleates at the allotriomorphic ferrite/austenite boundaries and grows as sets of parallel plates separated by thin layers of austenite, the latter subsequently being retained to ambient temperature or partially transforming to martensite and/or pearlite. On the other hand, primary Widmanstätten ferrite nucleates directly from austenite grain boundaries which are not covered by allotriomorphic ferrite, although its growth mechanism is identical to that of secondary Widmanstätten ferrite. Details of the transformation mechanism of Widmanstätten ferrite have been reported in Reference [18]. In Dubé`s classification [19], secondary Widmanstätten ferrite was referred to as a 'Widmanstätten ferrite side-plate' and primary Widmanstätten ferrite was called a 'Widmanstätten ferrite primary side-plate'.

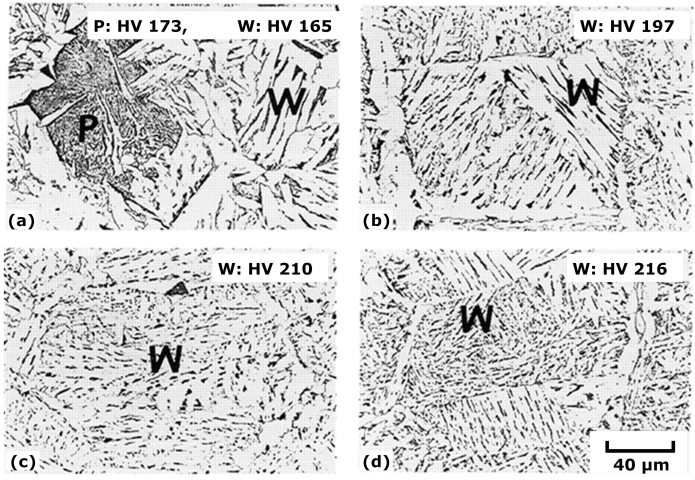

Figure 3. Optical micrographs obtained from four different steels after a simulated HAZ thermal cycle at 80 kJ/cm; (a) steel O, (b) steel L, (c) steel M and (d) steel H. Value of Vickers hardness, HV, for each phase is indicated. (W: Widmanstätten ferrite; P: pearlite).

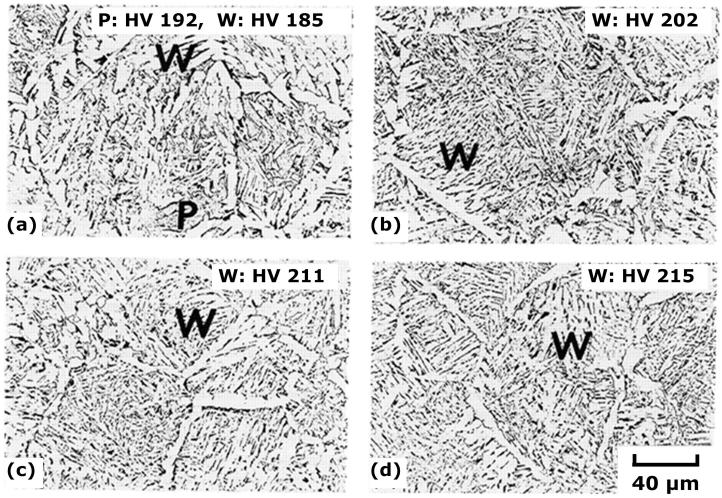

Figure 4. Optical micrographs obtained from four different steels after a simulated HAZ thermal cycle at 50 kJ/cm; (a) steel O, (b) steel L, (c) steel M and (d) steel H. Value of Vickers hardness, HV, for each phase is indicated. (W: Widmanstätten ferrite; P: pearlite).

The structures of the coarse-grained HAZ in the niobium-containing steels and the reference steel without Nb are significantly different, especially in the case of high energy inputs, 80 and 50 kJ/cm, and their corresponding optical micrographs are presented in Figures 3 and 4. Figure 3 shows that after 80 kJ/cm heat input, the HAZ microstructure of steel O, without Nb, Figure 3(a), was composed of large amounts of pearlite colonies with secondary Widmanstätten ferrite (containing a coarse layer of allotriomorphic ferrite). Whereas, after 80 kJ/cm heat input, the microstructures of steel L, 0.01 wt%Nb, Figure 3(b), steel M, 0.02 wt%Nb, Figure 3(c), and steel H, 0.039 wt%Nb, Figure 3(d), consisted mainly of secondary Widmanstätten ferrite (containing a thin layer of allotriomorphic ferrite) and retained microphases trapped between the Widmanstätten ferrite plates. The results from optical metallography imply that the small additions of niobium brought about the retardation of the $\gamma \rightarrow \alpha$ transformation kinetics. Consequently, pearlite colonies do not exist in the niobium-containing steels even after 80 kJ/cm heat input, which has a long cooling time between 800 to 500 °C of 220 s. The above results are consistent with those reported by several authors [20,21]. They claimed that small additions of niobium in solid solution in austenite would increase the hardenability of the steel. It has been suggested that because the niobium atoms have a large misfit within the iron lattice, the austenite grain boundaries are favourable sites for the location of niobium atoms. Grain-boundary segregation of niobium is presumed to raise the energy barrier to ferrite nucleation at the austenite grain boundaries; therefore, niobium has a strong retarding effect on the transformation of austenite to allotriomorphic ferrite and pearlite [21].

By comparing the micrographs in Figure 3 and Figure 4, it can be seen that, for the steels studied, the effect of Nb on $\gamma \rightarrow \alpha$ transformation after 50 kJ/cm heat input simulation is similar to that at 80 kJ/cm heat input. The above results indicate that under the conditions of 80 kJ/cm and 50 kJ/cm, additions of niobium retard the pearlite transformation. On the other hand, at a low energy heat input, 20 kJ/cm, the microstructure of the coarse-grained HAZ of niobium-containing steels consisted chiefly of interlocking ferrite plates with small amounts of bainite and Widmanstätten ferrite, Figures 5(b)–(d); while that of the niobium-free steel comprised Widmanstätten ferrite and martensite with a small fraction of pearlite, Figure 5(a).

At heat inputs of 80 kJ/cm and 50 kJ/cm, the secondary Widmanstätten ferrite can be obtained in all the steels studied as shown in Figures 3 and 4; whereas, at the heat input of 20 kJ/cm, the primary Widmanstätten ferrite replaces the secondary Widmanstätten ferrite as shown in Figure 5. The results indicate that at a slow cooling rate between 800 and 500 °C the formation of allotriomorphic ferrite may occur before that of Widmanstätten ferrite (i.e., secondary Widmanstätten ferrite forms). The evidence from optical metallography, Figures 3 and 4, also indicates that small additions of niobium have a significant effect on the secondary Widmanstätten ferrite transformation. For the same heat input, the width of the Widmanstätten ferrite plates in the niobium-free steel is much coarser as compared with that in the niobium-containing steels. Micralloyed niobium does depress the transformation start temperature of Widmanstätten ferrite, as a result, the width of the Widmanstätten ferrite plates in the niobium-containing steels becomes finer.

The major effect of niobium on HAZ microstructure in the case of the 20 kJ/cm heat input level appears to be the formation of interlocking ferrite plates, Figures 5(b)–(d). A similar structure is well known to be acicular ferrite in alloy-steel weld deposits [22], where non-metallic inclusions play an important role in development of intragranular nucleation. Another similar structure of intersecting acicular ferrite [23,24], which forms in deformed austenite under controlled-rolling and accelerated-cooling, has also been reported. The detailed morphology and toughness properties of the interlocking ferrite plates will be discussed in the following sections.

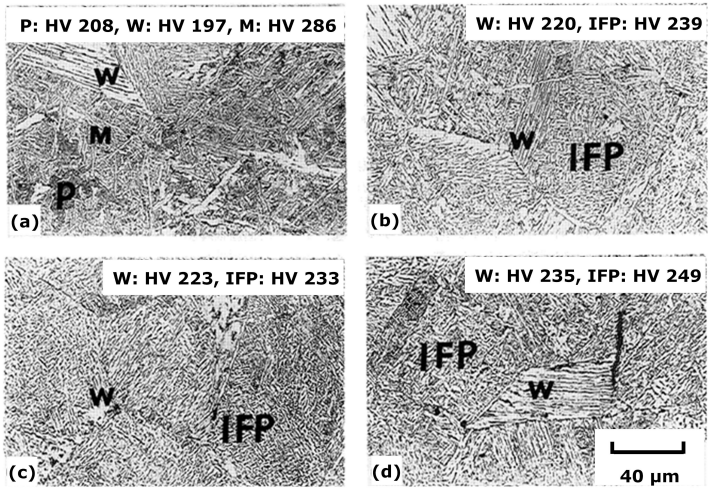

Figure 5. Optical micrographs obtained from four different steels after a simulated HAZ thermal cycle at 20 kJ/cm; (a) steel O, (b) steel L, (c) steel M and (d) steel H. Value of Vickers hardness, HV, for each phase is indicated. (W: Widmanstätten ferrite; M: martensite; P: pearlite; IPF: interlocking ferrite plates).

Transmission Electron Microscopy

In the optical micrographs, it is very difficult to reveal the microstructural details of the bainite, martensite and the interlocking ferrite plates. Attention was therefore focused on transmission electron microscopy. The electron micrograph shown in Figure 6 was taken from the 20 kJ/cm heat input specimen of steel H. It clearly illustrates the characteristics of the interlocking ferrite plates, which are usually found in the niobium containing steel specimens after simulation of 20 kJ/cm heat input, such as the regions marked **IFP** in Figures 5(b), (c) and (d). Figure 6 reveals that the individual interlocking ferrite plate has a high dislocation density which implies that the transformation mechanism could be displacive. In the upper left-hand region of the micrograph, a lower bainite plate (with intra-plate carbides precipitated in a single variant) can be found. Figure 7 illustrates transmission electron micrographs and corresponding diffraction patterns for the interlocking structures. The dark-field images, as shown in Figures 7(b) and (c), illuminate the packet structures which are made up of several parallel plates having essentially the same orientation. The orientation relationship between these two packets of interlocking ferrite plates has been investigated by analysing the corresponding electron diffraction patterns, as shown in Figure 7(e). The result is illustrated in Table II, where 24 equivalent axis-angle pairs relating these two packets of ferrite plates are shown. Judging from the highest angle of rotation, [0.0000 0.1524 0.9883]/180°, it appears that the orientation relationship between these two packets of interlocking ferrite plates may result from the existence of a Nishiyama-Wasserman orientation relationship with austenite, which has been documented in Reference [25]. The result

indicates that the transformation mechanism of the interlocking ferrite has a displacive characteristic. Widmanstätten ferrite also forms by a displacive mechanism, but it grows as sets of parallel plates without interlocking or intersecting. The morphology of interlocking ferrite plates is distinct from that of Widmanstätten ferrite; the former essentially forms through intragranular nucleation so that its distinctive feature can be developed. It has been claimed [26,27] that in HAZ structures of titanium-containing steels, titanium oxides and nitrides act as favourable nucleation sites for intra-granular ferrite plates within prior austenite grains. In this work, the nucleation mechanism of the interlocking ferrite plates involved is not yet understood.

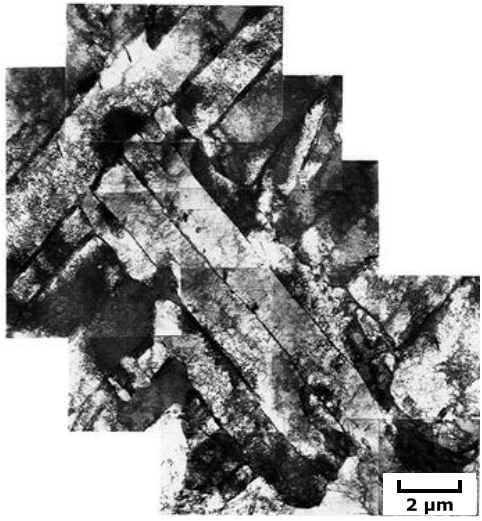

Figure 6. Transmission electron micrograph showing the interlocking structures obtained from steel H specimen after a simulated HAZ thermal cycle at 20 kJ/cm.

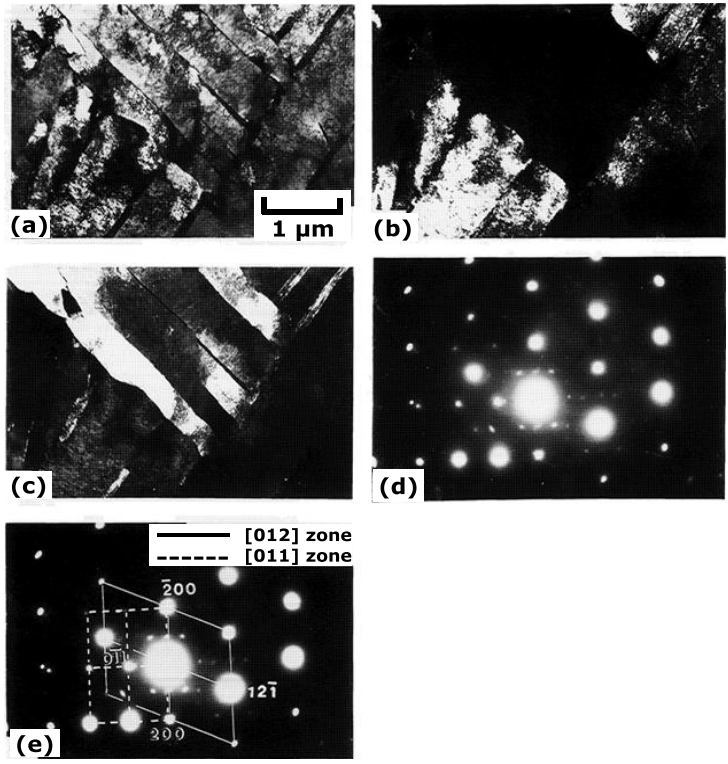

Figure 7. Transmission electron micrographs and corresponding diffraction patterns illustrating the interlocking structures; (a) bright field image, (b) and (c) dark field images, (d) corresponding diffraction pattern, (e) interpretation of (d).

Table II. 24 Equivalent Axis-Angle Pairs Relating Two Packets of Interlocking Ferrite Structure

No.	Axis			Angle (°)
1	1.0000	0.0000	0.0000	17.5
2	-0.5089	-0.6943	-0.5089	110.5
3	0.6278	0.6278	0.4601	130.6
4	0.0000	0.5911	0.8066	180.0
5	-0.7029	0.7029	-0.1084	167.6
6	-0.7029	0.1084	0.7029	167.6
7	-1.0000	0.0000	0.0000	72.5
8	0.1506	0.9771	-0.1506	91.3
9	-0.7029	-0.7029	0.1084	167.6
10	0.6278	-0.6278	0.4601	130.6
11	0.6278	-0.4601	0.6278	130.6
12	0.0000	0.1524	0.9883	180.0
13	1.0000	0.0000	0.0000	107.5
14	-0.7029	-0.1084	-0.7029	167.6
15	0.1506	-0.1506	0.9771	91.3
16	-0.5089	0.6943	0.5089	110.5
17	-0.5089	-0.5089	0.6943	110.5
18	0.0000	0.9883	0.1524	180.0
19	0.1506	-0.9771	0.1506	91.3
20	0.0000	0.8066	0.5911	180.0
21	0.1506	0.1506	0.9771	91.3
22	0.6278	0.4601	-0.6278	130.6
23	-0.5089	0.5089	-0.6943	110.5
24	-1.0000	0.0000	0.0000	162.5

Some of the microstructural features from the simulated HAZ specimens have also been studied by transmission electron microscopy. They are illustrated in Figures 8 to 12. Figure 8 shows the microstructure obtained from steel O after 80 kJ/cm heat input simulation. The corresponding optical micrograph is shown in Figure 3(a). It shows that pearlite and Widmanstätten ferrite transformed from the austenite after allotriomorphic ferrite grew from the prior austenite grain boundaries during the thermal cycle. Pearlitic structures were not found in the niobium containing steels studied under the same heat input. It is clear that with Nb in solid solution in austenite, a pearlite structure cannot be obtained even at the slow cooling rate associated with a 80 kJ/cm heat input. The result is consistent with the reports by several authors [8,10,12] who asserted that addition of a suitable amount of niobium (less than 0.04 wt%) increases the hardenability of steels. Figure 9 shows the microstructure obtained from steel H after a 50 kJ/cm heat input simulation. Its corresponding optical micrograph is shown in Figure 4(d). Secondary Widmanstätten ferrite nucleated at the allotriomorphic ferrite-austenite boundaries and grew as sets of parallel plates separated by thin regions of austenite, the latter subsequently being retained to ambient temperature or partially transforming to martensite, Figure 9(b). These small quantities of retained austenite and martensite mixtures are called M/A constituents. Abson et al. [28] therefore refer to this Widmanstätten ferrite and its associated microphases as “Ferrite with Aligned Martensite Austenite-Carbide”. As to the mechanical properties, Widmanstätten ferrite

in the HAZ is generally regarded as an undesirable constituent because its presence leads to poor toughness; the longer the plates of Widmanstätten ferrite, the poorer the toughness. Figures 10 to 12 (obtained from steel H after a heat input simuation of 20 kJ/cm) show separately, upper bainite, lower bainite and autotempered martensite. It is well known that upper bainite is more brittle than lower bainite. Cleavage fracture is definitely controlled by both the carbide particle size and morphology. The interplate carbides are much coarser in upper bainite and crack easily under the influence of the stress which accumulates as carbides block an active slip band. In steel H the martensite start temperature is about 445 °C and martensite formed at higher temperatures will be autotempered [29]. Autotempered martensite plates are also expected to possess good toughness due to the more uniform distribution of fine carbide particles within their plates. In the 20 kJ/cm heat input simulation specimens of niobium-containing steels, the amounts of bainite and autotempered martensite are very small. Optical micrographs in Figures 5(b) to (d) have shown that for a 20 kJ/cm heat input, the microstructures of the coarse-grained HAZ of niobium-containing steels consisted chiefly of interlocking ferrite plates with small amounts of bainite and Widmanstätten ferrite. Indeed, it is very difficult to distinguish lower bainite from autotempered martensite in the optical micrograph since both phases tend to produce grey etching structures owing to the existence of interplate or interlath carbides.

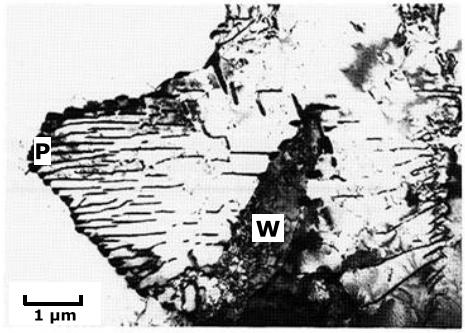

Figure 8. Transmission electron micrograph showing Widmanstätten ferrite obtained from steel O sample after a simulated HAZ thermal cycle at 80 kJ/cm
(W: Widmanstätten ferrite; P: pearlite).

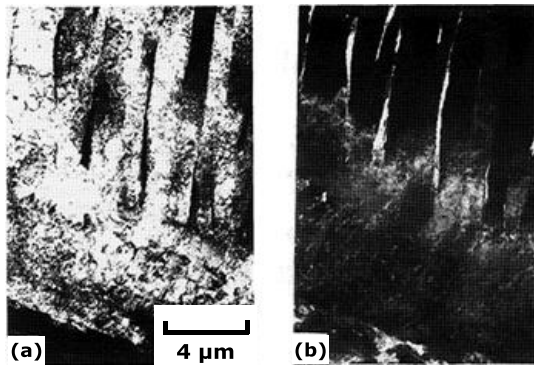

Figure 9. Transmission electron micrographs; (a) bright field and (b) dark field images showing secondary Widmanstätten ferrite obtained from steel H sample after a simulated HAZ thermal cycle at 80 kJ/cm.

Figure 10. Transmission electron micrograph showing upper bainite obtained from steel H sample after a simulated HAZ thermal cycle at 20 kJ/cm.

Figure 11. Transmission electron micrograph showing lower bainite obtained from steel H sample after a simulated HAZ thermal cycle at 20 kJ/cm.

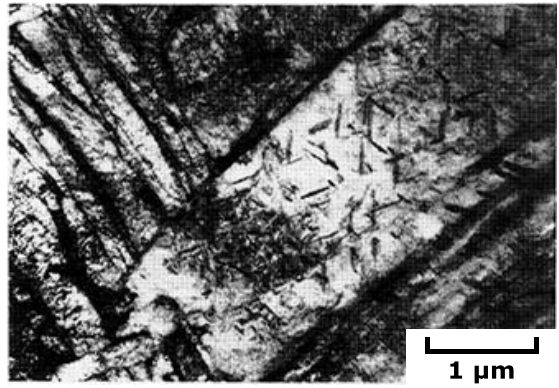

Figure 12. Transmission electron micrograph showing autotempered martensite obtained from steel H sample after a simulated HAZ thermal cycle at 20 kJ/cm.

It is well known that after a high-energy welding process such as submerged-arc or electro-slag welding, the HAZ of niobium-containing steels gives a typical structure of secondary Widmanstätten ferrite. Several authors have asserted [10,20,30] that the effect of niobium on transformation behaviour has been noted as the emergence of the acicular ferrite or bainite. However, there is no detailed transmission electron microscopy to identify the morphologies of acicular ferrite and bainite. The classification of microstructures on the basis of morphology is of considerable importance in the study of structure-property relationships. More research work on this aspect is needed.

Charpy Impact Test

Figure 13 presents the variation of Charpy impact energy as a function of test temperature for the simulated HAZ specimens. At 80 kJ/cm and 50 kJ/cm heat inputs, the niobium containing steels (steels H, M and L) and the niobium-free steel (steel O), possess nearly the same toughness at subzero temperatures as shown in Figures l3(a) and (b). However, at the 20 kJ/cm heat input level, the niobium containing steels have much higher toughness than the niobium-free steel as shown in Figure 13(c). The data also indicates that for the same niobium containing steel the specimens obtained from the simulation of a heat input of 20 kJ/cm possess higher toughness than those obtained from the simulations of heat inputs of 50 kJ/cm and 80 kJ/cm. This result is consistent with the published work [27], which demonstrates that at lower heat inputs an improved toughness is obtained if niobium is added to the steel.

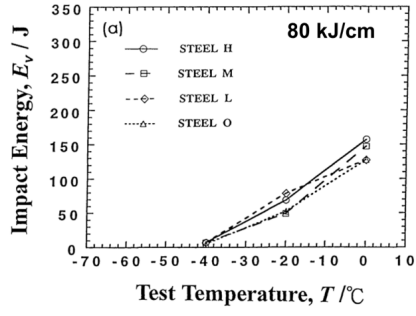

(a)

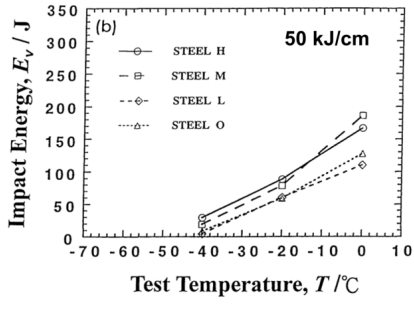

(b)

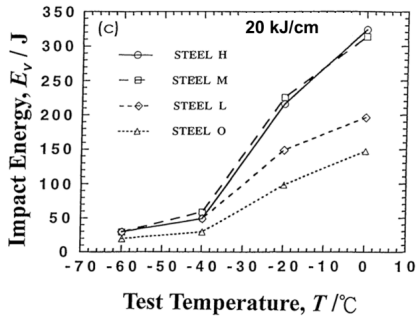

(c)

Figure 13. Plots of Charpy impact energy versus test temperature for four different steels after simulated HAZ thermal cycles at (a) 80 kJ/cm, (b) 50 kJ/cm and (c) 20 kJ/cm.

In the present work the results reflect that the interlocking ferrite structure, which forms in the niobium containing steels after 20 kJ/cm heat input simulation, improves the toughness property. Most studies of low-carbon steels agree that the important structural unit affecting toughness is the cleavage facet size since the cleavage crack is deflected at the packet boundaries. Each packet consists of a group of platelets, which have habit plane poles in close proximity and are essentially the same crystallographic orientation. It is conceivable that the transformation crystallography is vital because this exerts an influence on both the packet size and morphology. Widmanstätten ferrite, having a set of extremely long and parallel ferrite plates in identical orientation, is detrimental to toughness. Indeed, Widmanstätten ferrite leads to a more general condition that groups of plates with a common cleavage plane should be avoided. On the other hand, the reason why the structure of interlocking ferrite plates is a desirable microstructural constituent can be understood as follows. This structure possesses much finer packets which consist of several small platelets; adjacent packets have different habit planes and are different variants of the Nishiyama-Wasserman orientation relationship with austenite. It is suggested that the refinement of packets causes substantial crack deflections and hence improves the toughness of the interlocking ferrite plates microstructure.

Conclusions

An investigation has been made of the simulated heat-affected zone (HAZ) using thermal cycles equivalent to heat inputs of 20 kJ/cm, 50 kJ/cm and 80 kJ/cm in niobium-free and niobium-containing steels. The thermal cycles used corresponded to the actual thermal cycles that occur in the coarse grained region of the real HAZ. The microstructure and toughness of the simulated HAZ have been studied. The important conclusions of this work may be summarised as follows:

1. The results indicate that the addition of niobium can retard the pearlite formation in the steels studied for heat inputs of 50 kJ/cm and 80 kJ/cm; the corresponding microstructures in the coarse-grained region in the niobium containing steels consisted mainly of typical Widmanstätten ferrite, but that in the niobium-free steel was composed of a large amount of pearlite with some Widmanstätten ferrite.

2. At the low energy heat input level (20 kJ/cm), the microstructures in the HAZ of the niobium containing steels consisted mainly of interlocking ferrite plates with a small amount of bainite and Widmanstätten ferrite; whereas the niobium-free steel also contained a small quantity of pearlite.

3. At 80 kJ/cm and 50 kJ/cm heat inputs, the niobium containing steels and the niobium-free steel possessed approximately the same toughness at subzero temperatures. However, at the 20 kJ/cm heat input, the niobium containing steels had much higher toughness than the niobium-free steel. The evidence reflects that the interlocking ferrite structure, which forms in niobium-containing steels after the 20 kJ/cm heat input simulation, improves the Charpy impact toughness property.

Acknowledgement

This work was carried out with the financial support from China Steel Corporation. The authors thank China Steel Corporation for the supply of the steel plates.

References

1. M.J. Crooks et al., "Precipitation and Recrystallization in Some Vanadium and Vanadium-niobium Microalloyed Steels," *Metallurgical Transactions A*, 12 (12) (1981), 1999-2013.

2. H. Abrams et al., *HSLA Steels: Metallurgy and Applications*, (Philadelphia, PA: ASM, 1986), 579.

3. S.S. Hansen, J.B. Vander Sande, and M. Cohen, "Niobium Carbonitride Precipitation and Austenite Recrystallization in Hot-rolled Microalloyed Steels," *Metallurgical Transactions A*, 11 (3) (1982), 387-402.

4. H. Nakasugi, H. Matsuda, and H. Tamehiro, *Steels for Line Pipe and Pipe Line Fittings* (London, UK: Metals Society, 1981), 90-95.

5. H. Ohtani, T. Hashimoto, and T. Kyogoku, *HSLA Technology and Applications* (Philadelphia, PA: ASM, 1983), 843.

6. D. Webster and J.H. Woodhead, "Effect of 0.03% Niobium on the Ferrite Grain Size of Mild Steel," *Journal of the Iron and Steel Institute*, 202 (1964), 987-994.

7. G.T. Eldis and W.C. Hage, *Hardenability Concepts with Application to Steels*, (Warrendale, PA: TMS-AIME, 1978), 397-420.

8. K.J. Irvine, F.B. Pickering, and T. Gladman, "Grain-refined C-Mn Steels," *Journal of the Iron and Steel Instiute*, 205 (2) (1967), 161-165.

9. C. Fossaert et al., "The Effect of Niobium on the Hardenability of Microalloyed Austenite," *Metallurgical and Materials Transactions A*, 26 (1) (1995), 21-30.

10. N. Shams, "Microstructure of Continuous Cooled Niobium Steels," 37 (12) (1985), 21-24.

11. R. Otterberg, R. Sandstrom, and R. Sandberg, "Influence of Widmanstätten Ferrite on Mechanical Properties of Microalloyed Steels," *Metals Technology*, 7 (1) (1980), 397-408.

12. S. Suzuki, G.C. Weatherly, and D.C. Houghton, "The Response of Carbo-nitride Particles in HSLA Steels to Weld Thermal Cycles," *Acta Metallurgica*, 35 (2) (1987), 341-352.

13. J. Strid and K.E. Easterling, "On the Chemistry and Stability of Complex Carbides and Nitrides in Microalloyed Steels," *Acta Metallurgica*, 33 (11) (1985), 2057-2074.

14. R.W.K. Honeycombe and H.K.D.H. Bhadeshia, *Steels - Microstructure and Properties*, 2nd edition, (London, UK: Edward Arnold, 1995), 76.

15. H.K.D.H. Bhadeshia, L-E. Svensson, and B. Gretoft, "A Model for the Development of Microstructure in Low-alloy Steel (Fe-Mn-Si-C) Weld Deposits," *Acta Metallurgica*, 33 (7) (1985), 1271-1283.

16. L. Levine and D.C. Hill, "Structure-property Relationships in Low C Weld Metal," *Metallurgical Transactions A*, 8 (9) (1977), 1453-1463.

17. J.R. Yang and L.C. Chang, "The Effect of Stress on the Widmanstätten Ferrite Transformation," *Materials Science and Engineering A*, 223 (1) (1997), 158-167.

18. H.K.D.H. Bhadeshia, "A Rationalisation of Shear Transformations in Steels," *Acta Metallurgica*, 29 (6) (1981), 1117-1130.

19. C.A. Dube, H.I. Aaronson, and R.F. Mehl, "La Formation de la Ferrite Proeutectoide dans les Aciers au Carbone," *Revue de Metallurgie*, 55 (1958), 201-210.

20. A.J. DeArdo, J.M. Gray, and L. Meyer, *Fundamental Metallurgy of Niobium in Steel* Niobium, (Warrendale, PA: TMS—AIME, 1984), 685-759.

21. C. Fossaert et al., "The Effect of Niobium on the Hardenability of Microalloyed Austenite," *Metallurgical and Materials Transactions A*, 26 (1) (1995), 21-30.

22. J.R. Yang and H.K.D.H. Bhadeshia, "Continuous Heating Transformation of Bainite to Austenite," *Materials Science and Engineering A*, 131 (1) (1991), 99-113.

23. J.R. Yang, C.Y. Huang, and C.S. Chiou, "The Influence of Plastic Deformation and Cooling Rates on the Microstructural Constituents of an Ultra-low Carbon Bainitic Steel," *Iron and Steel Institute of Japan International*, 35 (8) (1995), 1013-1019.

24. Z. Huang and M. Yao, "Effect of Arrangement of Acicular Ferrite in a Widmanstatten Microstructure on the Fracture of Mild Steel," *Materials Science and Engineering* A, 119 (1989), 211-217.

25. J.R. Yang and H.K.D.H. Bhadeshia, "Orientation Relationships between Adjacent Plates of Acicular Ferrite in Steel Weld Deposits," *Materials Science and Technology*, 5 (1) (1989), 93-97.

26. F.J. Barbaro, P. Krauklis, and K.E. Easterling, "Formation of Acicular Ferrite at Oxide Particles in Steels," *Materials Science and Technology*, 5 (11) (1989), 1057-1068.

27. Ø. Grong and O.M. Akselsen, "HAZ Toughness of Micralloyed Steels for Offshore," *Metal Construction*, 18 (9) (1986), 557-562.

28. D.J. Abson and R.E. Dolby, (Document, IXJ-29-80, International Institute of Welding, 1980), 1.

29. R.W.K. Honeycombe and H.K.D.H. Bhadeshia, *Steels-Microstructure and Properties*, 2nd edition, (London, UK: Edward Arnold, 1995), 171.

30. J.M. Gray, "Weldability of Niobium Containing High Strength Low Alloy Steel," *Welding Research Council Bulletin*, 213 (1976), 1.

Fundamentals and Applications of Mo and Nb Alloying in High Performance Steels – Volume 1
Edited by Hardy Mohrbacher
CBMM, IMOA and TMS, 2014

SYNERGIES OF NIOBIUM AND BORON MICROALLOYING IN MOLYBDENUM BASED BAINITIC AND MARTENSITIC STEELS

Hardy Mohrbacher

NiobelCon bvba, 2970 Schilde, Belgium

Keywords: Molybdenum, Niobium, Boron, Recrystallization, Grain Refinement, Hardenability, Secondary Hardening, Quenching and Tempering, Precipitation, Strength, Charpy Toughness, Wear Resistant Plate, HSLA Steels, Phase Transformation, CCT

Abstract

Bainitic and martensitic steels have a great potential for structural as well as automotive applications due to the lean alloying concept and the favorable combination of strength and ductility. These steels are being considered as the material of choice for many advanced applications where yield strengths above 500 MPa are required to reduce component weight. Traditionally Mo has been a key alloying element in producing such steels. In order to expand the envelope of such steels it is interesting to combine Mo alloying with the microalloying element Nb and in some cases B. Cross effects between these elements bear synergies that cannot be achieved by single alloying. This paper demonstrates how these synergies can be beneficially used in combination with appropriate processing.

Introduction

Increasing attention is being paid to the economic advantages that high-strength low-alloy steels have to offer. These advantages include lower structural weight, Figure 1, increased resistance to brittle failure, economies during construction and transportation as a result of lower cost in handling lighter sections, fewer man-hours of welding and lower electrode consumption as a result of lighter sections, Figure 2. The advantages listed are of primary interest to the transportation and materials handling industry where the ratio of payload to dead weight load is of paramount importance. Fringe benefits resulting from this are greater speeds, less fuel consumption per load and smaller sized propulsion units. In addition to strength properties, structural steel selection is concerned with ease of forming, welding and other fabrication procedures. Service conditions require that the steel exhibits good toughness at the temperature of service, thus the candidate steel should possess adequate impact resistance at the lowest temperatures anticipated in service.

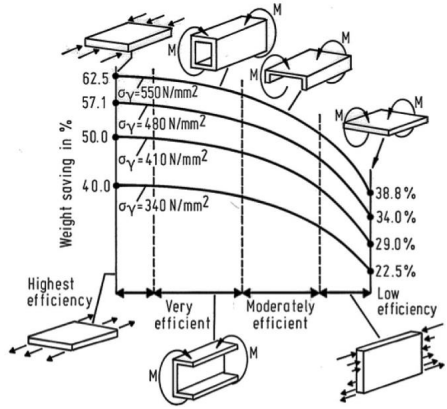

Figure 1. Weight saving potential by substituting 200 N/mm^2 steel with high strength steels for various loading conditions.

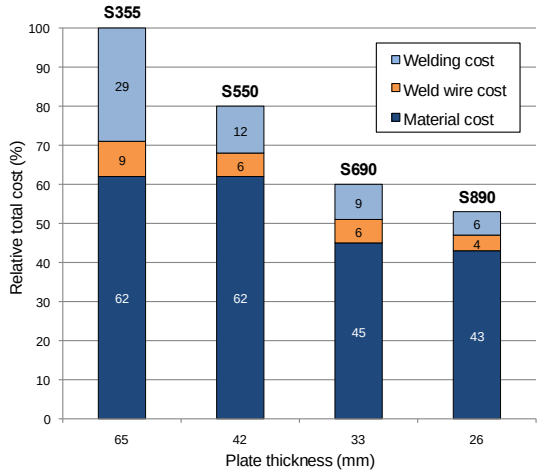

Figure 2. Material and welding cost of higher strength steels relative to S355.

Traditional high strength structural steel is produced based on a carbon-manganese alloy concept having a ferritic-pearlitic microstructure obtained by either normalizing or thermomechanical rolling. Such steels cover a yield strength range of up to around 460 MPa. To make the desired strength, different strengthening mechanisms are employed, Figure 3. The base strength originates from the carbon content ranging up to 0.2%, however increasing the carbon content severely deteriorates the steel's toughness. Solid solution strengthening is mainly obtained by

manganese and silicon bulk alloying. The most important contribution to increasing the strength is grain refinement and the most effective way to achieve this is by Nb microalloying in combination with thermomechanical rolling. Grain refinement is the only strengthening mechanism that also improves toughness. Niobium is, in that respect, by far the most effective element. The dispersion of fine precipitates, typically carbides or nitrides of the microalloying elements, further increases the strength.

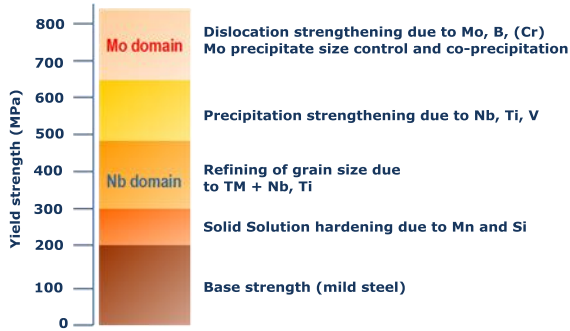

Figure 3. Strengthening effects in HSLA steel.

In modern high strength structural steels with strength levels above 460 MPa, it is necessary to modify the nature of the ferrite matrix and to avoid pearlite formation. One method is to force the austenite-to-ferrite transformation to temperatures below 700 °C and thereby increase the dislocation density and refine the subgrain size. The resulting microstructure is bainite or degenerate ferrite. The two alloying elements that prominently assist this transformation strengthening are molybdenum and boron. To a lesser extent chromium and niobium are also effective in this respect. With such alloy concepts a yield strength level of up to around 800 MPa can be achieved.

The highest strength is still obtained by martensitic microstructures. This microstructure is the result of quenching from austenite, which can be done by a separate heat treatment or directly after finish rolling, Figure 4. In order to obtain a fully martensitic structure, the cooling speed must be sufficiently high across the entire plate cross-section. Alloying of molybdenum and/or boron effectively help to reduce the critical cooling speed for martensite formation. The amount of alloys required depends finally on the gauge to be produced as well as on the cooling capacity of the production line. The strength of quenched martensite is controlled by the carbon content. With applicable carbon contents in the range of 0.1 to 0.2%, the tensile strength ranges from 1200 to 1600 MPa. However, the toughness of fully quenched martensite is quite low. Tempering is necessary in order to produce steels with minimum yield strengths from 690 to 1100 MPa with simultaneous high toughness and good processing behavior. Quenched and tempered steels can be alloyed with chromium, molybdenum, nickel, niobium, boron and vanadium at carbon contents up to 0.2%. During heat treatment this leads to a fine bainitic-martensitic microstructure with optimum strength and toughness properties.

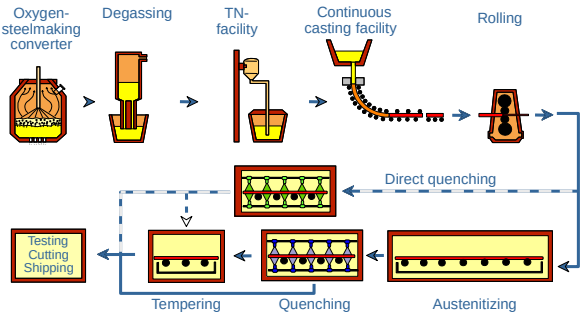

Figure 4. Processing routes for quenched and tempered steel.

Grain Size Control

Recrystallization

The addition of Nb to low carbon steel significantly retards the rate of static recrystallization (SRX). For instance, by microalloying with 0.04%Nb the time for 95% recrystallization (t_{95}) at 1060 °C is around 20 seconds, whereas it takes over 50 seconds to complete the SRX if the Nb content of the steel is increased to 0.095%. Also, an increase in the Mo content from 0.1% to 0.6% leads to a significant retardation of the SRX kinetics, Figure 5. Since it is the aim of roughing rolling to obtain a homogeneous, fully recrystallized austenite microstructure, this effect of Nb and Mo has to be taken into account when designing the rolling schedule. Taking the maximum interpass time in the roughing mill to be 20 seconds, full recrystallization must occur within that period, i.e., t_{95} must be less than the interpass time. This demand determines the temperature range of roughing rolling. On the other hand, the slab discharge temperature has to be considered and this typically has maximum values of 1150 °C and 1250 °C on plate mills and strip mills, respectively. Thus, the processing window, where fully recrystallizing roughing rolling passes can take place, is approximately 80-180 °C for the 0.1%Mo-0.04%Nb alloy, whereas it is reduced to approximately 30-l30 °C for the 0.6%Mo-0.04%Nb alloy.

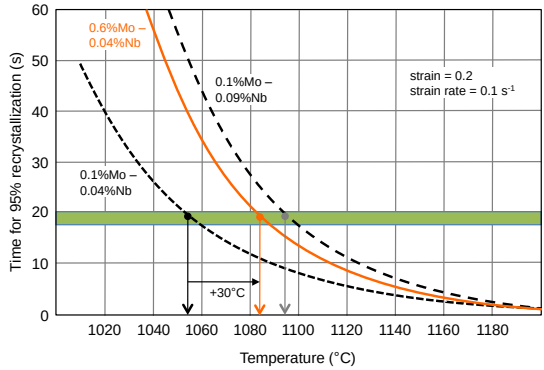

Figure 5. Influence of Mo-Nb alloy combinations on static recrystallization at high temperature.

It is well established that Nb is the most effective element in retarding the static recrystallization (SRX) of austenite at high temperature. This effect of Nb strongly increases up to an addition of 0.06% and then levels off [1]. Mo as a single alloying element does not remarkably retard SRX, however the combination of Mo and Nb leads to a synergetic increase in retardation of SRX. Earlier experiments performed by Akben et al. [2] revealed the effect of Mo additions on the dynamic recrystallization (DRX) of microalloyed steels. When microalloyed steels are deformed above the solution temperature of their respective carbonitrides, the addition of Mo leads to a distinct retardation in the initiation of dynamic recrystallization. The solute retarding effect of Mo alone is intermediate between that of Nb, which has the greatest, and that of V, which has the least effect on an equal atom fraction basis. The addition of B alone can slightly retard SRX. However, when B is combined with Nb the effect is larger than the sum of the separate effects. According to He et al. [3], this has been attributed to the formation of Nb-B complexes exerting a strong dragging force on the grain boundary and hence reducing its mobility. Figure 6 exemplifies these effects for the addition of Mo and B to high-Nb ULCB steel. It is interesting to note that the addition of Ni has an adverse effect promoting SRX. Increasing the recrystallization stop temperature (RST) to values of 900 °C or above results in a particularly large processing window for finish rolling. It also allows reducing or even eliminating the holding period between roughing and finishing. This can significantly improve the productivity of a hot strip mill. Finishing at higher temperatures also reduces the mill loads resulting in less maintenance efforts. The increased recrystallization limit temperature (RLT) by B co-addition however can be a concern, as full recrystallization is desired during roughing. Especially for plate mills, the operating window is narrowed due to the relatively low slab discharge temperature.

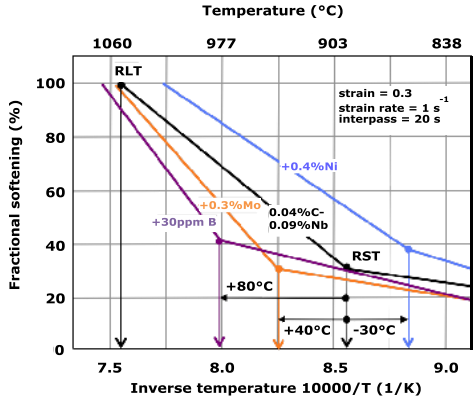

Figure 6. Effects of Mo, B and Ni addition to a low-C high-Nb base alloy on fractional softening behavior.

Strain Induced Precipitation

When Nb microalloyed steel is ausformed below the solution temperature of its carbide or carbonitride, in-situ precipitation of small particles results in a further component of retarding recrystallization. In this case the addition of Mo involves two opposing effects. One is an increased retardation of recrystallization due to its effect as a solute. The other is a decrease in the amount of precipitation due to a reduced activity of C and N, Figure 7. It was observed that the onset of precipitation of Nb in a 0.05%C-0.04%Nb steel takes twice as long when 0.3%Mo is added [2]. More recent results by Cao [4] confirmed this effect and indicated that the precipitation start in a 0.02%C-0.08%Nb steel is delayed by one order of magnitude after adding 0.15%Mo. It is evident that an increased portion of Nb can be retained in solid solution. Nb prevailing in solid solution after finish rolling has a significant capability to reduce the transformation temperature. Solute Mo and Nb strongly reduce the diffusivity of carbon in austenite as indicated by Figure 8 [5]. This effect is stronger for Nb than for Mo. However, Nb's solubility is limited and decreases with temperature whereas Mo remains fully soluble. Since Mo retards the Nb precipitation, as explained above, their individual effects on reducing the carbon activity are additive in dual alloyed steel. Hara et al. [6] have explained the effect of reduced carbon activity by Nb-C or Mo-C cluster formation. Microalloying elements available in solid solution after finish rolling have two important effects. Firstly, they delay the transformation from austenite to ferrite to a lower temperature. This effect increases with the cooling speed, Figure 9. Secondly, solute microalloying elements have the potential to precipitate during or after the phase transformation to a much finer particle size than that of precipitates formed in austenite. These precipitates can provide effective strengthening also known as secondary hardening.

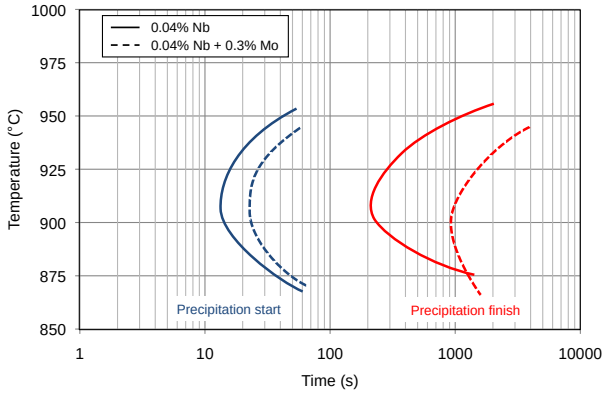

Figure 7. Influence of Mo addition on the strain induced precipitation behavior of Nb.

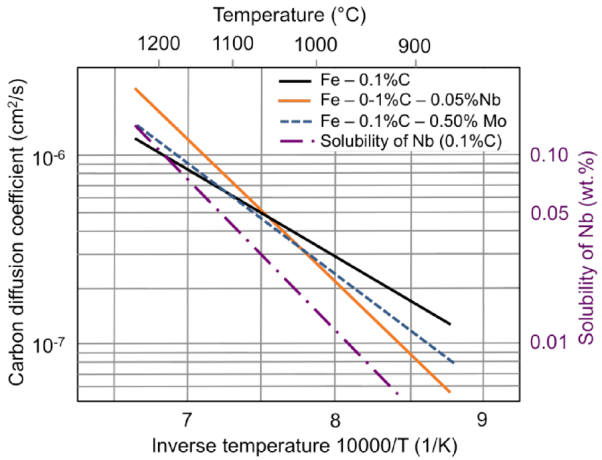

Figure 8. Solubility of Nb in 0.1%C steel and influence of solute Mo and Nb on the diffusivity of C.

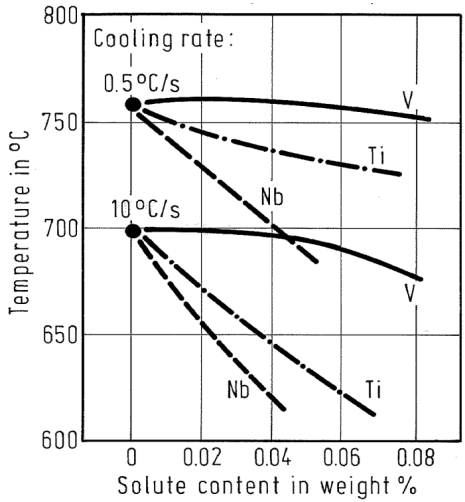

Figure 9. Effect of solute microalloying elements on the γ–α transformation temperature.

Hardenability

Molybdenum's effect of reducing the carbon activity was also found to be beneficial with respect to boron-alloyed steels. Boron is a very powerful hardenability element that is added to steel in minute amounts, usually not more than 50 ppm. As such it is used in (ultra-) low carbon bainitic steels as well as in quench-hardening steels. The effectiveness of boron in providing hardenability is based on its segregation to the austenite grain boundaries where it obstructs the formation of grain boundary ferrite at transformation temperature. This mechanism is however only possible if B is in solid solution. Since B is a strong nitride former, Ti is usually added at around stoichiometric ratio (Ti = 3.4×wt%N) to protect B, however, B can still be lost by forming a complex $Fe_{23}(C,B)_6$ precipitate. This happens at the austenite grain boundary, particularly when increased amounts of B and C are present due to segregation. Asahi [7] and Hara et al. [6] have identified this phenomenon for steels with ultra-low as well as hyper-peritectic carbon contents. In both cases the addition of Mo and/or Nb to the alloy improved the effectiveness of B. Nb in contrast to Mo has a limited solubility, which depends on the carbon content.

Besides rendering a better effectiveness of boron in preventing grain boundary ferrite formation, molybdenum acts as a hardenability element by itself. This effect of Mo additionally enhances the B effect as becomes evident from Figure 10 [6]. Compared to the Nb-B steel where only B acts as a hardenability agent, the Mo-B steel shows a lower transformation temperature as well as a higher hardness at any cooling rate. Figure 11 exemplifies the hardenability effect of molybdenum by adding different levels of Mo to a constant low carbon Mn-Cr base alloy [8]. Each alloy was heated to a temperature of 50 °C above the Ac3 temperature and held for

10 minutes. Afterwards the alloy was cooled at various rates and the microstructure was evaluated. Adding 0.25% Mo to the base composition significantly delays pearlite formation and lowers the transformation temperature. Simultaneously, the bainite field is greatly extended. As such, practically at all technically relevant cooling rates, a ferritic-bainitic microstructure is obtained. Increasing the Mo content further to 0.5% leads to a delay of ferrite formation and a complete suppression of pearlite formation. At cooling rates of above 30 K/s a fully bainitic microstructure exists. More detailed analysis of the bainitic phase revealed that the block size decreases with increasing Mo content whereas the misorientation angle between bainite laths, as well as the dislocation density, increases. These effects result in an increased hardness (strength) of bainite as the Mo content is raised. Increasing the cooling rate at a constant Mo content leads to the same effects. Simplified, this means that raising the Mo content in such low carbon steel can substitute for lack of cooling rate. This is relevant to mills equipped with less powerful accelerated cooling devices. On the other hand, Mo helps to achieve bainitic transformation and sufficient strengthening for heavier gauged strip or plate material.

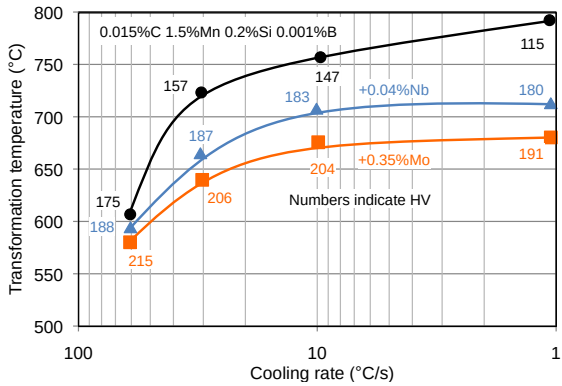

Figure 10. Effect of cooling rate on transformation temperature and hardness in ULCB steel with B, Nb-B and Mo-B alloying.

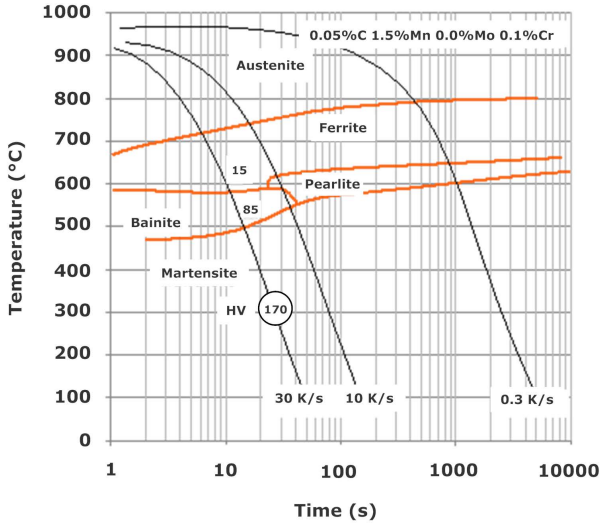
0.05%C 1.5%Mn 0.0%Mo 0.1%Cr
Austenite
Ferrite
Pearlite
Bainite
Martensite
15
85
HV
170
30 K/s
10 K/s
0.3 K/s
Temperature (°C)
Time (s)
1000
900
800
700
600
500
400
300
200
100
0
1
10
100
1000
10000

(a)

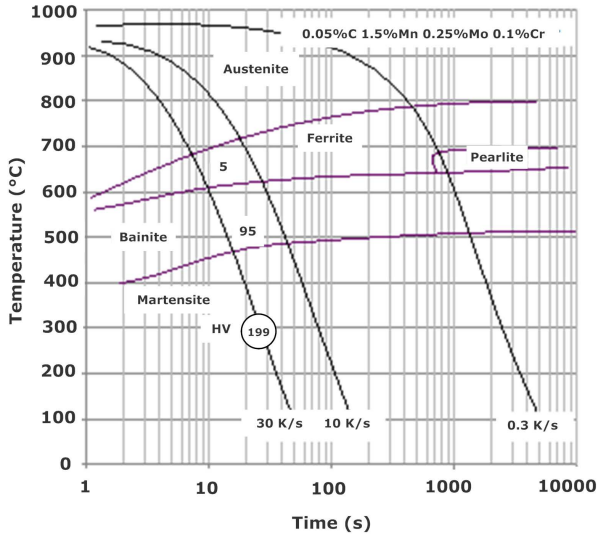
0.05%C 1.5%Mn 0.25%Mo 0.1%Cr
Austenite
Ferrite
Pearlite
Bainite
Martensite
5
95
HV
199
30 K/s
10 K/s
0.3 K/s
Temperature (°C)
Time (s)
1000
900
800
700
600
500
400
300
200
100
0
1
10
100
1000
10000

(b)

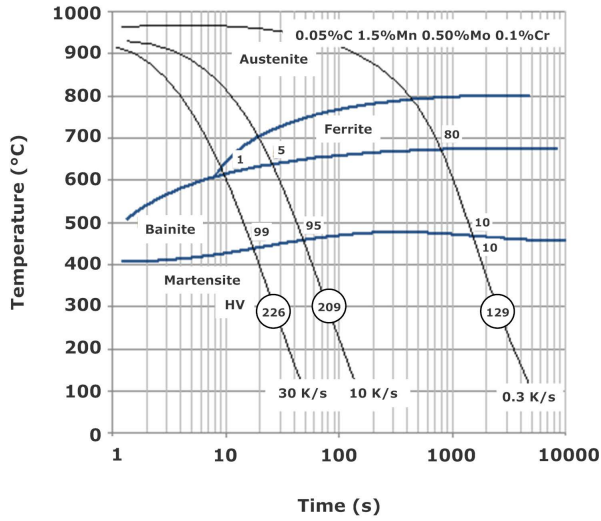

(c)

Figure 11. Effect of Mo alloying on the transformation behavior of a low-carbon base alloy (heating to A_{c3}+50 °C – holding for 10 minutes without deformation – cooling at various rates); (a) 0.05%C, 1.5%Mn, 0.0%Mo, 0.1%Cr, (b) 0.05%C, 1.5%Mn, 0.25%Mo, 0.1%Cr, (c) 0.05%C, 1.5%Mn, 0.50%Mo, 0.1%Cr.

Dissolved Nb and Mo substantially delay ferrite formation by reducing carbon diffusivity and exerting a strong drag force on moving grain (phase) boundaries. Other bulk alloying elements like Mn and Ni also delay ferrite formation, however the effectiveness of Mo is about 3x and 6x stronger than that of Mn and Ni respectively [9]. Besides alloying, two processing variables have a great influence on ferrite formation. Increasing the cooling rate (CRt) after finish rolling suppresses ferrite formation and reduces the transformation temperature. On the contrary, increasing the final deformation in the non-recrystallizing regime promotes ferrite nucleation and increases the transformation temperature. Figure 12 demonstrates the influence of process variables in combination with different alloy concepts. The bainite start (Bs) temperature increases with the accumulated deformation in austenite, Figure 12(a). Mo-Nb steels have a similarily low sensitivity of the Bs temperature to the degree of deformation. A higher Nb content in the Mo-alloyed HTP steel further raises the Bs temperature since in this steel recrystallization is very strongly suppressed and hence the driving force for transformation is particularly high. Adding boron to Mo-Nb steel results in a significant decrease of the Bs temperature in the undeformed austenite. Under this condition B can easily segregate to the austenite grain boundary. Deforming austenite in the non-recrystallizing regime enhances the austenite grain boundary area and generates deformation bands inside austenite grains that can act as nucleation sites.

The effectiveness of B is then reduced. Increasing the Mo content is the most efficient way of decreasing the Bs temperature in strain-accumulated austenite. This holds for all cooling rates, Figure 12(b). In Mo-Nb steels the Bs temperature is quite sensitive to the CRt. Adding B to the steel strongly reduces the CRt sensitivity. The Bs temperature has a direct influence on the strength of the steel, Figure 12(c). The present data indicate that the strength increases by approximately 17 MPa for every 10 °C reduction of the Bs temperature. This change is similar in magnitude for yield and tensile strength. In an earlier study, Wang et al. [9] found the influence to be around 15 MPa per 10 °C reduction of the Bs temperature. Bai et al. [10] investigated the influence of CRt and strain on the formation of transformation products in ultra low carbon steels. It can be concluded that Nb in combination with high deformation, under industrially feasible CRt, results in the partial formation of polygonal ferrite (PF) thereby reducing strength. The addition of B alone is not sufficient to prevent PF formation. However the further addition of Mo significantly facilitates the formation of bainitic microstructures under industrially achievable conditions.

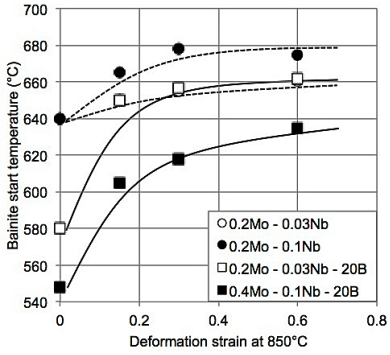

(a)

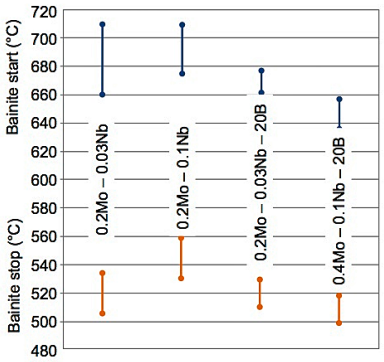

(b)

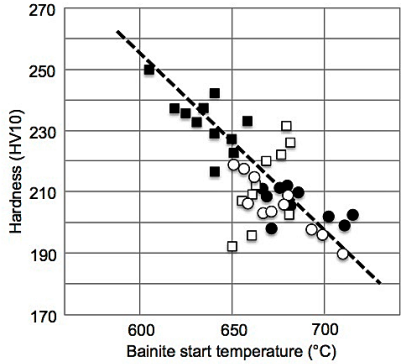

(c)

Figure 12. (a) Effect of Mo, Nb and B on bainite start temperature in 0.03%C steel at a cooling rate of 15 K/s, (b) bainite start and stop temperatures in 0.03%C steel; strain ε=0.6 at 850 °C; cooling rates: 1 – 15 K/s; Mo, Nb, B variable, other alloying elements constant, (c) hardness as a function of bainite start temperature (symbols correspond to (a)).
All compositions in wt% except B ppm.

Secondary Hardening

Nb has the lowest diffusivity and solubility in ferrite of the three carbide-forming microalloying elements (Nb, Ti, V). Both properties together promote the formation of very fine precipitates. NbC also has the largest lattice parameter of the three MC carbides consequently resulting in higher interfacial distortion for coherent precipitates, and thus in more effective strengthening. Obtaining the maximum precipitation strengthening effect depends furthermore on optimized selection of cooling pattern after finish rolling. Table I indicates the time – temperature dependence of precipitation strengthening in a 0.03%C steel alloyed with either Nb (0.02%) or Mo (0.15%) – Nb (0.10%) by isothermal holding at 600 °C and 650 °C after finish rolling at 930 °C and fast cooling at a rate of 30 °C/s. The isothermal holding time was varied between 5 and 60 minutes. From the results (Table I) it can be concluded that the Nb steel requires a lower holding temperature and shorter holding time to achieve optimum precipitation strengthening [11]. At longer holding times the Nb steel loses strength due to Ostwald ripening. The Mo-Nb steel has superior strength for any of the simulated isothermal conditions. It can be concluded that Mo delays the precipitation of NbC and obstructs Ostwald ripening [12,13]. The latter effect is well known and is being utilized for instance in fire-resistant steel [14].

Table I. Influence of Isothermal Holding Temperature and Time on Precipitation Strengthening in 0.03%C Steel with Nb and Mo-Nb Addition

	Isothermal holding for 1h		**Hardness change during isothermal holding time**	
	YS (MPa)	**TS (MPa)**	**5 → 30 min**	**30 → 60 min**
Nb/600 °C	458	602	+22	-53
Mo-Nb/600 °C	670	670	+16	+42
Nb/650 °C	429	575	-19	-17
Mo-Nb/650 °C	690	670	+11	+12

The combination of low carbon content, Mo alloying and fast cooling provides conditions for maintaining a substantial amount of Nb in solid solution after finish rolling. This Nb is available for nano-precipitation either by a secondary heat treatment (plate) or by appropriate coiling conditions (hot strip). Simulation of a DQ treatment with subsequent tempering at 600 °C for one hour, Figure 13(a), was used to estimate the strengthening potential at various C and Nb contents. It is obvious that with an enhanced amount of both elements the yield strength significantly increases. It is however not exactly clear how much C and Nb were effectively available to form fine precipitates and how much other carbide formers such as Mo and Cr were involved. Nevertheless, for the samples with a C content below 0.02% conditions were such that an interstitial free (IF) matrix can be obtained by carbide precipitation. In this case the DBTT (Ductile Brittle Transition Temperature) is further reduced to a level of below -100 °C, Figure 13(b). The higher C content leads to a more pronounced precipitation hardening. This also results in a loss of toughness, as expected. The increase in DBTT is moderate for the 0.05%Nb steels, yet quite significant in the 0.1%Nb steel. In the latter steel, Nb at full precipitation binds about 0.014%C. Since this steel also contains a relatively high amount of Mo it is possible that additionally Mo_2C precipitates have been formed. The needle-shaped morphology of Mo_2C precipitates can be harmful to impact properties [15]. Therefore a suitable balance between different carbide forming elements as well as appropriate tempering conditions has to be achieved in order to avoid precipitation of Mo_2C.

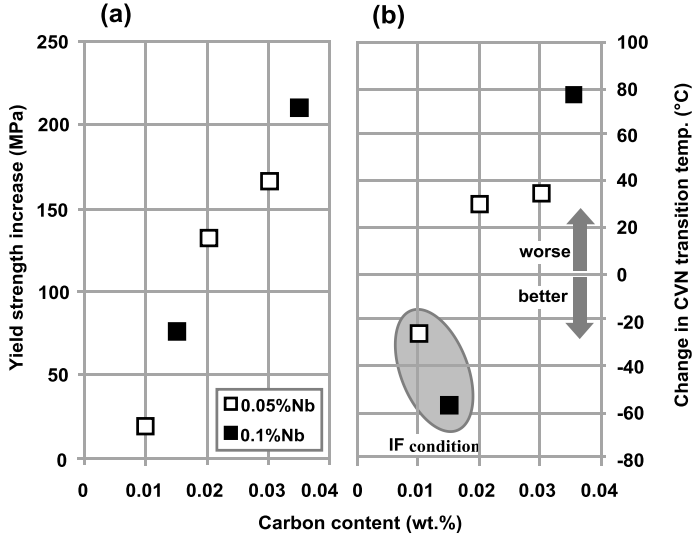

Figure 13. (a) Precipitation hardening effect after DQ cooling and subsequent tempering at 600 °C/1h in Mo-Nb ULCB steels, (b) corresponding change in the DBTT.

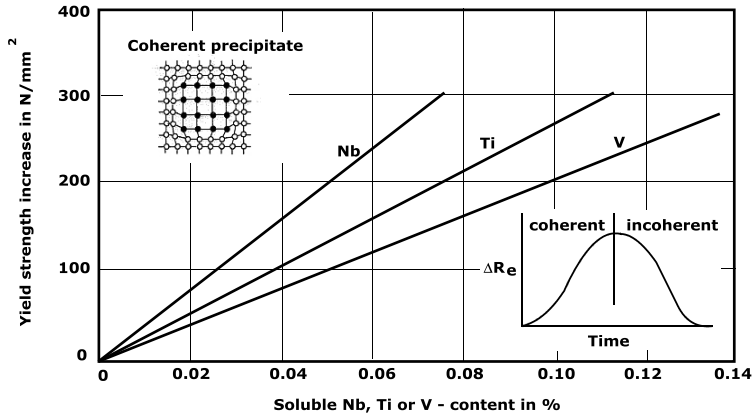

Figure 14. Strength increasing potential of microalloying elements by coherent precipitation.

The strengthening potential of nano-sized coherent precipitates of microalloying elements is in the order of 300 MPa, Figure 14. The actual strength increase by precipitation hardening depends on the amount (i.e. soluble microalloy content) and distribution of such particles. Furthermore, the lattice distortion and thus the resulting stress field at the particle-matrix interface is controlled by the lattice constant of the carbide species. The larger lattice constant of NbC as compared to that of TiC or VC consequently results in a higher strengthening potential of NbC for the same amount and size distribution of particles.

Advanced Processing Concepts

Direct Quenching of Plate

When producing steels of the highest strength level, quenching & tempering is an often-used treatment. The rolled material after cooling down from rolling is re-austenitized and then quenched, Figure 4. This results in a very strong but often brittle material. Subsequent tempering provides a much better toughness and ductility at the expense of strength. Molybdenum effectively enhances the so-called tempering resistance, which counteracts the loss of strength as described by Krauss [16].

In more recent processing concepts, the rolled material is fast cooled immediately after finish rolling. Depending on the cooling severity and the cooling stop temperature, the following cooling variants can be distinguished for plate mills [17]:

- ACC (Accelerated cooling) results in cooling with ideal cooling rate, i.e. the difference of cooling rate between surface and center is kept low.
- HACC (Heavy ACC) is a special variant of the classical ACC but with a lower final cooling temperature and somewhat higher cooling rate.
- DQ (Direct Quenching) with fastest possible cooling of the surface, similar to conventional quenching. The center of the plate is also cooled to below the martensite-start temperature by means of continuation of cooling.
- DQST (DQ + Self Tempering) means that the center heat still present is exploited after an extremely short cooling time and self-tempering is achieved.

Compared to the traditional Q&T procedure, DQ or DQST have the decisive difference that the steel only goes once through the α–γ phase transformation (instead of 3 times in conventional Q&T). Accordingly, the microstructure of the finish-rolled austenite has an influence on the properties of the quenched material, as it will not be normalized. The microstructure before direct quenching depends on the hot-rolling schedule. If the finishing temperature is above the recrystallizing stop temperature (HR = hot rolling), the austenite grain shape will be equiaxed and relatively coarse. On the contrary, if finish rolling is done below the recrystallization stop temperature (CR = controlled rolling), the austenite grain is elongated in the rolling direction and flattened in the normal direction.

Applying either of the rolling schedules to a 0.15%C-Mn-B steel without and with 0.25% Mo leads to the following results [18]:

- Strength and toughness are better for the HR/DQ than for the CR/DQ route in the Mo-free steel. The strength of the CR/DQ material is particularly low since ferrite has formed along the boundaries of the former austenite grains.
- The strength of the Mo-added material is nearly equal for the HR/DQ and CR/DQ material and in both cases significantly better than for the Mo-free steel.
- When comparing the toughness of HR/DQ treated steels, the Mo-free material performs better.
- The toughness of the Mo-added steel considerably improves when applying the CR/DQ route.

These differences can be explained by the cross effects between Mo and B as indicated before in Figure 9. In the Mo-free steel, part of the boron precipitates as $Fe_{23}(C,B)_6$ and is not available for hardenability. In the absence of free B at the austenite grain boundary, ferrite nucleation is facilitated, particularly when the finish rolling temperature is coming close to the A_{c3} temperature. Based on experiments by Asahi [7] with 0.15%C-Mn-B steels, the critical cooling rate to obtain 90% of the full martensite hardness is thus higher in the Mo-free steel, especially when the B-content is below 20 ppm, Figure 15.

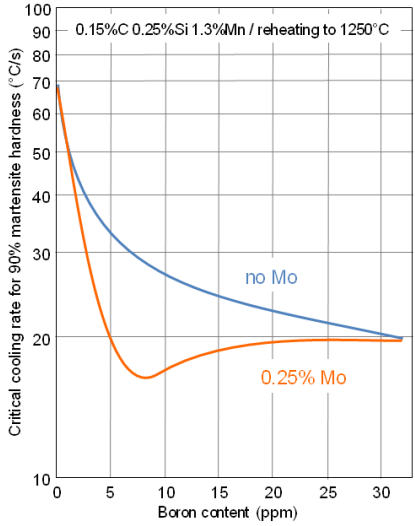

Figure 15. Influence of Mo on the effectiveness of B alloying with regard to the critical cooling rate to obtain 90% martensite hardness.

On the other hand, solute boron at grain boundaries reduces the cohesive forces that hold neighboring grains together, and thereby reduces impact toughness through grain boundary decohesion. This is seen as an increase in the fracture appearance transition temperature (FATT) with increasing free boron content in the steel, Figure 16 [19]. Consequently, grain boundary precipitation of boron carbide and boride particles improves toughness by essentially removing boron from (segregated) solid solution in the vicinity of the grain boundary, which explains the better HR/DQ toughness of the Mo-free steel. The toughness improvement in the Mo-added CR/DQ steel is related to the obstruction of crack propagation by the elongated austenite grain structure.

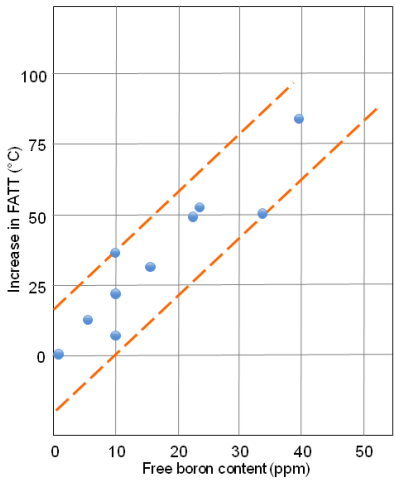

Figure 16. Influence of the free B content (not fixed as BN) on the fracture appearance transition temperature (FATT) in 0.10-0.12%C steels.

An alternative alloy design for good quench hardenabilty is Mo-Ni steel. When subjecting such an alloy concept to HACC or DQ cooling the obtained base microstructure is granular bainite, being a mixture of irregular ferrite with second phases (MA, bainite, or pearlite) distributed between the irregular ferrite grains [20]. Due to molybdenum's effect of retarding pearlite formation, only martensite-austenite (MA) or bainite are expected to appear as second phases. Figure 17 shows the yield-tensile behavior for the two cooling concepts. It is obvious that the DQ route leads to the highest tensile strength, yet the yield strength is lower than from the HACC route. Considering the yield ratio, the DQ route results in a particularly low value, as is typical for ferritic-martensitic dual phase steel. Therefore it is reasonable to assume that the second phase is MA in the DQ route. In the HACC route the yield ratio is much higher, indicating that bainite is the second phase. Adding Nb at different levels to this Mo-Ni alloy, the strength significantly increases for both routes. In the HACC route the yield ratio stays nearly constant whereas in the DQ route it increases. This indicates that the addition of Nb changes the

microstructure of the second phase towards bainite. Toughness is lowest for the Mo-Ni steel without Nb produced via the DQ route and significantly increases with the addition of Nb. In the HACC route, toughness is on a high level for all alloys.

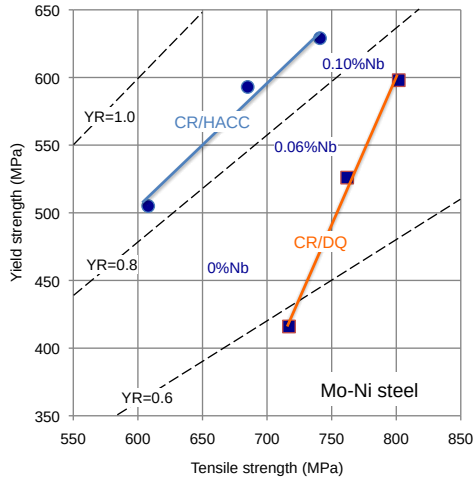

Figure 17. Influence of the cooling route on the strength of 0.07%C-0.2%Mo-0.3%Ni steel and effects of Nb alloying.

When applying a tempering treatment to the DQ route produced material, competing mechanisms such as the Cottrell effect, recovery and secondary precipitation influence the strength as shown in Figure 18. The tensile strength is decreasing for tempering temperatures up to around 550 °C, which is mainly due to a reduction of strength of the second phase. The regaining of strength in the tempering range of 550 to 650 °C is due to secondary precipitation, which is more pronounced in a Mo-Ni-Nb steel. The yield strength however shows a significant increase at low tempering temperatures due to pinning of mobile dislocations by carbon diffusion (Cottrell effect). This effect is most pronounced in the low yield ratio (Mo-Ni) steel. Secondary precipitation hardening is stronger in the Nb-added steel, indicating that a substantial amount of Nb is in solid solution. It is widely known that solute Mo and Nb have the effect of retarding the climb motion and recovery of dislocations as well as grain boundary migration. In low-carbon HSLA steel these solute elements retard dislocation recovery at temperatures up to 550 °C [21]. This can explain the moderate loss of strength in the Nb-added steel when tempering in the range of 400-500 °C. The retention of dislocation networks also has a beneficial secondary precipitation effect since such defects act as nucleation sites during tempering [22].

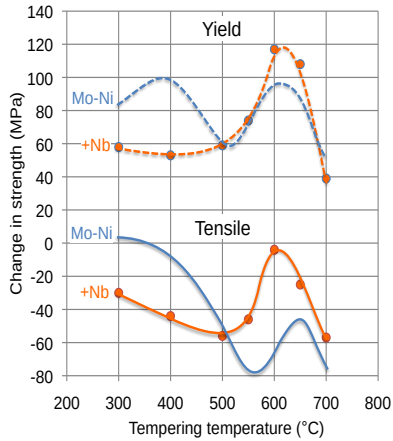

Figure 18. Influence of tempering temperature (30 min.) on the yield and tensile strength of 0.07%C-0.2%Mo-0.3%Ni steel and cross effects of Nb alloying.

Wear Resistant Plate

Machines and equipment for industry, mining, agriculture and other constructions often require heavy plates, which have to guarantee good wear resistance. The most typical application is for machines to excavate raw materials such as coal, ores, stone, etc. These steels comprise as characteristic alloying elements manganese, chromium, molybdenum and nickel and are based on carbon levels up to 0.40%. Consequently they attain high hardness values of 400 to 600 HB (Brinell Hardness), Table II. Typical plate thicknesses range up to 100 mm. The characteristic wear type in most applications is ploughing leading to abrasive wear. Thereby, usually the plate surface gets scratched when exposed to an abrasive and hard material such as sand or other minerals. High hardness of the material is one important feature for good wear resistance. Furthermore, a higher toughness of the material improves the wear resistance and thus reduces material loss.

The necessary high hardness is achieved by quenching the plate into a martensitic microstructure. The hardness of the as-quenched martensite directly correlates with the amount of carbon. For sufficient through-hardenability, especially of heavier plate gauge, the addition of alloying elements such as Mo, Ni, Cr, and Mn are used. Their hardening capabilities are demonstrated in Figure 19 for a 0.4%C steel (600 HB class). It is evident that Mo is particularly powerful in raising the hardening depth. To limit the Mo content to a maximum of 0.5% a micro-addition of boron (typically 20 ppm) can be used as a hardness booster. In this case, boron has to be protected from combining with nitrogen by microalloy additions of Ti or Nb plus Al. The Nb+Al combination was shown to be successful in reducing the free N to a level below which BN formation is suppressed. A substantially finer particle dispersion, which is beneficial for toughness, exists in the Nb microalloyed steel due to the lower formation temperatures of the AlN and Nb(C,N) particles compared to TiN [23].

Table II. Chemical Composition Boundaries for Abrasive Resistant Steel Plates

Target hardness (HB)	Max. plate gauge (mm)	Base alloy composition (max. %)						Typ. CET* (%) at gauge	
		C	Si	Mn	Cr	Ni	Mo	8 mm	40 mm
400	100	0.20	0.80	1.50	1.00		0.50	0.26	0.37
450	100	0.22	0.80	1.50	1.30		0.50	0.38	0.38
500	100	0.28	0.80	1.50	1.00	1.50	0.50	0.41	0.41
600	40	0.40	0.80	1.50	1.50	1.50	0.50	0.55	0.55

*CET = C + (Mn+Mo)/10 + (Cr+Cu)/20 + Ni/40

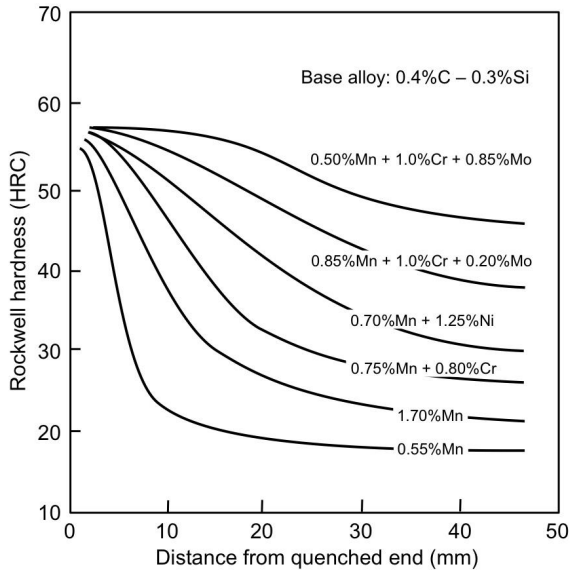

Figure 19. End quenching curves demonstrating the effect of various alloy combinations on through-hardenability.

Toughness is an important property for the application of wear plates and there are several ways of improving it. A common method is tempering of the as-quenched plate. This treatment leads to a trade-off of properties as hardness is reduced and toughness is increased. Sufficient additions of Mo and optional microalloying of Nb counteract the hardness loss under a given tempering condition by increasing the tempering resistance as shown in Figure 20. Toughness decreases with increasing hardness of untempered martensite according to Figure 21. However, there are metallurgical methods to still improve toughness at a given hardness level. It is beneficial to keep impurity levels of P, S and N as low as possible. P segregates to prior austenite grain boundaries reducing grain boundary cohesion. S can form MnS inclusions that are much softer than the martensitic matrix. Excessive N leads to the formation of coarse TiN particles, which can act as crack initiation sites. Adding Nb has the effect of refining the prior austenite grain structure. In

martensitic steels intragranular fracture propagates primarily interfacially along martensite lath boundaries. Lath boundaries develop within the prior austenite grain. The propagating intragranular crack is forced to stop or to change direction at the prior austenite grain boundary. Intergranular fracture separates prior austenite grain boundaries during propagation. Hence, refining the prior austenite grain size requires more energy for the crack to propagate and is thus beneficial. Figure 22 demonstrates the toughness increasing effect of Nb microalloying in a 450 HB grade. Over the entire range of testing temperatures the impact resistance is substantially improved. Additionally, alloying of Mo can help prevent P segregation to the austenite grain boundaries and thus counteract the P-induced loss of grain boundary cohesion [24]. This is particularly helpful when the steel shop has difficulties achieving ultra-low P levels. Studies on abrasive wear properties showed that the better toughness in the niobium microalloyed steel also results in an improvement of the wear resistance due to a change in wear mechanism. Under a given test condition of abrasive wear by hard minerals on a 450 HB grade, the service life could be increased by around 20% using niobium microalloying [25].

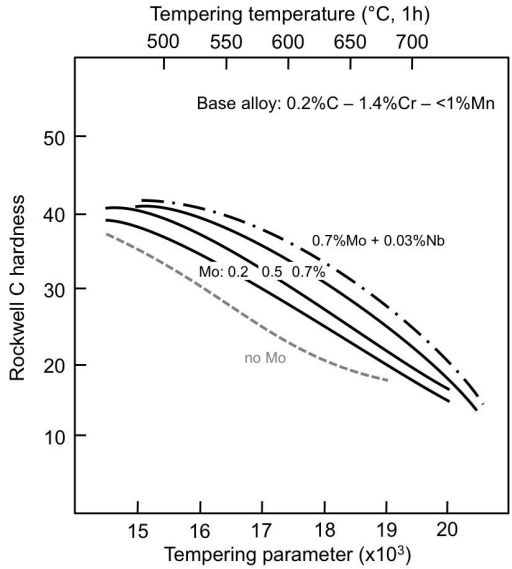

Figure 20. Effect of increasing Mo additions and Nb microalloying on the tempering resistance.

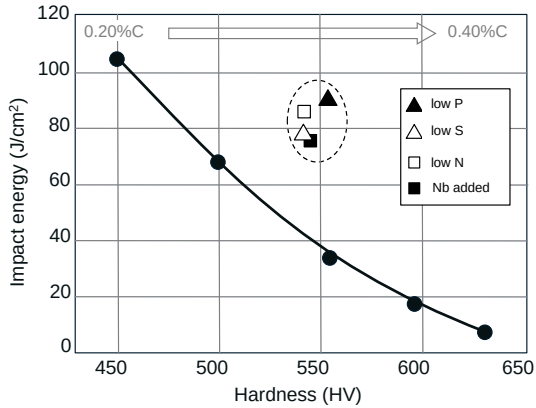

Figure 21. Dependence of impact toughness on hardness (C-content) of as-quenched martensite and metallurgical methods of increasing toughness.

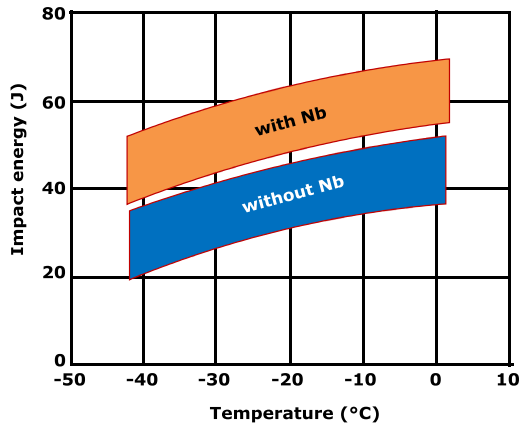

Figure 22. Toughness as a function of impact temperature for 450 HB abrasive resistant plate steels without and with Nb microalloying.

Conclusions

Additions of Mo and Nb to low carbon plate steel allow an increase in both yield and tensile strength. The two alloying elements have beneficial individual effects and reveal interesting synergies when alloyed in combination. Nb is particularly effective in retarding recrystallization. This is the basis for efficient grain refinement thus improving strength and toughness simultaneously. Secondly, Nb provides a high potential for precipitation hardening. Mo is a potent hardenability element as it retards ferrite formation and lowers the bainite transformation temperature. It also assists Nb in retarding recrystallization and optimizes the precipitation hardening effect of Nb. Both elements significantly enhance the tempering resistance. The simultaneous presence of solute Mo or Nb also increases the effectiveness of B microalloying. Solute B segregated to the austenite grain boundaries efficiently inhibits pro-eutectoid ferrite nucleation. On the other hand, B strongly enhances the recrystallization retarding effect of Nb. A well-considered coordination of these alloying elements with the plate processing conditions is required to exploit their metallurgical effects and thus obtain the optimum mechanical properties [22].

References

1. L. Cuddy and J. Raley, "Austenite Grain Coarsening in Microalloyed Steels," *Metallurgical Transactions A,* 14 (10) (1989), 1989-1995.

2. M.G. Akben, B. Bacroix, and J. Jonas, "Dynamic Precipitation and Solute Hardening in AV Microalloyed Steel and Two Nb Steels Containing High Levels of Mn," *Acta Metallurgica,* 29 (1) (1981), 111-121.

3. X. Wang and X. He, "Effect of Boron Addition on Structure and Properties of Low Carbon Bainitic Steels," *Iron and Steel Institute of Japan International*, 42 (S38-S46) (2002), 38.

4. J. Cao, "Study on the Precipitation of Carbonitride in Nb-Mo-bearing Steel" (Dissertation, Kunming University of Science and Technology, 2006).

5. T. Tanaka and T. Enami, "Metallurgical Variables Involved in Controlled Rolling of High Tensile Steels and Its Application to Hot Strip," *Tetsu-to-Hagane*, 58 (13) (1972), 1775-1790.

6. T. Hara et al., "Role of Combined Addition of Niobium and Boron and of Molybdenum and Boron on Hardnenability in Low Carbon Steels," *Iron and Steel Institute of Japan International*, 44 (8) (2004), 1431-1440.

7. H. Asahi, "Effects of Mo Addition and Austenitizing Temperature on Hardenability of Low Alloy B-added Steels," *Iron and Steel Institute of Japan International*, 42 (10) (2002), 1150-1155.

8. M. Masimov and N. Kwiaton, "A Study of Mo-induced Bainitic Transformation in Continuously Cooled Steels by X-ray and Electron Diffraction" (Paper presented at Euromat 7-10 September 2009, Glasgow).

9. S. Wang and P. Kao, "The Effect of Alloying Elements on the Structure and Mechanical Properties of Ultra Low Carbon Bainitic Steels," *Journal of Materials Science,* 28 (19) (1993), 5169-5175.

10. D. Bai et. al, "Effect of Deformation and Cooling Rate on the Microstructures of Low Carbon Nb-B Steels," *Iron and Steel Institute of Japan International,* 38 (4) (1998), 371-379.

11. Y. Ohmori, Trans. *Iron and Steel Institute of Japan International,* 15 (1975), 194.

12. R. Uemori et al., "AP-FIM Study on the Effect of Mo Addition on Microstructure in Ti-Nb Steel," *Applied Surface Science,* (76) (1994), 255-260.

13. Y. Funakawa and K. Seto, "Coarsening Behavior of Nanometer-sized Carbides in Hot-rolled High Strength Sheet Steel," *Materials Science Forum*, 539-543 (2007), 4813-4818.

14. R. Chijiiwa et al., "Development and Practical Application of Fire Resistant Steel for Buildings," (Nippon Steel Technical Report, Japan, 1993), 47-55.

15. S. Yamasaki and H. Bhadeshia, "Modelling and Characterisation of Mo 2 C Precipitation and Cementite Dissolution During Tempering of Fe–C–Mo Martensitic Steel," *Materials Science and Technology*, 19 (6) (2003), 723-731.

16. G. Krauss, "Heat-treated Low-alloy Carbon Steels: The Benefits of Molybdenum" (Paper presented at the Proceedings of the International Seminar on Applications of Mo in Steels, Beijing, 2010), 13.

17. H.J. Kirsch et al., "New Property Combinations in Heavy Plate via the Accelerated Cooling Process," *Stahl und Eisen,* 119 (3) (1999), 57.

18. C.S. Lee and W.Y. Choo, *Proceedings from Materials Solutions '97 on Accelerated Cooling/Direct Quenching Steels,* ASM (1997), 51.

19. A.P. Coldren, R.L. Cryderman, and N.L. Semchysheh, "Strength and Impact Properties of Low-Carbon Structural Steel Containing Molybdenum" (Report, Climax Molybdenum Company).

20. V. Schwinn, P. Fluess, and D. Ormston, "Low Carbon Bainitic TMCP Plate for Structural and Linepipe Applications," *Proceedings of Recent Advances of Niobium Containing Materials in Europe,* Verlag Stahl Eisen (2005), 43.

21. Y. Mizutani et al., "590 MPa Class Fire Resistant Steel for Building Structural Use" (Nippon Steel Technical Report No. 90, 2004), 45.

22. C. Klinkenberg, K. Hulka, and W. Bleck, "Niobium Carbide Precipitation in Microalloyed Steel," *Steel Research International,* 75 (11) (2004), 744-752.

23. A. Kern, B. Müsgen, and U. Schriever, Thyssen Technische Berichte, 25 (1993), 67.

24. P. Dumoulin et al., “Role of Molybdenum in Phosphorus-induced Temper Embrittlement,” *Metal Science*, 14 (1) (1980), 1-15.

25. A. Kern, P. Feinle, and U. Schriever, “Heavy Plate Made of Wear Resistant Special Structural Steels – Manufacture, Processing Application” (Paper presented at EUROMAT 01, Rimini 2001), 765.

Fundamentals and Applications of Mo and Nb Alloying in High Performance Steels – Volume 1
Edited by Hardy Mohrbacher
CBMM, IMOA and TMS, 2014

EFFECTS OF TI-MO AND TI-NB COMPLEX ADDITIONS ON INTERPHASE PRECIPITATION IN LOW-CARBON STEELS

Hung-Wei Yen[1], Ching-Yuan Huang[2] and Jer-Ren Yang[1]

[1]Department of Materials Science and Engineering
National Taiwan University, Taipei, Taiwan
[2]Iron and Steel R&D Department
China Steel Corporation, Kaohsiung, Taiwan

Keywords: Interphase Precipitation, Nanometer-sized Carbide, TEM, Thermal Simulation, Phase Transformation, Hardness, Niobium, Molybdenum, Titanium

Abstract

The purpose of this research was to study the effects of Mo and Nb additions on interphase precipitation in titanium-alloyed low-carbon steels. Sheet spacing and inter-particle spacing of interphase-precipitated carbides were quantitatively measured and evaluated by transmission electron microscopy. Besides, to elucidate these results, the transformation rate of ferrite was measured by dynamic dilatometer. Addition of 0.2 wt%Mo, which increases the super saturation for carbide nucleation, can further refine the inter-particle spacing of carbides. The Vickers microhardness has been achieved in this Ti-Mo containing steel after isothermal heat treatment at 650 °C for 20 min. Addition of 0.04 wt%Nb had no strong effect on refining the inter-particle spacing further. The precipitation of (Ti,Nb)(C,N) in the present alloy system increased the ferrite growth rate. It is suggested that the ability to refine the carbide dispersion in this Ti-Nb steel could be optimized by reducing the carbon content. These results and discussions provide guidance for alloy design to attain strong ferrite in steels by producing dense interphase-precipitated nanometer-sized carbides.

Introduction

Interphase precipitation (IP), leading to the sheeted dispersion of nanometer-sized, complex alloy carbides $(M_1,M_2)C$, has been shown to provide remarkable strength via precipitation hardening in advanced low-carbon ferritic steels. By this method, JFE and China Steel recently reported their developments of ultrahigh-strength hot-rolled steel strip for automotive use [1,2]. In these steels, the precipitation strengthening due to the IP of nanometer-sized carbides was estimated to be approximately 300 MPa.

Several mechanisms have been proposed in the literature [3-8] to explain the evolution of IP carbides. The most acceptable one is the ledge mechanism; during the austenite-to-ferrite transformation, the carbides nucleate densely on the terrace planes of the ledged α/γ interface. As the ledge trails a complete passage, another ledge moves over a new parallel interface, where the nucleation cycle begins again. This process can be repeated many hundreds of times in a particular austenite grain, thereby leading to the well-characterised form consisting of sheets of carbides with uniform sheet spacing, in a ferrite matrix. The ledge mechanism was proposed only for the semi-coherent interface associated with rational α/γ orientation relationships (ORs) and it

leads to a planar carbide dispersion of IP (PIP). The recent study by Yen et al. [9] claimed that the ledge mechanism can occur on interfaces associated with both rational and irrational ORs, thus leading to PIP or curved IP with a regular spacing (Regular CIP). Hence, by the ledge mechanism, the resulting density and distribution of tiny carbides relies on two factors, (1) the precipitation kinetics of carbides on the terrace plane and (2) the austenite-to-ferrite transformation kinetics. Both factors can be affected by the chemical composition of the steel. In general, the alloying elements expected to affect the interphase precipitation reaction can be categorised into four groups [10]:

(1) elements which have a strong affinity with carbon atoms to form carbides and encourage the ferrite transformation, e.g. vanadium, titanium, and niobium;
(2) elements which have some affinity with carbon to form carbides but slow down the ferrite transformation, e.g. molybdenum, tungsten, and chromium;
(3) elements which stabilise ferrite or austenite and greatly affect the kinetics of ferrite transformation, e.g. manganese, nickel, and silicon;
(4) interstitial elements which directly participate in carbide or carbonitride formation and also determine the kinetics of ferrite transformation, e.g. carbon and nitrogen.

The scope of the present work is to investigate, by using advanced TEM, the roles of Mo and Nb additions on the distribution of IP carbides in Ti containing low-carbon steels. Molybdenum and niobium solutes have a strong retarding effect on the ferrite growth but they are also supposed to participate in the formation of IP carbides. The interconnection between quantitative TEM results and dilatometry curves can provide further understanding of the effects of alloying on IP carbides.

Experimental Procedure

The present investigation involved three different steels and their chemical compositions are listed in Table I. A Ti-containing C-Mn-Si steel was selected as the reference material (**Steel A**). To study the synergistic effects of Ti-Nb and Ti-Mo additions, two other steels, having approximately the same base composition but alloyed with additions of 0.2 wt%Mo (**Steel B**) and 0.04 wt%Nb (**Steel C**), were also evaluated. All of the steels were prepared by vacuum melting, and then cast into 100 kg ingots with a thickness of 210 mm. The ingots were homogenised at 1200 °C for 2 h and then hot rolled in several passes, by 20% reduction per pass, to plates of 20 mm thickness. In the present work, all the heat treatments were carried out on a Dilatromic III RDP deformation dilatometer from Theta Industries, Inc.

Table I. Chemical Composition of Three Steels (in wt%)

	Fe	C	Si	Mn	Ti	Nb	Mo	S*	N*
A	Bal.	0.10	0.1	1.5	0.2	-	-	44	40
B	Bal.	0.10	0.1	1.5	0.2	-	0.20	44	40
C	Bal.	0.10	0.1	1.5	0.2	0.04	-	43	40

*(ppm)

Before the preparation of dilatometer specimens, the pieces of steel were homogenised at 1250 °C for 3 days while sealed in a quartz tube containing argon, and subsequently quenched in water. All dilatometer specimens were taken from the quarter thickness position below the plate surface, and orientated along the rolling direction before final machining to 3 mm diameter cylindrical rods of 6 mm length. The work was to study the effects of Ti, Ti-Mo and Ti-Nb additions on the precipitation of carbides during isothermal transformation. The processing schedules performed in the dilatometer are given in Figure 1. The specimens were austenitised at 1200 °C for 3 min (in order to dissolve all of the carbides), then cooled to 650, 680 and 700 °C respectively, at a cooling rate of 20 °C/s and held at these temperatures for different times, (20 and 60 min), and finally quenched to room temperature at a cooling rate of 100 °C /s.

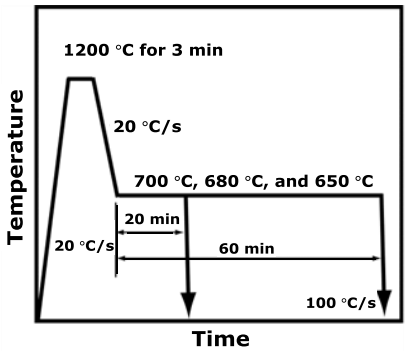

Figure 1. Schematic diagram of heat treatment process for isothermal transformation.

Optical metallography (OM) samples were prepared from the dilatometer specimens. The specimens were mechanically polished and then etched in 3% nital solution. For the purpose of revealing the precipitation hardening, hardness measurements were made on the ferrite phase in the optical specimens, using a Vickers hardness tester with a load of 100 g.

Transmission electron microscopy (TEM) samples were prepared from 300 μm thick discs slit from the dilatometer specimens. The discs were thinned to 60 μm by abrasion on SiC sandpaper and then electropolished in a twin jet electropolisher using a solution of 5% perchloric, 25% glycerol, and 70% ethanol at -20 °C and 35 V potential. The specimens were examined using a Tecnai G2 T20 TEM and FEI Tecnai F30 field emission gun TEM (FEG TEM). To measure the sheet spacing of IP carbides, a typical sheeted dispersion of carbides should be observed in TEM thin foils. Assuming the carbides precipitate on a terrace plane with index of $\{h\ k\ l\}$ in the ferrite grain, to display an image of well-aligned interphase-precipitated carbides, the specified zone axes $<u\ v\ w>$ must satisfy the condition [3]:

$$hu + kv + lw = 0\,. \tag{1}$$

The zone axes satisfying Equation (1) will intersect the terrace plane edge-on and the typical sheeted distribution of carbides will be visible under these zone conditions. To estimate the inter-particle spacing, the foil thicknesses were measured by the log-ratio method for analysing the corresponding electron energy loss spectrum (EELS), which was collected with a semi-collection angle of about 19.4 mrad in TEM mode, using the mean free path in iron of 108 nm for inelastic scattering of iron [3].

Results and Discussion

Phase Transformation of Ferrite

After the isothermal heat treatments for 20 min, two phases are observed using OM, (1) diffusional ferrite, which nucleated and grew during the isothermal transformation and (2) martensite, which originated from the rapid cooling of untransformed austenite. The volume fraction and grain size of ferrite in the three steels after the isothermal heat treatments for 20 min are listed in Table II. The volume fraction of ferrite is apparently lower in **Steel B**, which implies a strong retarding effect of molybdenum on the ferrite transformation kinetics though molybdenum also participates in the formation of IP. As illustrated by the example in Figure 2, the ferrite grain size is finer in **Steel C**. Moreover, the ferrite grain size displays a clear bimodal distribution as shown in Figure 2(c), because the precipitation of (Ti,Nb)(C,N) in austenite enhances the nucleation rate of ferrite.

After the holding time of 60 min, the volume fractions of ferrite remain nearly the same in the three steels (i.e. 0.76 in **Steel A**, 0.78 in **Steel B**, and 0.75 in **Steel C** at 680 °C). The corresponding dilatometric curves for the isothermal transformations at 680 °C in the three steels have been analysed and are presented in Figure 3. It is worth noting that in the early stages the transformation rate of austenite in the Ti-Mo steel is dramatically lower than in theTi and Ti-Nb steels. The slope of the linear portion of the transformation curve is lowest in **Steel B** and steepest in **Steel C** which means that the ferrite growth rate in **Steel B** was reduced. In this research, this effect is attributed to the retarding effect of molybdenum solutes on the interface mobility [11,12]. Niobium also has been reported to retard ferrite growth [13] but in **Steel C** this effect was not apparent. Instead, the ferrite transformation rate increases due to the addition of 0.04 wt% of Nb, compared with **Steel A**. The results from the dilatometer are consistent with the OM observations.

Table II. Volume Fraction and Grain Size of Ferrite in Three Steels Isothermally Heat Treated at Different Temperatures for 20 min

Vol. %	**650 °C**	**680 °C**	**700 °C**
Steel A	74(4)%	68(5)%	64(3)%
Steel B	66(5)%	58(6)%	47(6)%
Steel C	76(7)%	70(6)%	61(3)%
Grain size (μm)	**650 °C**	**680 °C**	**700 °C**
Steel A	48(9)	75(7)	92(9)
Steel B	43(10)	70(5)	87(11)
Steel C	28(12)	40(14)	71(9)

*The value in () is the standard deviation of the measurement

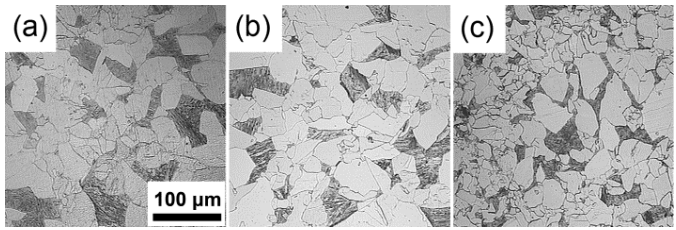

Figure 2. Optical micrographs taken from specimens; (a) **Steel A**, (b) **Steel B** and (c) **Steel C** isothermally treated at 680 °C for 20 min.

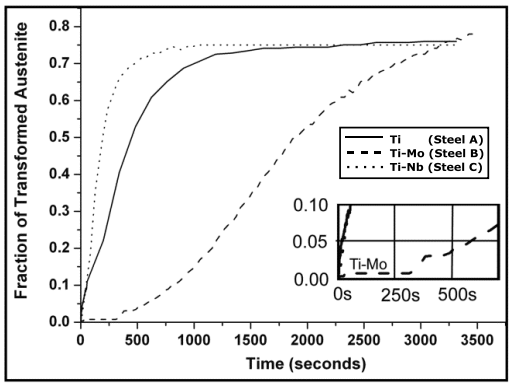

Figure 3. The isothermal transformation curves of three steels isothermally treated at 680 °C.

Interphase-precipitated Carbides in Ferrite

The distribution of interphase precipitated carbides is associated with two parameters, (1) the sheet spacing, the average distance between two neighbouring sheets of line-aligned carbides, and (2) inter-particle spacing, the average distance between two particles on the same sheet plane. To measure the sheet spacing, TEM images with exactly aligned sheets of carbides should be examined along some specified zone axes of ferrite grain as indicated by Equation (1). To obtain the inter-particle spacing, the thicknesses of specimens are measured by the log ratio method from EELS. This method provides higher accuracy, compared with some previous reports [14]. Typical TEM micrographs displaying sheeted carbides in each sample are shown in Figure 4. The sheet spacing and inter-particle spacing of the three steels, isothermally treated at 650, 680 and 700 °C for 20 min, are listed in Table III. Based on these results, three facts can be be highlighted. Firstly, both sheet spacing and inter-particle spacing are refined with decreasing isothermal treatment temperature, with the variation of sheet spacing with temperature change being more dramatic. Secondly, the selection of carbide forming element itself can have a strong influence on the inter-particle spacing. It is apparent that the inter-particle spacing in **Steel B**

shows the finest distribution. Thirdly, on the other hand, the sheet spacing is not significantly affected by the selection of the carbide forming element in the present alloys.

Table III. Sheet and Inter-particle Spacing of the Three Steels Isothermally Treated at Different Temperatures for 20 min

	Sheet Spacing (nm)		
	650 °C	**680 °C**	**700 °C**
Steel A	19.6(6.0)	29.4(5.5)	40.6(7.3)
Steel B	19.1(5.6)	30.3(7.0)	38.8(10.1)
Steel C	18.5(4.4)	27.2(5.8)	36.9(12.4)
	Inter-Particle Spacing (nm)		
	650 °C	**680 °C**	**700 °C**
Steel A	38.7(8.8)	43.3(11.7)	48.6(12.0)
Steel B	33.4(11.2)	36.7(10.3)	43.9(15.2)
Steel C	40.4(8.8)	47.2(9.8)	53.3(11.9)

*The value in () is the standard deviation of the measurement

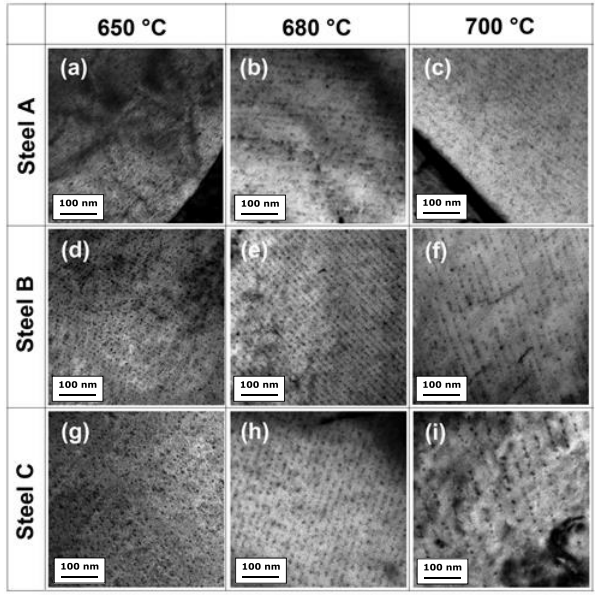

Figure 4. TEM micrographs showing the IP nanometer-sized carbides in the three steels isothermally heat treated at different temperatures for 20 min.

Effects of Mo and Nb on Interphase Precipitation

The discussion here is based on the dilatometer experiments, OM observations, and TEM investigations. It follows the recent proposition that most interphase precipitation events in low-carbon steels occur via the ledge mechanism during austenite-to-ferrite phase transformation [9]. In **Steel B**, it is clear that the relatively slow growth rate during phase transformation is due to the retarding effect of molybdenum solutes. The slower ledge velocity could contribute to finer inter-particle spacings because of more time for (Ti,Mo)C to nucleate on the terrace planes. Furthermore, compared with **Steel A**, adding 0.2 wt%Mo can raise the supersaturation for carbide nucleation. It has been confirmed that molybdenum can participate in the MC-type carbide reaction [15]. Niobium solutes have also been reported to retard the ferrite transformation [13]. In **Steel C**, the retarding effect of niobium solutes was not observed. If niobium atoms precipitate as (Ti,Nb)(C,N), it can enhance the nucleation of ferrite and the ferrite transformation as shown in Figure 3. Although the remaining niobium solutes still participate in the IP reaction, the rapid ferrite transformation reduces the amount of carbide formation. Therefore, to optimise the carbide density in Ti-Nb containing steels, the carbon and titanium content should be reduced to suppress the niobium consumption due to the precipitation of carbonitrides. However, a reduction of Ti will lead to a reduction of the total amount of carbide formation. In the present alloy systems (with 0.1 wt%C and 0.2 wt%Ti), molybdenum does not tend to participate in the carbide reaction at high temperatures (i.e. >900 °C) even though the alloy contains 0.2 wt%Mo.

Vickers Microhardness of Ferrite

The Vickers microhardness of ferrite has been measured for samples of the three steels, which have been isothermally treated at 650, 680 and 700 °C for 20 min, (using short holding times to prevent the coarsening of carbides), as shown in Figure 5. In the present conditions, the highest Vickers microhardness (301 HV) was obtained in **Steel B** isothermally transformed at 650 °C. The corresponding microstructure possesses the best combination of finest sheet spacing and finest inter-particle spacing as shown in Figure 4 and Table III. Such a high hardness of coarse-grained ferrite approximates to a yield stress of over 900 MPa. For this reason, it was defined as super ferrite [14]. In **Steel C**, heat treated at 650 °C for 20 min, a Vickers microhardness of 275 HV was also achieved with only a 0.04 wt% addition of Nb.

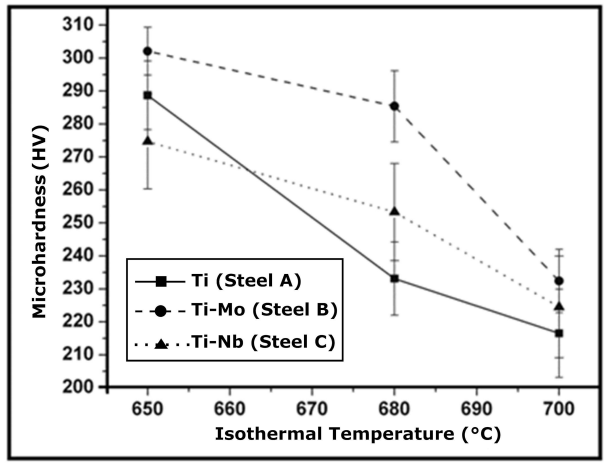

Figure 5. Vickers microhardness of three steels isothermally heat treated at 650, 680 and 700 °C for 20 min.

Conclusions

The effects of Mo and Nb additions on interphase precipitation in three experimental Ti-containing steels have been quantitatively examined by advanced TEM techniques. The following conclusions can be drawn:-

1. Both sheet spacing and inter-particle spacing are refined with decreasing isothermal treatment temperature, though the sheet spacing changes more significantly with temperature.

2. Molybdenum has the advantage of producing more IP nanometer-sized carbides due to its efficiency in suppressing the ferrite transformation rate.

3. Due to the synergistic effects of Ti-Mo additions, the highest Vickers hardness of 301 HV can be achieved in coarse-grained ferrite after isothermal transformation at 650 °C.

4. Niobium in the present alloy accelerates the ferrite transformation due to the precipitation of (Ti,Nb)(C,N), such that it loses the potential to refine inter-particle spacing by the solute retarding effect on ferrite growth.

5. To optimise the carbide density, it is suggested to reduce the carbon content, such that the ability of niobium solutes to interact with the moving interface can be recovered.

Acknowledgement

This work was carried out with financial support from the National Science Council of the Republic of China, Taiwan, under Contract NSC 98-2221-E-002-055-MY3. The authors thank China Steel Corporation for providing the alloy steels.

References

1. Y. Funakawa et al., "Development of High Strength Hot-rolled Sheet Steel Consisting of Ferrite and Nanometer-sized Carbides," *Iron and Steel Institute Japan International*, 44 (11) (2004), 1945-1951.

2. C.Y. Huang et al., "Development of Nano-size Precipitation Strengthening Hot-rolled Automobile Steels" (Paper presented at the AISTech 2010 Iron and Steel Technology Conference, Pittsburgh, PA, 3-6 May 2010), 849-857.

3. R.W.K. Honeycombe, "Transformation from Austenite in Alloy Steels," *Metallurgical Transactions A*, 7 (7) (1976), 915-936.

4. R.A. Ricks and P.R. Howell, "Bowing Mechanism for Interphase Boundary Migration in Alloy Steels," *Metal Science*, 16(6) (1982), 317-322.

5. R.A. Ricks and P.R. Howell, "The Formation of Discrete Precipitate Dispersions on Mobile Interphase Boundaries in Iron-base Alloys," *Acta Metallurgica*, 31 (6) (1983), 853-861.

6. P.R. Howell, R.A. Ricks, and R.W.K. Honeycombe, "The Observation of Interphase Precipitation in Association with the Lateral Growth of Widmanstätten Ferrite," *Journal of Materials Science*, 15 (2) (1980), 376-380.

7. R.M. Smith, and D.P. Dunne, "Structural Aspects of Alloy Carbonitride Precipitation in Microalloyed Steels," *Materials Forum* (11) (1988) 166-181.

8. D.V. Edmonds and R.W.K. Honeycombe, *Precipitation Processes in Solids*, ed. K.C. Russell and H.I. Aaronson, (New York, NY: The Metallurgical Society of AIME, 20-21 September, 1976).

9. H.W. Yen et al., "Interphase Precipitation of Nanometer-sized Carbides in a Titanium–molybdenum-bearing Low-carbon steel," *Acta Materialia*, 59 (16) (2011), 6264-6274.

10. R.W.K. Honeycombe, *Structure and Strength of Alloy Steels*, (London, UK: Climax Molybdenum Company, 1975).

11. G.J. Shiflet and H.I. Aaronson, "Growth and Overall Transformation Kinetics Above the Bay Temperature in Fe-C-Mo Alloys," *Metallurgical Transactions A*, 21(6) (1990), 1413-1432.

12. W. Reynolds et al., “The Incomplete Transformation Phenomenon in Fe-C-Mo Alloys,” *Metallurgical Transactions A*, 21 (6) (1990), 1433-1463.

13. M. Suehiro, Z.K. Liu, and J. Agren, “Effect of Niobium on Massive Transformation in Ultra Low Carbon Steels: A Solute Drag Treatment,” *Acta Materialia*, 44 (10) (1996), 4241-4251.

14. H.W. Yen, C.Y. Huang, and J.R. Yang, “The Nano Carbide Control: Design of Super Ferrite in Steels,” *Advanced Materials Research*, 89-91 (2009) 663-668.

15. H.W. Yen, C.Y. Huang, and J.R. Yang, “Characterization of Interphase-precipitated Nanometer-sized Carbides in a Ti–Mo-bearing Steel,” *Scripta Materialia*, 61 (6) (2009), 616-619.

Applications of Mo and Nb Alloyed Steels

Fundamentals and Applications of Mo and Nb Alloying in High Performance Steels – Volume 1
Edited by Hardy Mohrbacher
CBMM, IMOA and TMS, 2014

APPLICATION OF NIOBIUM-MOLYBDENUM STRENGTHENING MECHANISMS IN HIGH STRENGTH LINEPIPE STEELS

J. Malcolm Gray

Microalloyed Steel Institute, Houston TX, USA

Keywords: Linepipe Steels, Strengthening Mechanisms, Niobium, Molybdenum, CCT, X80, X100, X120, Mechanical Properties

Abstract

The synergistic effects of niobium and molybdenum in lowering austenite-to-ferrite transformation temperatures have been known for approximately 45 years. The benefits have been widely exploited in linepipe steels since 1971 when 485 MPa (X70) linepipe produced by IPSCO [1] was installed in Canada in the TransCanada and Novacorp gas transmission systems. At that time the steels were cast as semi-killed ingots and had inferior transverse Charpy properties due to the presence of MnS and silicate inclusions. Other applications have been found in hot-rolled long products [2] and Nippon Steel's HT80 quenched and tempered plate [3,4]. As linepipe yield strengths have increased to X80, X100 and above, and carbon contents have been reduced to 0.03-0.06 percent, the Nb-Mo combination has become indispensable for producing economical steels when used in combination with chromium, copper and nickel. This paper provides a brief chronology of the adoption of Nb-Mo and Nb- Mo-B alloying since the mid 1960s.

Research and Technological Development

Research by the author [5] was conducted at the U.S. Steel Research Laboratory in Monroeville, PA starting in 1966 and culminating in the casting of 30 ton BOF heats at South Works, Chicago in 1968 and 1969 [6].

The chemical composition of the pilot scale heat is shown in Table I below.

Table I. Chemical Composition and Mechanical Properties of 30 Ton BOF Heat of Nb-Mo-Ni Steel

	Yield Strength, MPa	**C**	**Mn**	**Ni**	**Nb**	**Mo**	**B (ppm)**	**Ti**	**N**
As rolled	509-558	0.045	1.25	0.80	0.09	0.37	19	0.023	0.007
Aged 600 °C – 1/2 h	695-758								

The Charpy V-notch transition temperatures of the as-rolled and aged plates were +15 and +30 °C respectively. This was due to the absence of appropriate austenite conditioning knowhow and the strong effect of $NbMo_4C_3$ precipitation in the bainitic microstructure. As time progressed and controlled rolling practices were developed, the steel (without nickel), Table II, was applied by IPSCO in 1971-1972 [7,8,9], and installed in large diameter gas pipelines in Canada which

are still operating safely today. In that early application the skelp was rolled on a reversing Steckel Mill in Regina, Saskatchewan and then water cooled.

Table II. Chemical Composition of IPSCO Linepipe, circa 1972 [1]

C	Mn	Nb	Mo	Cu	Ni	Si
0.05	1.75	0.095	0.32	0.25	0.12	0.08

Today almost all steels are fully-killed and continuously cast, and rolling mill and thermal cooling regimes have become very sophisticated, such that steel compositions similar to that presented in Table I are routinely capable of producing linepipe with yield strengths of 690 MPa (X100) and excellent notch toughness [10,11,12].

As part of the Nb-Mo research program, at U.S. Steel continuous cooling transformation (CCT) diagrams were developed for the four steels presented in Table III [13].

Table III. Chemical Compositions of Steels Investigated

Heat No.	Designation	C	Mn	P	S	Si	Al (Total)	N	Nb	Mo
W8583/1	Base Steel	0.018	0.49	0.013	0.017	0.12	<0.005	0.001	-	-
W8620/1	Base + Niobium	0.022	0.52	0.020	0.020	0.12	<0.008	0.001	0.10	-
Y9364/1	Base + Molybdenum	0.018	0.50	0.018	0.019	0.15	<0.002	0.001	-	0.51
Y9360/1	Niobium - Molybdenum (Nb-Mo)	0.014	0.50	0.016	0.017	0.13	0.001	0.001	0.10	0.50

The manganese content was deliberately kept low to facilitate the achievement of very low carbon contents, which thereby maximized solution of niobium carbide with its attendant benefits. The full CCT diagrams for the four steels are presented in Figures 1 to 4, and then are consolidated in Figure 5 where it is simple to compare the effects of the individual and combined (Nb-Mo) elements. The combination of niobium and molybdenum results in a reduction in ferrite/bainite start temperature of >100 °C for cooling rates as low as 0.1 °C/s compared with the individual effects of niobium and molybdenum. This makes it possible to produce uniform, non-polygonal microstructures in both thin and heavy (40 mm) plates.

The effect of niobium in reducing A_{r3} temperature is much greater than the effects of other microalloying elements, Figure 6. However, niobium and vanadium can be combined in some cases with good effect, Figure 7.

The Nb-Mo synergistic combination was adopted rapidly by Hoesch [14], Usinor [15], Italsider [16] and other linepipe producers especially for linepipe supplied to the former USSR. However, this came to an abrupt end in 1974 / early 1975 when the price of molybdenum skyrocketed. As a result manufacturers returned to Nb-V alloying, or in the case of Italsider to Nb-0.30 percent Chromium, alloy designs for API Grade X70 linepipe.

As yield strengths have moved upward to 550 MPa (X80), or to 690 MPa on a trial basis, molybdenum has been reintroduced into the linepipe arena, often in combination with higher niobium contents, Figure 8.

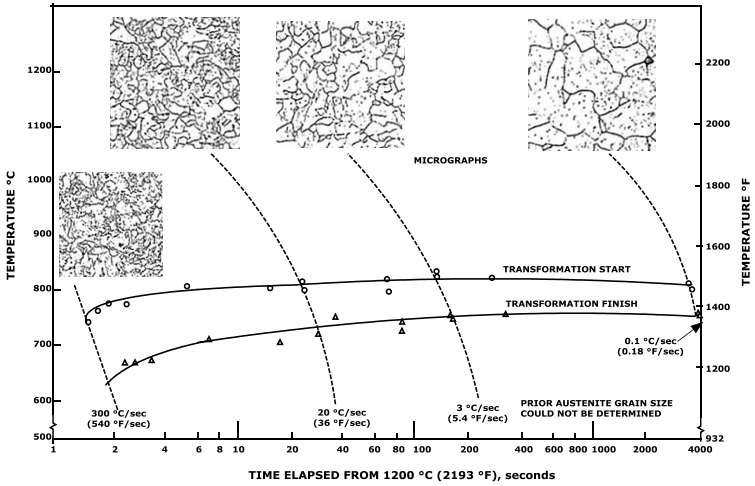

Figure 1. CCT diagram: 0.02%C 0.50%Mn.

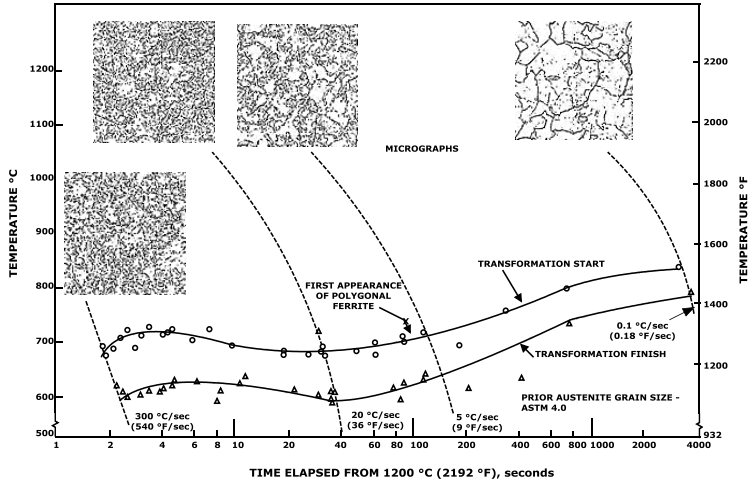

Figure 2. CCT diagram: 0.02%C 0.50%Mn 0.10%Nb.

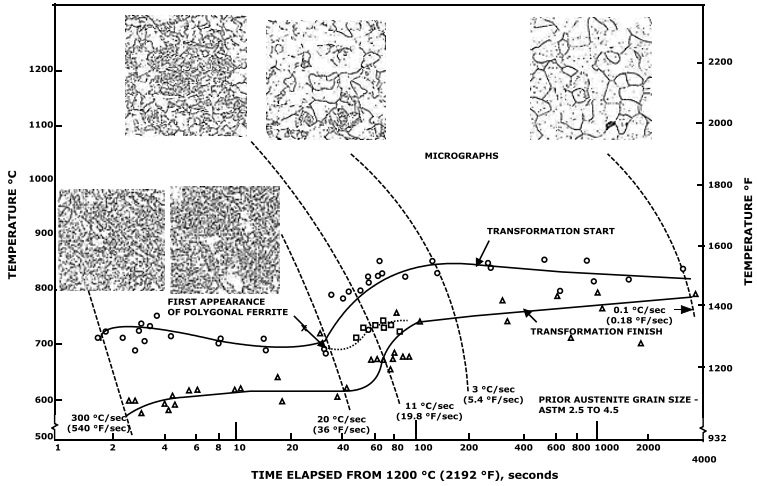

Figure 3. CCT diagram: 0.02%C 0.50%Mn 0.51%Mo.

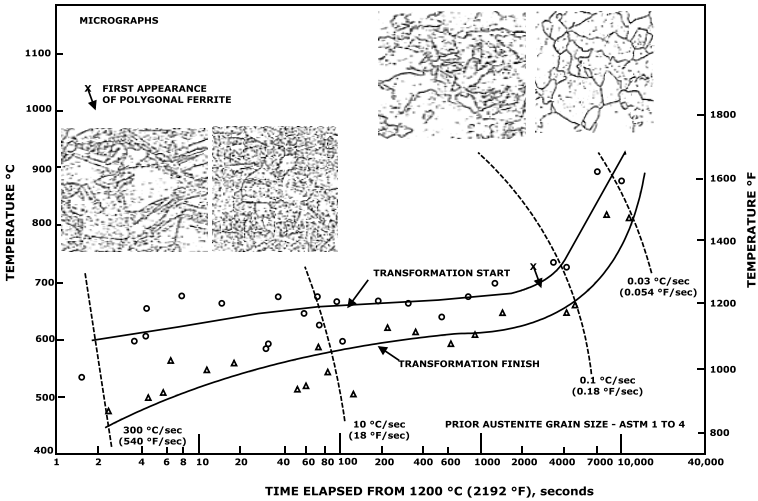

Figure 4. CCT diagram: 0.02%C 0.50%Mn 0.10%Nb 0.50%Mo.

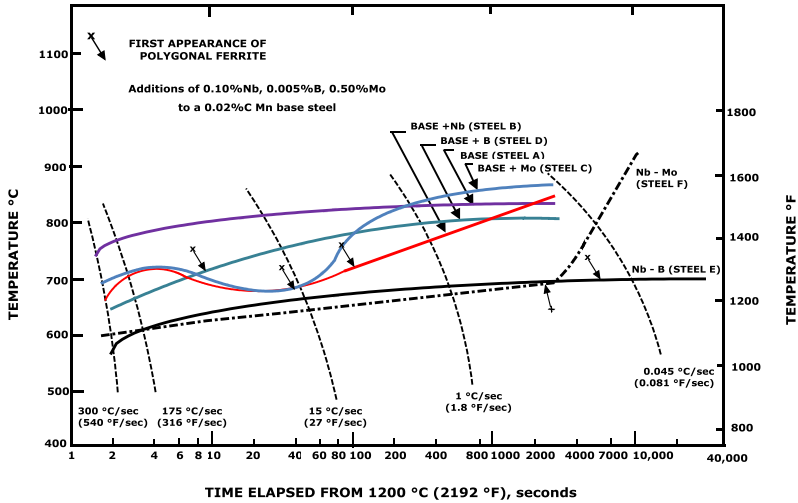

Figure 5. Comparison of transformation-start temperatures for all steels.

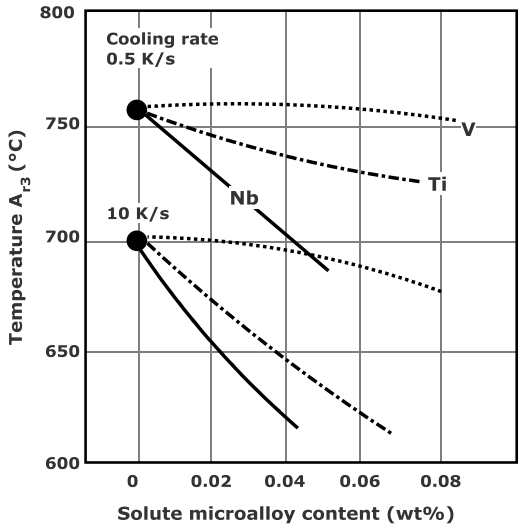

Figure 6. Effect of solute microalloying elements on the A_{r3} temperature.

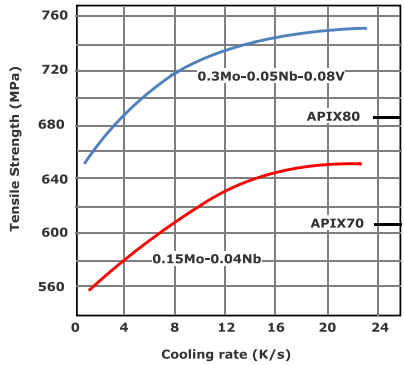

Figure 7. Tensile strength vs cooling rate in IAC processed 19 mm (0.75 in) plates.

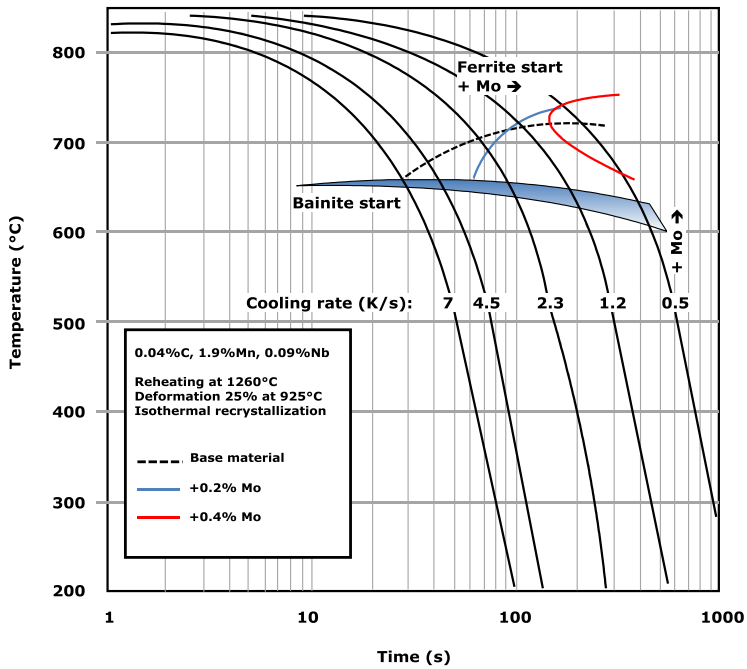

Figure 8. Influence of Mo content on transformation behavior of low-carbon 0.09%Nb steels (base: 0.04%C-MnCuNi).

The higher niobium (0.10%), molybdenum combination is particularly useful for production of spiral seam linepipe since strip mill rolling reductions tend to be limited compared with plate mill processing.

Recent examples have been presented by Salzgitter [17] for 14, 18.8 and 25 mm skelp. Data for 18.8 mm skelp are shown in Table IV.

Table IV. Chemical Composition for 18.8 mm Skelp wt%

C	Mn	Si	Nb	Ti	Mo	Cr	Al	N
0.05	1.78	0.31	0.092	0.018	0.12	0.18	0.04	0.004

Slabs 253 x 1550 mm cast using soft reduction were free of edge cracks and required no flame scarfing thereby permitting hot charging. A transfer bar size of 52 mm was utilized and the finish rolling temperature was 820-835 °C. Mechanical properties for the above and related trials are presented in Figure 9.

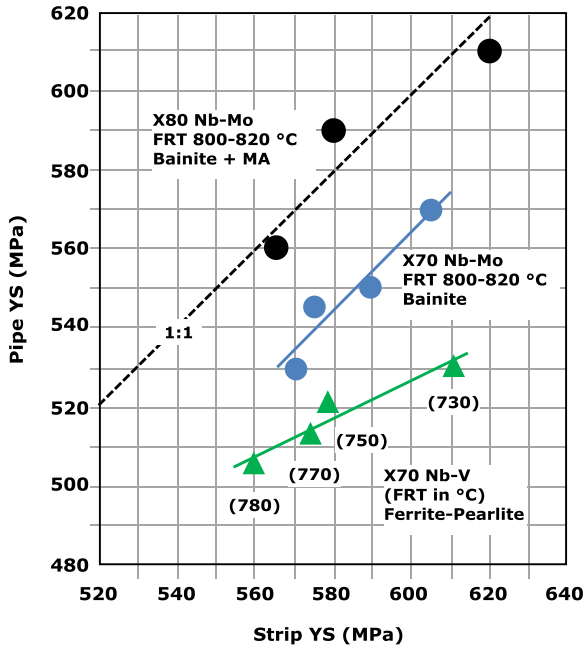

Figure 9. Influence of alloying concept and microstructure on the yield strength in as-rolled material and flattened pipe sample.

The low carbon Nb-Mo concept is appealing to the strip mill operator since the higher rolling temperatures for the HTP concept lead to less wear on rolls and bearings, reduced risk of mill overload, reduced load on the crop shear and generally faster processing time. The economic benefits claimed by the authors [17] are presented below:

Economic Comparison for Low Carbon 0.10 Percent Niobium versus Conventional Nb-V Concept

- Moderately higher alloying cost.
- Lower CE_{IIW} (-2 points) and P_{cm} (-5 points).
- Can be cast with a slab width bigger than the required final strip width:
  ⇒ Increased continuous casting capacity.
- Bending properties in the hot strand are improved:
  ⇒ Flame scarfing can be eliminated.
  ⇒ Hot charging becomes possible.
- Enhanced solubility of microalloying elements due to low C:
  ⇒ Reduced slab residence time in reheating furnace.
- High delivery temperatures after discharging from the furnace:
  ⇒ Slab width reduction of up to 300 mm in the sizing press.
- Increased processing temperatures due to higher T_{NR}:
  ⇒ Entire sequence of hot rolling is accelerated.
  ⇒ Larger processing window along the entire process chain from slab to pipe.
- Lower plastic deformation resistance at increased finishing temperature:
  ⇒ Higher rolling temperatures and shortened production times can be achieved.
  ⇒ Reduced wear on bearings, drives and rolls as well as crop shear.
- Wide bainitic (AF) range in the CCT:
  ⇒ Increases processing window on the run-out table / down coiler.
  ⇒ Enables synergies between microstructural and precipitation strengthening.
  ⇒ Reduces production complexity.

The discussion thus far concerning the benefits of the Nb-Mo synergy has concentrated on their combined effect in lowering the A_{r3} temperature. However, there is also a strong yet subtle effect related to the formation of $NbMo_4C_3$ carbides after transformation. A small amount of molybdenum (0.08–0.12%) dramatically increases the volume fraction of NbC type precipitation. This phenomenon was extensively studied by Kanazawa et al in the early 1960s [3,4]. The Nb-Mo-C ternary referenced in their publication(s) is presented below [17]. Examples of recent utilization of the concept will be presented later.

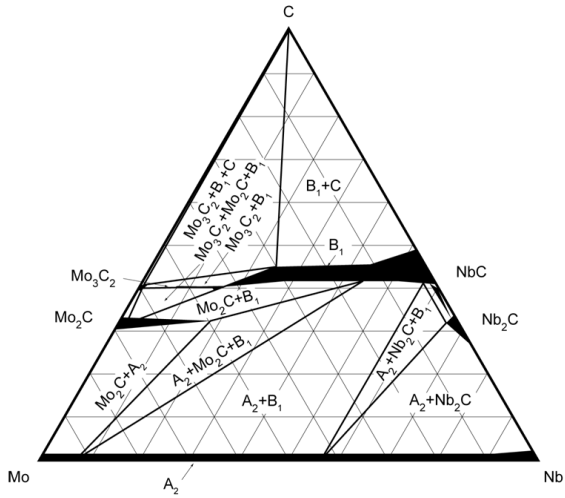

Figure 10. Phase diagram of Nb-Mo-C alloy at 1900 °F (1038 °C) (by Rudy [18]).

The use of niobium contents of 0.10 percent is not a recent phenomenon, although the trend towards 550 MPa (X80) designs has stimulated recent applications. A few milestones are presented in Table V below.

Table V. Commercialization of HTP Linepipe

Year	Manufacturer	Maximum Niobium Content	Project
1972	IPSCO	0.07 – 0.11	TCPL-Nova
1974	Algoma Steel-Canadian Phoenix	0.14	TCPL
1975	Hoesch	0.15	MA-75
1980	Hoesch	0.10	Czech Republic
1998	ArcelorMittal – PMT	0.095	Pemex (Cantarell)
2004	OSM – Napa Pipe	0.095	El Paso (Cheyenne Plains)
2005	Angang – Julong (JCO)	0.10	CNPC (X-70) First West East Project
2008	Multiple (7-8) Mills	0.11	CNPC (X-80) Second West East Project

The rapid growth of high quality linepipe manufacture is presented in Figure 11.

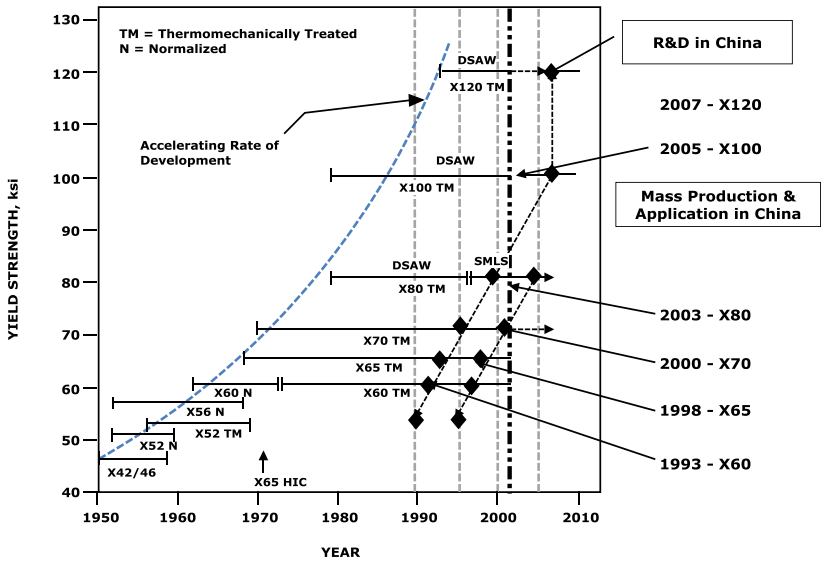

Figure 11. Development of high strength linepipe capability in China.

The most recent examples of Nb and Nb-Mo alloying as practiced in China have been presented in numerous papers at recent conferences [19,20] and several are summarized in Table VI.

Table VI. Chemical Compositions of Chinese Hot Rolled Coils API Grade X80 (550 MPa) [18]

Mill Name	C	Mn	Cr	Mo	Nb	V	Ti	N	Thickness
N. China Petroleum	0.06	1.88	-	0.33	0.056	-	0.023	0.005	14.6 mm
	0.07	1.89	-	0.24	0.055	0.05	0.011	0.004	14.6 mm
Jining	0.04	1.80	-	0.28	0.070	-	0.011	N.R.	18.4 mm
From TGRC Paper*	0.046	1.81	0.18	0.31	0.062	0.005	0.009	N.R.	18.4 mm
Angang	0.04	1.88	0.27	0.10	0.10	-	0.012	0.005	18.4 mm
Shougang	0.04	1.80	0.30	0.15	0.095	-	0.015	N.R.	18. 4 mm
Nanjing	0.045	1.82	0.27	0.12	0.092	-	0.012	N.R.	18.4 mm

*Tubular Goods Research Center of the China National Petroleum Corporation
N.R. – Not Reported

The route map(s) for the First and Second West-East Pipeline Projects are presented in Figure 12. The overall length of the Second Pipeline is 9226 km of which the mainline used 4770 km of 48" OD x 18.4 mm API Grade 550 MPa (X80) with the balance 42" OD API Grade 485 MPa (X70). Approximately 72 percent of the linepipe was manufactured using the spiral seam route, truly an impressive performance after only 10 years of serious Chinese pipelining. The future is likely to be even more impressive as plans emerge for the third, fourth and even sixth and seventh massive projects.

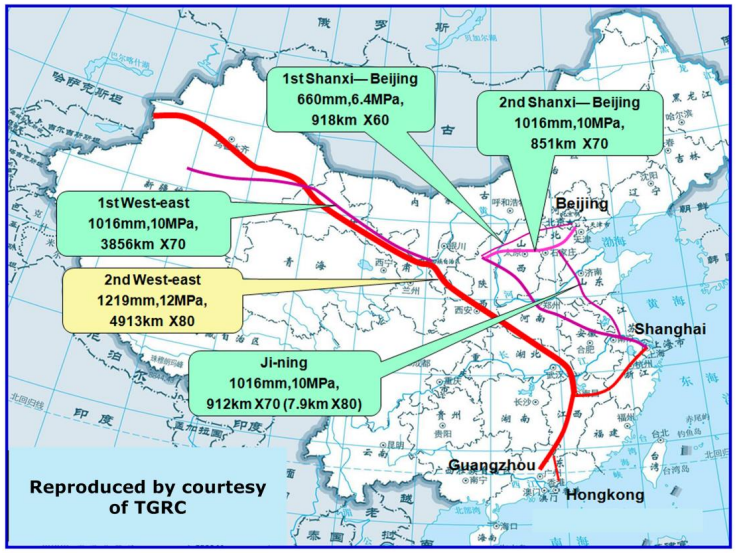

Figure 12. Recently installed pipeline systems in China.

Conclusions

There is a well documented strong synergistic effect of niobium and molybdenum on the austenite to ferrite transformation temperature which produces bainitic microstructures at relatively slow cooling rates. The effect is enhanced by reduction in carbon contents to 0.06 percent and below and by increasing niobium contents to close to the stoichiometric ratio with carbon and nitrogen.

The concept was first introduced commercially in 1971/2 by Canadian produced X70 linepipe installed in the TransCanada and Novacorp pipeline systems. The strengths levels have since moved up incrementally to X80, X100 and X120, but the latter two API 5L/ISO 3183 Grades have yet to find significant commercial usage. It is likely that the ultra-low carbon niobium-molybdenum alloying approach will continue to find favor amongst both producers and end

users based on the achievable strength, toughness, weldability and fracture arrest characteristics, all combined with relative ease of manufacture compared with the traditional Nb-V alloying approach.

References

1. E.C. Hamre and A.M. Gilroy-Scott, "Properties of Acicular Ferrite Steels for Large Diameter Linepipe," *Proceedings of Microalloying 75, International Symposium on High-strength, Low-alloy Steels*, Washington, DC, (1-3 October 1975), 375-381.

2. P. Maitrepierre et al., "Transformation Characteristics and Properties of Low-carbon Niobium-boron Steels," *Memoires Scientifiques de la Revue de Metallurgie*, (5 June 1978), 355-369.

3. S. Kanazawa et al., "Combined Effect of Nb and Mo on the Mechanical Properties of Nb-Mo Heat-treated High Strength Steel with 80 kg/mm^2 Strength Level," *Transactions of the Japan Institute of Metals*, 8 (2) (1967), 105-112.

4. S. Kanazawa et al., "On the Behavior of Precipitates in the Nb-Mo Heat-treated High Strength Steel having 80 kg/mm^2 Tensile Strength," *Journal of the Japan Institute of Metals*, 31 (171) (1962), 113-120.

5. J.M. Gray, "Mechanical Properties and Microstructure of Low-carbon Hot Rolled High Strength Low Alloy Steels" (Report 89-018-015 (1), U.S. Steel, 28 November 1969).

6. P.E. Repas, "Evaluation of Plate and Sheet Products from 30 Ton BOF Heats of an Experimental Mn-Ni-Cb-Mo-B Steel" (Report 89-018-011 (6), U.S. Steel Research Center, 28 May, 1971).

7. A.P. Coldren et al., "Microstructure and Properties of Low Carbon Mn-Mo-Cb Steels," *Proceedings of Processing and Properties of Low Carbon Steels, The Metallurgical Society of AIME*, New York, (1973).

8. G. Tither, A.P. Coldren, and J.L. Mihelich, "Influence of Processing on Properties of Molybdenum Steels for Pipeline" (Paper presented at the CIM Annual Conference of Metallurgists, Toronto, Canada, 25-28 August 1974).

9. R.L. Cryderman et al., "The Development of High Strength Hot-Rolled Mn-Mo-Cb Steel" (Paper presented at the 14th Mechanical Working and Steel Processing Conference, Iron and Steel Div. AIME, Chicago, Illinois, 19 January 1972), volume X, 114.

10. X. Dianxiu, S. Chengjia, and S. Weihue, "Microstructure and Mechanical Properties of X100 Grade High Strength Linepipe," *Proceedings of the Third International Seminar on High Strength Linepipe*, Xi'an, China, (28-29 June 2010), 81-85.

11. L. Yang, Z. Weiwei, and G. Shaotao, “Tensile Properties and Strain Ageing of X100 Pipeline Steel” ibid, 86-95.

12. L. Shaopo et al., “Development of X100 Pipeline Plates using TMCP and Tempering Technology” ibid, 235-238.

13. J.M. Gray, W.W. Wilkening, and L.G. Russell, “Transformation Characteristics of Very-low Carbon Steel” (Report 89-002-015 (3), US Steel, 15 May, 1969).

14. K. Taeffner et al., “Technology of Hot Strip and Plate Production for Large Diameter Line Pipe,” *Proceedings of Microalloying 75*, Washington, DC, (1-3 October 1975), 425-434.

15. M. LaFrance et al., “Use of Microalloyed Steels in the Manufacture of Controlled-rolled Plates for Pipe,” *Proceedings of Microalloying 75*, Washington, DC, (1-3 October 1975), 367-373.

16. M. Civallero, C. Parrini, and N. Pizzimenti, “Production of Large-diameter High-strength Low-alloy Pipe in Italy,” *Proceedings of Microalloying 75*, Washington, DC, (1-3 October 1975), 451-468.

17. S. Bremer, V. Flaxa, and F. Knoop, “A Novel Alloying Concept for Thermo-mechanical Hot-rolled Strip for Large Diameter HTS (Helical Two Step) Line Pipe,” *Proceedings of ASME 7th International Pipeline Conference 2008*, Calgary, Alberta, Canada, (29 September–3 October 2008), 489-495.

18. E. Rudy, Monatshefte für Chemie 92, volume 4, 846.

19. *Proceedings of CNPC Tubular Goods Research Institute 2nd International Seminar on X80 and Higher Grade Line Pipe Steel 2008*, Xi'an, China, (23-24 June 2008).

20. *Proceedings of 3rd (CNPC) International Seminar on High Strength Linepipe 2010*, Xi'an, China, (28-29 June 2010).

Fundamentals and Applications of Mo and Nb Alloying in High Performance Steels – Volume 1
Edited by Hardy Mohrbacher
CBMM, IMOA and TMS, 2014

EFFECTS OF MICROALLOYING AND HOT ROLLING PARAMETERS ON TOUGHNESS AND YIELD STRENGTH OF API X80 GRADE STEEL STRIPS

Kisoo Kim

Sheet Products & Process Research Group Technical Research Laboratories
POSCO, South Korea

Keywords: X80, Spiral Pipe, MA Phase, Charpy Toughness, Property Anisotropy, DWTT, Process Route, Niobium, Molybdenum, Titanium, Microstructure, Nickel, Mechanical Properties, Austenite Grain Size, Precipitation

Abstract

Recently API X80 grade has been increasingly used for UOE pipes and, furthermore, API X100 and X120 grades are being developed. However, the usage of hot rolled API X80 grade for spiral-welded pipes has been limited. This is partly due to metallurgical barriers which are the anisotropy of mechanical properties and the strength drop after pipe forming. Manufacturing conditions and metallurgical parameters causing these barriers have been reviewed. The effect of both size and distribution of MA constituent on the Charpy impact upper shelf energy has been investigated. In addition, the development of API X80 hot rolled strip and commercial production results from a 12,000 tonne API X80 grade order for a linepipe project have been summarised.

Introduction

Higher strength grades of hot rolled steel strip are now being used for pipeline construction to obtain high gas transport efficiency. The use of high strength steel strip allows higher operating pressures and gas transmission rates, Figure 1 [1,2]. These higher grades require both increased strength and enhanced toughness by adding more microalloying elements without deteriorating weldability, to ensure the safety and economy of the pipeline. It is therefore important to optimise chemical composition and processing parameters to satisfy the requirements of the entire production route, Figure 2.

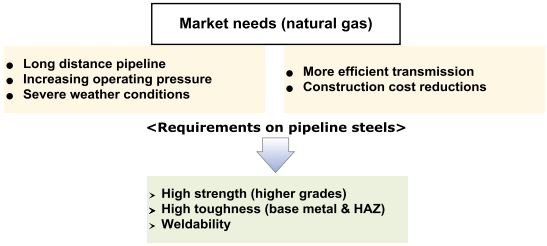

Figure 1. Recent requirements for pipeline steels.

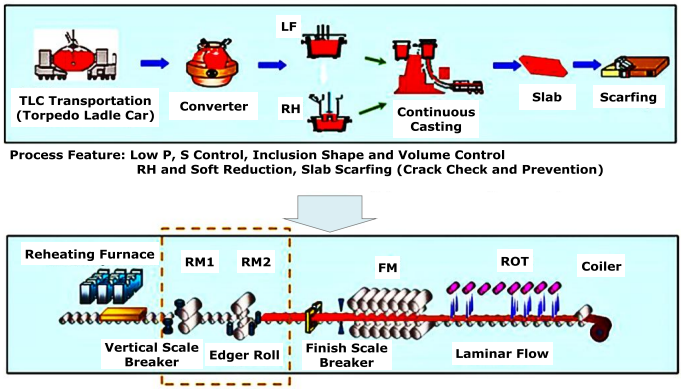

Figure 2. Production route of high strength steels for linepipe application.

To manufacture higher strength steels it is necessary to add more alloys, which potentially results in inferior weldability and toughness. An increased operating pressure in a pipeline system requires higher toughness values to achieve crack arrest when running ductile fracture occurs. This results in the API/ISO Standards for higher strength grades requiring higher values of Charpy energy. Metallurgically, unfortunately this requirement is contradictory to the nature of steel since higher strength usually results in lower toughness as shown in Figure 3. HSLA steels have firstly overcome this paradox and therefore have been widely used in high strength steel applications. Although no revolutionary development has been pushing the technological limit of steel manufacturing processes, as seen in the IT industry, deeper scientific understanding of metallurgical phenomena has become possible. It sould be noted that technology transfer from laboratory to mill is considered to be another technical problem in steel research, which is mainly due to the size difference. Small scale laboratory output cannot be directly implemented in the commercial production mill. Several thousand kilometer long pipelines made with higher strength grade steels have been successfully constructed in the world by using the mill as laboratory-like facilities, i.e. intensive metallurgical analysis and investigation on the mill, not using samples melted and processed in the lab. Practically speaking, 20 tonnes of slabs rolled as plates or strip with cooling water and oxide scale on the surface cannot be rolled in the same condition from head to tail or from surface to centre line of the stock. Statistical controls in the material processing that are based on and stick to metallurgical principles should be introduced in the mill in order to guarantee the target mechanical properties.

In the manufacturing of UOE pipes, an expansion process increasing yield strengths by straining of the pipe body is beneficial to the final dimension and also the mechanical properties. Meanwhile, it is more challenging to obtain the desired strength and toughness in the pipes due to anisotropy of mechanical properties originating from the crystallographic texture in hot rolled strip [3]. This is because more reduction (one-directional hot rolling) is applied in the strip manufacturing process, using a tandem hot rolling facility, compared with plate rolling. The mechanical anisotropy, illustrated in Figure 4, shows the diagonal direction which is coincident

with the hoop direction in the pipe body having poor toughness and lower yield strength. A crystallographic texture is traditionally believed to be responsible for this phenomenon but the temperature dependency of Charpy energy and the relationship between these properties before and after pipe making have not been clearly explained yet.

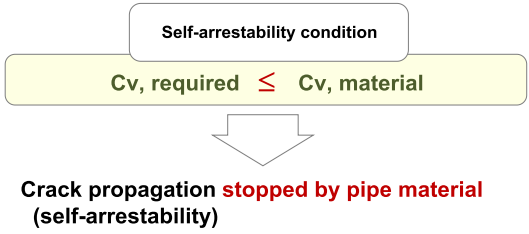

❋ Strength vs. Toughness (CVN)

Grades	CVN (API/ISO) J	CVN [J, -15 °C]	YS [MPa]
API X70	84 / 27	500	490
API X80	133 / 27	150-370	560

Figure 3. A comparison of toughness requirements for API X70 and X80.

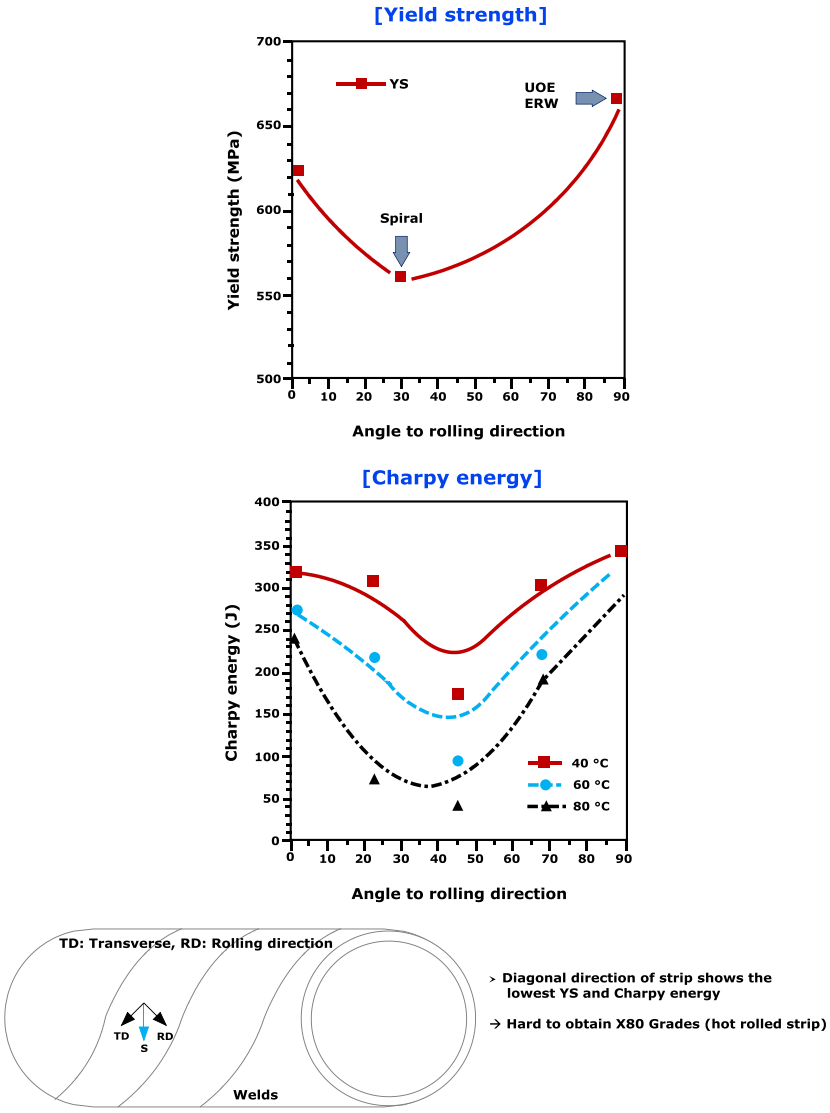

Figure 4. Anisotropy of yield strength and Charpy energy of strip.

One important empirical result indicates that the microstructure, including effective grain size and the distribution of precipitates, plays a key role in the mechanical anisotropy of properties. For example, the occurrence of cleavage observed on the fracture surface of a Charpy specimen has a strong dependency on hard phases contained within the microstructure. The resulting lower energy values are associated with brittle behaviour, while ductile fracture occurs by microvoid coalescence. The effective grain size and the second phase distribution, for acicular ferritic/bainitic microstructures, frequently shown in high grade API steels, cannot be well defined, which leads to the difficulty of understanding the basics of toughness behaviour. It is noted in Figure 4 that the anisotropy of toughness is weakened as temperature increases and at extremely low temperatures below -100 °C no toughness anisotropy has been observed.

The addition of microalloying elements, such as Nb, Ti, Mo and V which precipitate in austenite (γ) as carbides, nitrides, or carbonitrides are essential additions for API grade steels. The controlled rolling of microalloyed steels is performed to optimise metallurgical phenomena such as Nb dissolution in the reheating furnace, austenite conditioning, pancaking during finishing and finally phase transformation on the runout table. Even nano-precipitation at low temperature (below 600 °C) has to be considered after coiling. Effects of alloying elements can be summarised as follows [4]. Mo enhances strength and toughness by readily promoting the formation of low-temperature transformation phases and grain refinement. Cr enhances strength as it promotes low-temperature transformation phases but deteriorates low-temperature toughness due to coarse grain size. Nb is effective for enhancing both strength and toughness as it efficiently refines grains and raises the volume fraction of secondary phases. Considering only the effect of primary alloy addition, it can be concluded that high strength attained with increased alloying decreases toughness, Figure 5. Although it is known that a ductile ferrite matrix will give a Charpy energy level of 500 J, the microstructural parameters which affect DBTT (Ductile Brittle Tansition Temperature) and Charpy energy plateau (CVN), respectively, are not clearly, quantitively understood yet.

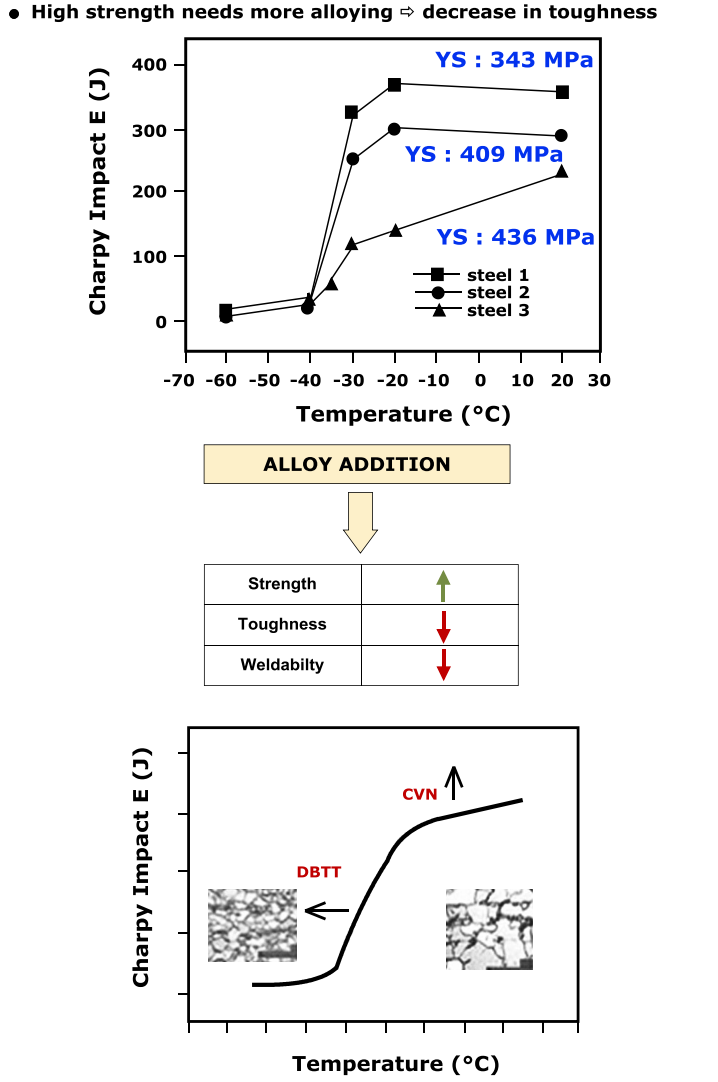

Figure 5. General alloying effect on the strength and toughness.

A schematic thermal history and the major metallurgical events occuring during strip manufacturing processes are shown in Figure 6. It is notable that the temperature is the most crucial property controlling factor. Alloys added to the steels, acting as a promoters/suppressors of phase transformation and precipitation, can be utilised as originally intended to determine the final microstructure, by mill-line temperature control. One of the difficult metallurgical issues is the kinetics of Nb(C,N) precipitation in deformed γ in roughing stands in Nb microalloyed steels. It is complicated to understand because several parameters are acting at the same time, such as alloying elements, temperature and deformation. It is known that the strain-induced precipitation of NbC in γ is delayed in Nb-Ti microalloyed steels compared with that in Nb-microalloyed steels because of incorporation of some of the Nb atoms in the undissolved (Ti,Nb)(C,N) particles during the solution treatment, Figure 7.

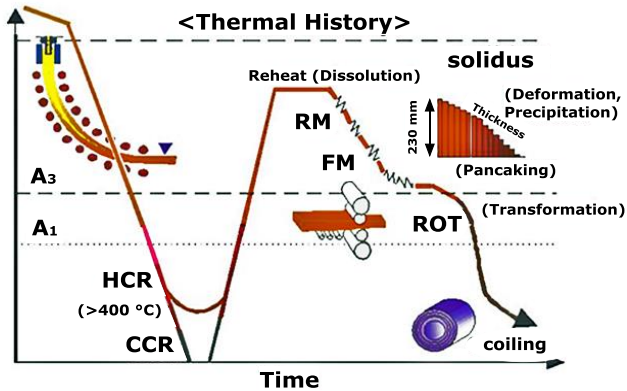

Figure 6. An overall thermal history during strip manufacturing processes.

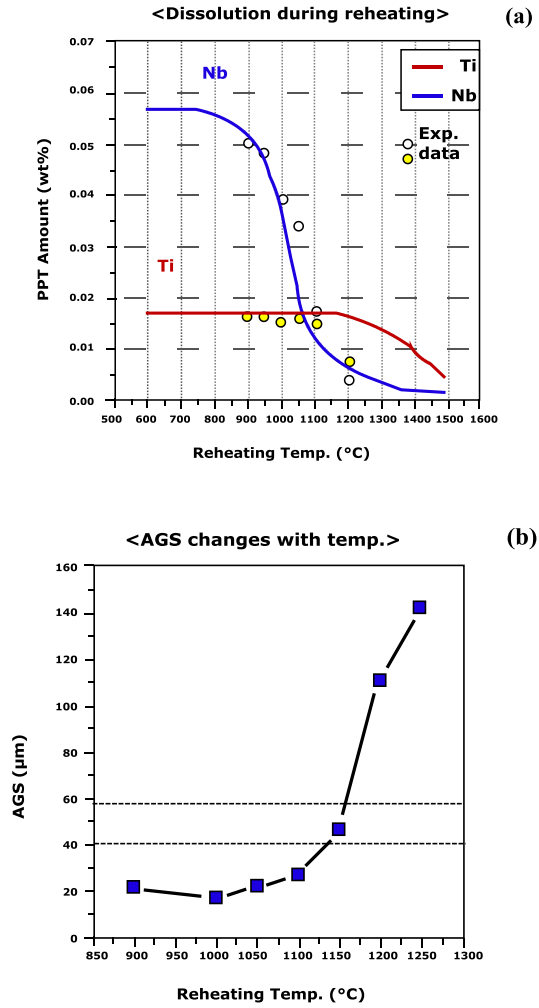

Figure 7. Dissolution behaviour of precipitates during reheating (a), and resulting AGS (Austenite Grain Size) (b).

It has been reported that (Ti,Nb)N precipitates are cuboidal, having a size of 45 to 300 nm, and (Ti,Nb,V)C or (Nb,V)C precipitates are spherical or irregular shaped, being 20 to 45 nm in size. Nb-rich precipitates of 30 to 150 nm tend to nucleate on Ti-rich precipitates or on grain boundaries, and fine NbC of less than 5 nm precipitate at low temperatures, as for example those encountered during coiling.

As explained before, optimisation of microstructure and precipitation behaviour is necessary to improve the strength and toughness of high grade pipeline steels. Appropriate design of the chemical composition together with thermo-mechanical controlled processing (TMCP) contribute to achieving effective microstructures and textures, and through them the desired mechanical properties. In this paper some key metallurgical points are summarised and discussed that were obtained during the development and commercialisation of API X80 hot rolled strip for spiral-welded pipes, at POSCO, mainly considering the effects of hot rolling conditions on mechanical properties.

Hot Rolling Condition

With the pipeline requirement, as seen in Table I, higher Charpy energies for securing safe transport of 1,300 psig max. (pounds per square inch gauge) gas had to be obtained. Thus, based on experience, the microstructure of API X80 steel was designed to have an acicular ferrite matrix, carbide-free cells of bainite with an isle-like dispersed martensite/austenite (MA) constituent. The addition of Nb, Mn, Ni, and Mo is effective for the formation of acicular ferrite to obtain high toughness as well as high strength. The carbon content is kept at about 0.07% or less. Chemical composition of the high grade linepipe steels were ≤0.07%C – ≤1.85%Mn – ≤ 0.085%Nb <0.025%Ti – ≤0.35%Mo – ≤0.6%Cr + Ni + V (wt%), and several heats were mill-trialled to determine the final chemistry and hot rolling conditions.

Table I. Requirement of CVN for API X80 Grade Steels

WT(mm)	Charpy E (J) @ -15 ^{o}C (Coil)	Remarks
10.85	**240**	-
	181	Each heat
14.45	**130**	-
	99	Each heat

Hot rolled strip with thicknesses of 10.85 and 14.45 mm were manufactured in oxygen converters and then cast to slabs with a final thickness of 250 mm. The slab reheating temperature was above 1200 °C in order to bring niobium carbides or nitrides into solution.

To determine slab reheating temperatures, Nb precipitation behaviour was analysed with respect to reheating temperatures, Figure 8, and also chemical composition because these precipitates control AGS (Austenite Grain Size) in the slab. Abnormally large grains in the slab can be a starting point of poor toughness in the final product because they are difficult to refine after the reheating process. As a result, reheating temperature should be high enough to secure the dissolution of the alloying element but not too high, in order to prevent abnormal grain growth.

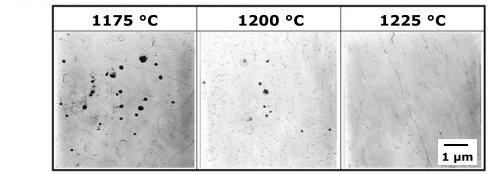

※ Dissolution temperature of Nb

Irvine's equation **	Laboratory simulation
1187 °C	1225 °C

** *log[Nb][C+[12/14]N]=2.26-6770/T*

Figure 8. Nb precipitates in a 0.05%Nb steel at reheating temperatures which control AGS (Austenite Grain Size) during reheating processes.

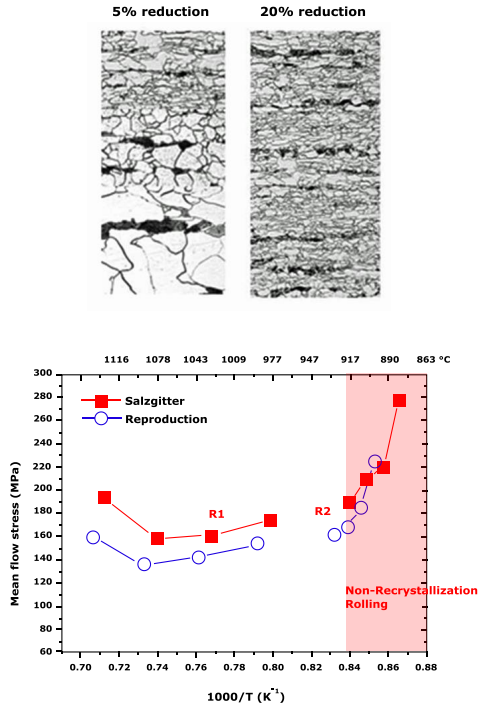

Figure 9. Through thickness grain refinement variation with the amount of rolling reduction and mean flow stress changes, showing non-recrystallisation in the roughing mill.

In Figure 9 the through thickness grain size changes, with the amount of reduction in the roughing mill, and mean flow stresses calculated using the roll force from the hot rolling mill are shown. These micrographs and the changes of mean flow stresses imply that reduction and temperature are keys to the control of microstructure, in conjunction with Nb precipitation. It is important because the final acicular ferritic or bainitic microstructure is strongly dependent on the accumulated strains in the non-recrystallised austenite phase (pancaked) in the roughing mill.

Figure 10 shows very fine (Nb,V)C precipitates which are believed to be formed after coiling, at lower temperatures. The table rows represent the sampling location corresponding to head (top row), middle (centre row) and tail (bottom row) of a strip. It can be seen that precipitation is stronger in the mid-section of a strip, because of slower cooling rates, compared to the outer or inner windings of the coiled strip.

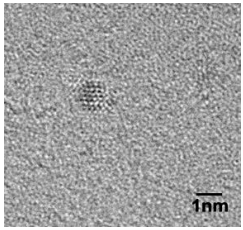

- Homogeneous precipitation in ferrite region

- Round shape (Nb,V)C

- Size <3 nm

Precipitated

Alloys (Total)	Ti (0.018)	V (0.051)	Nb (0.052)
Precipitated	0.019	0.0029	0.031
	0.019	0.0120	0.046
	0.019	0.0026	0.029

***Nb exists, both as precipitates and as solid solution**

Figure 10. Nb rich precipitates formed after coiling processes.

Mechanical Properties

Table II lists the mechanical properties of manufactured strips for a trial coil and 42" OD pipes, respectively, showing values higher than the API specification. The yield strength of the coiled strip is measured at 30 degrees to the rolling direction near the tail end, corresponding to the hoop direction of the pipes. Other mechanical properties such as Charpy and DWTT have also been measured along the 30 degree direction of the strip. Flattened tensile specimens were prepared from a coupon taken from ring samples. Yield and tensile strength in the transverse and longitudinal directions are always greater compared to that at the 30 degree to the rolling direction. This anisotropy of mechanical properties is undesirable, which is thought to be one of the difficulties of designing spiral welded pipelines.

Table II. Mechanical Properties of Strip Coil and Pipes

WT (mm)	Coil (MPa), 30°		Pipe (MPa), Hoop direction	
	YS	TS	YS	TS
10.85	676	838	595 (Avg.) (599/587/597)	756 (Avg.) (761/747/758)
14.45	597	760	580 (Avg.) (580/587/574)	760 (Avg.) (760/758/761)

Charpy Impact Energy

Charpy energy is of importance for designing pipelines to control fracture behaviour especially during high pressure gas transport. Charpy toughness values at different temperatures, as a function of specimen orientation, are displayed in Figure 11, showing a similar dependency as seen in tensile properties. The Charpy impact energies at 20~45 degrees to the rolling direction are decreased despite the low yield strength. This anisotropy originates from the major components of textures, which are {332}<113> and {113}<110> orientations, and the density of {001} cleavage planes in the Charpy specimen, which is highest at 30 degrees to the rolling direction compared with that of other orientations. Therefore, the highest susceptibility to cleavage fracture, i.e. increased ductile-brittle transition temperature, can be seen in the 30 degree direction [5].

Figure 12 shows photos of fractured Charpy specimens and fracture surfaces of longitudinal (L), transverse (C) and 30 degree (30°) samples tested at -80 °C. The shape of fractured specimens is an indication of the amount of plastic deformation experienced by the Charpy specimen when impacted by the striker of the impact machine. Lateral expansion or deformation on opposite side to the notch (striking face) is observed in L and C direction samples while no plastic deformation is observed in the 30 degree sample. It can be clearly seen in the SEM photos that cleavage fracture is dominant in the 30 degree sample.

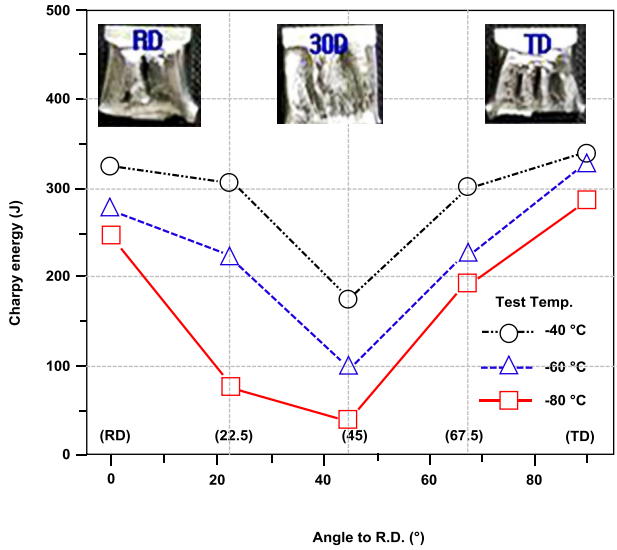

Figure 11. Changes of Charpy impact energy with hammer striking direction and temperature.

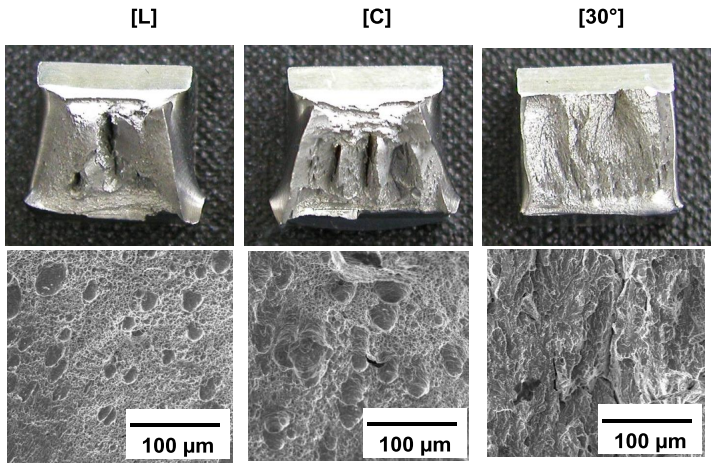

Figure 12. Fracture surface showing lateral expansion by plastic deformation (L-Longitudinal & C-Transverse) and brittle fracture without plastic deformation (30 degree). Charpy impact test was performed at -80 ^{o}C.

The Charpy impact energies of high strength linepipe steels can be affected by microstructural factors, such as initial centreline segregation and abnormal grains found in slabs. The AP (Ammonium Persulphate) method has been used to reveal centerline segregation in the slabs, which then allowed adjustment of the soft reduction condition during the continuous casting process. Abnormal grains, on the other hand, survive and increase the effective thickness and length of the pancaked austenite grains, generated during rolling in the non-recrystallisation regime, and remain as a source of anisotropy and poor toughness. When measured, the effect can be seen in the range of length and thickness of the pancaked austenite grains, 3~35 μm and 2~10 μm, respectively [6,7].

Effects of MA on Toughness

It is believed that the addition of Ni has a beneficial effect of improving toughness. This effect has been confirmed in this work, as shown in Figure 13. Ni additions up to 0.2% improve Charpy impact toughness however no big difference has been observed by increasing the Ni addition from 0.2 to 0.4%. To obtain a higher impact toughness all chemical elements should be balanced and optimised to minimise carbides and, more importantly, nitrides. The microalloy carbides and nitrides can be a source of crack initiation, resulting in poor toughness, so that the addition of Ti and V, for example, should be minimised. The effect of alloying elements, however, cannot fully explain the toughness of a steel composition. Hard phases spotted in the matrix result in poor toughness due to their lack of ductility. Small islands of martensite or retained austenite (MA constituent) can accelerate cracking and are frequently observed in an API X80 grade alloying system. Cracks can be initiated at and be propagated along the interface of MA and matrix as shown in Figure 14. The formation of MA is known to be strongly dependent on the amount of Mo and Cr added.

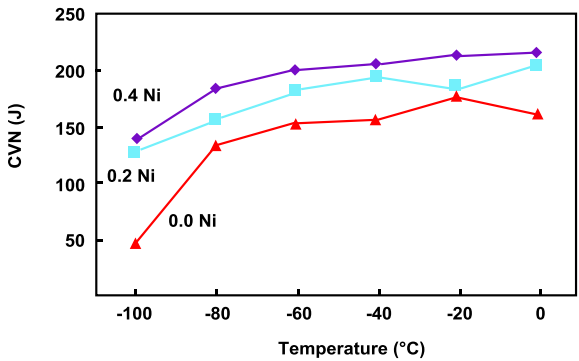

Figure 13. Effect of Ni addition on CVN.

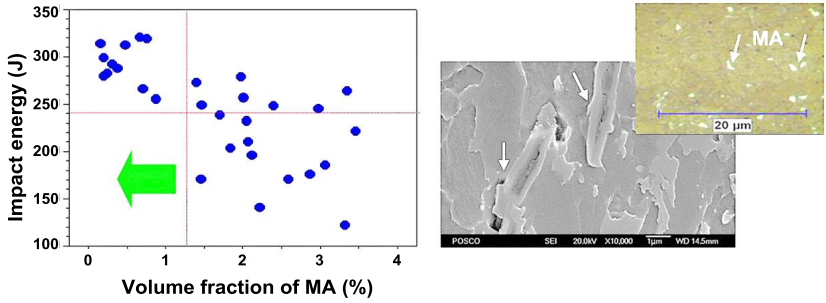

Figure 14. Relationship between MA volume fraction and Charpy impact energies.

Drop Weight Tear Test (DWTT)

Figure 15 shows changes of shear area, SA (%), measured from DWT tests at various temperatures, using 16.9 mm thick API X80 grade produced in mill trials. As observed in Charpy impact tests, similar anisotropic properties of SA can be seen, that is the lowest value of SA occurs at 30 degrees to the rolling direction, Figure 15 (a). A general relationship between the degree of reduction in the non-recrystallisation zone and 85% Shear Appearance Transition Temperature (SATT) can be derived from mill trial results, Figure 15 (c).

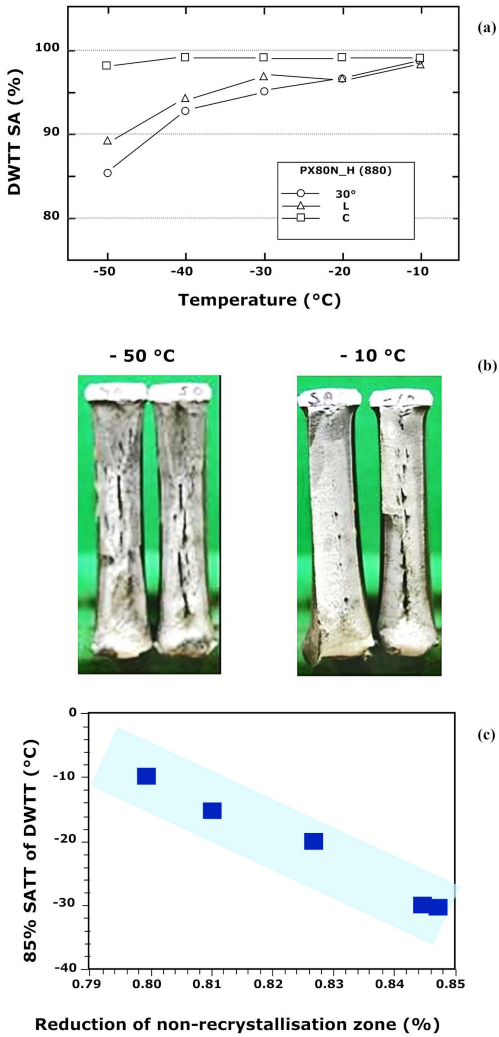

Figure 15. Variation in DWTT Shear Area (%) with temperature and sampling direction; (a) fractured surfaces, (b) the general relationship between % reduction in the non-recrystallisation zone and (c) 85% Shear Appearance Transition Temperature (SATT).

Commercial Production of API X80

The optimisation of chemical compositions and hot rolling conditions, by reviewing mill trials, has been done for commercial production. To achieve the high toughness level requirement of API X80, mill-line temperatures, such as reheating, roughing delivery and coiling temperatures, have to be finely tuned. Cooling water and rolling speed were adjusted to control roughing delivery temperature. Fine grained microstructures improve the ductile-brittle transition temperature, but do not appear to influence the upper shelf energy.

Figure 16 shows the Charpy energy distribution at -20 °C from commercial production of 12,000 metric tonnes of hot rolled strip. Produced coils with lower toughness than the requirement were rejected, however this concerned only a few coils. The microstructure of a sample coil is shown in this figure and reveals a bainitic microstructure.

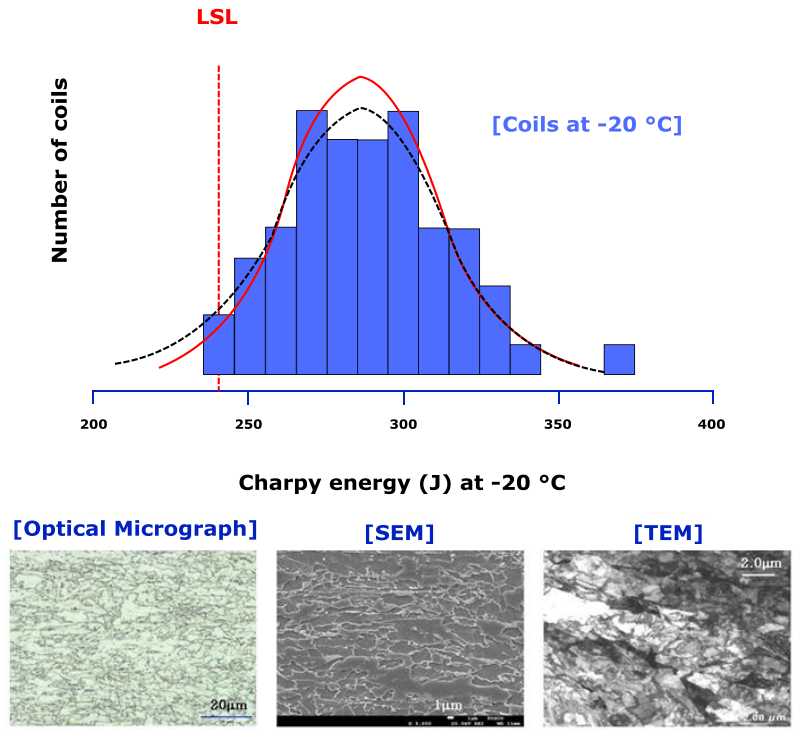

Figure 16. Distribution of Charpy energy measured at -20 °C for commercially produced API X80 grade with a thickness of 10.85 mm and typical steel microstructure at different scales.

For the construction of the Southeast Supply Header pipeline, Figure 17, 27,000 pipes were manufactured and supplied from a pipe mill. In conclusion, 300 miles of API X80 grade 42" spiral pipeline has been successfully constructed.

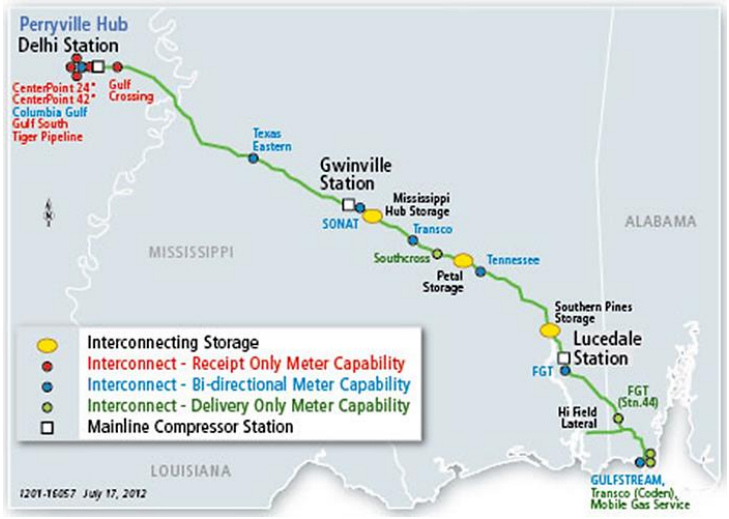

Figure 17. South East Supply Header pipeline.
(source: *www.spectraenergy.com/Operations)*

Summary

API X80 grade hot rolled steel strip with thicknesses of 10.85 and 11.45 mm has been developed. This API X80 grade satisfies the API requirements for commercial applications and has been successfully applied in a pipeline project. The DWTT shear area fraction at -20 °C was 100%, and the Charpy impact energies at -20 °C were more than 240 J in the strip. A combination of high strength and good toughness was obtained by controlling hot rolling parameters to obtain an optimised microstructure of acicular ferritic/bainitic matrix with a reduced MA content.

Acknowledgments

The authors would like to acknowledge Dr. J H Bae for their efforts on mill trials, Mr. Steve Rapp for a valuable discussion on the project (Spectra Energy Transmission), and CBMM for supporting a wonderful technical conference.

References

1. M. Okatsu, F. Kawabata, and K. Amano, "Metallurgical and Mechanical Features of X100 Linepipe Steel" (Paper presented at the Proceedings of the International Conference on Offshore Mechanics and Arctic Engineering, American Society of Mechanical Enginieers, New York: NY, 1997), (3) 119-124.

2. J.H. Cheng et al., "The Influence of Rolling Practice on Fracture Properties of Hot Rolled Plate," *Canadian Metallurgical Quarterly*, 21 (3) (1982), 299-308.

3. M.C. Kim, Y.J. Oh, and J.H. Hong, "Characterization of Boundaries and Determination of Effective Grain Size in Mn-Mo-Ni Low Alloy Steel from the View of Misorientation," *Scripta Materialia*, 43 (3) (2000), 205-211.

4. Y.M. Kim et al., "Effects of Molybdenum and Vanadium Addition on Tensile and Charpy Impact Properties of API X70 Linepipe Steels," *Metallurgical and Materials Transactions A*, 38 (8) (2007), 1731-1742.

5. D. Bhattacharjee, J.F. Knott, and C.L. Davis, "Charpy-impact-toughness Prediction Using an "Effective" Grain Size for Thermomechanically Controlled Rolled Microalloyed Steels," *Metallurgical and Materials Transactions A*, 35 (1) (2004), 121-130.

6. J.M. Hyzak, and I.M. Bernstein, "The Role of Microstructure on the Strength and Toughness of Fully Pearlitic Steels," *Metallurgical Transactions A*, 7 (8) (1976), 1217-1224.

7. Y.J. Park and J.M. Bernstein, "The Process of Crack Initiation and Effective Grain Size for Cleavage Fracture in Pearlitic Eutectoid Steel," *Metallurgical Transactions A*, 10 (11) (1979), 1653-1664.

Fundamentals and Applications of Mo and Nb Alloying in High Performance Steels – Volume 1
Edited by Hardy Mohrbacher
CBMM, IMOA and TMS, 2014

SEISMIC AND FIRE RESISTANT NIOBIUM-MOLYBDENUM-BEARING LONG AND PLATE PRODUCTS

Steven G. Jansto

CBMM North America, Inc., 1000 Old Pond Road
Bridgeville, PA 15017, USA

Keywords: Nano Co-precipitation, Fire Resistant, Molybdenum, Niobium, Seismic, Elevated Temperature Strength, Mechanical Properties, Thermal Simulation, Rebar, Plate, Intercritical Rolling, Specifications, HSLA Steels, Engineering Design, Construction, Strength

Abstract

The compelling need for development of higher performance steels for seismic and fire resistant steel applications is driven by the recent catastrophic earthquakes and/or tsunamis in Haiti, Peru, China and Japan. Current research and development projects throughout the world are focused on the development of a family of niobium-molybdenum-bearing S500 and S600 grades of bars, beams and plates with superior toughness, fatigue resistance, fire resistance, seismic resistance, reduced yield to tensile ratio variation within a heat of steel and overall superior performance. The engineered nucleation and controlled growth of complex nano-co-precipitation, containing Nb and Mo, contribute significantly to a mechanism that results in enhanced performance under seismic and/or fire environmental conditions. The successful high quality production of these Nb-Mo steels with higher strength and elongation behavior may require slight process metallurgy adjustments to the melting and hot rolling practices to consistently manufacture and initiate the optimum precipitate size, distribution and volume fraction of (Nb,Mo)(C,N) in these value added earthquake/fire resistant grades. Rebar, long product and plate producers, who intend to supply these earthquake and fire resistant steels, should incorporate the successful process metallurgy strategies and operating procedures exercised today in producing advanced high strength and toughness steels for automotive, pipeline and critical structural applications, such as fracture-critical beams, forging quality bars, ship plate and pressure vessels.

Introduction

The market trend for improved reinforcing bar and structural steel beam or plate for seismic and hurricane/typhoon regions is driving the development of new grades of steels, with exceptional properties, not available in currently manufactured reinforcing bars and construction steels for challenging civil engineering designs. The next generation of Nb-bearing seismic and fire resistant construction steels requires improved properties in such attributes as; (1) better toughness at lower temperature, (2) higher yield strengths for lower cross sectional area of structure, (3) higher elongations, (4) better weldability to reduce construction time, (5) improved heat affected zone (HAZ) toughness, (6) improved elevated temperature properties, (7) improved seismic performance and (8) better fatigue resistance. All of these properties are desired in both the weldment and the base metal.

The successful production of value added seismic and fire resistant steels requires the application of melt shop and rolling mill practices that in some cases are similar to those used for value added automotive, pipeline and structural grades. Tighter process control during the melting, casting, billet heating and rolling is necessary in order to meet the demanding properties necessary in seismic-prone environments. These practices are often considered unnecessary in conventional long product production, however, the future generation of value added long products will demand changes in operational practices. Different control strategies are required for the production of these high quality construction steels. These strategies include lower residual element levels, scrap segregation, lower sulfur and phosphorous levels, adopting a low carbon approach, and control of nitrogen levels at the basic oxygen furnace (BOF) or electric arc furnace (EAF) and at the billet caster.

Every rebar and plate producer that will manufacture these value added S500 and S600 reinforcing bars and plates should thoroughly understand their process metallurgy variables so the new practices fit their specific steel grade compositions, residual levels, clean steelmaking and hot rolling operation. In addition to the control of nitrogen, hydrogen and oxygen levels, control of scrap residuals, such as copper, lead, antimony and tin, is also very important in order to achieve exceptional toughness in the S500 and S600 products.

Quite often, steelmakers attempt to produce microalloy grades with exceptional toughness at higher carbon levels (approaching 0.12 to 0.20%C) and high residual contents due to poor scrap segregation. These high carbon and high residual contents can lead to a variety of quality problems such as cracking, poor surface quality, segregation issues and low toughness [1]. A reluctance to lower the base carbon level and achieve strength through precipitation and grain refinement can result in high strength reinforcing bars lacking superior toughness. The metallurgical cleanliness of the scrap and effectiveness of scrap segregation and preparation are often an opportunity area to improve overall structural steel quality.

Civil and Materials Engineering Developmental Trends

From a civil engineering design perspective, a performance-based design approach is applied. Such an approach involves the development of damage resistant systems that involve; (1) seismic isolation systems, (2) energy dissipation systems and (3) self centering frames and walls. Significant progress has been accomplished in the ability to better predict the occurrence and intensity of future earthquakes; however, through the course of these design changes, materials have not changed. Therefore, the designers have embraced the possibility of incorporating both improved fire and seismic resistant materials in construction to better withstand earthquakes, typhoons and other catastrophic events, thereby minimizing structural damage and saving human lives. Also, the development of new fire resistant steels for construction is necessary since fires are often associated with seismic events.

Material Engineering Integrative Design

Specified materials for construction have not changed significantly over the past decade. The global structural steel market development, research and industrial implementation require a shift in the traditional metallurgical approach, especially with designs requiring seismic and fire resistance capabilities. Current challenges confronting structural and long product steelmakers are identical in nature to the challenges faced by automotive steel and pipeline producers in their development of advanced high strength steels over the last decade.

For example, during the evolution of pipeline steel development from X52 through X100, similar challenges existed, resulting in steelmaking and processing changes to successfully apply High Temperature Processing (HTP) to overcome these production and product quality challenges. Some, but not all, of this technology can be transferred to the production of structural Nb-bearing steels. Many of the designs currently applied in the construction of high strength pipelines are strain-based. Unique materials have been developed to assist the designers in assuring that the proper stress-strain behavior occurs during loading of pipelines. Interestingly, structural designers and fabricators also desire a more uniform and predictable stress-strain behavior of beams, rebars and construction plates under severe loading and both low and high-cycle fatigue loading. Although the chemistries and hot rolling schedules of these newly developed pipeline steels do not necessarily apply directly to some of these construction applications, there are many elements of the metallurgical mechanisms that will apply in various bridge and building designs.

A second opportunity for materials improvement involves fatigue and fracture performance behavior under seismic and/or elevated temperature conditions. There is very limited data on fatigue and fracture toughness of recently developed construction steels.

Nb and/or Nb-Mo Steels for Earthquake Zones and Fire Resistance Requirements

The development of seismic resistant rebar was initiated with the introduction of Nb to existing rebar grades. Increased sizes of reinforcing bars, at greater than 40 mm in diameter, high yield strength (greater than 450 MPa), with improved weldability, are required in concrete reinforcing bars for seismic zone construction. Microalloyed steels with vanadium have been traditionally used in rebar, but recently the strong grain refinement effect of Nb has resulted in the increased development of Nb-bearing steels in concrete reinforcing bars for 450 to 550 MPa strength levels, improving ductility and toughness. The addition of Mo also offers improved fire resistant properties for an evolving market.

Currently a large quantity of rebar is produced with no microalloys, using the Tempcore process, however, ductility is reduced. The cooling scheme achieved through application of the Tempcore process with a Nb-Mo grade may be modified or eliminated in the lower strength grades, resulting in reduced operating cost and increased mill productivity. The Tempcore process is applied to reinforcing bars to increase the yield strength, but elongation, toughness and fatigue performance may be impaired due to the microstructure produced.

Fire Resistant Plate Steels

Fire resistant constructional steels have been commercialized in some parts of the world (China and Japan) and are being examined in the USA. Current activities are focused on development of specifications for testing of elevated temperature properties. Some material specifications and niche applications (e.g. high-rise building columns, structures where friable insulated coatings are undesirable) will follow. Selected metallurgical studies are reviewed, with a focus on Nb-containing steels that are intended to help understand the microstructure/property relationships that control fire resistant (FR) properties. Specific examples are cited which illustrate the apparent benefit of Mo in suppressing precipitate coarsening rates at elevated temperature, beneficial effects of microstructure refinement, microalloy precipitation, and warm working of ferrite on the FR properties.

Since structural steels usually maintain most of their strength at 350 °C (and indeed some steels may be stronger at 350 °C than at room temperature due to strain aging effects of interstitials), this high yield strength requirement is effective but conservative. Consequently a need developed to design and implement newer steels with improved yield and tensile strength properties at even higher elevated temperatures than 350 °C. The FR steels produced in Japan for the past several years guarantee a minimum yield strength at 600 °C that is 2/3 of the room temperature yield strength, i.e. having a minimum yield strength ratio of 2/3, and these developments have already stimulated implementation of FR steels in some niche applications. Some other design codes cite minimum yield strength ratios of 50% at 600 °C [2].

With the evolving demand for fire resistance, it became apparent that a Nb-Mo based structural steel design could also improve fire resistance at the same time. Therefore, it was decided to study various compositions focused upon fire resistance behavior. So, the need for fire resistance in construction steels, for high strength at elevated temperatures, was defined in the USA. Also, there are very limited commercially available fire resistant plates produced globally. Simultaneously, work is being performed in China at Baoshan Iron and Steel Company as a result of the increasing demand for high performance fire resistant structural steels for use in commercial building-type applications and a low Mo-Nb approach via TMCP has demonstrated acceptable high temperature strength [3].

Based upon the research and development within the USA, as well as other previous developments in Japan, specifically Nippon Steel [4], it was decided to create a task force within ASTM to study the possibility of writing an ASTM specification. At this time, an ASTM specification for FR steels has been written and will be balloted. To meet this requirement, a new fire resistant Nb-Mo structural steel grade is under development. Much of this work is the underpinning for development of the specification.

Experimental Nb-Mo Fire Resistant Steel Comparison

The goal of the current research is to further develop a Nb-Mo alloy design that will retain 2/3 of its yield strength at 600 °C. Table I compares the compositions to the commercially available Japanese FR steel plate.

Table I. Compositions of Experimental Fire Resistant Steels wt% [5]

	C	Mn	P	S	Si	Cu	Ni	Cr	Mo	V	Nb	Al	N
Base	0.11	1.16	0.018	0.013	0.19	0.25	0.08	0.17	0.02	0.004	0.001	0.002	0.010
Nb	0.10	1.06	0.005	0.031	0.27	0.39	0.16	0.09	0.047	0.001	0.021	0.003	0.016
Mo+ Nb	0.10	0.98	0.008	0.028	0.30	0.38	0.15	0.10	0.48	-	0.017	0.004	0.010
V+Nb	0.08	1.13	0.005	0.030	0.27	0.32	0.11	0.13	0.036	0.047	0.021	0.003	-
NSC I	0.11	1.14	0.009	0.020	0.24	-	-	-	0.52	-	0.03	-	-
NSC II	0.10	0.64	0.009	0.050	0.10	-	-	-	0.51	-	-	-	-

Figure 1 exhibits the superior elevated temperature properties of Nb-Mo plate steels compared to other ASTM A572 or ASTM A992 type construction steels.

The Nb + Mo steel exhibits the best high temperature performance. The strengthening mechanism involves the co-precipitation of (Nb,Mo)(C,N) in a fine dispersion of 3 to 5 nanometers diameter within the ferrite matrix. Figure 2 illustrates the co-precipitation of the (Nb,Mo)(C,N).

Basis for New ASTM FR Steel Specification

The diffusion of Nb and Mo at different carbon concentrations influences the precipitation kinetics. Initially, solute Nb and Mo will retard dislocation climb motion, dislocation recovery and grain boundary migration. However, as the temperature increases, the dislocations can become mobile at approximately 400 to 500 °C and, consequently, the yield strength reduces as exhibited in Figure 1. Finally as the fire ensues, the secondary precipitation of (Nb,Mo)(C,N) occurs and the traditional Ostwald ripening mechanism takes place. Figure 3 below illustrates the retardation of the dislocation climb.

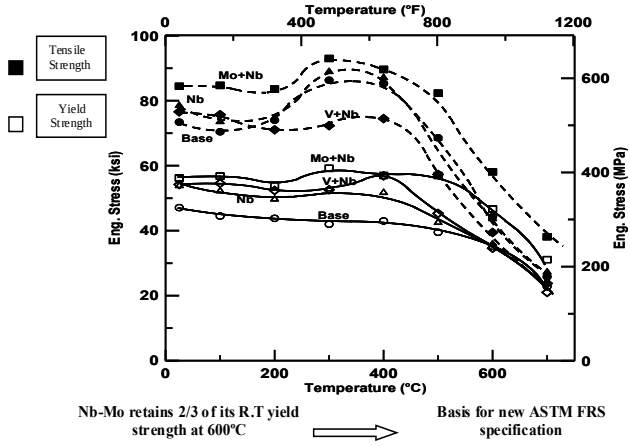

Figure 1. Yield and tensile strength vs. temperature (25-700 °C) for base, Nb, Mo+Nb and V+Nb alloys [5].

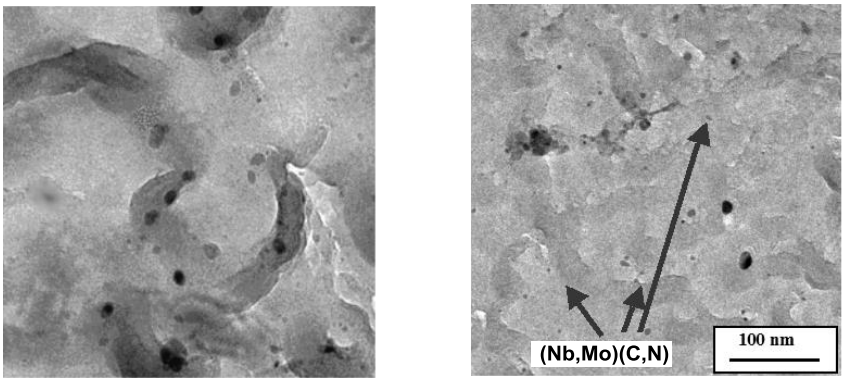

Figure 2. Co-precipitation of duplex (Nb,Mo)(C,N) precipitates in the ferrite matrix.

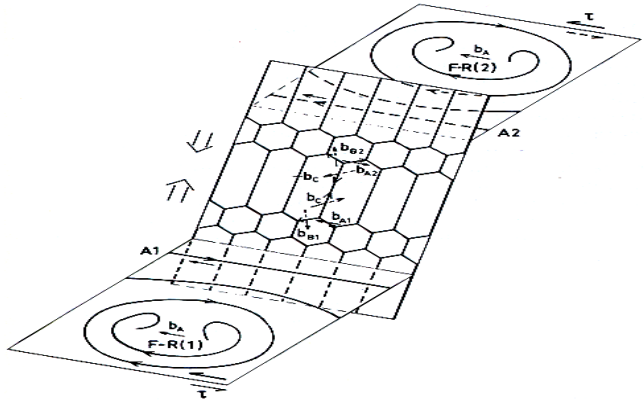

Figure 3. Retardation of dislocation motion during fire.

It is widely known that solute Mo and Nb have the effect of retarding the climb motion and recovery of dislocations as well as grain boundary migration. In low-carbon HSLA steel these solute elements retard dislocation recovery at temperatures up to 550 °C [6]. This can explain the moderate loss of strength of the Nb-added steel when heated in the range of 400-500 °C.

The important parameters of Nb-Mo production of FR steel plate, beams and rebar are:

- Through proper hot rolling thermal practices, create duplex 3-5 nm co-precipitates of (Nb,Mo)(C,N).
- The TMCP rolling process and appropriate finishing temperature must be controlled for a given Nb-Mo composition to assure both the proper size of the ferrite microstructure and the fine Nb-Mo precipitate distribution in the ferrite sub-structure.
- Secondary precipitation during fire.
- Clean steel process metallurgy at Basic Oxygen Furnace (BOF) or Electric Arc Furnace (EAF) and Secondary Steelmaking.
- Reheating furnace practices and combustion control to drive nano-precipitation homogeneity in the final microstructure (i.e. the kinetics of the reaction).

Co-precipitation of Microalloy Carbonitrides

Extensive research is underway to study the synergistic effects of Nb,V, Ti and Mo in duplex and ternary combinations. The research-to-date is evaluating the precipitate size, shape, morphology, precipitate crystallographic structure, precipitate volume fraction, precipitate chemical stoichiometry and the coherency with the ferrite matrix. Figure 4 schematically illustrates the classical strain in the matrix dependent upon the degree of coherency between the precipitate and the matrix and illustrates the effect of soluble solute content on yield strength.

The diffusivity, mobility and solubility of the Nb, Ti, and V carbide forming elements will affect precipitate formation, volume and distribution. Depending upon the amount of interfacial

distortion between the ferrite matrix and the precipitate, the amount of effective strengthening is determined, as shown in Figure 4. Also, the thermal practice during rolling and cooling after the last rolling stand affects the ferrite matrix grain size and the effective precipitate size, volume fraction and distribution and hence the resultant strength levels. The TMCP research relating the effect of different finishing temperatures and cooling on the Nb-Mo FR steel alloy composition is further discussed later in this paper.

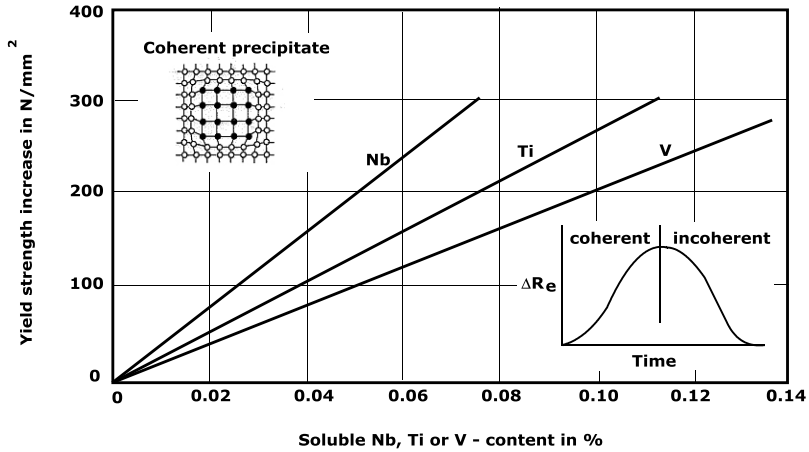

Figure 4. Effect of soluble solute content on increase in yield strength depending on coherency of precipitate with matrix and optimal time at temperature.

Since Mo delays the precipitation of NbC and obstructs Ostwald ripening, an increase in yield strength occurs during the fire [7]. Although the coarsening effect (i.e. Ostwald ripening) is well known, current Nb-Mo research is in progress to better understand the precipitate interaction with the matrix under elevated temperature conditions (i.e. simulation of actual fire conditions).

However, it is apparent in Figure 1 that the Nb-Mo combination results in the highest elevated temperature strength, retaining 2/3 of its room temperature yield strength up to 600 °C, thereby meeting the JIS and soon to be approved ASTM fire resistant steel specifications. Research will continue in order to gain a deeper understanding into the diffusion of Nb and Mo at different carbon concentrations and the influence on precipitation kinetics.

Fire Resistant Steel in China

A new, low Mo bearing FR steel design, containing Nb and other microalloy elements, has been commercially produced via the TMCP process. The new FR steel demonstrates acceptable high temperature strength and ambient temperature mechanical properties. The high temperature behavior of B490RNQ is better than that of Q345B for nominally the same room temperature strength level, by a remarkable margin as shown in Figure 5 [8].

Based upon the Chinese test results, molybdenum significantly improves the elevated temperature yield strength of steel. The steel microstructure is predominantly composed of ferrite, and a molybdenum addition of about 0.5% and 0.02% niobium are considered essential for FR steels with a tensile strength of 400 to 490 MPa. The addition of niobium to the base steel increases the elevated temperature yield strength by 20 MPa. The niobium addition reduces the ferrite grain size and increases the room temperature yield ratio by about 10% (the room temperature yield ratio is the elevated temperature yield strength at a given test temperature divided by the room temperature yield strength). The base composition of the developed FRS grade is shown below in Table II.

Fire resistant weathering steels (FRW) have been developed by Baosteel for many users for the construction of industrial buildings and civil architecture. Numerous welding tests, process evaluation and fireproof tests, carried out jointly with the relevant owners and engineering firms, have been completed. The results prove that these FRW steels can completely satisfy the users' requirements in terms of welding, shaping, earthquake resistance, fire resistance, weather resistance, and are considered the premium products among the constructional steels in China.

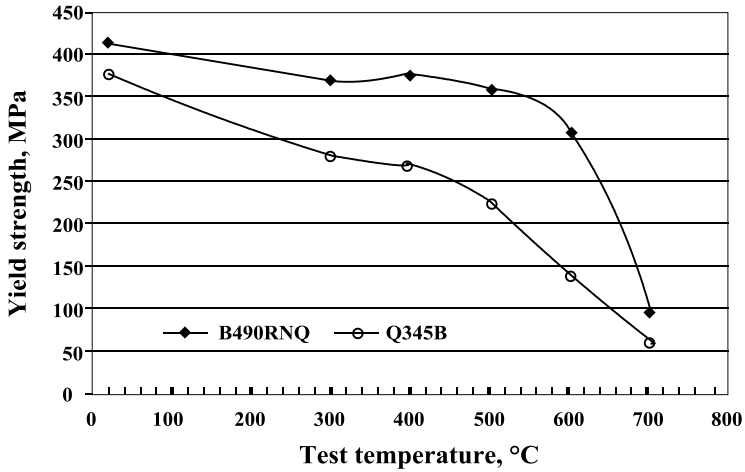

Figure 5. Comparison of elevated temperature yield strength properties of Q345 and B490RNQ FRS.

Table II. China FRS Composition (wt%) [8]

Steel	Base composition	Varied elements
A	0.12%C-0.25%Si-1.0%Mn-0.5%Cr	0.5%Mo
B	0.12%C-0.25%Si-1.0%Mn-0.5%Cr	0.02%Nb
C*	0.10%C-0.25%Si-0.9%Mn-0.5%Cr	0.5%Mo-0.02%Nb

* Steel C – Optimum Nb-Mo FRS composition

TMCP Considerations for FRS Plate Production

Thermomechanical processing laboratory simulations were developed to investigate the effect of finish rolling temperature on the room and elevated temperature strength of a Nb alloyed steel that might be considered for FR applications. Results suggest that finish rolling at low temperatures such as 650 °C can improve the elevated temperature strength of FR steel. This may be due to the presence of warm-worked ferrite generated from finish rolling at this temperature. The greater ability to maintain strength at elevated temperature may be due to the stability of the dislocation substructure that is created during warm working of the ferrite [9].

The constant-load test results illustrate differences between steels, with a Mo + Nb steel exhibiting better FR properties than comparative C-Mn, V, or Nb steels tested identically [10]. The good elevated temperature strength and creep properties are due to the high lattice friction stresses, which are the result of a very fine distribution of MC precipitates, Mo in solid solution, and a strong wave of secondary precipitation at approximately 650 °C. It is the lattice friction stress that maintains strengths up to 600 °C when grain boundary sliding initiates [11]. Nevertheless, it is observed that small additions of 0.017%Nb result in a greater elevated temperature strength offsetting the influences of significant changes in the base microstructure at these temperatures [12].

Thermomechanical processing of HSLA steels within the warm working regime of 0.4-0.6 T_m (where Tm is the absolute melting temperature) is known to produce a stable, recovered ferrite substructure [13]. The formation of a dislocation substructure in the ferrite occurs when the combination of strain and temperature allows sufficient dislocation motion and recovery to occur [14]. It has been shown that the presence of a bainitic microstructure can improve the elevated temperature strength of FR steels in comparison to a ferrite/pearlite microstructure [2,6]. Bainitic ferrite has some characteristics in common with recovered ferrite, specifically the presence of low angle boundaries. Therefore, it was decided to consider whether stable substructures may provide enhanced elevated temperature properties. Thermomechanical processing laboratory simulation cycles were developed and tested on a low Mo-Nb-Cu alloy to investigate the effect of finishing temperature on both the room temperature and elevated temperature strengths of a Nb-steel considered for FR applications. The composition of the rolled steel for the TMCP laboratory simulation is shown below in Table III.

Table III. Chemical Composition of FR Steel Used in TMCP Laboratory Simulation (wt%) [9]

C	**Mn**	**P**	**S**	**Si**	**Cu**	**Ni**
0.10	1.06	0.005	0.031	0.27	0.39	0.16
Mo	**Sn**	**V**	**Nb**	**Cr**	**Al**	**N**
0.047	0.011	0.001	0.021	0.09	0.003	0.011

TMCP Laboratory Rolling Simulation [9]

A schematic diagram of this processing experiment is illustrated below in Figure 6.

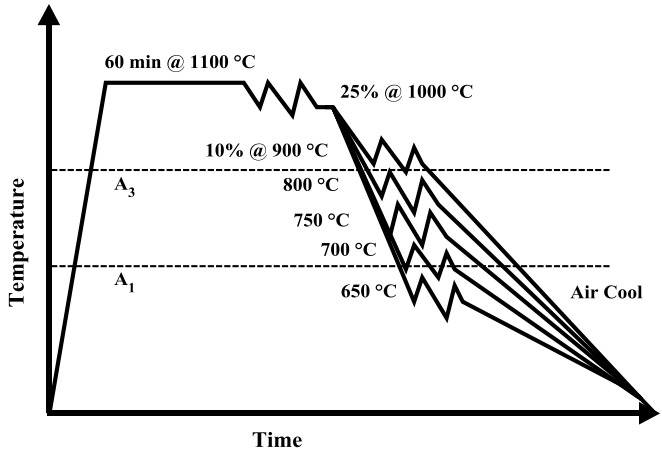

Figure 6. Schematic representation of the processing profile for study of effects of finishing temperature on fire resistant steel properties.

Room temperature tensile test results for the warm rolled experimental FR alloy are shown in Figure 7, as a function of finish rolling temperature. The results show that room temperature strength decreases with an increase in the finish rolling temperature of the FR steel. At the lowest finish temperature of 650 °C the highest yield and tensile strength values are observed, 424 MPa (61.5 ksi) and 574 MPa (83.3 ksi), respectively. As the finish rolling temperature increased into the two-phase region, the yield strength and tensile strength both decreased. During deformation at these finish temperatures there is a mixed microstructure of ferrite and austenite. At the highest finish rolling temperature of 900 °C, the microstructure consists entirely of austenite. Results show that the corresponding room temperature strength was lowest for this condition, probably because of the absence of warm worked ferrite grains and air-cooling to room temperature.

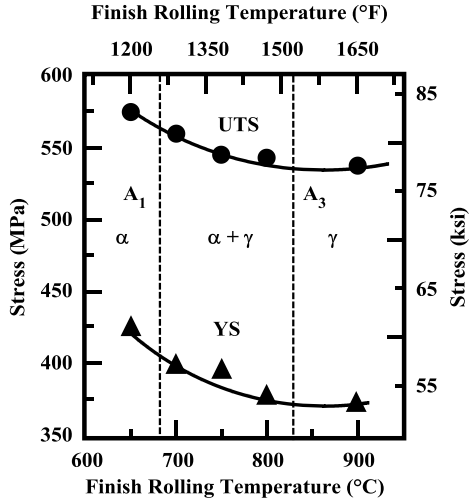

Figure 7. Room temperature yield and tensile strengths for FRS as a function of finish rolling temperature.

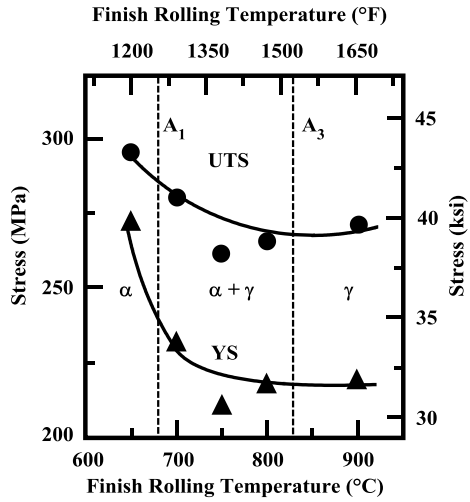

Figure 8. Elevated temperature (600 °C) yield and tensile strengths for FRS as a function of finish rolling temperature.

Elevated temperature mechanical property data at 600 °C for each finish rolling temperature are shown in Figure 8. The highest yield and tensile strength values are found to result from the lowest finishing temperature of 650 °C. The overall trend indicates that the highest yield and tensile strengths occur at the lowest finishing temperatures, presumably due to an increasing presence of warm worked ferrite. Intercritical rolling with higher finishing temperatures did not appear to increase the strength relative to austenitic rolling. The resulting elevated temperature strength ratio $YS_{600°C}/YS_{RT}$ and room temperature yield ratio YS_{RT}/UTS_{RT} were greatest for a finish rolling temperature of 650 °C, producing the highest 600 °C/RT yield strength ratio of 63%.

These results suggest that warm-working at low temperature may offer an attractive opportunity to increase the elevated temperature strength for FRS plate applications. Although this value does not surpass the JIS G 0567 standard of 66%, the rolling reduction was limited to 10% in the laboratory simulation. Also, because of these light reductions at very low rolling temperatures, adjustments to this low Mo-Nb composition are anticipated to easily meet the JIS standard.

Reinforcing Bar for Earthquake Zone Steel Development

With the projected increased intensity and frequency of hurricanes, earthquakes and cyclones, there is a market demand to develop and then consistently produce S500 and S600 rebars with elongations of 25 to 30%. Civil engineers are requesting steelmakers to produce reinforcing bar with elongation levels approaching 30%. Microalloying with Nb and Mo offers the possibility to achieve 600 MPa strength levels with elongations of 25 to 30% and an ultimate tensile strength to yield strength (UTS/YS) ratio of 1.28-1.30 [15]. The S500 Nb grade with a 700 °C self temper has a 1.24 tensile to yield ratio compared to a 1.18 ratio for a Nb-V chemistry. Specifications need to include a tensile to yield ratio similar to ASTM A706 in North America for seismic applications. In addition to a Nb or Nb/Mo chemistry, customized and disciplined quenching practices are of critical importance in order to successfully meet the properties required for this demanding application.

The S500 and S600 rebar alloy design strategy involves; (1) lower carbon equivalent to improve weldability, (2) improved ductility and toughness, and (3) achievement of good yield point elongation. Niobium is added at the 0.020 to 0.035% level to promote precipitation strengthening, improve grain refinement and enhance hardenability to compensate for the strength loss due to the reduced carbon and manganese levels. Additions of Mo in the 0.05 to 0.10% range will enhance hardenability in order to meet stringent earthquake applications and improve fire resistance, achieving elongations exceeding 25% and approaching 30% consistently. Nb and Mo have a synergistic effect helping to achieve a ferrite and bainite core in place of the conventional ferrite and pearlite core obtained with Tempcore. An alloying combination of Mo + Nb + Cr + Ni < 0.30%, C between 0.10-0.20% and Mn between 0.60-1.20% with specially designed coil cooling conditions and low sulfur/low phosphorous should consistently meet S500, and with further adjustments to rolling temperature and cooling, meet S600. This is an area of continuing research [16].

Niobium and molybdenum have a synergistic precipitation effect creating nano-precipitates, 5 to 10 nanometers in size, uniformly distributed throughout the matrix. The combination of grain refinement and nano-precipitation are significant factors in helping to achieve a finer ferrite and bainite core in place of the conventional ferrite and pearlite core with Tempcore [15]. The future seismic rebar recipe is an alloying combination of Mo + Nb, C between 0.10-0.20%, restriction of Mn to less than 1.00%, utilization of specially designed coil cooling practices and incorporation of low sulfur (less than 0.007%) and low phosphorous levels (less than 0.020% if possible). Such practices will significantly improve a given mills capability to consistently meet S500 property requirements, and with further adjustments to rolling temperature and cooling, meet S600 product requirements. As there has been limited published research on the impact and fracture toughness properties of rebar, some fundamental process metallurgy considerations should be incorporated into the production scheme to effectively manufacture S420, S500 and S600 seismic rebars. Three key elements that require strict control to improve ductility are illustrated in Figure 9.

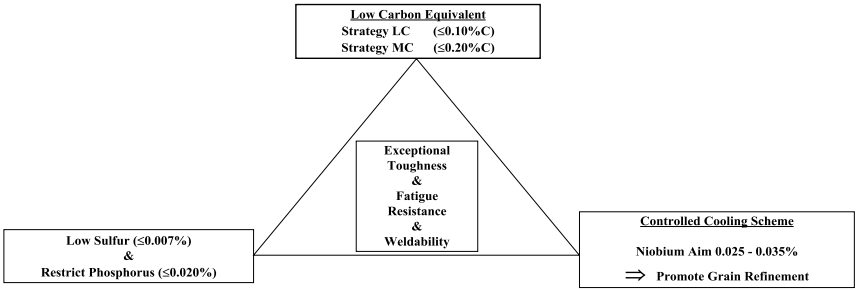

Figure 9. Ultra tough seismic rebar approach [17].

A lower total cost of production may be achieved through a low carbon-Nb alloy design incorporating the selective accelerated cooling approach in conjunction with better control of reheat furnace temperatures. For example, in comparing a Nb chemistry rebar with a V chemistry rebar, the Nb chemistry exhibits the more consistent elongation between 1100 and 1150 °C which is the optimal soak zone temperature for both ductility and efficient lower cost energy consumption (i.e. mmbtu per tonne). Reduced yield-to-tensile strength ratio variation is experienced as well with Nb-bearing versus V-bearing rebar when rolled with these thermal practices which offers quality improvements and reduced rejection rates [18].

Nb-Mo EQR Rebar (Earthquake Resistant)

The basic guidelines for designing this developmental Nb-Mo reinforcing bar are given in the Japanese Industrial Standard on Rolled Steel for Building Structures (JIS G3136-1994). The specification encompasses the mechanical property requirements as shown below in Table IV.

Table IV. Mechanical Property Requirements in JIS G3136-1994

Yield Strength (MPa) YS	Ultimate Tensile Strength (MPa) UTS	UTS/YS	Elongation (%)	Charpy @ 0 °C Joules
>325	>490	>1.25	>25	>27

Industrial heats of the Nb-Mo EQR chemistry nominally containing 0.14%C, 0.85%Mn, 0.25%Si, 0.024%Nb and 0.18%Mo were produced and evaluated. A variety of cooling practices were evaluated at various rebar diameters as shown below in Table V [19].

The Nb only and Nb-Mo grades of EQR exhibited excellent ductility (>36%) and a very high UTS/YS ratio (>1.24). The best balance of properties was obtained for the Nb-Mo combination with the partial water quenching cooling scheme as shown in Table VI.

Table V. Finish Temperatures (°C) by Size and Cooling Scheme

Thickness mm	80	62	47	35	25	18	12	Quenching Conditions
Nb-Mo 1	1070	1040	1010	990	950	890	800	AC
Nb-Mo 2	1070	1040	1010	990	950	890	825	AC
Nb-Mo 3	1070	1060	1050	1035	1020	990	950	Water cooling start at 730 °C
Nb-Mo 4	1070	1060	1050	1030	1015	1005	990	Water cooling start at 750 °C for few seconds and taken out

AC – Air Cool

Table VI. EQR Mechanical Properties [19]

Steel	Cooling Condition	YS (MPa)	UTS (MPa)	UTS/YS	Elong. (%)
Nb-Mo 1	AC	399	528	1.32	48
Nb-Mo 2	AC	386	532	1.38	46
Nb-Mo 3	WQ	533	780	1.46	37
Nb-Mo 4	PWQ	422	578	1.37	42
Nb	AC	400	500	1.25	48

AC – Air Cool

Summary

The future trend for successful development of higher strength FR steels and EQR S500 and S600 structural plate and bar grades will continue to incorporate Nb-Mo synergies for improved toughness performance at elevated temperatures. Seismic and fire resistant grades with Nb and Mo exhibit opportunities to increase toughness and maintain 2/3 of room temperature yield strength at 600 °C. The future for these grades is a dual Nb-Mo product as shown by the developments described in China, India, Japan and the USA. Further research and development activities are needed to transfer this Nb-bearing low carbon "clean steel" plate technology into the S500 and S600 value added long product structural sectors globally. The current fire resistant Nb-containing plate research provides a valuable foundation for the continuation of this development of a family of Nb-Mo chemistries which can be transferred to fire resistant and seismic resistant beam, rebar and plate research. Additionally, the civil and materials engineering communities need to collaborate more effectively to optimize structural design, tensile to yield ratio criterion and Nb-Mo bearing steel materials selection for fire and seismic resistant structural steel applications.

References

1. S. Jansto, "Successful Melting and Casting of Nb-bearing Carbon Steel Billets, Slabs and Beams" (Paper presented at the Roundtable Meeting on the Quality of Billets, Slabs and Beams of Nb-bearing Steels, Beijing, China, 29-30 June 2009).

2. J.C. Cross, "Effects of Microstructure on the Fire-resistant Properties of HSLA Structural Steels" (M.S. thesis, Colorado School of Mines, Golden, CO, 2006).

3. D. Wen, Z. Li, and J. Cui, "Development of Fire-resistant Weathering Steel for Buildings in Baosteel," (Niobium Bearing Structural Steels, TMS, October 2010), 157-164.

4. Y. Sakumoto, "Use of FR Steel: Design of Steel Frames to Eliminate Fire Protection, New Developments in Steel-frame Building Construction" (Nippon Steel Corporation, October 1993), 1-21.

5. J.G. Speer, R.W. Regier, and S. Jansto, "Elevated Temperature Properties of Nb-microalloyed Fire-resistant Constructional Steels" (Paper presented at the International Symposium on New Developments and Applications of High Strength Steels, Buenos Aires Hotel, Argentina 26-28 May 2008).

6. Y. Mizutani et al., "590 MPa Class Fire-resistant Steel for Building Structural Use" (Nippon Steel Technical Report No. 90, 2004), 45.

7. R. Chijiwa et al., "Development and Practical Application of Fire-resistant Steel for Building Construction" (Nippon Steel Corporation Technical Report, No. 58, 1993) 47-55.

8. D. Wen, Z. Li, and J. Cui, "Development of Fire-resistant Weathering Steel for Buildings in Baosteel" (Niobium Bearing Structural Steels, TMS, October 2010), 157-164.

9. R. Regier et al., “Thermomechanical Processing Effects on the Elevated Temperature Behavior of Niobium Bearing Fire-resistant Steel” (Paper presented at the Materials Science & Technology Conference, Detroit, Michigan, 16-20 September 2007).

10. J. Speer and S. Jansto, “Nb Microalloyed Fire-resistant Steel,” (Niobium Bearing Structural Steels, TMS, October 2010), 139-156.

11. W. Sha, F.S. Kelly, and Z.X. Guo, “Microstructure and Properties of Nippon Fire-resistant Steels,” *Journal of Materials Engineering and Performance*, 8 (5) (1999), 606-612.

12. J.G. Speer et al., “Elevated Temperature Properties of Niobium-microalloyed Steels for Fire-resistant Applications,” (Paper presented at the 2005 HSLA Conference, Sanya, China, 8-10 November, 2005).

13. N. Hansen and R. Mehl, “New Discoveries in Deformed Metals,” *Metallurgical and Materials Transactions A*, 32 (12) (2001), 2917- 2935.

14. C.M. Young and O.D. Sherby, “Subgrain Formation and Subgrain-boundary Strengthening in Iron-based Materials,” *Journal of the Iron and Steel Institute*, 211 (9) (1973), 640-647.

15. S. Jansto, “Niobium-bearing Steel Development for Weldable Structural Steel Applications” (Paper presented at the International Roundtable on Yield to Tensile Ratio, Beijing, China, 17-18 June 2009).

16. V. Kumar et al., “Development of Earthquake Resistant TMT Bars,” *Steel Scenario*, 15 (Q3) (2006), 76-77.

17. S. Jansto, “Production and Application of High Strength Earthquake Resistant Nb-bearing Reinforcement Bar” (Paper presented at the Seminar on Niobium Bearing Structural Steels, New Delhi and Mumbai, India, March 2010).

18. S. Jansto, “Production and Niobium Application in High Strength and Earthquake Resistant Reinforcing Bar” (Paper presented at the International Reinforcing Bar Symposium, Beijing, China, 18-20 May 2009).

19. A. Deva et al., “SAIL’s Effort Toward Development of Nb-microalloyed High Strength Steels for Structural Applications” (Paper presented at the International Symposium on Niobium Bearing Structural Steels, New Delhi, India, 12-15 April 2011).

Fundamentals and Applications of Mo and Nb Alloying in High Performance Steels – Volume 1
Edited by Hardy Mohrbacher
CBMM, IMOA and TMS, 2014

METALLURGY OF TWO TYPES OF PRECIPITATION HARDENED HIGH STRENGTH FLAT-ROLLED PRODUCTS FOR AUTOMOBILE APPLICATIONS

Yoshihiro Hosoya, Toshiaki Urabe, Yoshimasa Funakawa and Yoshihiko Ono

Steel Research Laboratories, JFE Steel Corp., Japan

Keywords: High Strength Steels, Interphase Precipitation, Stretch Flangeability, Niobium, Molybdenum, Automotive, IF Steel, TEM, SEM, r–value, Grain Size, Hole Expansion, Microstructure

Abstract

Two types of high strength flat-rolled products, which were originally developed by JFE, are presented in this paper. One is a high strength cold-rolled sheet for automobile body panels aiming to achieve a strength of 440 MPa with excellent formability, sufficient galvannealing (GA) applicability and anti-secondary work embrittlement. The other is a hot-rolled strip for under-body or chassis parts aiming at a strength of 780 MPa and having an excellent balance between elongation and stretch-flangeability, less scatter of mechanical properties and sufficient thermal stability of strength for GA application. From the metallurgical viewpoint, both products have unique features. The former contains around 50-60 ppm carbon, and Nb at the stoichiometric level in relation to carbon, which forms fine NbC precipitates in a ferrite matrix and subsequently promotes the formation of a PFZ (Precipitation Free Zone). Since the PFZ acts as a micro-yielding site, a low yield to ultimate strength ratio is attained with a fine grain structure. The latter steel contains Ti and Mo, which form MC type complex carbides by interface precipitation during γ/α transformation after hot-rolling. Since the matrix structure is composed of a ferritic single phase, excellent stretch flangeability is achieved compared to multi-phase high strength steel types with the same strength.

Introduction

Since the mid-1990s, the ULSAB, ULSAS, ULSAC and ULSAB-AVC projects have given the opportunity to not only reassess the conventional high strength steels (HSS) but also to work on the development of new types of HSS to achieve further weight-reduction of the car body whilst maintaining the collision safety and the stiffness of the body structure. Consequently, many new hot- and cold-rolled HSS have been developed up to the present day. For example, ultra-HSS with a tensile strength higher than 980 MPa with sufficient ductility, TRIP (Transformation Induced Plasticity) steels containing sufficient amounts of retained austenite which markedly improves the stretch formability. Regarding hot-rolled HSS, in particular, the types with a microstructure composed of a bainite or ferrite single phase, strengthened by fine precipitates, have been developed to take into account the need for enhanced stretch flangeability.

However, the body weight reduction achieved by use of HSS alone is already facing the following limitations:

(1) Limit of formability (lack of shape retention and surface distortion),
(2) Limit for the improvement of mechanical properties (large gap between weight saving target and expected value with improved mechanical properties),
(3) Limit for the improvement of rigidity (required component's rigidity has, despite strength improvements, restricted the component thickness reduction attainable through the use of HSS).

Thus, the share of HSS used in the structure and safety related parts appears to be almost saturated in recent car designs.

Considering the recent research activities on HSSs for automotive applications, it seems that the TRIP and TWIP (TWinning Induced Plasticity) types, which have excellent strength and ductility balances, have attracted a lot of global research activity. However, their alloy design, with high Mn content, makes it difficult to use them widely in automobiles for economical as well as metallurgical reasons. Regarding strengthening of interstitial free (IF) steels, on the other hand, it has also been found that the addition of Mn as a solid-solution hardening element up to 2.0% markedly deteriorates the r-value. These examples indicate the definite limitation of alloying with substitutional solid-solution elements, in particular Mn, in the development of flat-rolled HSSs for automotive applications.

In this paper, two types of HSS, which were developed based on the common concept to intentionally utilize fine precipitation hardening, are introduced by extracting typical data from the technical articles presented by the authors so far. One is a high strength cold-rolled steel sheet for automobile body panels aiming up to a strength of 440 MPa which has excellent formability, sufficient GA applicability and anti-secondary work embrittlement [1-3]. The other is a high strength hot-rolled strip for under-body or chassis parts aiming at a strength of 780 MPa and having an excellent balance between elongation and stretch-flangeability, less scatter in mechanical properties and sufficient thermal stability of strength for the subsequent reheating required for GA application [4-6].

Cold-rolled HSS with a Tensile Strength Higher than 390 MPa, Strengthened by Fine NbC Precipitates.

Materials Design Concept

Regarding the solid-solution hardening of IF steels used for exposed panels, unavoidable problems have been experienced such as:

(1) Addition of a high amount of Mn deteriorates the r-value,
(2) Solid-solution hardening of the ferrite matrix by alloying with Mn, Si and P deteriorates the resistance to secondary work embrittlement,
(3) GA qualities are detrimentally affected by high contents of Mn, Si and P.

Although grain refinement is an effective way to improve the toughness of steel, this has not been intentionally applied to flat-rolled products because the increase in yield stress deteriorated the shape retention capability of stamped panels.

Figure 1 shows the alloy design concept of grain-refined IF steels. Grain refinement and precipitation hardening are combined with solid-solution hardening to improve galvanizability and resistance to secondary work embrittlement.

The grain refinement and the precipitation hardening were achieved by an appropriate combination of a fine distribution of carbides with relatively high carbon content close to 60 ppm and a niobium (Nb) addition, enough to form NbC precipitates. By adding the precipitation strengthening on top of the base strength, the content of solid solution elements could be reduced. In particular, reduction of Si was effective in improving the GA quality.

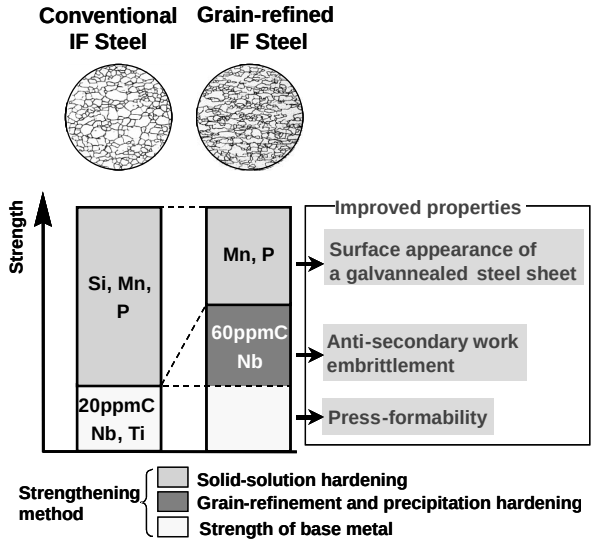

Figure 1. Schematic diagram showing the metallurgical concept of the newly developed steel compared to the conventional IF steel.

Outstanding Mechanical Properties

In general, the mean r-value of cold-rolled steel sheets is directly related to the ASTM grain size number as shown in Figure 2 [7]. The mean r-value can be improved by elevating the annealing temperature because of the further growth of the {111} grains, and can reach over 2.5 in IF steels. However, steel sheets with coarse grains cause a rugged surface, so-called "orange-peel," after stamping, which is not suitable for the surface quality required for exposed panels. The

newly developed grain-refined IF steel exhibited an outstanding balance of mean r-value and grain size compared to conventional cold-rolled sheets as shown in Figure 2. This was caused by a nucleation and growth of γ-fibre texture which was dominated by the grain refinement of the ferrite structure in the hot-band material.

Another feature of this steel was the unique yielding behavior, i.e. yield stress was kept low despite the tensile strength being increased by the precipitation hardening and the grain refinement as shown in Table I. For example, the 390 MPa grade steel has a yield stress which is comparable to that of the present 340 MPa BH steels which are currently applied widely for the exposure panels with anti-surface deflection.

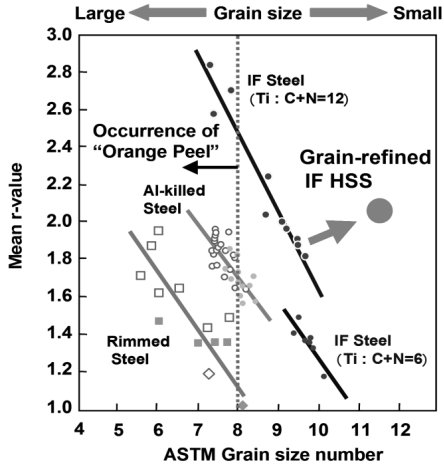

Figure 2. Correlation between ASTM grain size number and mean r-values of cold-rolled steel sheets.

Table I. Mechanical Properties of 340 to 440 MPa Grade, Grain-refined IF HSS, SFG-HITEN [16]

Type	Grade	Thickness (mm)	YS (MPa)	TS (MPa)	El (%)	Mean r-value	Tc (˚C)
CR	SFG390	1.0	235	405	40	1.9	-85
	SFG440	1.0	290	446	37	1.9	-65
GA	SFG390	1.0	227	400	38	1.7	-65
	SFG440	1.0	285	442	35	1.7	-45

CR : Cold-rolled steel sheet, GA: Galvannealed steel sheet
Tensile specimen : JIS No.5, Transverse direction
Tc : Transition temperature for anti-secondary work-embrittlement with a cup-height of 35 mm and a drawing cup ratio of cup-diameter to blank diameter, 2.1 for 340 grade and 2.0 for 390 and 440 grades.

Formation of Microstructure

A surprising characteristic of this steel was the formation of a PFZ (Precipitation Free Zone) during annealing which dominated the unique mechanical properties as briefly discussed in the previous section. Figure 3 shows the distribution of fine precipitates observed in the 390 MPa grade steel. Fine NbC precipitates with diameter of 10 to 40 nm were observed. The arrays of relatively coarser precipitates seem to be distributed along the grain boundaries. Some of the arrays of coarse precipitates accompany the parallel precipitate arrays along the grain boundaries. In the areas between these pairs of arrays, very few fine precipitates are observed, which is close to the precipitation free zone (PFZ) besides the small numbers of coarser precipitates. While the so-called PFZ is formed on both sides of a grain boundary, in general, these areas with few precipitates were observed to be located along one side of the grain boundaries.

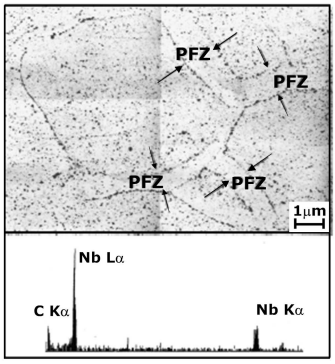

Figure 3. TEM image from replica and EDS spectra of precipitates, observed in the annealed sheet of 390 MPa grade of grain-refined IF HSS [10].

The increment in strength due to precipitation hardening and grain refinement is approximately 30 MPa. Therefore, it can be considered that the strength of the PFZ is lower than that of the grain matrix due to the absence of precipitation hardening. This is the dominant feature, which leads to the lower yield strength. However, with progress of deformation after yielding, intergranular deformation mainly takes place, and the tensile strength nearly equalizes the level of the grain matrix, strengthened by the fine NbC precipitates. Although it is well known that both grain-refinement and precipitation hardening increase the yield strength of steel, the grain-refined IF-HSS exhibits a yield/TS ratio lower than that of conventional solid-solution hardened IF-HSS, which is not consistent with conventional understanding.

Figure 4 shows a TEM micrograph highlighting the sub-structure, which was developed near the grain boundaries in the early stage of deformation after 0.5% tensile straining, in which the yielding has just occurred. It was observed that the dislocations were pinned by the NbC precipitates at the boundary between the PFZ and the precipitation dispersed matrix, and they bowed from the grain boundary side to the matrix side as indicated in the figure by the white

arrows. It was also found that the dislocation density was very low in the PFZ. Since the grain boundary is considered to act as the effective Frank-Reed source, it is suggested that the dislocations were generated at the grain boundaries and moved towards the matrix through the PFZ.

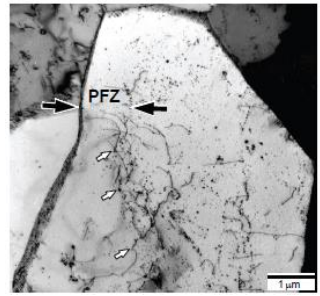

Figure 4. TEM micrograph of specimen deformed with 0.5% tensile strain [18].

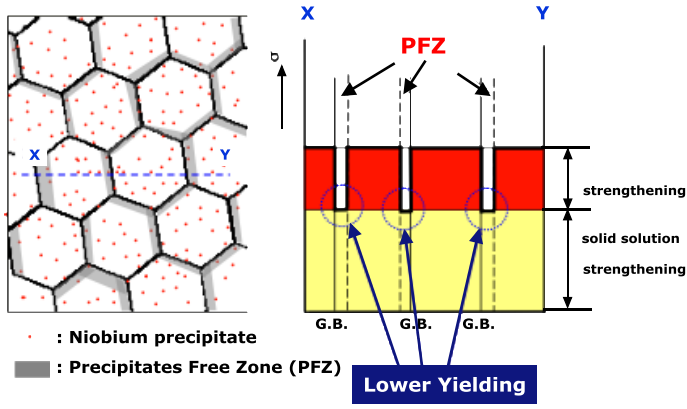

Figure 5. Mechanism of providing low yield strength.

Furthermore, the PFZ region should be softer than the matrix where the NbC particles are dispersed homogeneously. Therefore, it was inferred that the dislocations could easily be generated at the grain boundaries accompanied by a PFZ. This is the probable reason why this steel exhibits a low yield strength with a fine grain structure as schematically depicted in Figure 5. Other results also clearly demonstrated that the yield strength of this steel depended on the volume fraction of the PFZ, which was controlled by the heating rate during annealing.

Regarding the anti-secondary work embrittlement, it was also improved by the grain refinement. The micro alloying of boron (B) was effective in further improving the anti secondary-work embrittlement**.**

Hot-rolled HSS with Tensile Strength Higher than 780 MPa Strengthened by the Interphase Precipitation of (Ti,Mo)C Fine Complex Carbides.

Concepts of the Material and Process Design

Several problems for utilizing TRIP steel have been experienced, such as:

(1) High amount of Mn addition to obtain a sufficient volume fraction of meta-stable retained austenite is costly,
(2) Variation of mechanical properties over the entire coil was large, caused by the instability of austempering condition,
(3) Deterioration of the stretch-flangeability by secondary working, such as shearing and blanking, was large caused by the high susceptibility for deformation,
(4) Softening of the hard phase was unavoidable during reheating such as in hot-dip galvanizing and welding.

As a solution to these problems, precipitation hardening by TiC with suppressed ferrite and pearlite transformation promoted by the addition of Mn and Mo was used, as schematically depicted in the CCT diagram in Figure 6.

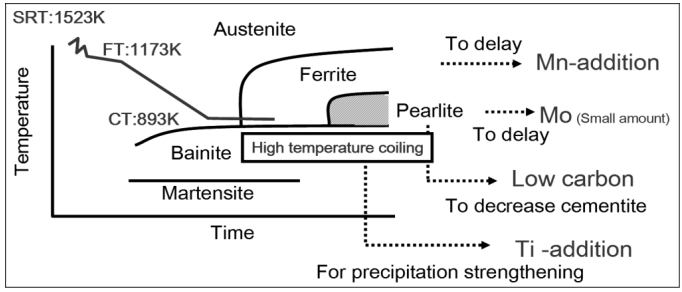

Figure 6. Schematic CCT diagram of alloy design and on-line microstructure control.

Outstanding Mechanical Properties

The most outstanding mechanical property characteristic of the 780 MPa HSS was the excellent balance between elongation and stretch flangeability as shown in Figure 7. (Stretch flangeability as measured by the hole expansion test). This balance was achieved by the steel microstructure which was composed of single phase ferrite in comparison to other steels whose microstructure is composed of mixed phases containing bainitic and/or martensitic hard phases.

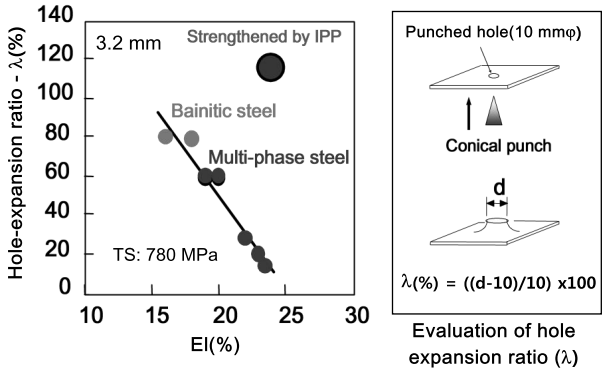

Figure 7. Outstanding El- λ balance of hot-band strengthened by interphase precipitation (IPP).

Formation of Microstructure and Origin of Mechanical Properties

The remarkable feature of this steel was the achievement of a tensile strength of up to 780 MPa with a ferrite single phase. This resulted from the precipitation of MC type (Ti,Mo)C, nano-scale fine complex carbides which were formed by interphase precipitation during the γ/α transformation after the finish of hot-rolling, as shown in Figure 8. Against initial expectation, the results proved that Mo formed complex carbides, substituting half of the Ti atoms in TiC, formed by interphase precipitation.

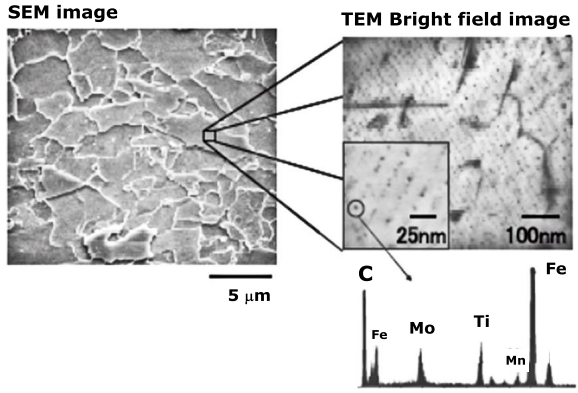

Figure 8. Typical microstructure of 780 MPa class hot-strip, hardened by nano-scale interphase precipitates.

XRD analysis of the precipitates revealed that the (Ti,Mo)C formed a super lattice and satisfied the Baker-Nutting relationship with the ferrite matrix as shown in Figure 9. This precipitation was the dominant cause of both the marked increase in hardenability and the thermal stability of the ferrite phase in this steel.

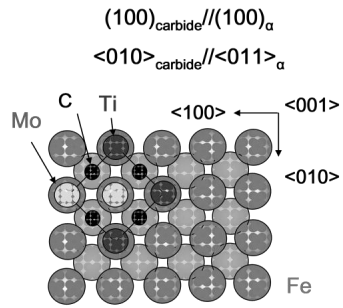

Figure 9. Lattice structure of precipitates and crystallographic relationship with ferrite matrix.

The strengthening mechanisms in this steel were estimated as follows. Since the yield stress caused by the sum of solid-solution hardening of the given chemistry and hardening by grain refinement is around 400 MPa, the remaining 300 MPa must be made up by precipitation hardening ($\Delta\sigma$).

The Δσ was calculated by applying the Orowan model to the nano-scale precipitates. From the results shown in Figure 10, the gap in strengthening from 400 MPa to 700 MPa, which was the yield stress of this steel, could be made up by precipitation hardening based on the Orowan mechanism.

Regarding the outstanding thermal stability of the strength of this steel, the hardness change of three steels, i.e. Steel A(Ti-Mo), Steel B(Ti-Nb), Steel C(Ti), isothermally held for $8x10^5$ seconds at 650 °C, was evaluated. In this experiment, the average size of the precipitates in each steel was 3 nm, 6 nm, and 13 nm in steels A, B, C, respectively. The hardness of Steel A was very stable compared to steels B and C as shown in Figure 11. Subsequent studies revealed that the thermal stability of the precipitates was improved by reducing their interfacial energy which was dominated by the excess amount of carbide forming elements in solution.

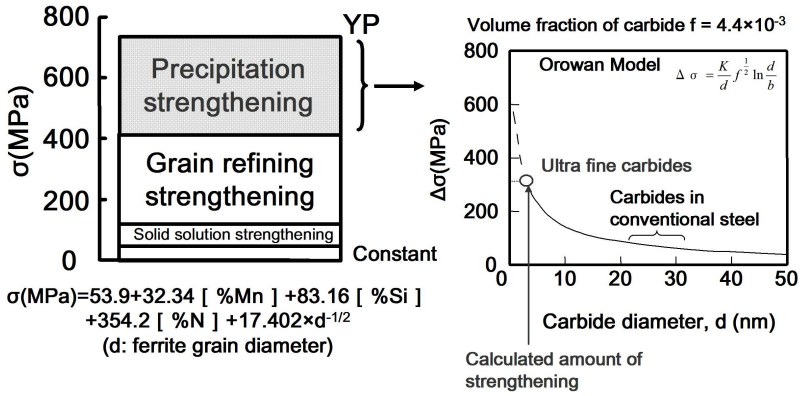

Figure 10. Strengthening of ferrite matrix by nano size fine carbides.

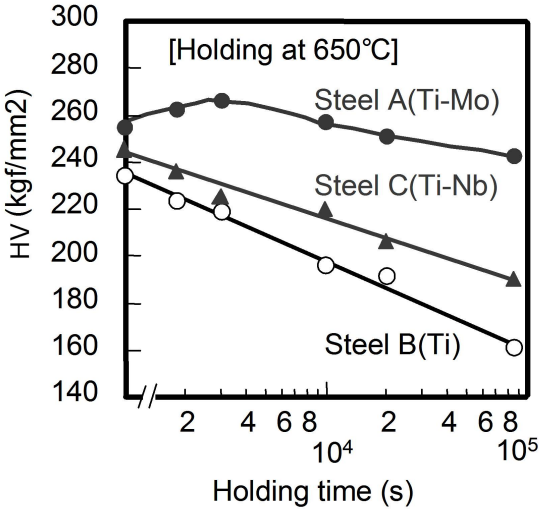

Figure 11. Softening behavior of three types of steels after isothermal holding at 650 °C.

Summary

The typical features of the two types of steel developed by the authors were introduced. Most of the unique features of the steels were hard to predict at the beginning of the investigation.

When starting the R&D program, adding C up to around 60 ppm and coiling at a temperature higher than 600 °C appeared to be an unlikely way for the development of cold-rolled and hot-rolled HSSs, respectively. Yet, it led to the discovery of metallurgically innovative flat-rolled products.

There might be more undeveloped concepts that are worthy of assessment. It also seems interesting to further explore the feasibility of precipitation hardening with Nb, Mo and Ti, compared to conventional strengthening by solid-solution hardening and phase transformation hardening in flat-rolled products.

References

1. F. Kitano et al., “New Type of IF-high Strength Steel with Superior Anti-secondary Work Embrittlement,” *Iron and Steel Institute of Japan International*, 41 (11) (2001), 1402-1410.

2. Y. Ono et al., “Effect of NbC Distribution on Mechanical Properties of IF High Strength Steel with Fine Grain Structure,” *Materials Science Forum*, 426-432 (2003), 1481.

3. Y. Hosoya et al., “Current Progress in High Strength Cold-rolled and Coated Steel Sheets for Automobile Body Panels”, *Iron and Steel Institute of Japan International, Asia Steel International Conference, 9-11 May*, (2006), 102-107.

4. Y. Funakawa et al., “Development of High Strength Hot-rolled Sheet Steel Consisting of Ferrite and Nanometer-sized Carbides,” *Iron and Steel Institute of Japan International*, 44 (11) (2004), 1945-1951.

5. K. Setoand and Y. Funakawa, “Coarsening Behavior of Nanometer-sized Carbides in Hot-rolled High Strength Sheet Steel,” *Materials Science Forum*, 539-543 (2007), 4813-4818.

6. Y. Funakawa, K. Seto, and H. Nakamichi, “Strengthening of Ferritic Steel by Interface Precipitated Carbides in Rows,” *Materials Science Forum*, 638-642 (2010), 3218-3223.

7. D.A. Karlyn, R.W.Vieth, and J.L. Forand, *Mechanical Working and Steel Processing VII* (New York, NY: The Metallurgical Society of AIME, 1969), 127.

Fundamentals and Applications of Mo and Nb Alloying in High Performance Steels – Volume 1
Edited by Hardy Mohrbacher
CBMM, IMOA and TMS, 2014

THE USE OF MOLYBDENUM AND NIOBIUM IN ULTRA-HIGH STRENGTH MULTIPHASE STEELS

Hardy Mohrbacher

NiobelCon bvba, 2970 Schilde, Belgium

Keywords: Molybdenum, Niobium, Ultra-high Strength, Multiphase Steels, Strip, Automotive, DP Steel, CP Steel, Hole Expansion, Annealing Strategies, TRIP Steel, Phase Transformation

Abstract

Multiphase steels such as DP (Dual Phase), TRIP (Transformation Induced Plasticity) and CP (Complex Phase) can be produced either directly from the as rolled heat or via an additional heat treatment, usually after cold rolling. The latter has become the dominating route in automotive steel production. The primary effect of Mo alloying is to modify the phase fields in the CCT diagram in such a way that a sufficiently large processing window enables stable production with little property scatter in the final product. Niobium microalloying can improve the strength of multiphase steels in various ways. It is also particularly beneficial with regard to the phase morphology and homogeneity leading to a significant improvement of the mechanical properties. This paper will show processing strategies involving Mo and Nb and explain their metallurgical effects.

Challenges to Modern Vehicle Construction

No other industrial sector has pursued weight reduction as vigourously as the automotive industry. This has been motivated by the need to reduce fuel consumption and emissions as well as the requirement to improve crash safety, and these continue to be major technical targets. The total vehicle weight has an important impact in this respect as indicated in Figure 1. Indisputably, the fuel consumption and thus the CO_2 emissions decrease with reducing vehicle weight. Several studies have indicated that a weight reduction of 100 kg can lead to savings in fuel consumption of 0.15 to 0.5 liters per 100 km [1]. This corresponds to a reduction in CO_2 emissions of between 4 and 12 g/km. The intensive use of lighter materials is effectively offering a significant weight reduction potential. Another possibility for reducing emissions is to use hybrid engine technology, however in this case vehicles tend to become heavier due to a weight increase of the power train. Very efficient in terms of emission reduction is engine downsizing which simultaneously leads to a weight reduction of the power train. Lighter vehicles not only reduce fuel consumption but also feature faster acceleration, shorter braking distances and overall better handling.

The body-in-white (BIW), i.e. the body structure, including all hang-on parts such as fenders, doors and lids, constitutes the largest contribution to the total vehicle weight. Furthermore, the BIW is also primarily responsible for the weight increase from one vehicle generation to the next as bodies usually become bigger and crash requirements are increased. The weight of the BIW ranges roughly from 300 to 500 kg depending on vehicle size [2]. Consequently, many efforts have been made by the industry to lighten the BIW [3]. Bodies using an advanced steel design

usually account for 28 to 35% of the total vehicle weight. In some sports cars and larger sized luxury vehicles, bodies are manufactured from aluminum, reducing the BIW weight contribution to between 16 and 20%. Many of today's mid-size vehicles apply a mixed materials concept for the BIW where the body structure is made with an advanced steel concept and hang-on parts are made from aluminum or plastics. This appears to be a good compromise between weight reduction, manufacturing complexity and cost.

The advanced steel BIW is the most cost-efficient way of reducing the vehicle weight. Weight reductions of 20 to 25% compared to a conventional steel body can be achieved at a simultaneously reduced cost [4]. Alternatively, when applying low-density materials such as aluminum, magnesium or plastics, weight reduction leads to a significantly increased cost of the BIW. Therefore steel remains the preferred material for vehicle construction. Additionally, established manufacturing technology such as press stamping, roll profiling and welding can still be used. In terms of steel development, the requirements of modern steels for vehicle construction are defined as being strong, formable, weldable and cost attractive.

Most of the components used for BIW, suspension, chassis or frame are produced from flat steel that comes either as hot rolled strip (for heavier gauges) or cold rolled strip (typically for gauges below 3 mm). The BIW of modern passenger cars contains up to 80% high strength steel of which the majority is covered by traditional (ferritic, ferritic-pearlitic or bainitic) HSLA steel. Multiphase steels, Figure 2, offering a good compromise of high strength and adequate elongation, have been gaining a significant share since the late 1990s. More recently, press-hardening steel (PHS) with a typical strength of above 1200 MPa has been introduced for applications requiring an extreme resistance against crash impact.

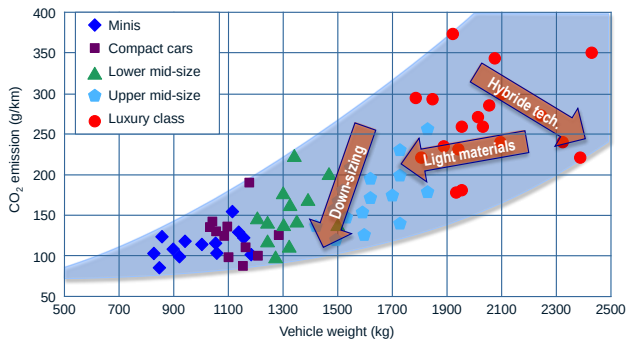

Figure 1. Influence of vehicle (curb) weight on CO_2 emission and concepts for reducing weight and emissions.

Molybdenum and niobium alloying is applicable to both hot rolled and cold rolled high strength steels. Niobium can be considered as an essential microalloying element in almost all high strength automotive flat steels. Besides its effect of grain refinement, niobium is also used for scavenging carbon (applicable to IF and BH steels), precipitation hardening and transformation

control. Mo alloying brings about valuable metallurgical advantages, especially when producing automotive steels with strengths exceeding 500 MPa. Mo suppresses the formation of ferrite and pearlite allowing the formation of bainite or martensite which are essential ingredients of multiphase steels.

Multiphase steels such as DP (Dual Phase), TRIP (Transformation Induced Plasticity) and CP (Complex Phase) steel can be produced either directly from the as rolled heat or via an additional heat treatment, usually after cold rolling. The latter has become the dominating route in automotive steel production.

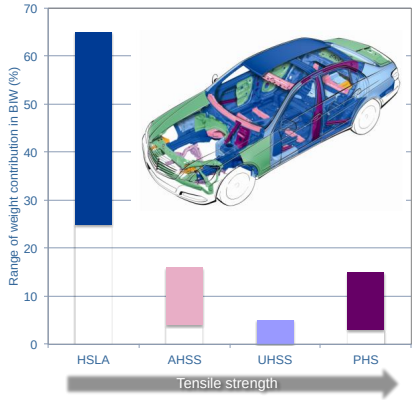

Figure 2. Contribution (min-max) of high strength steel classes to the total body-in-white (BIW) weight in the vehicle generation 2009-2010.

Hot Rolled Multiphase Steels

Hot rolled multiphase steel is used for heavier gauge applications such as used in chassis parts, anti-intrusion beams, reinforcements, and wheels. Hot-rolled dual phase and complex phase steel with tensile strengths of 600 and 800 MPa are the grades of most relevance.

Dual Phase Steel

Dual phase (DP) steels are characterized by a unique combination of strength and formability. Their soft ferritic matrix accounts for a low yield strength and good ductility whereas dispersed hard martensite islands ensure a high tensile strength. The resulting low yield-to-tensile strength ratio provides a high strain hardening capacity making these steels particularly suitable for uniaxial or biaxial stretching. With regard to crash deformation, this behavior also guarantees high energy absorption capability. Due to their high tensile strength, DP steels are also very suitable for applications subjected to cyclic loading.

During the production of dual phase steel directly from the rolling, the cooling strategy on the run-out table must allow sufficient formation of pro-eutectoid ferrite (matrix phase) without nucleation of pearlite. The carbon is partitioned to the remaining austenite phase, increasing its stability against transformation to ferrite. The boundary conditions are defined by the exit speed of the strip from the last finishing stand, the length of the run-out table, the configuration of the cooling headers and the coiling temperature. Accordingly, it becomes necessary to modify the CCT diagram by alloying in order to produce a ferritic-martensitic dual phase microstructure. The challenge is to avoid bainite or pearlite formation and to have the desired share of soft polygonal ferrite in the microstructure, typically 70-85% for the most common grades. The remaining carbon enriched austenite is transformed into martensite upon further cooling.

By way of reducing carbon diffusivity and exerting a strong drag force on moving grain (phase) boundaries, Mo delays ferrite formation and, to a much stronger extent, pearlite formation. Other bulk alloying elements like Mn and Ni also delay ferrite and pearlite formation. However the effectiveness of Mo is about 3 times stronger than that of Mn and 6 times stronger than that of Ni [5].

Two principal cooling strategies can be practiced depending on the capabilities of the run out table cooling arrangement, Figure 3. In single-step cooling the activation of accelerated cooling by water is delayed to allow sufficient formation of ferrite after finish rolling. Accelerated cooling is then applied to enable coiling below the martensite start temperature. The position of the ferrite nose in the CCT diagram has to be adapted to the required cooling path, by alloying. Using two-step cooling, fast cooling to a temperature of around 700 °C is applied right after finish rolling. Cooling is then interrupted and a stage of quasi-isothermal holding allows sufficient ferrite formation. Finally, the second cooling step aims for a coiling temperature of below 250 °C converting carbon-enriched austenite into martensite. It is apparent from Figure 3 that increasing the time gap between the initial bainite-martensite phase field and the pearlite phase field enhances the processing window regardless of the cooling strategy. Yet, the two-step cooling process is the preferable strategy. Molybdenum alloying can most efficiently influence the phase fields in the CCT diagram [6]. Figure 4 demonstrates the effect of Mo on the relevant times of ferrite start, pearlite start and 75% ferrite formation. It is evident that, for the given base alloy, the addition of 0.1% Mo sufficiently delays the pearlite start to allow the formation of 75% ferrite. Mo has a pronounced effect on the pearlite nose, shifting it by several orders of magnitude in time as the Mo content is raised from 0% to 0.50%. Its retarding effect on the polygonal ferrite reaction is much smaller; with the net result being that Mo increases the window of allowable cooling rates (CR_{max}/CR_{min}) very strongly. The effects of Cr and Si on the allowable cooling rates are much smaller than that of Mo, however, an inherent benefit of Si is the acceleration of polygonal ferrite formation. Si and Cr also contribute to the hardenability of austenite islands. Thus Mo additions in the range of 0.1-0.2% appears a reasonable compromise between processing conditions and alloy cost. More severe austenite conditioning, promoted by a microalloy addition of Nb and the consequent faster ferrite nucleation, can counteract the small delay in ferrite formation caused by Mo.

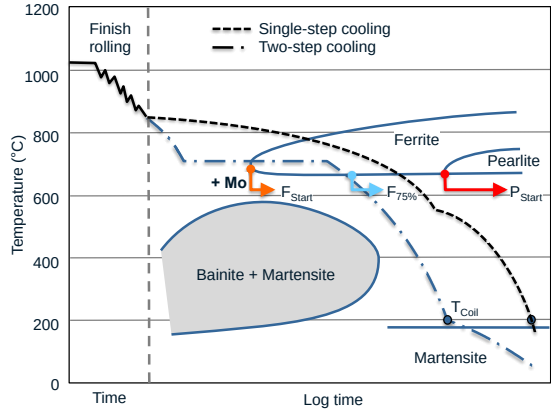

Figure 3. Finishing strategies for hot-rolled dual phase steel and the effect of Mo-alloying on the ferrite and pearlite phase fields.

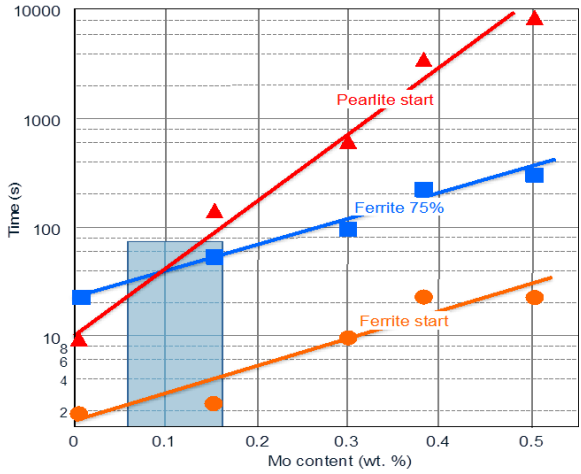

Figure 4. Effect of Mo-alloying on the ferrite and pearlite start time after finish rolling and typical alloy range for production of hot-rolled DP600.

Nb microalloying of hot rolled DP steel results in a significantly higher yield and tensile strength. The total elongation (A_{80}) for this much stronger Nb microalloyed variant is only slightly reduced at low coiling temperatures (<250 °C). A small addition of 0.04%Nb to the base alloy (0.11%C, 0.1%Si, 1.2%Mn, 0.8%Cr) lifts the tensile strength by around 200 MPa at lower

coiling temperatures and by around 100 MPa at higher coiling temperatures, Figure 5. The Nb-alloyed variant would still meet the strength requirements of DP600 after coiling at 350 °C. However, the yield to tensile strength ratio also increases from around 0.6 to above 0.7 indicating that the typical dual phase character is being lost at increasing coiling temperatures. The total elongation is only slightly reduced for the Nb-alloyed variant at lower coiling temperatures. Thus, Nb microalloying of the DP600 base grade can achieve a DP780 strength level with comparably good elongation and low yield-to-tensile ratio.

The tensile strength of DP steel is basically controlled by the martensite content and increases linearly with the martensite fraction. The addition of 0.05%Nb to a 0.18%C-Mn-Si-Cr base alloy results in an increase of the tensile strength by 100-150 MPa, Figure 6, at any martensite level [7]. Consequently by Nb microalloying, a specified strength level can be achieved with a lower martensite content and hence a better elongation. Niobium microalloying in combination with a high cooling rate results in an extremely fine-grained microstructure, as demonstrated in Figure 6. The finish rolling temperature appears to have no significant influence on the grain size.

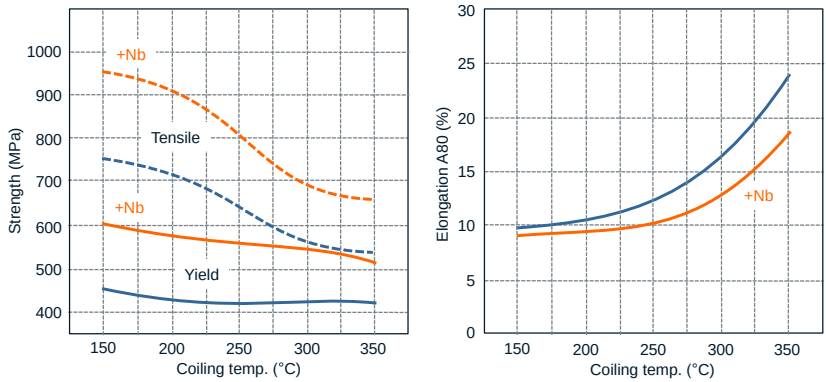

Figure 5. Effect of 0.04%Nb on strength and elongation of hot-rolled DP steel (0.11%C, 0.1%Si, 1.2%Mn, 0.8%Cr) as a function of coiling temperature.

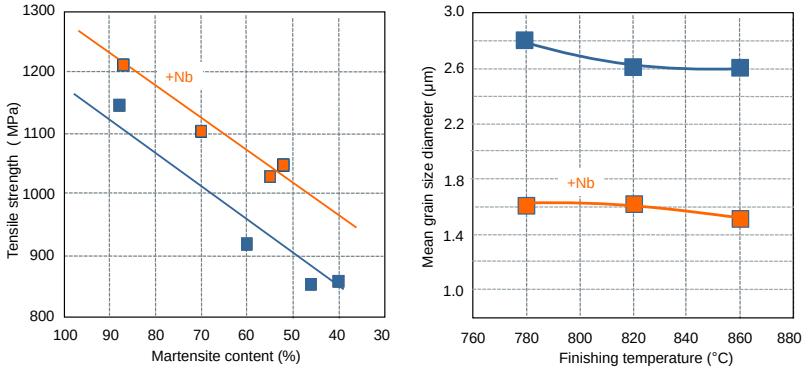

Figure 6. Effect of 0.05%Nb on tensile strength as a funtion of martensite fraction (coiling temperature 200 °C) and average grain size of hot-rolled DP steel (0.18%C-Mn-Si-Cr) as a function of finish rolling temperature.

Complex Phase Steel

Complex phase (CP) steels cover the very high tensile strength range of 800 to 1000 MPa and still offer reasonably good cold forming properties. Compared to DP steels of the same tensile strength, CP steel has a considerably higher yield strength but lower elongation. CP steel is very suitable for components that require high deformation resistance in the event of a crash, therefore most applications are found in the lateral crash reinforcement structure.

CP steels have a microstructure consisting of ferrite, bainite and martensite together with a small amount of retained austenite. The best compromise between high strength and good elongation essentially depends on the combination of microstructural constituents. The amount of martensite primarily determines the tensile strength. The yield strength is influenced by the grain size, the amount of bainite as well as by possible precipitation of microalloy carbides. Retained austenite ensures sufficient elongation. The excellent bendability and stretch-flangeability of these steels are due to the considerable amounts of bainite and/or tempered martensite, and suppression of the formation of polygonal ferrite, which results in a lower hardness difference between the microstructural constituents present. Also, the extremely fine-grained microstructure of CP steel (ASTM 14-15) is favorable with regard to strength and hole-expansion behavior. This grain refinement is mainly promoted by Nb microalloying in combination with intensive non-recrystallizing rolling and fast cooling after finish rolling.

The characteristic microstructure of CP steel is achieved when austenite transforms into several phases such as ferrite, martensite, bainite and retained austenite. The alloying concept and processing differ from that of a hot rolled DP steel. The cooling rate is adjusted so that only a relatively small amount of soft, polygonal ferrite is formed, and coiling occurs at a higher temperature in the bainite phase field. During bainite formation, carbon partitions to the remaining austenite phase, and the latter decomposes into martensite and retained austenite. In order to achieve sufficient carbon enrichment in the untransformed austenite it is important not to

lose carbon by carbide precipitation, i.e. formation of pearlite at higher temperatures, and cementite precipitation in bainite should be suppressed. When the coiling temperature is set to a low value, below 550 °C, the kinetics of microalloy carbide formation is very slow. Therefore, most of the microalloy content, which was not precipitated during austenite conditioning, will remain in solution. The optimum coiling temperature for a Mo-Nb alloyed CP steel, to achieve maximum precipitation hardening, was found to be in the range of 585-610 °C [8].

To bring all effects together, a stepped cooling schedule on the run-out table is necessary. Fast cooling after finish rolling into the ferrite phase field prevents recrystallization thus providing transformation from a pancaked austenite structure. Slow cooling in the ferrite phase field allows sufficient formation of ferrite phase which provides reasonable elongation in the final product. This is followed by a second fast cooling step to the coiling temperature.

Molybdenum alloying can contribute to the production of CP steel in different ways. During finish rolling it helps prevent partial dynamic recrystallization caused by high strain accumulation. This effect supports the transformation into a very fine-grained and homogeneous final microstructure. Molybdenum also retards the strain-induced precipitation of microalloying elements making them available for strengthening in the final product. As in DP steel, Mo prevents the formation of pearlite, which would result in a loss of solute carbon (stabilizing austenite) and deteriorate the final properties. The decomposition of undercooled austenite preferably occurs into carbide-free bainite, promoted by Si or Al alloying. Thus the remaining austenite is further enriched with carbon and the martensite-start temperature drops, and hence the chance of stabilizing retained austenite in the final product increases. Solute microalloying elements, typically Nb and Ti, together with Mo, provide excellent tempering resistance. This is important when the hot rolled strip is to be coated on a hot dip galvanizing line. By using an appropriate time-temperature cycle, the solute microalloying elements mainly co-precipitate with Mo thus increasing the yield and tensile strength [9].

Figure 7 summarizes the characteristic features of hot rolled high strength steels. Single-phase steels with bainitic or ferritic microstructures are the best performers with regard to hole expansion ratio. These steels also have a high yield to tensile ratio (YR) indicating limited work hardening. Multi phase steels perform well with regard to elongation. They have a low yield-to-tensile ratio thus featuring pronounced work hardening capability.

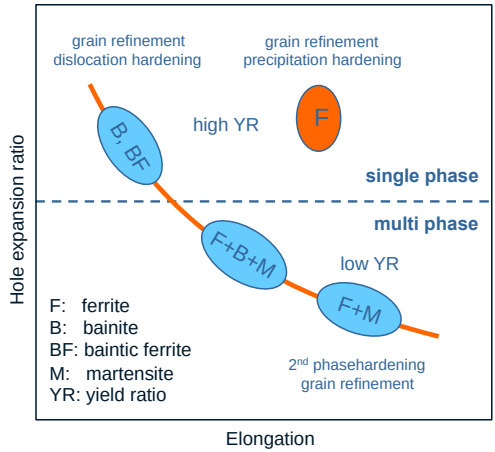

Figure 7. Relationship between elongation and hole-expansion ratio in single and multiphase steels.

Cold Rolled Annealed Multiphase Steels

The majority of flat steels used for light vehicle body construction are cold rolled and annealed materials covering the gauge range from 0.5 to 2.5 mm. The hot strip is mainly conditioned to have a ferritic or ferritic-pearlitic microstructure prior to cold rolling in order to keep the rolling loads low. For conventional steels, the annealing temperature after cold rolling is below A_{r1}. In this case, recrystallization of the heavily deformed cold rolled microstructure occurs but the phase composition of the hot rolled precursor strip is retained. When producing multiphase steels, the annealing temperature is raised into the intercritical region between A_{C1} and A_{C3}. In this case, some part of the cold deformed material recrystallizes whereas the rest transforms into austenite and existing cementite is dissolved. The actual annealing temperature determines the share of austenite generated. The cooling strategy after annealing controls the decomposition of austenite into phases like martensite, bainite or retained austenite. A continuous annealing line or a hot dip galvanizing line is necessary for such processing of multiphase steels. The grain size in the cold rolled annealed strip is always somewhat larger than that of the hot rolled mother strip due to grain growth during annealing.

Cold rolled multiphase steels can be divided into three groups: DP steels, TRIP (Transformation Induced Plasticity) steels, and partially martensitic steels (PM). The superior strength-ductility balance of multiphase steels is due to the tailored combination of soft and hard phases and, additionally, in the case of TRIP steels, the presence of metastable austenite. The tensile strength of these steels ranges between 450 and 1000 MPa and minimum total elongation (A_{80}) values lie between 7 and 27%.

In cold rolled strip, the amount of ferrite in the multiphase microstructure is adjusted by intercritical annealing between the A_{C1} and A_{C3} temperatures, Figure 8. The newly formed austenite fraction enriches in carbon and transforms into ferrite, bainite, martensite or stays as retained austenite, depending on the cooling program. The production of such steels requires a continuous annealing line (CAL) or a continuous galvanizing line (CGL).

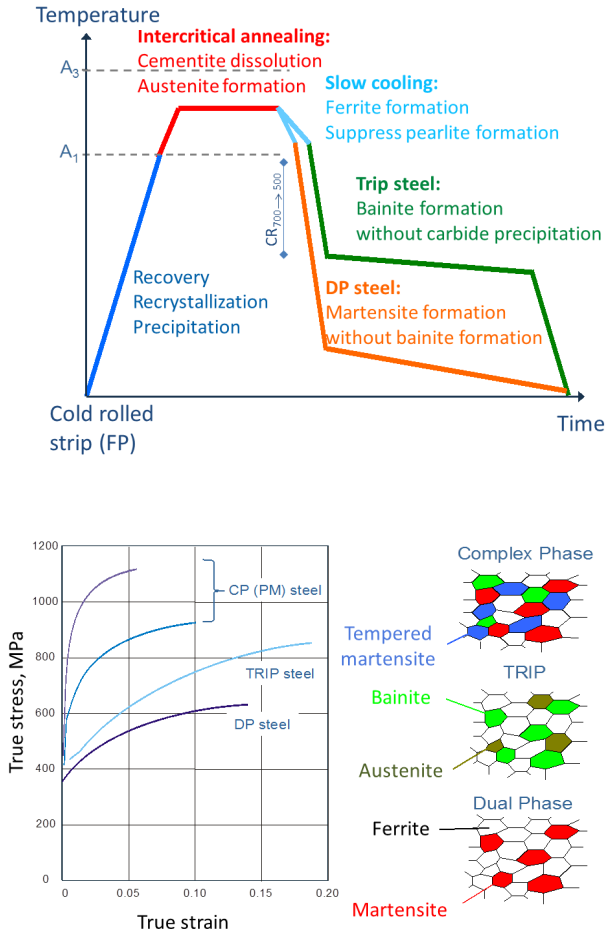

Figure 8. Schematic continuous annealing time-temperature curve for production of multiphase microstructures in low carbon steel and characteristics of multiphase steels.

Intercritical Annealed Dual Phase Steel

In the DP production route the carbon-enriched austenite is rapidly cooled below the martensite start temperature without forming any other phases. Obviously, for the DP steel route it is important to apply a high cooling rate to avoid bainite formation. This becomes particularly relevant for low-carbon DP alloys, which are preferred by carmakers due to their better weldability. Figure 9 indicates the critical cooling rate for a 0.05% C-Mn steel [12]. Increasing the Mn content indeed reduces the critical cooling rate, however, a too high Mn content can cause significant casting problems and centerline segregation. Therefore it is common to add other hardenability elements such as Cr or Mo or a combination of both. Molybdenum is approximately 3 times more effective than Cr in reducing the critical cooling rate. It allows the production of DP steel even on less powerful galvanizing lines that are not specifically equipped with a high speed cooling section. Furthermore, a small addition of Mo tremendously widens the process window, making production more robust against line speed and cooling rate variations. These can occur when a wider spectrum of sheet gauges has to be processed. Table I demonstrates several DP steel concepts currently in industrial production. Many of these concepts (B, D, F) use Mo in combination with Cr. Only galvanizing lines equipped with fast cooling sections specifically designed for multiphase steel production use Cr-only alloy concepts (A, E, G). The more exotic alloy concept, C, combines high Al with Mo alloying and appears to be a derivative of a TRIP steel concept. The production of DP780 (H, I, J) often involves an increase of the Mn content in combination with Cr and Mo alloying. Nb microalloying is more common in these grades as compared to DP600.

Nb microalloying has multiple effects with regard to the metallurgical mechanisms occurring during the intercritical annealing cycle. Nb precipitates usually exist in the hot rolled strip when coiling at conventional temperatures in the range of 600-650 °C. Any Nb remaining in solid solution has the potential to precipitate in-situ during the annealing cycle. The precipitation potential is enhanced when the coiling temperature is lowered to 500-550 °C as more Nb is retained in solid solution. This coiling condition also results in a very fine bainitic microstructure. Figure 10 shows the evolution of Nb precipitation during a CGL cycle. It is obvious that Nb precipitation is practically complete after reaching the intercritical soaking phase. For the bainitic coiling condition, most of the Nb is retained in solid solution, which then precipitates during the heating cycle as very fine particles giving a significant contribution to strengthening. The existing precipitates, produced in larger amounts after conventional coiling, are subjected to some degree of coarsening during the heating phase of the annealing cycle and hence have less effect on strength.

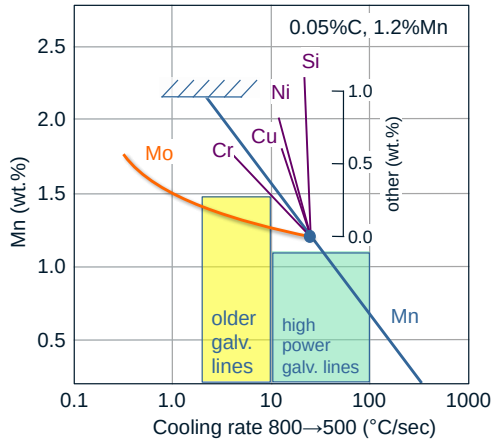

Figure 9. Relationship between critical cooling rate and alloying elements to produce ferritic-martensitic dual phase microstructure.

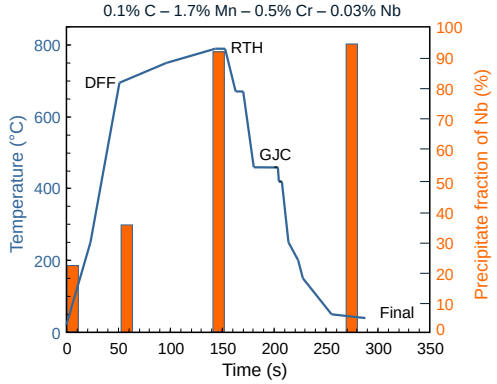

Figure 10. Progress of NbC precipitation (hot strip CT: 525 °C) during the intercritical annealing cycle.

Table I. Industrial Alloying Concepts for Dual Phase (DP) Steel Grades with 600 and 780 MPa Minimum Tensile Strength (wt%)

Grade		C	Si	Mn	Al	Cr	Mo	Ti	Nb
DP600	A	0.09	0.13	1.5	0.05	0.75	-	-	-
	B	0.12	0.30	1.4	0.03	0.25	0.08	0.01	-
	C	0.10	0.07	1.2	0.91	-	0.19	-	-
	D	0.10	0.18	1.4	0.04	0.15	0.20	-	-
	E	0.11	0.21	1.5	0.03	0.45	-	0.03	
	F	0.07	0.15	1.9	0.05	0.21	0.18	-	-
	G	0.09	0.25	1.8	0.04	0.40	-	-	0.03
DP780	H	0.16	0.17	1.7	0.03	0.32	0.16	-	-
	I	0.15	0.18	2.1	0.04	0.26	-	-	0.03
	J	0.08	0.05	1.9	0.03	0.50	0.15	-	0.02

Nb delays the recrystallization of cold deformed ferrite either by precipitation or by the solute drag effect of Nb on the grain boundaries. Experience with Nb alloyed DP steel indicated that the recrystallization temperature is typically raised by around 20 °C as compared to the same base composition without a Nb addition. The retarded recrystallization also preserves dislocation networks that act as nucleation sites for austenite. Hence, austenite formation should be accelerated in Nb alloyed DP steels. On the other hand, the grain-refined microstructure of Nb microalloyed strip additionally provides an increased grain boundary area which increases nucleation sites for austenite when annealing in the intercritical temperature range. Measurements have indeed confirmed that at a given intercritical annealing temperature the amount of austenite in the Nb alloy is higher compared to the Nb-free base alloy [13]. During the soaking phase, carbon partitioning is accelerated and more homogeneous in the finer grained microstructure of the Nb alloyed strip due to the shorter diffusion distances in the smaller grains. By slow cooling to the quenching temperature, a defined amount of new ferrite is nucleated from the existing austenite. Again, the refined microstructure of the Nb microalloyed steel exhibits quicker kinetics of this ferrite formation. A consequence of the enhanced amount of ferrite is that the remaining austenite phase is further enriched in carbon. This means that the hardenability of the carbon enriched and smaller austenite grains is increased. With regard to mechanical properties, Nb microalloyed DP steel should have less but stronger martensite as a second phase when subjected to a given annealing cycle as compared to the Nb-free base alloy. The systematic variation of annealing and quenching temperatures reveals that the Nb microalloyed DP steel always has the higher tensile strength, Figure 11, however its yield strength decreases with increasing annealing temperature due to delayed recrystallization at lower annealing temperature. In combination, this leads to better formability expressed by a lower yield-to-tensile ratio and higher total elongation. The variation of quenching temperature shows a significantly smaller impact on the properties of the Nb microalloyed variant since the transformation kinetics in the finer grained material is faster. The work hardening rate is directly proportional to the square root of the martensite share and inversely proportional to the square root of the martensite island size [14,15]. Hence, it is particularly interesting to reduce the martensite island size with regard to improving the stretch forming behavior, as was demonstrated by experimentally based data in forming limit diagrams (FLD) [16].

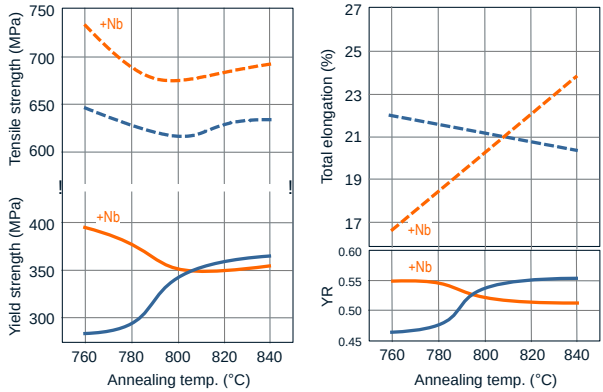

Figure 11. Effect of annealing temperature (QT = 750 °C) on the mechanical properties of cold rolled DP steel.

A recent trend in DP steel production is to further increase the tensile strength from the mainstream level of 590 MPa to 780 and 980 MPa. Simultaneously, steelmakers try to reduce the carbon level from around 0.15% to below 0.1% for better weldability. The strength increase demands a higher martensite fraction in the microstructure. Consequently, the average carbon content in the intercritical austenite is markedly reduced and the tendency of forming bainite at the expense of martensite is enhanced. This requires adapting the alloy concept as well as the annealing and cooling strategy.

When large fractions of austenite have to be transformed into martensite, the critical cooling rate is very much greater for low-carbon austenite than for high carbon austenite. The critical cooling rates required for the transformation of 90% and 50% of the intercritical austenite to martensite are plotted, as a function of carbon content of the austenite, in Figure 12 [17]. The data indicate that the hardenability of the austenite decreases slowly with decreasing carbon content at austenite carbon contents above 0.2%, but very rapidly at lower carbon contents. Furthermore, the cooling rate for converting 50% of the existing austenite into martensite is much lower than that for converting 90% austenite into martensite. These observations have a clear influence on the methodology of producing dual phase steels. Over the range of austenite carbon content within which martensitic hardenability varies slowly, i.e. above 0.2%C, it is beneficial to increase the intercritical annealing temperature in order to obtain a desired volume fraction of martensite at a lower cooling rate. This strategy would apply for dual phase steels containing up to about 20% martensite, covering the grades DP600 or lower. For the production of DP780 however, 40% martensite is needed in the microstructure. It is then more favorable to work with a lower intercritical annealing temperature. To enhance the stability of retained austenite with low carbon concentration during the galvanizing step it is necessary to delay bainite transformation by a suitable alloy concept. From research on TRIP steels it appeared that Mo makes the bainite transformation very sluggish [18]. The grain refinement induced by Nb

microalloying is also beneficial in this respect since the carbon distribution in the smaller austenite islands is more homogeneous due to the shorter diffusion path.

Figure 13 demonstrates the capabilities of different alloying concepts with respect to producing different strength levels. The low-C, high-Mn base alloy with Cr is capable of achieving strength levels up to 700 MPa. Adding a small amount of Nb raises the strength level to around 780 MPa, but the process window of applicable intercritical annealing temperatures is very narrow. The combined addition of Mo and Nb provides a strength level of around 900 MPa over a much wider range of intercritical annealing temperatures. Industrial low-C alloy concepts for hot dip galvanized DP980 apply Mo, Cr and Nb alloying in combination with an increased Mn addition.

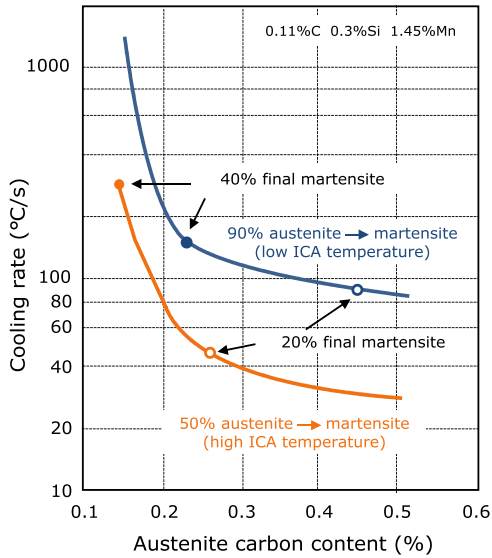

Figure 12. Annealing strategy with respect to carbon content and cooling rate.

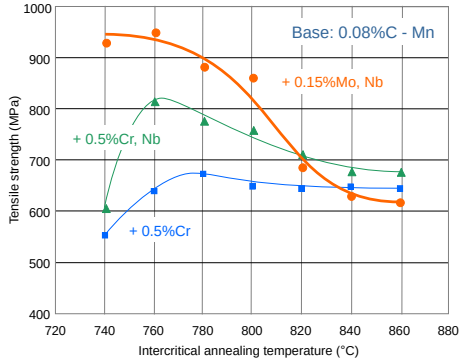

Figure 13. Effect of intercritical annealing temperature and various alloying concepts on achievable strength of dual phase steel with sub-peritectic carbon content [13].

Intercritical Annealed TRIP Steel

When producing TRIP steel, the annealed strip is quenched to an intermediate temperature to form carbide-free bainite. Increased additions of Si or alternatively Al help suppress carbide precipitation. During holding in this temperature range the progressing formation of carbide-free bainite leads to enrichment of carbon in the remaining austenite phase. A sufficiently high level of carbon concentration stabilizes this share of austenite down to room temperature. Depending on the average carbon content in the steel the amount of retained austenite in the final microstructure can be in the range of 10 to 20%.

Figure 14 exemplifies the development of different phase fractions as a function of the bainitic holding time. Short holding times result in the efficient formation of martensite, rendering only a small share of retained austenite which produces steel with DP characteristics. Very long holding times lead to carbide precipitation which also lowers the amount of austenite with sufficient carbon enrichment. The amount of retained austenite obtained for intermediate holding times depends on the absolute carbon content, the intercritical annealing temperature as well as the formation kinetics of pro-eutectoid ferrite and carbide-free bainite. The mechanical properties of an exemplary TRIP steel are displayed in Figure 15 as a function of the bainitc holding time at a temperature of 410 °C [19]. It is evident that at short holding times the DP character is pronounced whereas the TRIP character is established at longer bainitic holding times. It also becomes clear that a conventional galvanizing line (CGL) is not the best option to produce TRIP steel as it allows only a relatively short holding period. Better suited is a galvanizing line with an overageing (OA) section. The best conditions concerning the time temperature schedule are offered by continuous annealing lines (CAL), which would however require ad hoc galvanizing on an electro galvanizing line.

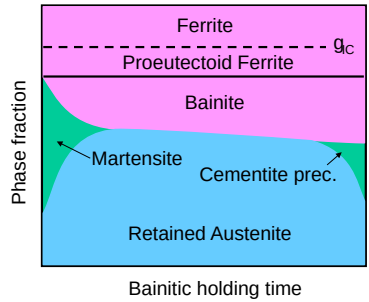

Figure 14. Development of phase fractions during bainitic holding after intercritical annealing of TRIP steel.

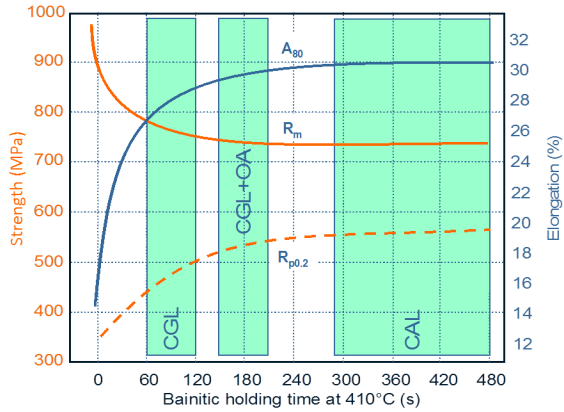

Figure 15. Development of strength and elongation in TRIP steel as a function of bainitic holding time.

As mentioned before, Mo makes the bainite transformation sluggish [18] leading to a higher amount of austenite with lower carbon enrichment at a given bainitic holding time and temperature. The martensite transformation-start temperature increases with reduced carbon enrichment. Consequently, Mo alloying promotes the formation of martensite and hence increases the tensile strength, especially for short bainitic holding times. Simultaneously, the amount of retained austenite and thus elongation is reduced. According to the findings shown in Figure 10, Nb is nearly completely precipitated after intercritical annealing and thus it is metallurgically inactive during bainitic holding. However, the grain refinement provided by Nb microalloying has a clear effect on the phase transformation kinetics through the intercritical annealing cycle as was already experienced for DP steels. During down cooling from the intercritical annealing temperature, the formation kinetics of pro-eutectoid ferrite is accelerated

due to the enhanced amount of nucleation sites offered by the refined microstructure. Thus the average carbon content in the remaining smaller austenite fraction is correspondingly higher. Similar to molybdenum, niobium is also known to delay bainite formation but this effect is only apparent at a rather low bainitic holding temperature [20]. At temperatures typically applied in galvanizing lines, the kinetics of bainite formation is hardly affected by niobium. Based on these effects, one can expect that Mo alloying of TRIP steels provides higher strength and lower elongation due to a higher martensite fraction. Nb microalloying has an opposite effect as it increases the share of ferrite and retained austenite leading to higher elongation and lower strength.

Accordingly, dual alloying with Mo and Nb has the potential of combining higher strength with good elongation. Figure 16 demonstrates that for an Al-Mo-Nb alloy concept, the processing robustness is considerably improved as compared to the Al-TRIP concept. The amount of retained austenite is less sensitive to the bainitic holding temperature, which is particularly advantageous when galvannealed grades have to be produced. Also, processing in a horizontal CGL configuration yields sufficient retained austenite with the Al-Mo-Nb TRIP concept. Figure 17 indicates the possibilities of the Al-Mo-Nb alloy concept by varying the bainitic holding time. With shorter holding times, so-called TRIP aided DP steel can be obtained by producing a fair amount of retained austenite within a primarily ferritic-martensitic microstructure. For longer holding times the TRIP character is more pronounced as the share of retained austenite is increased whereas the tensile strength is reduced. In a continuous annealing line, the duration of bainitic holding can be adjusted over a wide range, Figure 15. The bainitic holding period in a continuous galvanizing line depends on the specific design of the equipment. Lines with a horizontal furnace allow only a short holding period and thus promote the DP character [21]. Longer bainitic holding can be achieved by operating with reduced line speed, however, this reduces the productivity of the line thus increasing production cost.

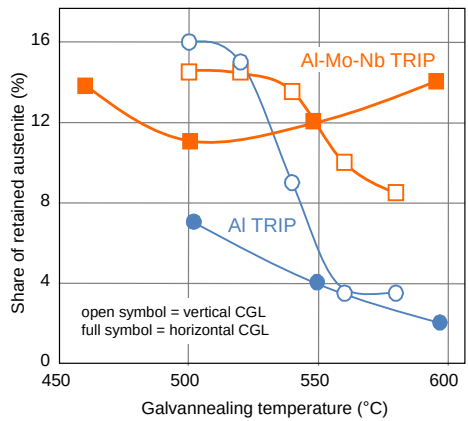

Figure 16. Influence of galvannealing temperature on the retained austenite share in Al and Al-Mo-Nb TRIP steel for different CGL configurations.

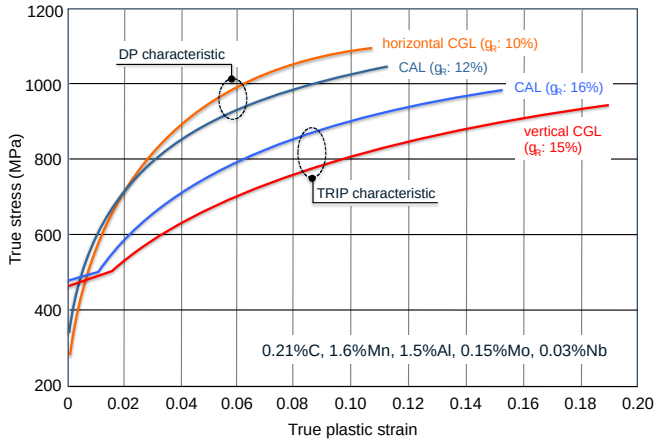

Figure 17. Influence of the annealing cycle and the amount of retained austenite (γ_R) on the stress-strain characteristics of multiphase steels.

Improvement of Microstructural Damage Resistance

Although multiphase steels have good elongation and formability, they are sensitive to microstructural damage when intensive localized straining is applied. In this situation all plastic flow is concentrated in a few grains of the softer phase. Dislocation pile-up against the hard undeformable phase may lead to microvoid formation as shown in Figure 18(a). The size of such microcracks is related to the grain size of the material and the mean free path length between hard and soft phases. Individual micro voids link up forming a microcrack, Figure 18(b), and it is evident that larger grains or inhomogeneously distributed phases accelerate the progress of microcracks and lead to faster macroscopic damage. Niobium microalloying considerably improves the microstructural resistance against the above mentioned damage initiation. As shown in Figure 19, the addition of Nb to DP steel results in a significant refinement of both ferrite and martensite phases. Furthermore, agglomeration of hard phase particles is reduced and the phase distribution is more homogeneous.

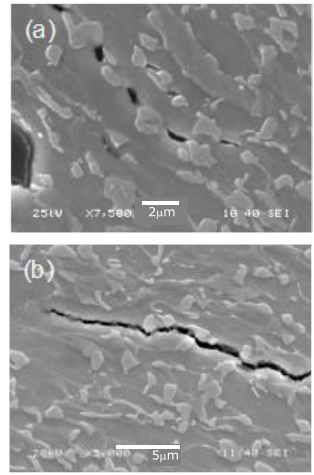

Figure 18. (a) Micro void formation in soft phase of DP600 and (b) macroscopic crack propagation in DP600 steel.

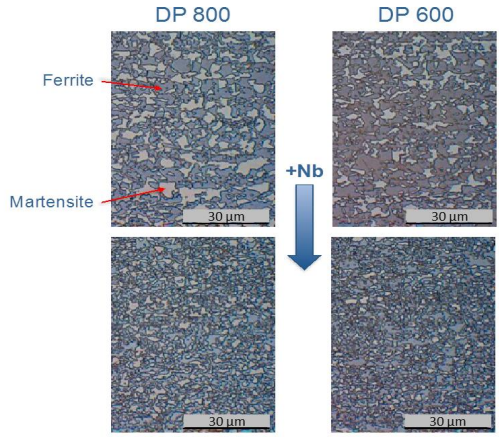

Figure 19. Grain refining effect of Nb microalloying in DP600 and DP800 steel.

The finer grained and more homogeneous microstructure leads to better results under forming conditions where highly localized straining predominates. These are sheared edge flanging, hole expansion and bending. Figure 20 shows the hole expansion ratio for a DP600 steel. The Nb microalloyed variant achieves an improvement of more than 50%. More critical is the situation in DP800 as the amount of martensite is much increased and clustering of the hard particles is more likely than in DP600. Here Nb microalloying results in an improvement of around 90% for the hole expansion ratio, Figure 21. Likewise the bending behavior is drastically improved which is particularly important for roll profiling operations. For this reason Nb microalloying is already well established in DP800 or higher strength grades. These positive effects of Nb microalloying have also been observed in TRIP steel [19].

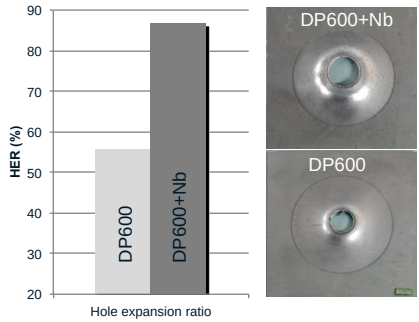

Figure 20. Influence of Nb microalloying on hole expansion behavior of DP600 (punched hole, sheet thickness 2.5 mm).

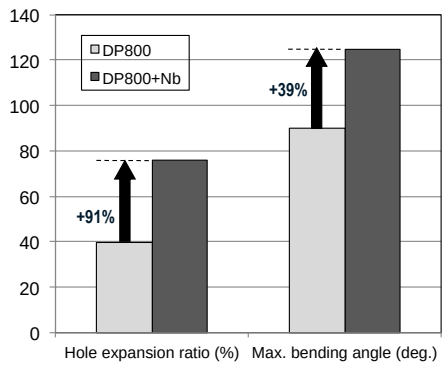

Figure 21. Influence of Nb microalloying on hole expansion and bending behavior of DP800 (punched hole, sheet thickness 1.5 mm).

Conclusions

Molybdenum and niobium alloying have distinct effects in the production of multiphase steels. Their effects are partly similar and in some respects complementary. Molybdenum exists in solid solution in multiphase steels and is as such metallurgically active in reducing the diffusivity of carbon. This effect retards ferrite formation and, to a much larger degree, pearlite formation from austenite. Molybdenum also efficiently retards the decay of metastable austenite into bainite. Therefore molybdenum is particularly useful in promoting dual phase microstructures even under critical processing conditions. Consequently, molybdenum is very beneficial for all multiphase steels aiming at very high strength levels. Niobium, like molybdenum, has the effect of reducing the carbon diffusivity when present in solid solution. However, niobium's solubility is much lower than that of molybdenum, thus it precipitates almost completely during hot rolling and intercritical annealing. The grain refining effect of niobium accelerates the kinetics of phase transformations and therefore ferrite formation is promoted after intercritical annealing. The resulting smaller amount of martensite has a higher and more equalized carbon content promoting a higher stability. During bainitic holding, the grain refined microstructure promotes the nucleation and growth of carbide-free bainite and thus supports the accumulation of retained austenite. When molybdenum and niobium are alloyed in combination they facilitate producing multiphase steels of the highest strength level. Depending on the processing conditions, such steels can be adjusted to have either a DP-like or a TRIP-like character. All grain-refined multiphase steels exhibit substantially improved hole expansion behavior and bendability.

References

1. T. Hallfeldt, "Possibilities and Challenges Using Advanced High Strength Sheets for Automotive Applications," *Proceedings of the International Symposium on Niobium Microalloyed Sheet Steel for Automotive Application*, Araxá, MG, Brazil, (5-8 December 2005), eds. S. Hashimoto, S. Jansto, H. Mohrbacher, and F. Siciliano, TMS, 2005), 117.

2. *Proceedings of the Automotive Circle International, EuroCarBody Conference (2008 – 2010)*, Vincentz Verlag.

3. B. Lüdke and M. Pfestorf, "Functional Design of a Lightweight Body in White – How to Determine Body in White Materials According to Structural Requirements," *Proceedings of the International Symposium on Niobium Microalloyed Sheet Steel for Automotive Application*, Araxá, MG, Brazil, (5-8 December 2005), eds. S. Hashimoto, S. Jansto, H. Mohrbacher, and F. Siciliano, TMS, 2005), 27.

4. Ultralight Steel Auto Body (ULSAB) Advanced Vehicle Concepts (AVC) Study, International Iron and Steel Institute.

5. S. Wang and P. Kao, "The Effect of Alloying Elements on the Structure and Mechanical Properties of Ultra Low Carbon Bainitic Steels," *Journal of Materials Science*, 28 (19) (1993), 5169-5175.

6. A.P. Coldren and G.T. Eldis, "Using CCT Diagrams to Optimize the Composition of an As-rolled Dual-Phase Steel," *Journal of Metals*, 32 (3) (1980) 41.

7. T. Heller and A. Nuss, "Effects of Alloying Elements on the Microstructure and the Mechanical Properties of Hot Rolled Multiphase Steels," *Proceedings of the 2nd International Conference on Thermomechanical Rolling*, Liège, (15-17 June 2004), 85-94.

8. S. Sarkar and M. Militzer, "Microstructure Evolution Model for Hot Strip Rolling of Nb–Mo Microalloyed Complex Phase Steel," *Materials Science and Technology*, 25 (9) (2009), 1134-1146.

9. K. Nakagawa, T. Yokota, and K. Seto, *Proceedings of the International Conference on New Developments in Advanced High-Strength Sheet Steels*, AIST, (15-18 June 2008), 209.

10. M. Kurosawa et al., "Age-hardening Behavior and Dent Resistance of Bake-hardenable and Extra Deep-drawable High Strength Steel," *Kawasaki Steel Technical Report*, (18) (1988) 61-65.

11. H. Taniguchi et al., "Effect of Mo on Strain Aging Behavior in Ultra Low Carbon Steel Sheets," *Tetsu-to-Hagane, Journal of the Iron and Steel Institute of Japan*, 88 (11) (2002), 808-813.

12. T. Irie et al., "Characteristics of Formable Cold Rolled High Strength Steel Sheets for Automotive Use," *Kawasaki Steel Technical Report*, (2) (1981), 14-22.

13. O.A. Girina, N.M. Fonstein, and D. Bhattacharya, *Proceedings of New Developments on Metallurgy and Applications of High Strength Steels*, Buenos Aires (2008).

14. N.K. Balliger and T. Gladman, "Work Hardening of Dual-phase Steels," *Metal Science*, 15 (3) (1981), 95-108.

15. C. Lanzillotto, F. Pickering, "Structure–property Relationships in Dual-phase Steels," *Metal Science*, 16 (8) (1982), 371-382.

16. Y. Granbom, "Influence of Niobium and Coiling Temperature on the Mechanical Properties of a Cold Rolled Dual Phase Steel," *Revue de Metallurgie*, 104 (04) (2007), 191-197.

17. R. Priestner and M. Ajmal, "Effect of Carbon Content and Microalloying on Martensitic Hardenability of Austenite of Dual-phase Steel," *Materials Science and Technology*, 3 (5) (1987), 360-364.

18. B. Ehrhardt et al., "Progress in the TM Process for New Cold Rolled Low Alloy Steel Grades with Minimized and with Maximized Strength," *Proceedings of the 2nd International Conference on Thermomechanical Processing of Steel*, Liège (15-17 June 2004), 425.

19. S. Traint et al., "Low Alloyed Trip Steels with Optimized Strength, Forming and Welding Properties," *Steel Research International*, 77, (9-10) (2006), 641.

20. W. Bleck, A. Frehn, and J. Ohlert, "Niobium Science and Technology," *Proceedings of the International Symposium Niobium 2001*, Orlando, TMS (2001), 727.

21. T. Heller et al., "Potential of Niobium in Sheet Steels, for the Automotive Industry," *Recent Advances of Niobium Containing Materials in Europe*, ed. K. Hulka, C. Klinkenberg, and H. Mohrbacher, (Dusseldorf, Verlag Stahleisen, 2005), 21.

Fundamentals and Applications of Mo and Nb Alloying in High Performance Steels – Volume 1
Edited by Hardy Mohrbacher
CBMM, IMOA and TMS, 2014

INFLUENCE OF TITANIUM AND NIOBIUM ON THE STRENGTH–DUCTILITY–HOLE EXPANSION RATIO BALANCE OF HOT-ROLLED LOW-CARBON HIGH-STRENGTH STEEL SHEETS

K. Kamibayashi, Y. Tanabe, Y. Takemoto, I. Shimizu and T. Senuma

Graduate School for Nature Science
Okayama University, Okayama 700-8530 Japan

Keywords: Automotive, High Strength Steel, Hole Expansion Ratio, Precipitation Hardening, Ductility, Niobium, Titanium, Mechanical Properties, r-value, Charpy Toughness, Hardness, EBSD

Abstract

It has been demonstrated that the demand for high strength sheet steels with excellent balances of strength, ductility and hole expansion ratio could be met by steels with a ferrite or bainitic-ferrite matrix strengthened by a large amount of finely dispersed precipitates. In this study, the influence of the precipitation forming elements, Ti and Nb on the balance of strength, ductility and hole expansion ratio has been investigated. Individually, neither Ti nor Nb produces optimum performance but it has been proposed that a carefully selected balance of added Ti and Nb can succeed in meeting the desired combination of properties. The reasons why the individual elements, when used alone, produce inferior performance is explored and the role of sulphides and the formation of textural colonies are both highlighted as playing important roles. Titanium alone can go part way towards satisfying the property demands whilst this has been shown to be more difficult with niobium as a single alloying addition. These observations are thoroughly discussed and explained.

Introduction

A remarkable number of high-strength steels have been developed and used in practice to reduce automotive body weight. Improvement in formability is one of the most important research items in the development of modern high-strength steels. Successful developments of advanced high-strength steels with a good strength−ductility balance are DP and TRIP steels [1,2]. The hole expandability of these steels is, however, poor. On the other hand, bainite or tempered martensite steels show excellent strength–hole expansion ratio balances but their ductility is low. In recent research and development, a large effort has been made to develop steels with a good strength–ductility–hole expansion ratio balance [3-13]. A newly developed steel of this kind consists of a ferrite matrix strengthened by a large amount of finely dispersed precipitates [5-8]. Funakawa and his co-workers [14] investigated the precipitation behavior of these kinds of steels containing Ti, Nb and Mo, and reported the occurrence of interphase precipitation. They also reported the mechanical properties of the steels developed. The influence of the separate or combined addition of Ti, Nb and Mo on the strength–ductility–hole expansion ratio balance was, however, not investigated in detail.

In this study, the influence of the addition of Ti and Nb on the strength–ductility–hole expansion ratio balance of the 600 MPa class steels consisting of a ferrite matrix strengthened by a large amount of precipitates has been investigated.

At first, an experiment was carried out using a Ti and a Nb-bearing steel. The microstructure and texture, the condition of the pierced surface, the behavior of crack initiation and propagation during hole expansion, precipitates and inclusions, etc., were studied in the two steels. By comparing the obtained results from both steels, the main factors influencing the ductility–hole expansion ratio balance were discussed and clarified. The discussion indicated that there exists an optimum ratio of Ti/Nb addition, and to determine this, an additional experiment was carried out using steels with various ratios of Ti and Nb additions.

Finally, we propose an adequate combination of Ti and Nb addition to produce steel with a good ductility–hole expansion ratio balance.

Experimental Conditions

Table I shows the chemical composition of the steels used in the experiment. The chemical composition was designed to obtain a tensile strength of around 600 MPa and a microstructure consisting of a ferrite matrix strengthened by finely dispersed precipitates. The Ti or Nb content of these steels are designed to almost fulfil stoichiometry with C, to avoid the formation of pearlite and grain boundary cementite that lower the hole expandability.

Table I. Chemical Composition of the Steels Used in the Experiment (wt%)

Steel	C	Si	Mn	P	S	Al	Nb	Ti	N
Ti	0.033	0.1	1.49	0.01	0.0062	0.037	-	0.12	0.0018
Nb	0.028	0.1	1.48	0.01	0.0053	0.037	0.22	-	0.0018

The steels were melted in a vacuum furnace and then cast into 50 kg ingots. Figure 1 shows the thermal history of the hot-rolling process. Ingots of 110 mm thickness were reheated at 1250 °C for 60 min for the solution treatment and subsequently hot-rolled at a finishing temperature around 930 °C according to a reduction schedule of: $110 \rightarrow 80 \rightarrow 60 \rightarrow 45 \rightarrow 30 \rightarrow 15 \rightarrow 8 \rightarrow 4.5 \rightarrow 2.8$ mm. The coiling process was simulated using an electrical furnace kept at a temperature of 600 °C, in which the hot-rolled sheets were held directly after hot-rolling for 60 min without a temperature drop below the furnace temperature and then cooled in air.

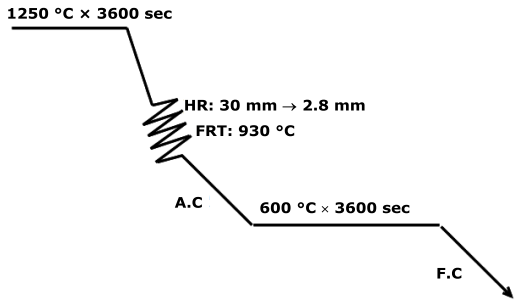

Figure 1. Thermal history of the hot-rolling process.

The microstructure was characterized using optical microscopy (OM), field emission scanning electron microscopy (FE-SEM) and transmission electron microscopy (TEM). The grain size of ferrite and the size of dimples observed on the pierced surface were analysed with an image analysis device (IAD). The texture of the steels was measured and analysed using electron backscatter diffraction patterns (EBSP). The calculation of the r-value from EBSP data was carried out using self-developed software. The chemical composition of precipitates was determined using energy dispersive X-ray (EDX) spectroscopy mounted on the TEM.

The hardness was measured on a micro-Vickers tester with a load of 2.94 N. Each plotted point is an average value of five measurements. Tensile tests and hole expansion tests were carried out to determine the mechanical properties of the steels. The tensile test was performed only in the rolling direction. A Charpy impact test was also carried out in both the rolling and the transverse directions. The test piece of the Charpy impact test consisted of two hot bands glued to each other.

The hole expansion test was performed according to the Japan Federation of Iron and Steel Standard (JFS T1001). The hole was pierced by a 10-mm-diameter punch. The clearance was 12%. For the hole expansion test, an Erichsen testing machine was used. The burred surface was facing upwards. The hole expansion was performed by moving a vertical conic punch of 60° angle upwards. Figure 2 shows schematic diagrams of the devices used for piercing and hole expansion.

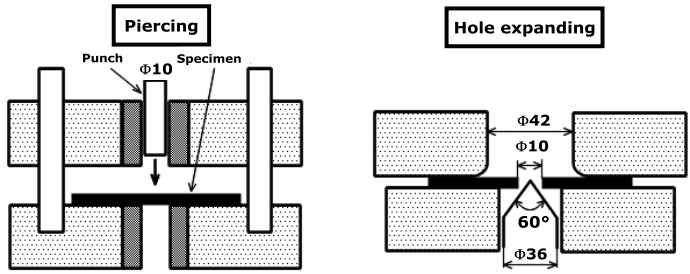

Figure 2. Schematic diagrams of the devices used for piercing and hole expanding.

The hole expansion ratio was calculated by Equation 1. Here, d_0 is the initial diameter of the hole and d is the diameter of the hole expanded so far as a through-thickness crack is just observed. To investigate the propagation behavior of cracks during hole expansion, specimens with hole expansion ratios of 20%, 40% and 70% were produced.

$$\lambda = \frac{d - d_0}{d_0} x100\% \quad (1)$$

Experimental Results

Figure 3 shows the mechanical properties of the Ti and Nb steels. TSxElxλ is a quantity used for evaluating the strength–ductility–hole expansion ratio balance. (A high value of this quantity means a good strength–ductility–hole expansion ratio balance.) It is clearly seen that the strength–ductility–hole expansion ratio balance of the Ti steel is superior to that of the Nb steel.

Table II shows the impact energy determined by the Charpy impact test at a temperature of 22 °C. The difference in impact energy between specimens L, whose notch was perpendicular to the rolling direction, and specimens C, whose notch was parallel to the rolling direction, was larger in the Nb steel than in the Ti steel. Specimen L of the Nb steel had the highest value of impact energy of the four cases, but Specimen C had the lowest. To clarify the reason for the superiority of the ductility–hole expansion ratio balance in the Ti steel, we investigated the microstructure, the condition of the pierced surface, the evolution of cracks during hole expanding, etc.

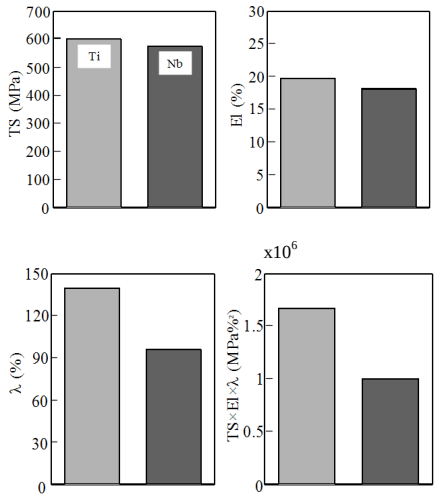

Figure 3. Mechanical properties of Ti and Nb steels.

Table II. Impact Energy Determined by Charpy Impact Test at a Temperature of 22 °C

	Impact energy (J/cm^2)
Ti steel specimen L	171
Ti steel specimen C	161
Nb steel specimen L	209
Nb steel specimen C	138

Figure 4 shows the pierced surface after the hole expansion test. As for the Ti steel, many cracks were observed over the entire circumference. On the other hand, the number of cracks in the Nb steel was limited, and the penetration crack always propagated parallel to the rolling direction. Figure 5 shows the evolution of the surface morphology during hole expansion. As for the Ti steel, many fine cracks were observed in the outer fractured surface of the hole expanded to $\lambda = 20\%$. These cracks reached the boundary between the sheared and fractured surfaces at $\lambda = 40\%$. As the expansion ratio increased to 70%, the number of cracks increased, but none of them propagated inside the sheared zone.

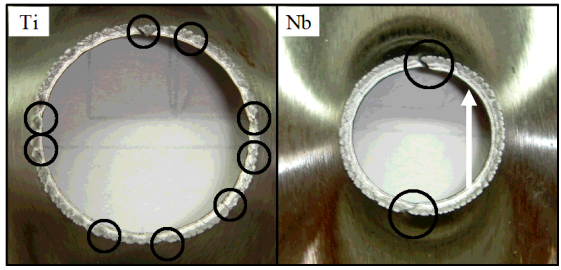

Figure 4. Pierced surfaces after the hole expansion test of Ti and Nb steels.
(The arrow shows the rolling direction).

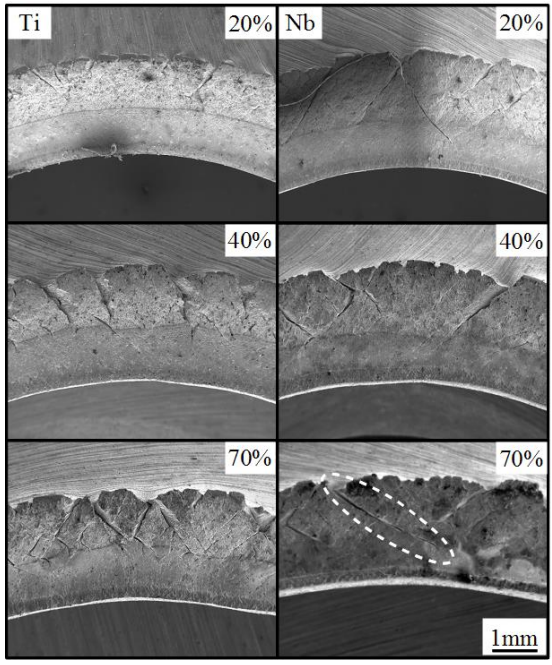

Figure 5. Evolution of morphology of the pierced surface during the hole expansion test.

At λ = 20%, the number of micro-cracks in the Nb steel was smaller than in the Ti steel, but some of them reached the boundary between the sheared and fractured surfaces. At λ = 70%, some cracks penetrating the sheared surface were observed in the Nb steel. It was also observed that the thickness of the pierced surface of the Ti steel was markedly reduced by hole expansion, and the change in the thickness of the Nb steel was not apparent. Thickness reduction in the Ti steel was realized by large numbers of cracks distributed over the entire circumference.

It is well known that the state of the pierced surface markedly affects the hole expansion ratio. The state of the pierced surface is characterized by the ratio of the sheared to fractured surface areas, the numbers and size of micro-cracks and dimples in the fractured surface, and work hardening in the vicinity of the pierced surface.

Figure 6 shows the pierced surface of the Ti and Nb steels. The ratio of the sheared to fractured areas was 56:39 for the Ti steel and 46:49 for the Nb steel. The increase in the ratio of the fractured areas seems to lower hole expandability.

If the vicinity of the pierced surface is significantly hardened by piercing, the hole expansion ratio may be lowered, and therefore the hardness in the vicinity of the pierced surface was measured. Figure 7 shows the hardness distribution up to 2 mm from the surface at three different positions, namely the centre of the sheared area, the centre of the fractured area and the boundary between the sheared and fractured areas. The increase in hardness in the sheared area was lower than in the fractured and boundary areas. The work hardening in the Nb steel was slightly less than that in the Ti steel. Because a higher hardness in the vicinity of a pierced surface is supposed to result in a lower hole expansion ratio, the work hardening behavior cannot explain the inferior ductility–hole expansion ratio balance in the Nb steel.

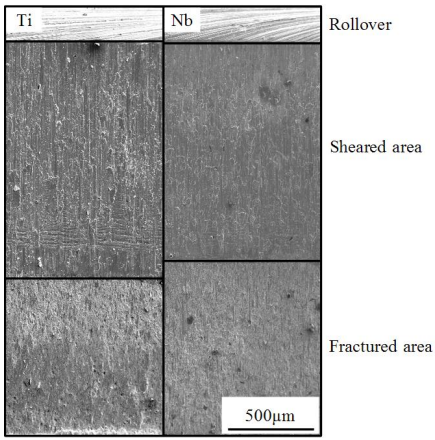

Figure 6. Appearance of the surfaces pierced by punch.

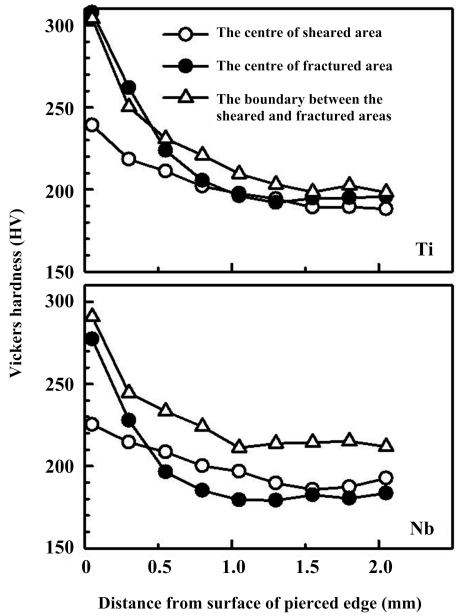

Figure 7. Hardness distribution up to 2 mm from the surface at three different positions.

Figure 8 shows the SEM pictures of fractured surfaces of both steels. To quantify the surface condition, the numbers and size of dimples were measured. The mean diameter and standard deviation of dimples observed were 3.62 and 2.45 μm, respectively, in the Nb steel and 2.31 and 1.24 μm, respectively, in the Ti steel. For the latter, 70% of the dimples were between 1.07 and 3.55 μm and the largest dimple size was around 6 μm, whereas 70% of the dimples in the Nb steel were between 1.17 and 6.07 μm and the largest size was more than 11 μm. Both the size and standard deviation of dimples in the Nb steel were clearly larger than those in the Ti steel.

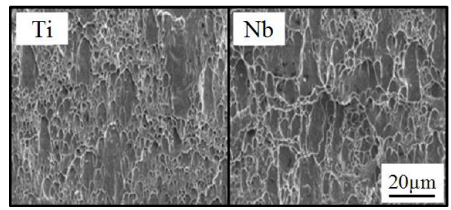

Figure 8. SEM micrographs of the fractured surfaces of the punched hole.

Figure 9 shows a cross section of the vicinity of the pierced surface. A number of micro-voids were observed. The number, average size and standard deviation of micro-voids observed in the cross section area in the vicinity of the fractured surface of a representative area of 100 μm x 30 μm of the Ti steel were 87, 1.4 μm and 1.6 μm, respectively, whereas those of the Nb steel were 45, 2.9 μm and 3.3 μm, respectively. The fact that the Ti steel has more micro-voids than Nb steel may relate to the fact that, as shown in Figure 4, in the initial stage of hole expansion more cracks were observed in the Ti steel than in the Nb steel. The fact that the micro-voids in the Nb steel were larger than in the Ti steel may also relate to the fact that the propagation rate of through-thickness cracks in the Nb steel was higher than in the Ti steel.

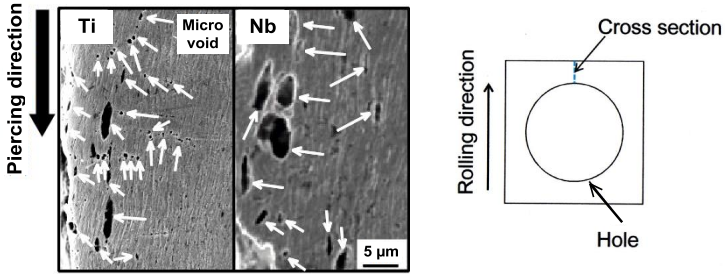

Figure 9. Micro-voids observed in the vicinity of the pierced surface.
The cross section is parallel to the rolling direction.

To examine whether the lower hole expansion ratio of the Nb steel could be mainly attributed to the state of the pierced surface, an additional hole expansion test was carried out using the specimens with a hole machined by electric discharged wire cutting. Although the hole expansion ratio of the machined holes of the Nb and Ti steels increased markedly to 187% and 205%, respectively, a clear difference still remained between the two steels.

To clarify this difference, the microstructures of the two steels were examined, Figure 10. The microstructure of the Nb steel was finer than that of the Ti steel. The average ferrite grain size of the Nb and Ti steels was 2.27 and 3.37 μm, respectively. It was also observed that the microstructure of the Nb steel was more heterogeneous than that of the Ti steel. This heterogeneity was probably caused by partial recrystallization of austenite because of the strong retardation effect of Nb on recrystallization. It is well known that heterogeneity of microstructure is detrimental to the hole expansion ratio.

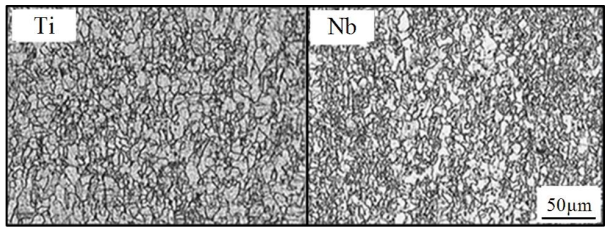

Figure 10. Microstructures of Ti and Nb steels.

To examine the microstructural heterogeneity in detail, a micro-scale textural analysis was carried out. Figure 11 shows the crystal orientations measured in the Ti and Nb steels by EBSP. The ellipses in the Nb steel indicate the presence of colonies (aggregates of grains with similar orientations), which is evidence for the microstructural heterogeneity of the Nb steel.

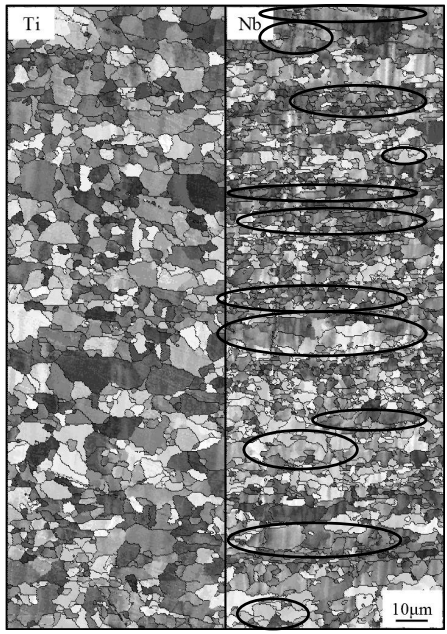

Figure 11. ND crystal orientation maps of Ti and Nb steels.

The hole expansion ratio is also affected by the planar anisotropy of the texture [15]. Figure 12 shows the planar anisotropy of r-values calculated using the orientation distribution function (ODF) data obtained by EBSP measurements at mid-thickness. It is recognized that the Ti steel had a larger planar anisotropy of r-values and a higher average r-value than the Nb steel. Phillips et al. reported that the hole expansion ratio was chiefly affected by the minimum r-value [15]. The minimum r-values of both steels are nearly the same, and therefore the inferior hole expansion ratio of the Nb steel compared to the Ti steel cannot be explained from the viewpoint of the textural anisotropy.

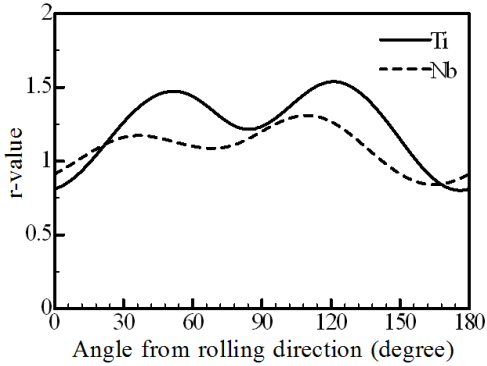

Figure 12. Planar anisotropy of r-values of Ti and Nb steels calculated with the orientation distribution function (ODF) data obtained by EBSP measurements.

At the bottom of the dimples in fractured surfaces, large precipitates were often observed. Figure 13 shows some results of the chemical composition of the precipitates in the Ti and Nb steels analysed by EDX. The precipitates analysed were $Ti_4C_2S_2$ and TiN in the Ti steel, and MnS and NbCN in the Nb steel. Besides these large precipitates, there were numerous nano-size precipitates that contributed to the precipitation hardening.

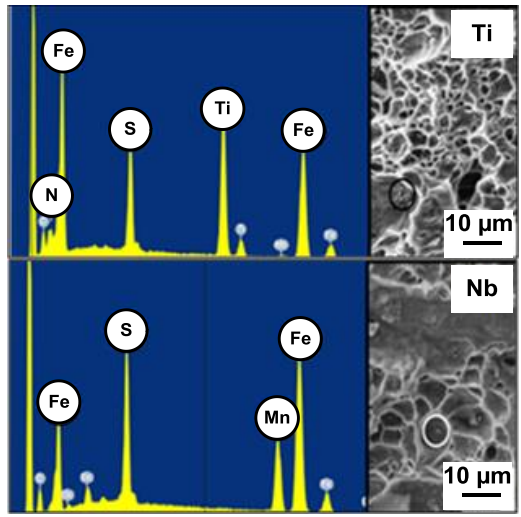

Figure 13. Analysis of the chemical compositions of large precipitates found at the bottom of dimples.

Discussion

Table III shows a comparison of the experimental results of the Ti and Nb steels. The reason for the difference in the hole expansion ratio between the two steels is discussed by considering these results and the microstructural analyses.

Table III. Comparison of Experimental Results of Ti Steel and Nb Steel

	Ti	**Nb**
Ratio of sheared-to-fractured areas	59/39	46/49
Cracks observed during hole expansion	Many	Few
Micro-voids in the vicinity of pierced surface	Many	Few
Ferrite grain size	3.37 μm	2.27 μm
Dimple size	2.31 μm	3.62 μm
Micro-void size	1.4 μm	2.9 μm
Sulphide	$Ti_4C_2S_2$	MnS
Textural colonies	Not recognized	Present
Hardness at the pierced surface	310 HV	295 HV

As seen in Figure 6, the fraction of the fractured area of the pierced surface of the Nb steel was markedly higher than that of the Ti steel. It is understandable that the high fraction of the fractured area of the pierced surface in the Nb steel has lowered hole expandability. The reason why the Nb steel has a high fraction of the fractured surface should be discussed. A high ratio of the fractured areas indicates that the Nb steel was more prone to fracture than the Ti steel. It is well known that grain refinement is effective for suppressing fracture. The measured mean ferrite grain size of the Nb steel was smaller than that of the Ti steel. This experimental finding led us to expect that the Nb steel would have the higher resistance to fracture, but this was not the case. This contradiction can be interpreted as follows. The resistance to fracture is enhanced by the existence of high angle boundaries, which hinder crack propagation. The formation of the textural colonies (with low angle boundaries) in the Nb steel meant a reduction in the effective grain boundary suppression of crack propagation. As a result, the effective grain size of the Nb steel increased, as indicated by the fact that the size of dimples and micro-voids of the Nb steel was large.

As seen in Figures 4 and 5, there were more cracks in the Ti steel than in the Nb steel, and there were also more micro-voids formed by piercing in the Ti steel than in the Nb steel. The higher sensitivity to crack initiation in the Ti steel may be caused by the existence of rectangular-shaped large TiN. The initiation of many cracks in the pierced surface during hole expansion contributes to stress release at the tip of the crack, and this release is supposed to suppress propagation of through-thickness cracks in Ti steel.

In the Ti steel, cracks were observed over the entire circumference of the pierced surface during hole expansion. In contrast, the cracks in the Nb steel were usually formed along the rolling direction, as seen in Figure 2. It is not obvious that the hole expansion ratio has a close relationship with toughness. However, Takahashi et al. [16] indicated a certain relationship between the hole expansion ratio and toughness by revealing a tight correlation of the hole expansion ratio with the Jc value. Therefore, the reason that the through-thickness cracks of the Nb steel are restrictedly formed in the direction parallel to rolling is discussed with the result of the Charpy impact test. As seen in Table II, the Nb steel has a large planar anisotropy of impact energy, and the impact energy in the direction parallel to rolling is significantly lower. The low impact energy parallel to the rolling direction is inferred to be caused by the existence of elongated large textural colonies and flattened (“pancaked”) MnS.

It is well known that the presence of MnS deformed by rolling lowers hole expandability. To examine the quantitative influence of MnS on the hole expansion ratio, a steel was produced by adding 0.0074%Ca to the Nb steel. By addition of Ca, the sulphide formed in the Nb steel became CaS instead of MnS. CaS is hard, and is not pancaked by hot-rolling. The formation of the so-called ‘shape-controlled sulphide’ was expected to improve the hole expansion ratio. Through this measure, the hole expansion ratio improved from 96% to 113% for the pierced specimens and from 187% to 202% for the machined specimens, respectively. There is still a clear difference in the strength–ductility–hole expansion ratio balance between the Nb and Ti steels. This result indicates that a large amount of the Nb addition itself detrimentally affects hole expandability. Because the quantity and size of NbC in the Nb steel and TiC in the Ti steel hardly differ from each other, the detrimental effect of Nb is inferred to be mainly caused by the formation of the heterogeneous microstructure with elongated, large textural colonies.

From these considerations, the suppression of the formation of large textural colonies and MnS seems to be important to achieve a good strength–ductility–hole expansion ratio balance in steel consisting of a ferrite matrix strengthened by finely dispersed precipitates. Since we supposed that a moderate addition of Nb would result in grain refinement without forming textural colonies, and could improve hole expandability, we carried out an additional experiment using a steel based on the Ti steel with moderate addition of Nb (hereafter called Ti–Nb steel). A small amount of Ti in the Ti steel was substituted by Nb. Table IV shows the chemical composition of the Ti–Nb steel. Table V shows the mechanical properties of the Ti–Nb steel compared with those of the Ti steel and Nb steel. The strength–ductility–hole expansion ratio balance of the Ti–Nb steel was the best among the steels investigated. The sulphide in the Ti–Nb steel was exclusively $Ti_4C_2S_2$. Figure 14 shows the microstructure of the Ti–Nb steel. The large and elongated textural colonies observed in the Nb steel were hardly evident in the Ti–Nb steel, and the mean ferrite grain size was 2.87 μm which is smaller than that of Ti steel.

Table IV. Chemical Composition of Ti–Nb Steel (wt%)

Steel	**C**	**Si**	**Mn**	**P**	**S**	**Al**	**Nb**	**Ti**	**N**
Ti-Nb	0.035	0.1	1.46	0.0048	0.0057	0.038	0.021	0.112	0.0029

Table V. Mechanical Properties of Ti Steel, Ti-Nb Steel and Nb Steel

	TS (MPa)	**T.El (%)**	**U.El (%)**	**L.El (%)**	**λ (%)**	**TS×El×λ (MPa %^{2})**
Ti	604	19.8	10.6	9.2	140	1674288
Ti-Nb	607	20.9	11.2	9.7	151	1915631
Nb	575	18.2	10.9	7.3	96	1004640

This result supported the conclusion that the inferior strength–ductility–hole expansion ratio balance in the Nb steel was caused by the formation of large and elongated textural colonies and deformable sulphide, and that the strength–ductility–hole expansion ratio balance of the Ti steel can be improved by proper addition of Nb, which refines the ferrite microstructure without formation of textural colonies.

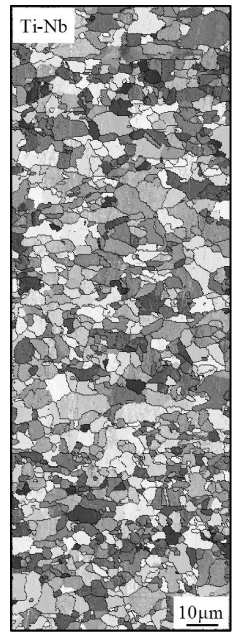

Figure 14. ND crystal orientation map of Ti-Nb steel.

Conclusions

1. An alloy composition incorporating a carefully balanced combination of Nb and Ti has been shown to provide a favourable combination of properties including the required strength-ductility-hole expansion ratio balance.

2. The enhanced properties have been achieved by optimum strengthening of the ferrite matrix by a large volume of finely dispersed precipitates as well as grain refinement.

3. Neither Ti nor Nb on its own, within the experimental composition limits studied, was capable of providing the best result.

4. Ti-only microalloyed steel resulted in a higher shear area at the edge of a punched hole and exhibited many microcracks over the entire circumference after hole expansion. However these cracks were not growing into a macroscopic crack.

5. Nb-only microalloyed steel resulted in a smaller shear area at the edge of a punched hole and exhibited fewer microcracks, which however propagated into macroscopic cracks at a smaller hole expansion ratio.

6. The ferrite grain size of the Nb steel was finer than that of the Ti steel but the former also contained large textural colonies. Such textural colonies can provide an easy crack path and may lead to larger dimples on the fracture surface compared to the Ti steel.

7. MnS and NbCN particles were observed in the fracture dimples of the Nb steel, whereas in the Ti steel TiN and $Ti_4C_2S_2$ particles were primarily observed.

8. The size and volume fraction of precipitates in the two steels (Nb and Ti alone) were similar.

9. It is postulated that larger textural colonies and the presence of deformable MnS may have been responsible for the poorer strength-ductility–hole expansion ratio in the first Nb steel studied.

10. A dual Ti+Nb microalloyed steel using a Nb level providing efficient grain refinement but avoiding the formation of textural colonies appears to deliver the optimum combination of properties.

Acknowledgements

We thank CBMM (Companhia Brasileira de Metalurgia e Mineração) for the financial support of this study. Special appreciation is extended to Dr. Hardy Mohrbacher for stimulating discussions.

References

1. S. Hayami and T. Furukawa (Paper presented at the Micro Alloying '75 Symposium on High-strength, Low-alloy Steels, Products and Process, Washington, D.C. 1975), 59.

2. O. Matsumura, Y. Sakuma, and H. Takechi, "Enhancement of Elongation by Retained Austenite in Intercritical Annealed 0.4 C - 1.5 Si - 0.8Mn Steel," *Transactions of the Iron and Steel Institute of Japan*, 27 (7) (1987), 570-579.

3. K. Sugimoto et al., "Retained Austenite Characteristics and Tensile Properties in a TRIP Type Bainitic Sheet Steel," *Iron and Steel Institute of Japan International*, 40 (9) (2000), 902-908.

4. K. Sugimoto et al., "Ductility and Formability of Newly Developed High Strength Low Alloy TRIP-aided Sheet Steels with Annealed Martensite Matrix," *Iron and Steel Institute of Japan International*, 42 (8) (2002), 910-915.

5. Y. Funakawa et al., "Development of High Strength Hot-rolled Sheet Steel Consisting of Ferrite and Nanometer-sized Carbides," *Iron and Steel Institute of Japan International*, 44 (11) (2004), 1945-1951.

6. M. Morita et al., "Development of Hot-rolled High Strength Steels Hardened by Precipitation Hardening with High Stretch Flanging," *CAMP - Iron and Steel Institute of Japan International*, 5 (1992), 1863.

7. M. Morita et al., “Development of Precipitation Hardened Ferrite and Martensite Dual Phase Steel for Automotive Wheel,” *Materia Japan*, 37 (6) (1998), 513-515.

8. Y. Mukai, “Development of New High-strength Steel Sheets for Automobiles,” *Kobe Seikou Giho*, 55 (2) (2005), 30.

9. T. Nonaka et al., “Developments of Ultra High-strength Cold-rolled Steel Sheets for Automotive Use,” *Shinnittetsu Giho*, 378 (2003), 12-14.

10. T. Tsumashika, K. Hasegawa, and H. Kawabe, “Ultra High-strength Steel Sheets Leading to Great Improvement in Crashworthiness,” *JFE Giho*, 4 (2004), 33.

11. Y. Omiya, “Developments and Trends Related to High-strength Steel Sheet for Automotive Use,” *Kobe Seikou Giho*, 50 (2000), 20.

12. N. Yoshinaga, “Symposium on Materials for Automobiles,” (2006), 15, (ISIJ).

13. T. Kashima and Y. Mukai, “Materials for Automotive Industry: Development of 780 MPa Class High Strength Hot Rolled Steel Sheet with Super High Flange Formability,” *Kobe Steel Engineering Reports*, 52 (3) (2002), 19-22.

14. Y. Funakawa and K. Seto, “Stabilization in Strength of Hot-rolled Sheet Steel Strengthened by Nanometer-sized Carbides,” *Tetsu-to-Hagane (Journal of the Iron and Steel Institute of Japan*), 93 (1) (2007), 49-56.

15. A. Phillips et al., “Effect of Microstructure and Texture on the Edge Formability of Light Gauge Strip Steel,” *Iron and Steel Institute of Japan International*, 51 (5) (2011), 832-842.

16. Y. Takahashi et al., “Fracture Mechanical Study on Edge Flangebility of High Tensile-strength Steel Sheets,” *Proceedings of the Materials Science and Technology Conference 2009*, Pittsburgh, USA, (25-29 October 2009), 1317-1402.

Fundamentals and Applications of Mo and Nb Alloying in High Performance Steels – Volume 1
Edited by Hardy Mohrbacher
CBMM, IMOA and TMS, 2014

PROGRESS IN PRESS HARDENING TECHNOLOGY AND INNOVATIVE ALLOYING DESIGNS

Jian Bian

Niobium Tech Asia
068868 Singapore

Keywords: Hardenability, Weight Reduction, Hot Forming, Grain Refinement, Press Hardening, Automotive, Strength, Niobium, Molybdenum, Coating, Precipitation

Abstract

The worldwide automobile industry is currently focusing on developing a new generation of vehicles with more safety, less CO_2 emission and alternative energy. The key to success is the lightweight technology. As a perfect example of lightweight technology, press hardening is presented in 3 major aspects: material, design and manufacturing. The press hardening technology resolves the conflicting issues for application of ultra-high strength steels and makes it possible for carmakers to increase the strength level up to 1500 MPa or more for the safety-critical components and to achieve a weight reduction of about 20% without compromising safety or increasing cost. The good formability at high temperature gives carmakers much more flexibility to design and to form the components in a very precise way. During the cooling process in the die it is possible to control the microstructure transformation locally by changing the local temperature of the die accordingly so that different microstructures and mechanical properties can be realized in a single component. The ongoing developments are focused on the improvement of the toughness and the resistance to delayed fracture of press hardening steels. Finally the author would like to introduce an innovative alloying concept for press hardening steel, which can meet the challenges of automotive application at the present time.

Introduction

There are three major reasons for using press hardening technology:

- Good formability.
- Lightweight.
- Safety.

Over the last decade advanced (AHSS) and ultra-high strength steels (UHSS) have been developed. But with increasing strength, the formability of the steels becomes very limited on the one hand and on the other hand springback during the forming operation becomes larger. Therefore the automobile and the supply industries are facing new challenges to form the high strength steels using the conventional press shop. That is the reason why the application of AHSS and especially UHSS has not reached the level which the automotive industry would like to have. According to the European Car Body exhibition in Germany in 2010, the advanced high strength steels (tensile strength approaching 800 MPa) are currently used up to 15% on average in the European car body structure and the ultra-high strength steels (tensile strength from 800-

1200 MPa) are only used for less than 5% so far. In contrast, the press hardening technology has developed very fast over the last decade. Due to forming at high temperature, even high strength steels have excellent formability and there is no springback after forming. The high strength level makes it possible to reduce the weight of crash relevant components by 20 to 30% without safety compromise and cost increase. The major advantages of press hardening in comparison with the cold forming process are:

- Good formability due to high temperature.
- No springback during forming process.
- Very high strength after forming process.
- Low forming load.
- Less wearing of die.
- Design flexibility and dimensional accuracy.

Figure 1 shows that the number of car components made by the press hardening process increased from 3 million in 1987 to 107 million in 2007 [1]. It is estimated that it will reach 360 million car components by 2016. The typical components made by press hardening are A/B-pillar, bumper, roof rail and tunnel [2]. The rapid increase of car components made by the press hardening process clearly demonstrates that press hardening represents the future for the automobile industry in the years to come.

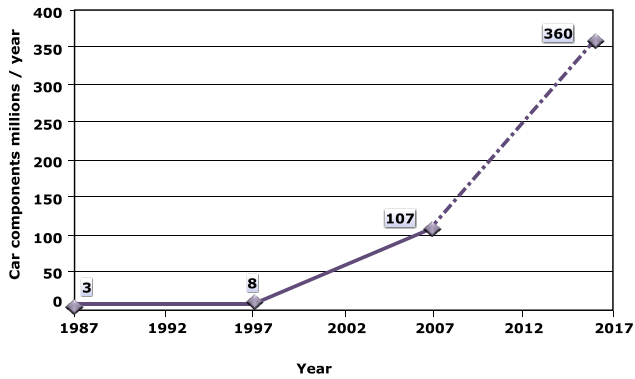

Figure 1. Number of car components produced by press hardening process from 1987 to 2007.

Press Hardening Steels

The standard press hardening steel is 22MnB5 which belongs to the manganese-boron steel group. This steel was developed about 40 years ago mainly as hot rolled or forged for a Q&T process with thick gauge. This steel was found to be suitable for press hardening due to its moderate carbon content and good hardenability. The critical cooling rate for martensite transformation is only about 27 K/s, therefore the first generation press hardening lines usually did not have water-cooled dies. But the disadvantage of uncooled dies is the extended cooling

time in the die and consequently lower productivity. For automotive application the press hardening steel will normally be cold rolled down to a thickness below 1.5 mm and subsequently coated with aluminum-silicon alloy or zinc alloy. The mechanical properties of 22MnB5 in the different process stages are listed in Table I.

Table I. Mechanical Properties of 22MnB5 in the Different Process Stages

Condition	YS, MPa	TS, MPa	Elongation, % (A80)
Hot rolled	500-650	650-820	>12
Cold rolled /annealed	310-400	480-560	>18
Cold rolled /AlSi coated	360-500	540-680	>10
Press hardened	950-1100	1450-1650	>5

Apart from the mechanical properties, 22MnB5 possesses a high bake hardening potential up to 100 MPa or more in the press hardened condition, good weldability (spot welding) and coatability, which are also very important criteria to be considered for automotive applications.

Coating System for Press Hardening

The most widely used coating system for the press hardening process is aluminum-silicon (AlSi for short) developed by ArcelorMittal [3]. This coating can protect the steel surface from scaling during the reheating process, but does not provide cathodic protection to the steel in corrosive media like a zinc coating does. The AlSi coating undergoes two major changes during the reheating period in the furnace:

1) Formation of rough surface of coating layer for good paint adherence.
2) Alloying of coating layer with the substrate.

Figure 2 shows that the coating layer becomes thicker and the surface becomes rougher after reheating. According to the investigation made by Arcelor-Mittal, the minimum reheating time for the coating layer should be about 4 minutes in order to get the desired surface condition for the subsequent painting process [3]. Figure 3 shows the alloying process of the coating layer during reheating in the furnace. Through diffusion of Fe to the coating layer, the weldability of the coating will be improved.

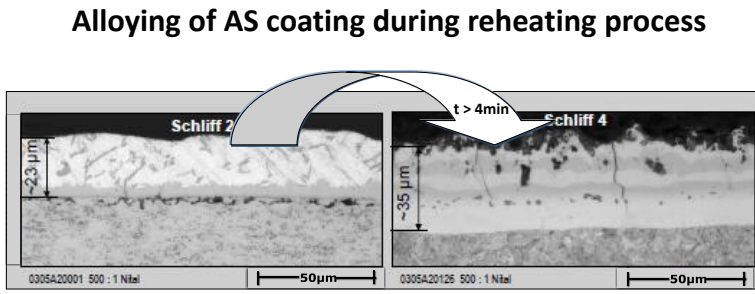

Figure 2. Influence of reheating process on the AlSi coating during press hardening process.

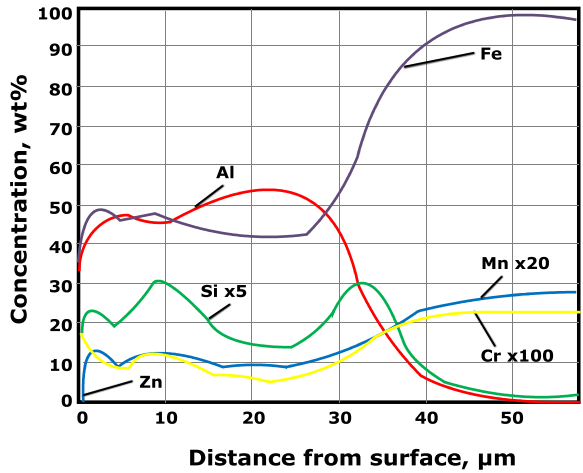

Figure 3. Alloying process of coating layer during reheating.

Process Technology

There are two process approaches for press hardening, namely one-step and two-step processing. For the one-step process, hot forming and quenching take place in the same die and the standard product is Usibor 1500 from ArcelorMittal [3]. For two-step process, which was developed by Voestalpine, the cold forming and quenching take place separately in two different dies and the standard coating is a zinc alloy [4]. The majority of operating press hardening lines are based on one-step processing which is more economical due to shorter process times with only one die. The temperature profile and the microstructure development during press hardening is demonstrated in Figure 4.

The process begins with reheating of coated steel sheet to a temperature between 880 and 950 °C. After that it will be transferred by a robot to the press die for final forming and quenching, which takes normally about 12 s, before the components are released from the die at a temperature between 150 and 200 °C, if the press die is not cooled at all. The martensite-start and finish temperatures of 22MnB5 are about 400 and 200 °C respectively and, due to this reason, the component should be cooled down below 200 °C before release from the die.

The steel microstructure before the press hardening process consists of ferrite and pearlite and at the end of reheating it is fully austenite, which will transform to martensite after quenching in the die.

The bottleneck of the conventional press hardening process is related to reheating time in the furnace and the quenching time in the die. In order to increase the productivity, new developments are being focused on alternative heating technology, for example induction heating to shorten the reheating time, or to alloy the coating outside of the press hardening process. As for the quenching process, a hydraulic press with a water-cooled die and pressure control during quenching represents the state of the art.

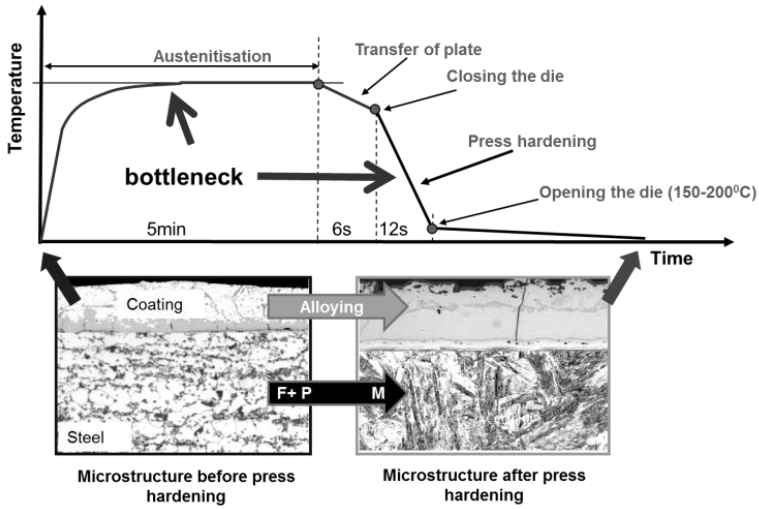

Figure 4. Temperature profile and the microstructure development during press hardening process.

Press Hardening into Dual Phase Microstructure

The standard microstructure after press hardening is martensite with very high strength but poor toughness. Since press hardening is a high temperature process, it is possible to control the microstructure development by controlling the process temperature and cooling rate during press hardening accordingly. Figure 5 shows just one example of how to make a DP steel by using the press hardening process.

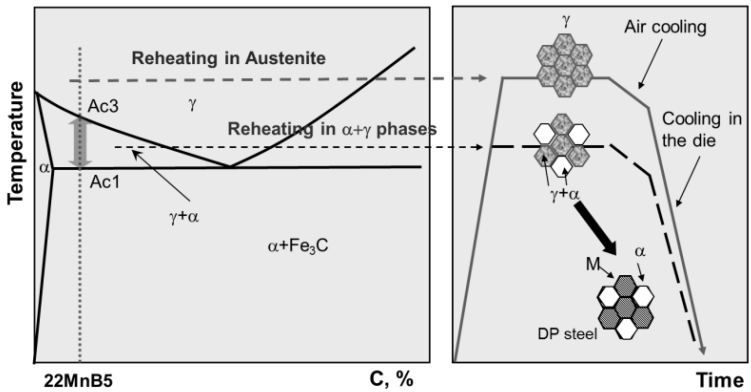

Figure 5. Press hardening into dual phase microstructure.

The only difference between dual phase press hardening and conventional press hardening is the reheating temperature. In order to produce a DP microstructure the steel sheet is reheated in the $\alpha+\gamma$ region instead of in the γ region as usual, and after quenching the dual phase microstructure can be realized. The influence of reheating temperature on the mechanical properties after press hardening is shown in Figure 6.

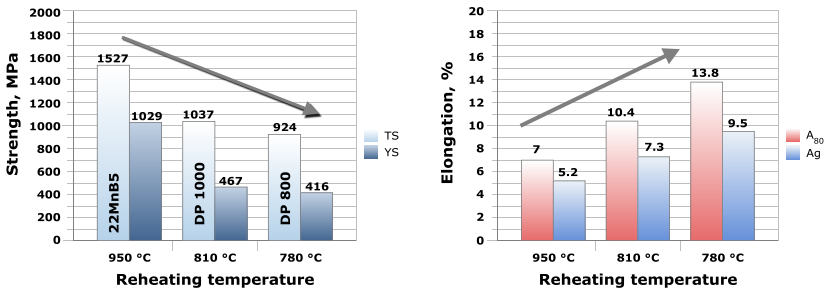

Figure 6. Influence of reheating temperature on the mechanical properties of dual phase steels after press hardening.

The major advantages of the process are:

- Dual phase microstructure with significantly improved elongation.
- Mechanical properties can be adjusted by varying the reheating temperature.
- To produce different products with the same steel composition by adjusting the furnace temperature accordingly.
- Energy-saving due to the lower furnace temperature.

Press Hardening with Higher Strength

The standard press hardening always produces a martensite microstructure. Since the hardness of martensite (strength) is solely related to the carbon content in the steel, it is easy to increase the martensite strength by increasing the carbon content. As mentioned above, the final strength of car components will be realized in the final step of forming and quenching; in this case the increase of strength will not have any evident negative effect on the whole process and especially on the forming process. As we know for the cold forming process, the strength level of the steel always has the dominant influence. Based on this consideration, higher strength can be reached by using a higher grade of manganese-boron steel for the press hardening process. Figure 7 shows some test results from ThyssenKrupp Steel Europe [5].

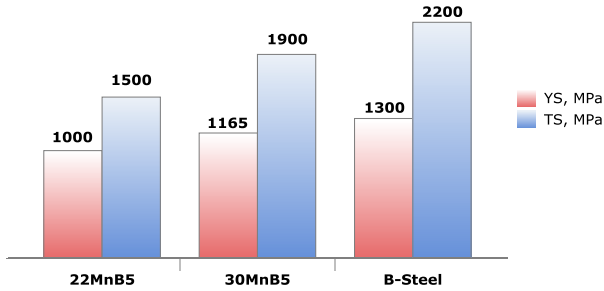

Figure 7. Higher strength up to 2200 MPa can be reached by using press hardening process [5].

By increasing carbon content accordingly, both yield strength and tensile strength can be increased and the total elongation remains at the same level due to the character of martensite. Due to this development, some carmakers in Europe are considering increasing the strength level up to 1900 MPa for some components like bumper and door beams by using the press hardening process. Mazda has already made the very first step to use 1800 MPa press hardening steel in the new CX-5 model [6]. Right now some developments are being focused on new press hardening steels with tensile strength of more than 2000 MPa.

Innovative Alloying Designs for Novel Press Hardening Steels

As mentioned before, the manganese-boron steels are suitable for press hardening due to the moderate carbon content and good hardenability. But manganese-boron steels do not provide the best solution to solve the specific problems with regard to the press hardening process like grain size coarsening during reheating and poor toughness and delayed fracture of the martensite microstructure. Currently these problems remain the major concerns for the automotive application of press hardening steels. Based on these considerations, an innovative alloying concept for the press hardening process, which is shown in Table II, has been developed.

Table II. Innovative Alloying Concept for Press Hardening Process

Mo = 0.15% Nb = 0.05%

Lower P and S

Steel grade	C Max	Si Max	Mn Max	P Max	S Max	Cr+Mo Max	Ti Max	B Max
22MnB5	0.25	0.40	1.40	0.025	0.010	0.50	0.05	0.0050

OUT OUT

Firstly, boron should be removed from the concept because boron can only increase the hardenability. However, hardenability is not an issue for the press hardening process due to the thin gauge of steel sheet for automotive application on the one hand and on the other hand the cooling rate in the die is much faster than the critical cooling rate for martensite transformation. Without B in the steel, Ti should also be taken out in order to avoid large TiN precipitates. The central point of the new concept is to use Nb alloying (about 0.05%) in order to control the grain growth from hot rolling to press hardening. Furthermore, Nb precipitates will help to increase the resistance to delayed fracture. The addition of Mo at 0.15% will compensate the hardenability due to the absence of B and slow down the precipitation process of Nb which will make Nb more effective at refining the microstructure and improving the toughness. Finally S and P should be further limited in order to improve the toughness of the steel. Figure 8 shows the the influence of Nb alloying on the microstructure of manganese-boron steels.

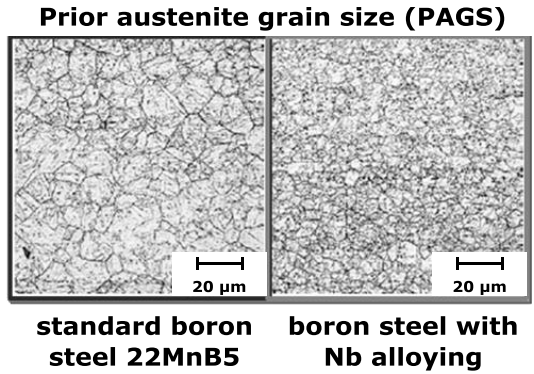

Figure 8. Influence of Nb alloying on the grain refinement of microstructure after press hardening process [7].

Due to the pinning effect of NbC precipitates, the prior austenite grain size at the end of reheating is much smaller than the conventional 22MnB5. Subsequently, the martensite packet size is also much smaller after quenching. The fundamentals of the new concept are to reduce or to avoid the crack initiation by avoiding large particles and inclusions on the one hand and on the other hand to increase the resistance to crack propagation by refining the microstructure and strengthening the grain boundaries (by reducing P, S and B); thus high strength, good toughness and high resistance to HIC can be achieved for press hardening steels. The following advantages of the new concept can be expected:

- Removal of B and Ti will make steelmaking and casting less problematic (clogging).
- Controlling the segregation of tramp elements to the grain boundaries.
- Refining microstructure.
- Avoiding large particles (TiN) and inclusions.
- Improving toughness.
- Trapping hydrogen and making martensitic steel less sensitive to delayed HIC.

Automotive Application

Press hardening steel is now used in almost every car model in Europe, and up to 12 different types of components and 20 parts can be used in the car body structure overall, as shown in Figure 9.

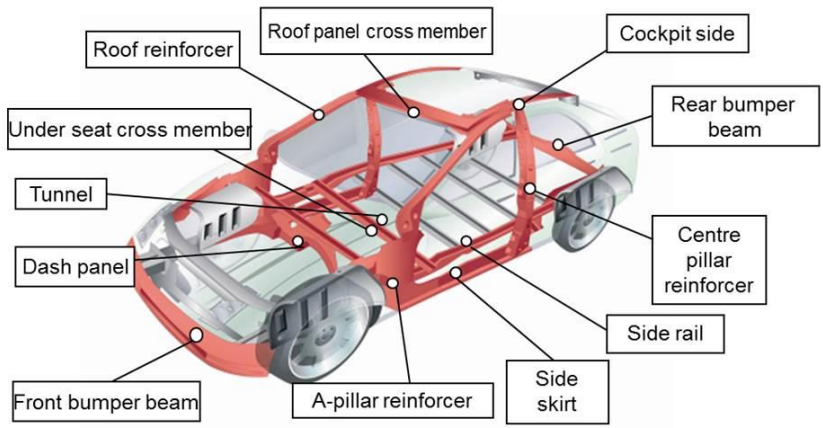

Figure 9. Application of press hardening steels in the car body structure.

The following diagram, Figure 10, shows the application of high strength steels from conventional HSS to PHS in some chosen European car models, which were demonstrated during the European Car Body Exhibition in 2009 and 2010 in Germany.

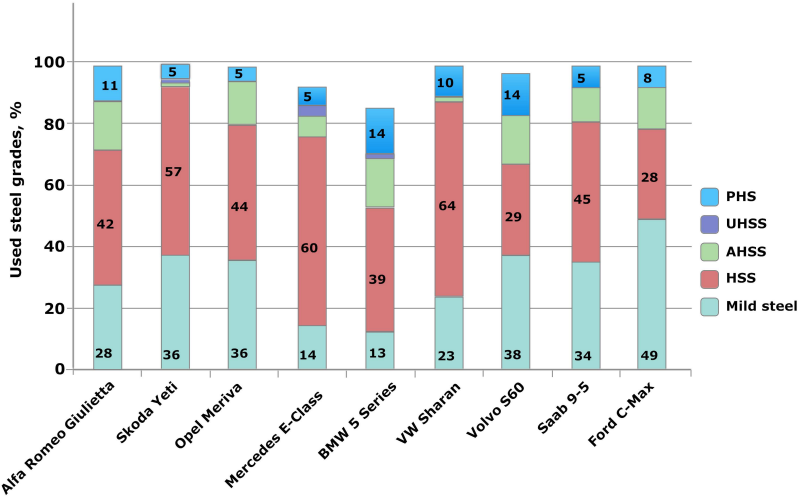

Figure 10. Used steel grades of some European car models from 2009 and 2010.

From Figure 10 the following development trends for car body structure can be concluded:

- Mild steels comprise less and less of the car body.
- Conventional HSS is still the major group used in the car body (up to 64% in the body structure).
- Advanced high strength steels continue to grow (up to 16% in the body structure).
- Ultra-high strength steels are still very limited in automotive application (less than 5%).
- Press hardening steels are present in every car model and used up to 15% in the body structure.

Conclusion

Press hardening technology has been proven to be a good solution to solve the problems of forming ultra-high strength steels like poor formability, springback, high forming load and wearing of the die. Press hardening broke the bottleneck for the application of ultra-high strength steels in the automobile industry and makes it possible to increase the strength level up to 1500 MPa or more for the safety-critical components and to achieve a weight reduction of about 20% without compromising safety or increasing cost. Press hardening is becoming both a technically and economically attractive lightweighting technology for the automotive industry,

especially with regard to the reduction of CO_2 emission. Niobium alloying provides an innovative alloying concept to make press hardening steels more suitable for automotive application.

References

1. J. Aspacher, "Forming Hardening Concepts" (Paper presented at the First International Conference on Hot Sheet Metal Forming of High Performance Steel, Kassel, Germany, 2008), 77-81.

2. Stahl im Automobil, Leicht und Sicher: Stahl-Information-Zentrum. 2009, www.stahl-info.de.

3. Arcelor-Mittal , "A New Method to Increase the Productivity of a Press Hardening Line Using Aluminized Boron Steel," *Proceedings of Conference of Materials in Car Body Engineering*, May 2011, Bad Nauheim, Germany.

4. PHS-Ultraform, Press Release, Voestalpine Stahl, 2011.

5. J. Bian, T. Heller, European Patent 1 865 086, "Verwendung Eines aus Einem Mangan-Bor-Stahl Hergestellten Flachproduktes und Verfahren zu Dessen Herstellung."

6. *Proceedings of Conference of Materials in Car Body Engineering*, May 2011, Bad Nauheim, Germany.

7. H. Mohrbacher, "Benchmark of Current Body Structures and Future Material Strategies," *Proceedings of Conference of Materials in Car Body Engineering*, May 2011, Bad Nauheim, Germany.

Common Acronyms and Abbreviations

ΔRe	Change in Yield Stress
Δt8/5	Cooling Time 800-500 °C
α	Ferrite
γ	Austenite
γ_R	Retained Austenite
A80	Percentage Elongation after Fracture, 80 mm Original Gauge Length
AC or ACC	Accelerated Cooling
Ag	Percentage Plastic Elongation at Maximum Force
AGS	Austenite Grain Size
AHSS	Advanced High Strength Steel
API	American Petroleum Institute
ASTM	American Society for Testing and Materials
BH	Bake Hardening
BIW	Body in White
BOF	Basic Oxygen Furnace
Bs	Bainite Start Temperature
CAL	Continuous Annealing Line
CCR	Cold Charging Rolling
CCT	Continuous Cooling Transformation
CET	Cold Cracking Susceptibility
CGL	Continuous Galvanizing Line
CIP	Curved Interphase Precipitation
CP	Complex Phase
CR	Controlled Rolling
CR/DQ	Control Rolled and Direct Quenched
CRt	Cooling Rate
CT	Coiling Temperature

CVN	Charpy V-notch
DBTT	Ductile-brittle Transition Temperature
DFF	Direct Fired Furnace
DP	Dual Phase
DQ	Direct Quench
DQST	Direct Quench and Self Temper
DRX	Dynamic Recrystallization
DWTT	Drop Weight Tear Test
EAF	Electric Arc Furnace
EBSD(P)	Electron Back Scattered Diffraction (Pattern)
EDS	Energy Dispersive Spectrum
EDX	Energy Dispersive X-ray Analysis
EELS	Electron Energy Loss Spectrum
El	Elongation
EQR	Earthquake Resistant
ERW	Electric Resistance Welding
FATT	Fracture Appearance Transition Temperature
FE(G)	Field Emission Gun
FLD	Forming Limit Diagram
FM	Finishing Mill
FR(S)	Fire Resistant (steel)
FRW	Fire Resistant Weathering
FSB	Finish Scale Breaker
GA	Galvannealed
GJC	Gas Jet Cooling
HACC	Heavy Accelerated Cooling
HAZ	Heat Affected Zone
HB	Brinell Hardness

HCR	Hot Charging Rolling
HR	Hot Rolled
HR/DQ	Hot Rolled and Direct Quenched
HRTEM	High Resolution Transmission Electron Microscopy
HSLA	High Strength Low Alloy
HSS	High Strength Steel
HTP	High Temperature Processed
HV	Vickers Hardness
IAD	Image Analysis Device
IAP	Intercritical Austenite Processing
IF	Interstitial Free
IFP	Interlocking Ferrite Plates
IP(P)	Interphase Precipitation
ISO	International Standards Organization
IT	Information Technology
JIS	Japanese Industrial Standard
LF	Ladle Furnace
LSL	Lower Specified Limit
MA or M/A	Martensite-austenite (phase)
MDRX	Metadynamic Recrystallization
MFS	Mean Flow Stress
MMBTU	Millions of British Thermal Units
OA	Overaging (Section of Annealing Line)
OD	Outside Diameter
ODF	Orientation Distribution Function
OM	Optical Metallography
OR	Orientation Relationship
PF	Polygonal Ferrite

PFZ	Precipitate-free Zone
PHS	Press Hardening Steel
PIP	Planar Interphase Precipitation
PM	Partially Martensitic (Steel)
PPT	Precipitate
Q&T	Quenched and Tempered
QT	Quench Temperature (in Annealing Cycle)
RD	Rolling Direction
RH	Vacuum Degassing Unit
RLT	Recrystallization Limit Temperature
RM	Roughing Mill
Rm	Tensile Strength
ROT	Run-out Table
RST	Recrystallization Stop Temperature
RT	Room Temperature
$Rt_{0.5}$	Yield Strength at 0.5% Total Elongation
RTH	Radiant Tube Heating
SA%	Percentage Shear Area
SATT	Shear Appearance Transition Temperature
SEM	Scanning Electron Microscopy (Microscope)
SRT	Start Rolling Temperature
SRX	Static Recrystallization
Sv	Grain Boundary Area per Unit Volume
TD	Transverse Direction
TEM	Transmission Electron Microscopy
TM	Thermomechanical
TMCP	Thermomechanical Controlled Processing
TN (facility)	Powder Injection Process

Tnr	No Recrystallization Temperature
TRIP	Transformation Induced Plasticity
TS	Tensile Strength
TWIP	TWinning Induced Plasticity
UHSS	Ultra-high Strength Steel
ULCB	Ultra-low Carbon Boron
ULSAB	Ultra Light Steel Auto Body
ULSAB-AVC	Ultra Light Steel Auto Body - Advanced Vehicle Concepts
ULSAC	Ultra Light Steel Auto Closure
ULSAS	Ultra Light Steel Auto Suspension
UOE	Pipe Manufacturing Process
UTS	Ultimate Tensile Strength
VSB	Vertical Scale Breaker
WT	Wall Thickness
XRD	X-ray Diffraction
YP	Yield Point
YS	Yield Strength

AUTHOR INDEX
Fundamentals and Applications of Mo and Nb Alloying in High Performance Steels

B
Bian, J. 227

F
Fazeli, F. 23
Funakawa, Y. 173

G
Gray, J.M. 121

H
Hosoya, Y. 173
Huang, C.Y. 63, 109

J
Jansto, S.G. 155
Jia, T. 23

K
Kamibayashi, K. 209
Kim, K. 135

M
Miao, C.L. 37
Militzer, M. 23
Mohrbacher, H. 83, 185

O
Ono, Y. 173

S
Senuma, T. 209
Shang, C.J. 37
Shimizu, I. 209
Subramanian, S.V. 3, 37

T
Takemoto, Y. 209
Tanabe, Y. 209

U
Urabe, T. 173

Y
Yang, J.R. 63, 109
Yang, Y. 3
Yen, H.W. 109

SUBJECT INDEX
Fundamentals and Applications of Mo and Nb Alloying in High Performance Steels

A
Annealing Strategies 185
Atom Probe 3
Austenite Grain Size 37, 135
Austenite Processing 37
Automotive 173, 185, 209, 227

B
Bainite 63
Boron 83

C
CCT 23, 37, 83, 121
Charpy Toughness 3, 63, 83, 135, 209
Coarse Grained Heat Affected Zone 63
Coating 227
Construction 155
CP Steel 185

D
Dislocation Density 37
DP Steel 185
Ductility 209
DWTT 135

E
EBSD 3, 209
Elevated Temperature Strength 155
Engineering Design 155

F
Fire Resistant 155

G
Grain Refinement 3, 83, 227
Grain Size 173

H
Hardenability 83, 227
Hardness 109, 209
HAZ 3
Heat Input 63
High Angle Boundaries 3
High Performance Steel 37
High Strength Steel 209
High Strength Steels 173
Hole Expansion 173, 185
Hole Expansion Ratio 209
Hot Forming 227
HSLA Steels 83, 155

I
IF Steel 173
Intercritical Rolling 155
Interlocking Ferrite Structure 63
Interphase Precipitation 109, 173

K
Kinetics 23

L
Linepipe 3, 23
Linepipe Steels 121

M
MA Phase 135
Mechanical Properties 121, 135, 155, 209
Microstructure 3, 37, 37, 63, 135, 173
Modelling 23
Molybdenum ..... 3, 23, 37, 83, 109, 121, 135, ... 155, 173, 185, 227
Multiphase Steels 185

N
Nano Co-precipitation 155
Nanometer-sized Carbide 109
Nickel 135
Niobium ..... 3, 23, 37, 63, 83, 109, 121, 135, 155, ... 173, 185, 209, 227

P
Phase Transformation ..... 3, 23, 37, 63, 83, 109, ... 185
Plate 155

Precipitation ... 3, 83, 135, 227
Precipitation Hardening ... 209
Press Hardening ... 227
Process Route ... 135
Property Anisotropy ... 135

Q

Quenching and Tempering ... 83

R

R-value ... 173, 209
Rebar ... 155
Recrystallization ... 3, 37, 83

S

Secondary Hardening ... 83
Segregation ... 3
Seismic ... 155
SEM ... 173
Solute Drag ... 23
Specifications ... 155
Spiral Pipe ... 135
Strength ... 83, 155, 227
Strengthening Mechanisms ... 121
Stress Relaxation ... 37
Stretch Flangeability ... 173
Strip ... 185

T

TEM ... 3, 63, 109, 173
Thermal Simulation ... 23, 37, 63, 109, 155
Titanium ... 109, 135, 209
TRIP Steel ... 185

U

Ultra-High Strength ... 185

W

Wear Resistant Plate ... 83
Weight Reduction ... 227
Widmanstätten Ferrite ... 63

X

X100 ... 3, 121
X120 ... 3, 121
X65 ... 23
X70 ... 37
X80 ... 23, 37, 121, 135